Reconstitution of the herpesviral pUL31 - pUL34 nuclear egress complex function

Dissertation

der Mathematisch-Naturwissenschaftlichen Fakultät

der Eberhard Karls Universität Tübingen

zur Erlangung des Grades eines

Doktors der Naturwissenschaften

(Dr. rer. nat.)

vorgelegt von

Michael Lorenz

aus Schlema

Tübingen

2015

Gedruckt mit der Genehmigung der Mathematisch-Naturwissenschaftlichen Fakultät der Eberhard Karls Universität Tübingen.

Tag der mündlichen Qualifikation:	15.04.2015
Dekan:	Prof. Dr. Wolfgang Rosenstiel
1. Berichterstatter:	PD Dr. Wolfram Antonin
2. Berichterstatter:	Prof. Dr. Gerd Jürgens

Acknowledgements

All this work would not have been possible without the help, inspiration and support of many wonderful people.

First and foremost, I am especially very grateful to my supervisor Dr. Wolfram Antonin for all the help, his excellent guidance and support, the scientific discussions and ideas throughout all the years of my PhD. I am infinitely grateful for the good advices, the untiringly support and the great opportunity to work in his lab.

I would also like to thank all members of my Thesis Advisory Committee: Prof. Dr. Gerd Jürgens, Dr. Michael Hothorn and Dr. Christian Liebig. I am greatly thankful for their support and guidance throughout the course of my PhD.

I am truly grateful to all the present and former members of the Antonin lab for their help and continuous support: especially Benjamin Vollmer for all his help, discussions, ideas, fun and the (badly missing) coffee breaks, Allana Schooley for all the critical scientific discussions and fun, Daniel Moreno for all his help, Marion H. Weberruss for the great time at the end, Katharina Schellhaus for the nice time, Paola DeMagistris don't worry be happy, Susanne Astrinidis for her help and support, Cornelia Sieverding, Adriana Magalska, Ruchika Sachdev, Nathalie Eisenhardt and Cathrin Gramminger.
Furthermore, I want to thank a lot of people from FML and the Max Planck Institute for Developmental Biology for their help. I thank Dr. Christian Liebig for helping me with the microscopes, Dr. Matthias Flötenmeyer and Jürgen Berger for their help with the TEM. A special thank you goes to Herta Soffel for all the help with administrative things and to the cleaning ladies, as well as the whole staff of the FML, without their support a lot of things would not have been possible.
I am also grateful for having received a scholarship from the Max-Planck-Society.
I want to thank all of my friends for their patience due all the years. I know it was not always easy.

Most importantly, I want to thank Rahel for her infinite support and patience over all these years and thank you for believing in me. Finally I want to thank my mother and my brother Christian, my sister Kathrin and her husband Udo for their support and believing in me.

Table of contents

Abbreviations

Δ	Delta
µm	Micrometer
nm	Nanometer
aa	Amino acid
AAA+	ATPases Associated with diverse cellular activities
AFM	Atomic force microscopy
APS	Ammonium peroxodisulfate
AT	Adenine thymine
ATP	Adenosine triphosphate
ATPase	Adenosine triphosphatase
BSA	Bovine serum albumin
C-terminus	Carboxyl-terminus
cAMP	Cyclic adenosine monophosphate
Chol	Cholesterol
CCSC	C capsid-specific complex
cm	Centimeter
CR	Constant region
CTAB	Cetyl trimethylammonium bromide
CVSC	Capsid vertex specific component
DAPI	4’,6-Diamidino-2-phenyindole
DiD-C_{18}	1,1'-Dioctadecyl-3,3,3',3'-tetramethylindodicarbocyanine perchlorate
DiI-C_{18}	1,1'-Dioctadecyl-3,3,3',3' tetramethylindocarbocyanine perchlorate
DMSO	Dimethyl sulfoxide
DNA	Deoxyribonucleic acid
dNTP	Deoxyribonucleoside triphosphates
E	Early
E. coli	Escherichia coli
EB	Elution Buffer
EDTA	1-(4-Aminobenzyl)ethylenediamine-N,N,N’,N’-

	tetraacetic acid
EGFP	Enhanced green fluorescent protein
EM	Electron microscopy
ER	Endoplasmic reticulum
FG	Phenylalanine glycine dipeptide
GEF	Guanosine triphosphate exchange factor
GSH	Glutathione
GST	Glutathione-S-transferase
GTP	Guanosine triphosphate
GTPase	Guanosine triphosphatase
GUV	Giant unilamellar vesicle
HEK293T	Human Embryonic Kidney 293 cells with T-antigen of SV40
HEPES	4-(2-hydroxyethyl)-1-piperazineethanesulfonic acid
His_6	Hexa Histidine
ICTV	International Committee on Taxonomy of Viruses
IE	Immediate early
ILV	Intra lumenal vesicle
INM	Inner nuclear membrane
ITO	Indium tin oxide
kbp	Kilo base pair
kDa	Kilo Dalton
L	Late
L_d	Liquid disordered
L_o	Liquid ordered
LB	Lysogeny broth
M	Mol
mA	Milliampere
mAb414	Mouse Monoclonal antibody 414
MALLS	Multi angle laser light scattering
MISTIC	Membrane-integrating sequence for translation of integral membrane protein constructs

ml	Milliliter
mRNA	Messenger RNA
MWCO	Molecular weight cut-off
N-terminus	Amino-terminus
NE	Nuclear envelope
NEC	Nuclear egress complex
NETC	Nuclear envelope targeting cassette
Ni-DGS	1,2-dioleoyl-sn-glycero-3-[(N-(5-amino-1-carboxypentyl)-iminodiacetic acid)succinyl] (nickel salt)
Ni-NTA	Nickel-nitrilotriacetic acid
NLS	Nuclear localization signal
NPAR	Nuclear pore complex assembly region
NPC	Nuclear pore complex
Nup	Nucleoporin
OD	Optical density
ONM	Outer nuclear membrane
ORF	Open reading frame
OSER	Organized smooth endoplasmic reticulum
PA	Phosphatidic acid
PBS	Phosphate buffered saline
PC	Phosphatidylcholine
PCR	Polymerase chain reaction
PE	Phosphatidylethanolamine
Pen/Strep	Penicillin / Streptomycin
PFA	Paraformaldehyde
PI	Phosphatidylinositol
PIPs	Phosphatidylinositol phosphates
PKC	Protein kinase C
PMSF	Phenylmethylsulfonylfluorid
PRV	Pseudorabies virus
PS	Phosphatidylserine
Ran	Ras-related nuclear protein
RCC1	Regulator of chromatin condensation 1

RK13	Rabbit kidney cell line 13
RNA	Ribonucleic acid
rpm	Round per minute
SDS-PAGE	Sodium dodecylsulfate - polyacrylamid gel electrophoresis
SEM	Standard error of the mean
SLB	Supported lipid bilayer
SM	Sphingomyelin
SuHV-I	Suid herpes virus-I
TBE	Tris-borate-EDTA
TE	Tris-EDTA
TEMED	N,N,N′,N′-Tetramethylethan-1,2-diamin
TEV	Tobacco etch virus
TMR	Trans membrane region
UL	Unique long
US	Unique short
VDAC	Voltage-dependent anion channel
v/v	Volume / volume
VZV	Varicella zoster virus
w/v	Weight / volume
Xenopus	Xenopus laevis

Summary

Herpes viruses adapted successfully during their evolution in order to reproduce themselves in a variety of hosts. After initial infection they can establish a state of viral latency in their host organism. The assembly of herpes virus capsids takes place in the cell nucleus. As these capsids exceed the size limit of nuclear pore complexes, they are transported by a virus-mediated vesicular transport through the nuclear membranes into the cytoplasm.

This transport involves the induction of membrane deformation, followed by capsid integration and subsequent scission of membrane vesicles at the inner nuclear membrane into the periplasm. This process is known as primary envelopment. The enveloped capsids fuse with the outer nuclear membrane and are released for further maturation into the cytoplasm.

It is believed that envelopment of capsids at the inner nuclear membrane is mediated by only two viral proteins, conserved among all herpes viruses. These essential proteins termed pUL31 and pUL34, interact at the inner nuclear membrane and form the so-called nuclear egress complex (NEC). The direction of the nuclear envelope passage is defined by a pUL31 and pUL34 gradient between the nucleus and cytoplasm and thus, might be the reason for maintaining the conserved two component nuclear egress complex.

The involvement of cellular proteins in primary envelopment, as well as the underlying mechanism is not known.

By employing a minimal artificial membrane test system I was able to demonstrate that the interaction of these two viral proteins is sufficient to mediate membrane invagination and scission. Strikingly, this process required no additional cellular factors. My further characterization of pUL31 revealed that artificial membrane tethering is sufficient to mediate membrane restructuring. The initial binding and subsequent oligomerization of pUL31 to membranes induces the formation of a protein coat in the absence of the interaction partner pUL34 that drives membrane budding and scission.

My results confirm that this complex of two viral proteins is sufficient to deform membranes in a minimal system. The important features of this complex, namely membrane deformation and membrane scission are mediated most interestingly only by the viral protein pUL31. Thus, pUL34 acts as a recruitment factor for pUL31.

Nevertheless, essential functions of the conserved protein pUL34 and its homologues in the replication cycle of herpesviruses cannot be excluded.

Taken together this study demonstrates how in contrast to the complexity of cellular membrane deformation and scission processes, a single viral protein combines these essential functions. Additionally, the presented results further emphasize the advantage of in vitro systems to investigate molecular mechanisms of membrane related processes.

Zusammenfassung

Um sich in einer Vielzahl von Wirten vermehren zu können, haben sich Herpesviren im Laufe ihrer Evolution erfolgreich angepasst. Sie sind die bisher einzig bekannten Viren, die nach einer Erstinfektion ein Leben lang in ihrem Wirtsorganismus persistieren, indem sie in eine Art Ruhezustand (Latenz) übergehen. Eine weitere Besonderheit von Herpesviren, ist der im Zellkern erfolgende Zusammenbau von Viruskapsiden. Diese werden aufgrund ihrer Größe die das Größenlimit von Kernporenkomplexen übersteigen, durch einen virusvermittelten, vesikulären Transport durch die Kernhülle in das Zytoplasma transportiert.

Dieser Transport umfasst die Induktion von Membrandeformation, sowie darauf folgende Membranabschnürungen der inneren Kernmembran. In diese werden Kapside integriert und liegen im periplasmatischen Raum vor. Dieser Prozess wird als primäre Umhüllung bezeichnet. Im weiteren Verlauf fusionieren die umhüllten, periplasmatischen Kapside mit der äußeren Kernmembran und geben diese zum weiteren Transport in das Zytoplasma frei.
Es wird angenommen, dass für diesen Einschnürungsprozess an der inneren Kernmembran zwei in allen Herpesviren konservierte, virale Proteine entscheidend sind. Diese essentiellen Proteine sind pUL31 und pUL34. Sie interagieren miteinander an der inneren Kernmembran und formen den sogenannten Kern-Austritts-Komplex. Konzentrationsunterschiede von pUL31 und pUL34 zwischen Zellkern und Zytoplasma, definieren die Richtung des Kerndurchtritts und sind vermutlich der Grund für die Beibehaltung eines konservierten Zwei-Komponenten Kern-Austritt-Komplexes.

Die Beteiligung zellulärer Proteine an der Umhüllung, sowie der zugrunde liegende Mechanismus sind bisher nicht bekannt.
Mit Hilfe eines minimalen, artifiziellen Membranvesikel Testsystems konnte ich nachweisen, dass die Interaktion der beiden viralen Proteine ausreichend ist, um Membraneinstülpungen und deren Fusion zu vermitteln. Dies erfordert keine weiteren zellulären Faktoren. Weiterhin konnte ich zeigen, dass das virale Protein pUL31 künstlich an Membranen gebunden, ausreichend ist, um deren Umstrukturierung

hervorzurufen. Die initiale Bindung und folgende Oligomerisierung von pUL31 an Membranen, induziert die Ausbildung einer Hülle in Abwesenheit des Interaktionspartners pUL34, was zu Membrandeformation und Abschnürungen führt. Meine Ergebnisse legen nahe, dass lediglich der Komplex aus zwei viralen Proteinen in einem minimalen System ausreichend ist, um Membranen zu deformieren. Die wichtigen Funktionen dieses Komplexes: Membrandeformation und Membranabschürung vermittelt lediglich das virale Protein pUL31. pUL34 fungiert somit in dem minimalen Vesikelsystem als Rekrutierungsfaktor für pUL31. Weitere, mitunter essentielle Funktionen des konservierten Proteins pUL34 und seiner Homologen im Vermehrungszyklus der Herpesviren können jedoch nicht ausgeschlossen werden.

Zusammenfassend demonstriert diese Arbeit, dass im Gegensatz zur Komplexität zellulärer Membrandeformations- und Abschnürungs-Prozesse, ein einzelnes virales Protein diese grundlegenden Funktionen vereint. Die weiteren vorgestellten Ergebnisse unterstreichen zudem den Vorteil von *in-vitro*-Systemen, um molekulare Mechanismen membranbezogener Prozesse zu untersuchen.

1 Introduction

1.1 Herpesviruses

Herpes viruses are enveloped DNA viruses with a double-stranded linear genome. The virus family of *Herpesviridae* is part of the order *Herpesvirales*, according to „The International Committee on Taxonomy of Viruses“ (ICTV) and is categorized in three families, three subfamilies, 17 genera and 90 species in total (Davison et al., 2009). The family of the *herpesviridae* is divided in three subfamilies, the *alpha*-, *beta*- and *gamma-herpesviridae* and further into several genera. In total, until to today 90 categorized and at least 48 unassigned species are known among the *Herpesvirales* (Davison, 2010).

Herpesviruses are characterized by the same basic structure and replication cycle (Fig. 1.1 - Fig. 1.3). One main property of herpes viruses is their ability to establish latent infections in dividing and non-dividing cells dependent on the cell tropism (Block & Hill, 2007). In the latent phase, the viral genome is circularized, located in the nucleoplasm and genes encoding factors involved in the lytic (replicative) cycle are transcriptionally and functionally repressed (Roizman & Knipe, 2001; Preston, 2000). Thus, no infectious viral particles are produced, resulting in suspended virus dissemination and appears thereby clinical inapparent. Latent infections last the lifespan of the host and can undergo reactivation anytime. Stimuli resulting in reactivation can be physical or psychological and induce viral gene expression and entry in the lytic cycle. The underlying mechanisms regulating establishment, maintenance and reactivation of latent infections are highly complex.

Alpha-herpesviruses are the “*prototypes*” of the *Herpesviridae,* including several human pathogenic herpes viruses such as human herpes virus I (HHV-1, HSV-1), human herpes virus II (HHV-2, HSV-2), and the human herpes virus 3 (HHV-3, VZV). In addition, several animal pathogenic species, e.g. suid herpesvirus-I (SuHV-1, PRV) are assigned to the subfamily.

Alpha-herpesviruses are commonly used to study virus related processes, as they can infect a broad range of cell types, accompanied by a high infectivity. Interestingly, many of the viral genes are not essential and can be replaced by genes of interest for

the creation of virus vectors (Burton et al., 2002). For this, the human not pathogenic suid herpesvirus-I (PRV) was the selected as model organism.
Unless otherwise indicated, the alpha-herpesviruses shall be examined more detailed in the following. Furthermore, herpesviral genes are designated to their location in the viral genome which consist of a long and short region as unique long (*UL*) or unique short (*US*) and corresponding, viral proteins as *pUL* or *pUS.*

1.1.1 Structure of herpesviruses

The overall morphology of herpesviruses is conserved. The main structural features of this family are the viral capsid of a typical viral particle. It comprises the viral DNA genome of about 152 kbp (HSV-I) and is of toroidal shape. The genome of herpesviruses is described as containing a unique long (U_L) and a unique short (U_S) region, each flanked by inverted repeat sequences (McGeoch et al., 1988; Furlong et al., 1972).
The viral capsid, a main structural element, is assembled in the nucleoplasm from about seven viral proteins (pUL6, pUL17, pUL18, pUL19, pUL25, pUL35, pUL38) (Brown & William, 2011; Loret et al., 2008; Rozen et al., 2008; Zhu et al., 2005; Johannsen et al., 2004). Capids have an icosahedral shape and are composed of 162 capsomers. These represent the smallest subunits of all herpesviruses and can be subdivided in 150 hexons and 12 pentons interconnected by triplexes (Fig. 1.1)

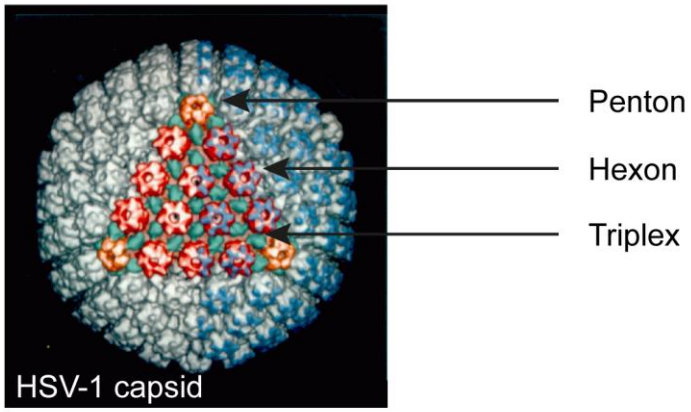

Figure 1.1: Structure of the HSV-1 capsid
Surface-shaded representation of a Cryo-EM reconstruction of a 125 nm HSV-1 capsid. One capsid face is coulored, highlighting hexons, pentons and triplexes (red, orange and blue). Adapted and modified from Brown & Newcomb (2011).

The layer between the viral capsid and the viral envelope is termed as the tegument, composed of a multitude of proteins (at least 20 to 23 for HHV-1) (Kelly et al., 2009; Loret et al., 2008; Zhu et al., 2005; Mettenleiter, 2004; Grünewald et al., 2003). Multiple roles are assigned to individual tegument proteins during viral entry and exit as well as in regulation of viral transcription and host translation (Kelly et al., 2009). The viral envelope represents the outer layer of herpes virions. The membrane originates from infected hosts and is aquired by secondary envelopement at the *trans*-Golgi network. The membrane is modified with serveral viral encoded glycoproteins playing an important role in viral attachment and fusion upon infection (Eisenberg et al., 2012; Farnsworth & Johnson, 2006; Turcotte et al., 2005; Wisner & Johnson, 2004). Additionally, viral glycoproteins are also found in budded virions and the inner nuclear membrane in HHV-I infected cells (Baines et al., 2007; Farnsworth et al., 2007; Stannard et al., 1996). Interestingly, viral glycoproteins are not present in budded virions of suid herpes virus-I (Klupp et al., 2008) and thus, appear not to be involved in budding at the inner nuclear membrane.

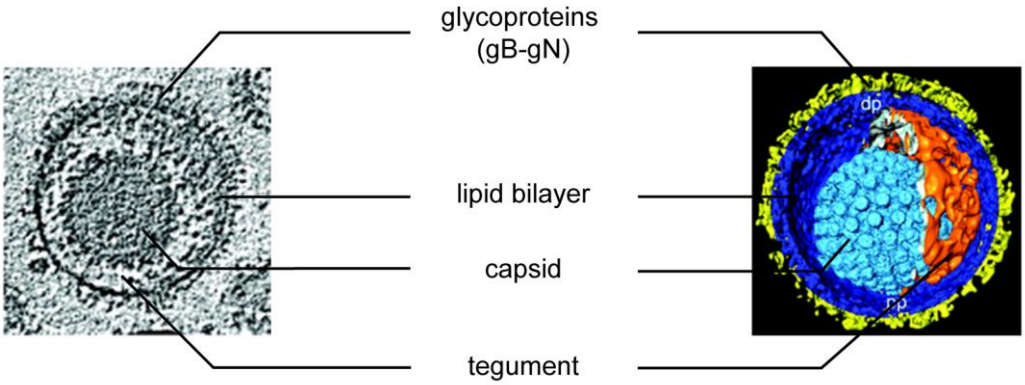

Figure 1.2: The structure of herpesviruses
The main structural components of herpesviruses are indicated in a 3D illustration (right) and in an electron microscopical image (left) for a single herpesviral particle. Adapted and modified from Gruenewald et al. (2003). Dp - distal pole, pp - proximale pole

1.1.2 Replication of herpesviruses

The initial steps of viral attachment to the surface of the target cell are the binding of viral glycoproteins to the target cell membrane receptors, including heparan sulfate proteoglycans (Bender et al., 2005), chondroitin sulfate proteoglycans (Banfield et al., 1995), as well as cellular integrins (Cheshenko et al., 2014) and presumably other cell surface receptors. Four membrane glycoproteins (gD, gB, and a heterodimer, gH/gL) are required for HHV-1 entry into cells (Forrester et al., 1992; Cai et al., 1987; Ligas & Johnson, 1988). These initial interactions are followed by fusion of the target cell membrane with the virus envelope, after which the nucleocapsid and tegument are released into the cytoplasm. Subsequently, the viral capsid is transported to the nucleus mediated by dynein and dynactin (Döhner et al., 2002). Interactions between the tegument protein pUL36 and NPC protein Nup358, mediate capsid binding to nuclear pore complexes (Copeland et al., 2009). This binding is thought to iniiate the release of the viral DNA bound to viral core proteins into the nucleoplasm (Pasdeloup et al., 2009).

Viral DNA translation is divided into three temporal phases (Honess & Roizman, 1974) immediately early (IE), early (E) and late (L) gene expression. The immediately early (IE) genes are the first viral genes being expressed, encoding mainly for non-structural proteins and further regulate gene expression of the (delayed) early (E) and late (L) genes.

After fusion of the viral envelope with the cell membrane, liberated tegument proteins pUL48 (VP16) and pUL41 (VHS) are of particular importance for viral progression. The binding of the viral protein pUL48 (α-TIF, α-trans inducing factor) to the cellular transcription factor oct-1 and the cellular protein hcf-1 (host cell factor-1) are assumed to be important for the initiation of transcription of the early genes (Nogueira et al., 2004; Liu et al., 1999; Kristie et al., 1989; Stern et al., 1989; Gerster & Roeder, 1988).

In addition, pUL41 (virion host shutoff protein, UL41) a viral protein with ribonuclease activity (Taddeo & Roizman, 2006; Matis & Kúdelová, 2001) degrades cellular mRNA, as well as to some extend viral mRNA, causing polysome breakdown. Thus, aquisition of the cellular translation machinery for the expression of viral early and late gene products is promoted.

How herpesviruses enter the lytic cycle from latency, after application of reactivation stimuli, is still not well understood. So far the viral protein pUL48 (VP16) appears to be crucial for reactivation (Kim et al., 2012) and entry into the lytic cycle (Sawtell et al., 2011; Thompson & Sawtell, 2010; Campbell et al., 1984; Batterson & Roizman, 1983; Post et al., 1981).

Reactivation is assumed to begin by expression of regulatory early gene products, inducing replication of viral DNA, present in the cell nucleus according to the "rolling circle" principle (Boehmer & Lehman, 1997).

Regulatory early gene expression induces the expression of the late gene, encoding mainly structural proteins, necessary for the production of new virus particles. These are synthesized in the cytosol and imported into the nucleus. Structural proteins allow the assembly of new capsids, by spontaneous aggregation of viral major capsid proteins and minor capsid proteins in the nucleoplasm (Newcomb et al., 1996). The viral concatemeric DNA is cleaved and packed into newly formed capsids by a yet ill defined mechanism. This involves the HHV-1 viral proteins pUL6, pUL15, pUL17, pUL25, pUL28, pUL32, and pUL33 (Heming et al., 2014; Conway & Homa, 2011; Toropova et al., 2011; White et al., 2003; Boehmer & Lehman, 1997).

Since newly formed capsids with a diameter of about 125 nm exceed the nuclear pore size limit (Panté & Kann, 2002), herpes viruses have developed a unique and yet not fully understood mechanism in order to egress from the nucleus via translocation through the inner (INM) and outer (ONM) nuclear membrane.

Capsids bud at the nucleoplasmic site of the inner nuclear membrane into the perinuclear space, resulting in fully enwrappment by the inner nuclear membrane (Fig. 1.4). In this process, termed *primary envelopement,* viral proteins as well as cellular proteins become part of the tegument layer, surrounding the capsid (Padula et al., 2009; Read & Patterson, 2007; Naldinho-Souto, 2006; Baines et al., 1995). In order to acquire the primary envelope two viral proteins, pUL31 and UL34, are essential and conserved among the *herpesvirales* (Reynolds et al., 2001; Roller et al., 2000; Chang et al., 1997). After full enwrappment of capsids by the inner nuclear membrane, these vesicles reside in the perinuclear space (Fig. 1.4B, Fig. 1.5).

The fusion process of enveloped virions with the outer nuclear membrane is ill defined and is assumed to involve viral glycoproteins, initially involved in fusion of the viral envelope with the cell membrane (Farnsworth et al., 2007; Stannard et al., 1996). In addition, the not conserved but essential viral U_S3 kinase plays an

important role in fusion of capsids with the outer nuclear membrane since a lack of U_S3 results in accumulation of enveloped capsids in the perinuclear space (Klupp et al., 2001).

After the release of the capsids into the cytoplasm they are actively transported via the microtubule plus end motor kinesin-1 towards the cell periphery (Radtke et al., 2010; Miranda-Saksena et al., 2009). The final viral envelope is aquired by budding through Golgi, trans-Golgi and endosomal membranes. This process is termed *secondary envelopment* and respresents a maturation step, as viral capsids aquire tegument proteins and glycoproteins, important for cell to cell transmission.

Enveloped capsids are finally released into the extracellular space after vesicle transport to the plasma membrane. This transport to the cell periphery is assumed to involve actin-based motor protein Myosin Va, but the underlying mechanism is not yet defined (Roberts & Baines, 2010).

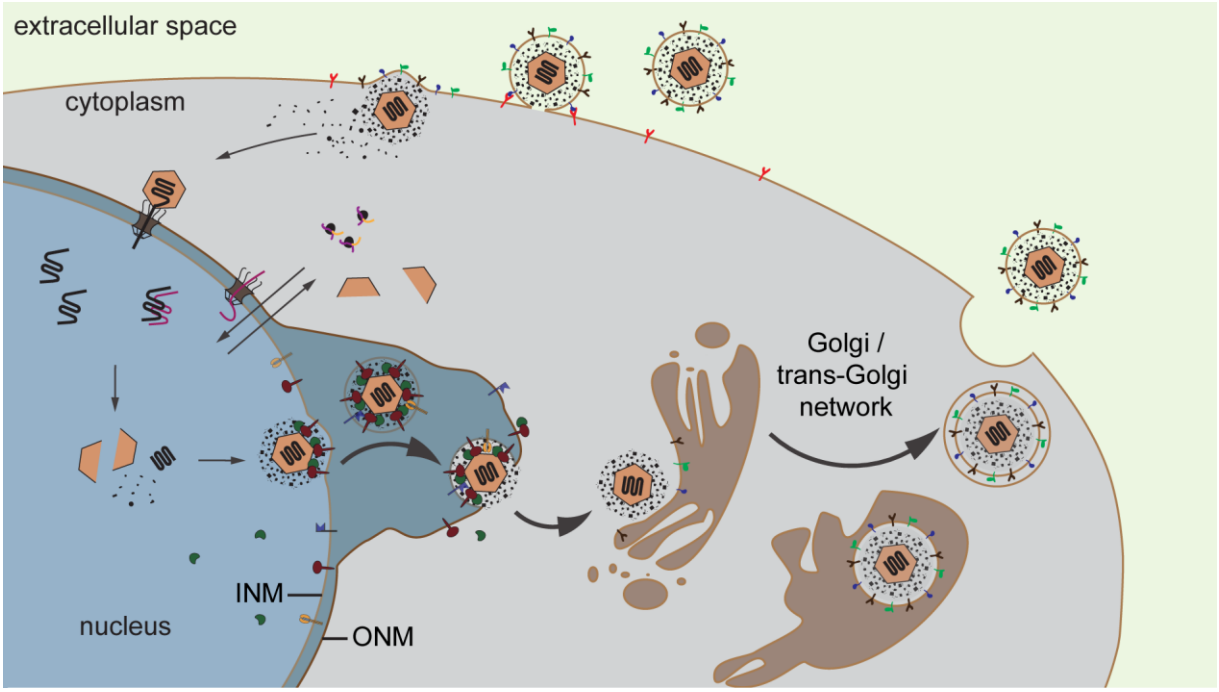

Figure 1.3: Illustration of the general herpesviral lifecycle
Infectious herpes viruses fuse with the cell membrane releasing the viral capsid into the cytoplasm. The capsid is transported to the nucleus were it interacts with NPC proteins releasing the viral DNA into the nucleoplasm where viral DNA is replicated and transcribed. Messenger RNA is exported into the cytoplasm and new structural viral proteins are synthesized which are imported in the nucleus. Assembly of new capids is performed in the nucleoplasm. Capsids are engulfed by the inner nuclear membrane resulting in periplasmatic enveloped particles which subsequently fuse with the outer nuclear membrane releasing the capsids into the cytoplasm. Cytoplasmic capsids are transported to the Golgi apparatus where a second budding step is performed, acquiring membranes to fuse with the cell membrane to release the new virus in the extracellular space.

1.1.3 The role of the nuclear egress complex in passing the nuclear envelope

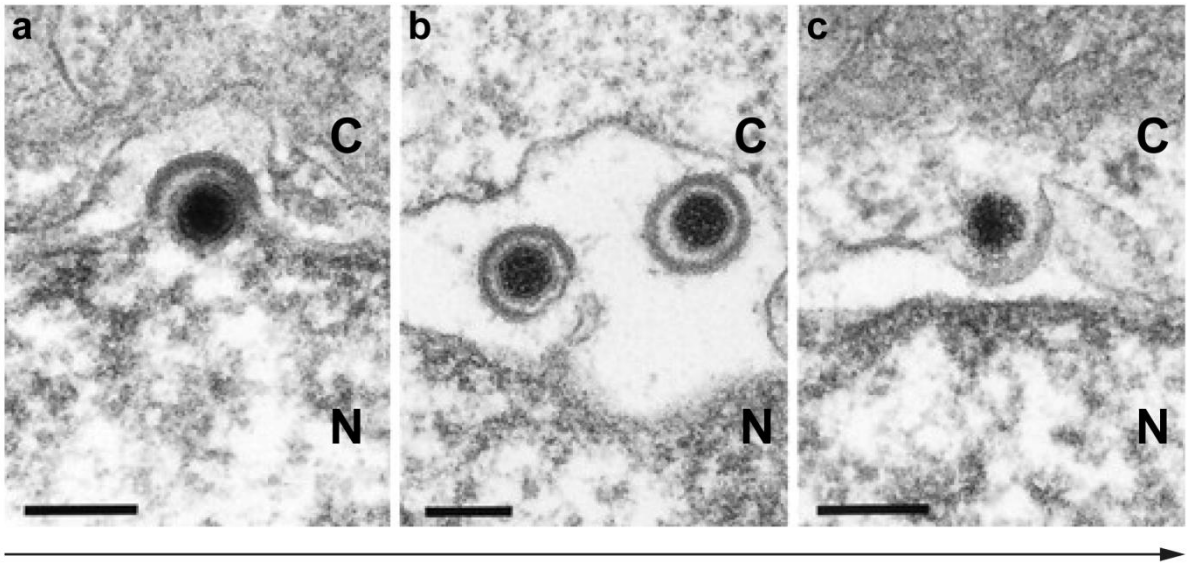

Figure 1.4: Transport of herpesviral capsids through the nuclear envelope
Herpesviral capsids aquire a primary envelope at in the inner nuclear membrane (A). Completely enveloped capsids reside in the perinuclear space (B) and subequently fuse with the outer nuclear membrane releasing the capsid into the cytoplasm (C). Budding direction (arrow), as well as nucleoplasm (**N**) and cytoplasm (**C**) are indicated. Bars: 150 nm, adapted and modified from Mettenleiter (2002).

Viral capsids acquire a primary envelope by constrictions at the inner nuclear membrane. How exactly capsids are transported and attracted to local accessible areas is unclear. In the process of the primary envelopment, two viral proteins pUL31 and pUL34 are essential and form the hetero-dimeric *nuclear egress complex* (NEC) (Loetzerich et al., 2006; Schnee et al., 2006; Mettenleiter, 2002) at the nucleoplasmic side of the inner nuclear membrane.

Both proteins are conserved among the *herpesvirales.* pUL31 is nucleoplasmic localized protein, interacting with the tail anchored viral protein pUL34, an integral type-II membrane protein, residing in the endoplasmic reticulum and nuclear envelope.

Infection experiments with viruses lacking either the UL31- and UL34 genes or both resulted in accumulation of non-enveloped capsids in the nucleoplasm (Liang & Baines, 2005).

The formed nuclear egress complex at the inner nuclear membrane is assumed to be involved in several ways during nuclear egress. Viral capsids need to access the inner nuclear membrane in order to cross the nuclear envelope covered at the nucleoplasmic site by the lamina, a dense meshwork consisting mainly of the proteins lamin A/C and lamin B. The pUL31/pUL34 complex locally disrupts the nuclear lamina (Bjerke & Roller, 2006; Reynolds et al., 2004; Simpson-Holley et al., 2004). This is mediated by recruiting additional viral and cellular factors to the membrane. Factors shown to be involved are cellular protein kinase C isoforms (PKC) (Leach & Roller, 2010; Park & Baines, 2006; Muranyi et al., 2002) and the viral kinases pUS3 (Mou et al., 2007; Kato et al., 2005; Reynolds et al., 2001; Purves & Roizman, 1991), conserved only in alphaherpesviruses, and pUL13 (Cano-Monreal et al., 2009; Romaker et al., 2006), as well as their homologues in all herpesviruses. The cellular and viral kinases phosphorylate components of the nuclear lamina: lamin A/C (Mou et al., 2007), lamin B1/B2 (Scott & O'Hare, 2001) and lamin interacting proteins e.g. lamin B receptor (LBR) (Scott & O'Hare, 2001; Cano-Monreal et al., 2009) and emerin (Leach et al., 2007).

Interestingly, also the NEC by itself can interact directly with lamin A/C *in vitro* (Reynolds et al., 2004). Thus, NEC-lamin interaction can interfere with lamin-lamin-interaction and additionally weakens the local integrity of the nuclear lamina (Reynolds et al., 2004).

Another important function of the NEC is implied in selecting capsids containing viral DNA (C-capsids) over immature capsids (A and B capsids) (Brown & Newcomb, 2011; Homa, 1997). This selection was assumed to include the viral proteins pUL17 and pUL25, two minor capsid assocciated proteins (Cockrell et al., 2011; Toropova et al., 2011) forming a complex, termed *C-capsid-specific complex* (CCSC) (Yang & Baines, 2011). As the C-capsid-specific complex was also found on immature

capsids, it was renamed to *capsids vertex specific component* (CVSC) (Toropova et al., 2011).

Most importantly, pUL31 and pUL34, forming the nuclear egress complex, are the main factors mediating capsid envelopment at the inner nuclear membrane (Bigalke et al., 2014; Roller et al., 2010; Mou et al., 2009; Klupp et al., 2007).

The NEC is assumed to remodel the inner nuclear membrane, preferentially around the viral capsids, but the precise mechanism, how pUL31 and pUL34 mediate inner nuclear membrane deformation remains enigmatic. Interestingly, in transfected cells the NEC is sufficient to induce perinuclear vesicle formation in the absence of other viral proteins (Klupp et al., 2007; Luitweiler et al., 2013). However, the key question remains, whether the NEC mediated membrane deformation requires additional cellular proteins as well as their potential involvment in scission of enveloped vesicles into the perinuclear space.

Recent findings indicate that the NEC only is indeed sufficient in mediating herpes viral primary envelopement (Bigalke et al., 2014).

In further respects, interactions between pUL31 and the pUL17-pUL25 complex may provide the physical link between attraction and attachment of capsids with the nuclear egress complex (Yang & Baines, 2011).

After complete enclosure of capsids by the inner nuclear membrane these vesicles have to fuse with the outer nuclear membrane. A direct role of the NEC in fusion of perinuclear vesicles is so far unknown. As pUL31 and pUL34 are found only associated with perinuclear enveloped capsids (Reynolds et al., 2002) and the C-terminus of pUL34 extends only three aminoacids into the periplasm, a potential interaction with soluble periplasmic or integral outer nuclear membrane proteins is uncertain, but cannot be excluded. Interestingly, overexpression of a cellular AAA+ ATPase in the lumen of the endoplasmic reticulum, torsinA, results in production and accumulation of enveloped vesicles in the cytoplasm and impaires HHV-I reproduction in infection experiments (Maric et al., 2011). TorsinA is implied to be involved in nuclear envelope maintenance (Ozelius et al., 1997). However, upon fusion of periplasmic vesicles with the outer nuclear membrane the fate of pUL31 and pUL34 is not defined. Both proteins are either degraded or reimported into the nucleus to promote another round of budding at the inner nuclear membrane.

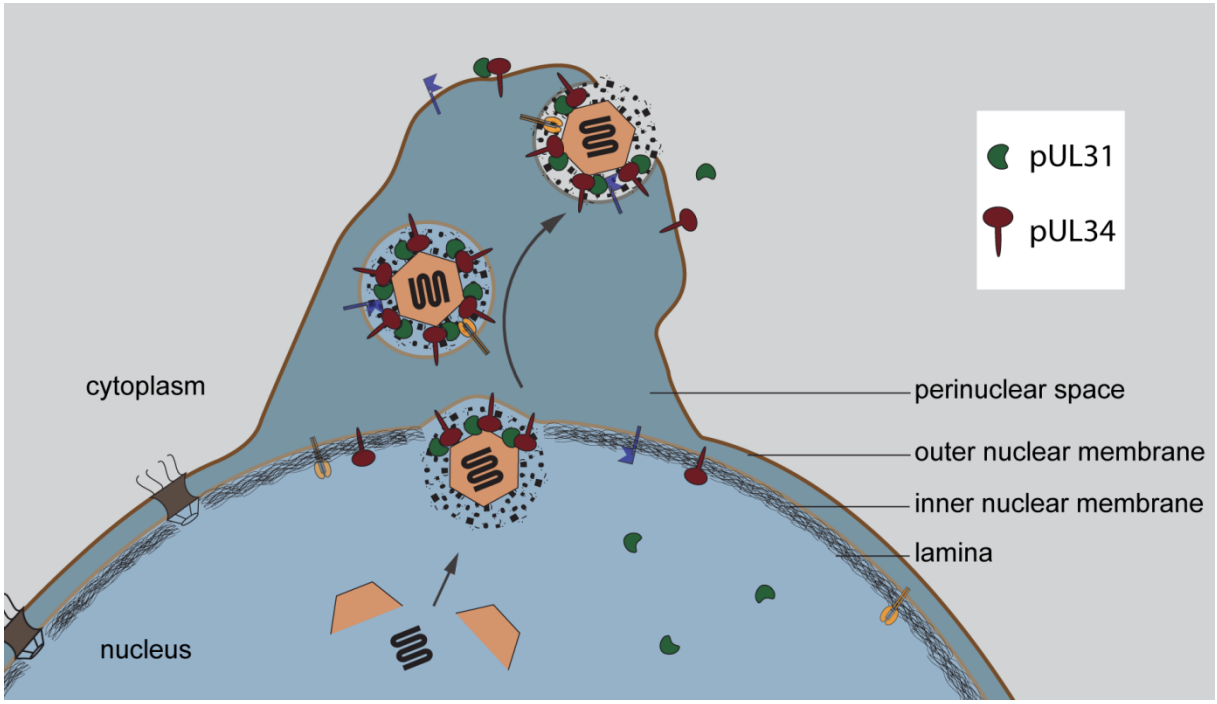

Figure 1.5: Illustration of inner nuclear membrane budding
Assembly of new capids is performed in the nucleoplasm with incorporation of viral DNA. Capsids are recruited and engulfed at the inner nuclear membrane (INM). The main factors for budding of viral capsids are the soluble protein pUL31 (green) and the viral membrane protein pUL34 (red). Complex formation of pUL31 and pUL34 results in constriction of capsids completely sheathed by the INM and scission of the vesicle with subsequent location in the perinuclear space. Enveloped viral particles fuse with the outer nuclear membrane releasing the capsids into the cytoplasm.

1.1.4 GUVs – a versatile tool to study membrane associated processes

Giant unilamellar vesicles provide a powerful, versatile tool for quantitative and qualitative biochemically analysis of membrane related processes. GUVs allow, due to their size, direct observation by light microscopy and enable simple manipulation of physical factors e.g. lipid composition, pH values or temperature. Thus, GUVs provide a tool to study membrane properties in terms of lipid dynamics, membrane budding, fission or fusion as well as lipid domain formation. In addition, GUVs can serve as a model system to test the interplay between proteins and lipids as well as integral membrane or membrane-associated proteins with soluble interactors. Countless cellular processes involve integral membrane proteins. Thus, GUVs can be used to address and understand the interplay of factors or individual functions.

Some integral membrane proteins were successfully integrated in GUVs and demonstrated functionality. These included the sarcoplasmic reticulum Ca2+-ATPase and the H+ pump bacteriorhodopsin (Girard et al., 2004) or voltage-dependent anion channels (VDAC) (Betaneli et al., 2012; Aimon et al., 2011).

GUV generation can be performed in many ways (Walde et al., 2010). The rehydration of dried lipid films provides an easy, although time consuming, way for generation of large quantities of GUVs. Applying an alternating field can assist the underlying natural swelling process (Angelova & Dimitrov, 1986) and is performed between conductive glass electrodes (ITOs) or platinum wires. Many adaptations and variations for the electroformation protocol exist reflecting the individually addressed issues.

1.2 The nucleus and the nuclear envelope

The nuclear envelope is composed of two membranes: the inner nuclear membrane and the outer nuclear membrane continuous with the endoplasmic reticulum. They are part of the most prominent structure of the cell: the cell nucleus, a compartment having a multitude of functions (Dulz & Ellenberg, 2007)**.** The nuclear membranes do not form an impermeable barrier surrounding the chromatin. This membrane structure is interrupted by nuclear pore complexes (NPCs). NPCs are large protein assemblies and are composed of about 30 different proteins termed nucleoporins (Nups) arranged in an eightfold symmetry (Fig. 1.2.1). They are integrated at sites where the inner and outer nuclear membranes fuse. NPCs mediate and regulate the bidirectional transport of factors across the nuclear envelope and are able to perform hundreds of transport events every minute (Gorlich & Mattaj, 1996).

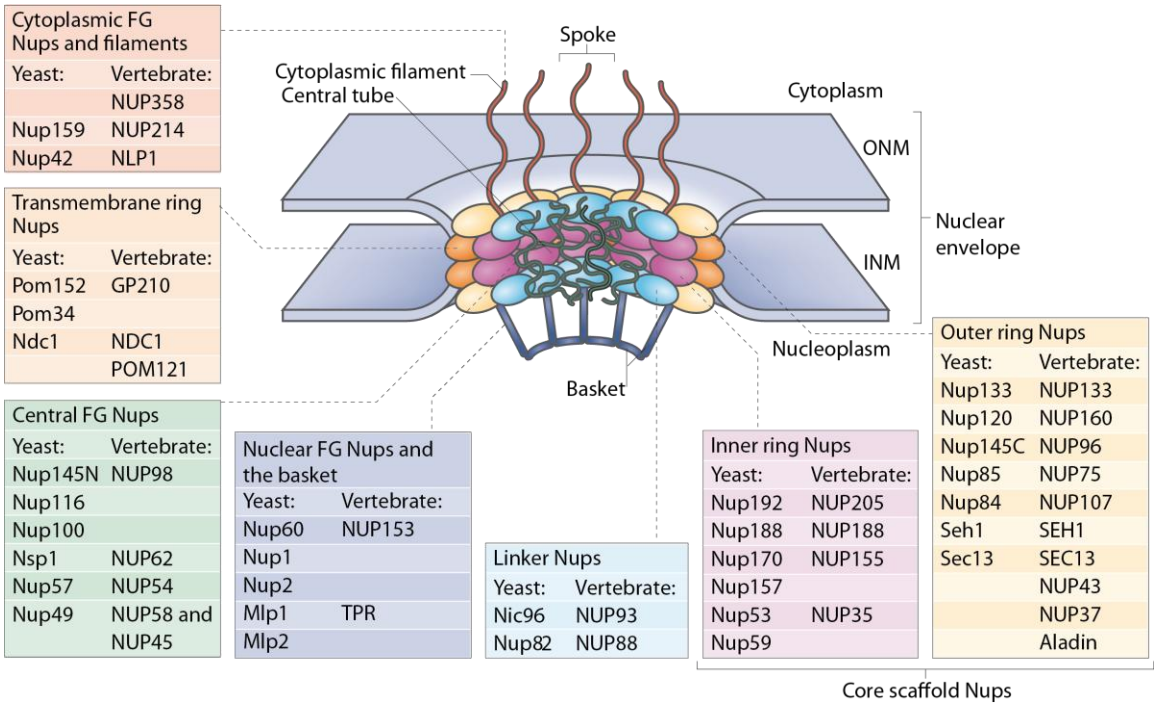

Figure 1.2.1: Nuclear pore complex structure and components
Nuclear pore complexes (NPCs) are comprised nucleoporins (Nups) arranged in an eight fold symmetry surrounding a central channel, connecting the nucleoplasm and cytoplasm. The NPC is anchored to the nuclear envelope by a transmembrane ring structure that connects to the core scaffold and comprises inner ring and outer ring elements. Linker Nups assist in anchoring the FG (phenylalanine-glycine)-repeat-Nups, filling the central tube. Peripheral structures are the cytoplasmic filaments, the nuclear basket with a distal ring. Yeast and vertebrate homologues are shown. Adapted from Strambio-De-Castillia (2010).

1.2.1 NPC assembly at the end of mitosis

In mitosis the nuclear envelope and integrated nuclear pore complexes undergo dramatic morphological changes. NPC reassembly in the reforming nuclear envelope starts by recruitment of the nucleoporin Mel28/ELYS to the decondensing chromatin depending on the AT hook binding motif to AT rich areas on the chromatin, followed by recruitment of the Nup107-160 complex (Franz et al., 2007; Rasala et al., 2008). The GEF RCC1 bound on chromatin generates a spatial ran-GTP gradient around the chromatin, releasing Importin-β bound factors crucial for further NPC assembly (Chen et al., 2007; Hutchins et al., 2004; Li et al., 2004; Walther et al., 2003; Hetzer et al., 2000). Subsequently, membranes are attracted containing the transmembrane nucleoporin Ndc1, interacting with Nup53 and thereby recruiting Nup155 to the assembling NPCs (Franz et al., 2005; Eisenhardt et al., 2014). Additionally, membranes containing the transmembrane nucleoporin Pom121 are recruited to assembly sites, interacting with the Nup107/Nup160 complex. Nup93 is recruited via Nup53 and strengthens the interaction between Nup53 and Nup155 (Sachdev et al., 2011). After Nup93 tethering, Nup188 and Nup205 are recruited. The final steps of nuclear pore assembly are recruitment of the central channel components, forming the FG repeats containing diffusion barrier in the central channel as well as peripheral nucleoporins forming the nucleoplasmic and cytoplasmic extensions.

1.2.2 NPC assembly in interphase

Nuclear pores are also assembled *de novo* in an intact nuclear envelope during interphase. It is generally assumed, that assembly has to start at the intact nuclear envelope and both, inner and outer nuclear membranes have to come in close proximity to assemble a new functional pore spanning the nuclear envelope (D'Angelo et al., 2006). So far, the spatial and temporal requirements for recruiting nuclear pore components to assembly sites as well as the order of assembly during interphase are unknown.

At least one of the three transmembrane nucleoporins, Pom121, although not conserved, is assumed to be important in interphasic pore formation. Pom121 is needed for early Nup107/Nup160 complex recruitment (Doucet et al., 2010; Dultz &

Ellenberg, 2010). Nup133, member of the Nup107/Nup160 complex forms an amphipathic helix and might assist recruitment of the whole complex to the membrane by sensing curvature, known to be required for interphasic NPC assembly (Doucet et al., 2010).

1.2.3 Nup153 is involved in a variety of processes

The 153 kDa nucleoporin Nup153 is a protein located at the nucleoplasmic side of the NPC. Together with TPR, it forms the nuclear basket, a 60–80 nm structure protruding in the nucleoplasm.

Orthologues of Nup153 are found in many organisms but not in yeast, although several nucleoporins share specific functions of Nup153.

The N-terminus of the protein contains the nuclear envelope targeting cassette (NETC), containing apotential amphipathic helix, targeting Nup153 to the inner nuclear membrane.

Furthermore, the N-terminus harbors the nuclear pore associating region (NPAR), sufficient for incorporation in nuclear pore complexes and a RNA binding motif. The central part of Nup153 contains a zinc-finger-region for interaction with DNA. The C-terminus contains FG rich motifs, assumed to be unfolded (Denning 2003) and interacting with transport receptors to facilitate transport of proteins (Kerr & Schirmer, 2011).

The overall domain architecture of Nup153 illustrates a multitude of interactions with factors, therefore involved in many processes (Ball & Ullman, 2005).

To characterize the role Nup153 in NPC assembly two prominent interactions with the small GTPase ran and the Nup107-Nup160-complex (Y-complex) are examined in more detail. Ran plays a major role in the bidirectional transport of cargo through nuclear pore complexes and is implied in liberating building blocks of the nuclear pore in the nucleoplasm from transport receptors (Walther et al., 2003; Hetzer et al., 2000).

The Nup107-Nup160-complex is a major component of the NPC. It forms mainly the cytoplasmic ring, anchoring the cytoplasmic filaments and the nucleoplasmic ring, anchoring the nuclear basket to the nuclear pore complex (Grossman et al., 2012).

1.3 Aims of this study

Herpesviruses are pathogens evolving over 200 million years (McGeoch et al., 1988). They are perfectly adapted to infect a wide range of vertebrates including humans. Several special features in herpesviral replication mediate a fast dissemination. Herpesviral capsids assemble in the nucleus and mature by passing the inner and outer nuclear membrane, termed nuclear egress. The nuclear egress involves the envelopment of new viral capsids at the inner nuclear membrane and the subsequent de-envelopment at the outer nuclear membrane, thus, releasing the capsids in the cytoplasm. Two conserved herpesvirus protein families, pUL31 and pUL34, are essential for the passage through the nuclear envelope and form the nuclear egress complex (NEC). The NEC formation is conserved among all herpesvirus subfamilies and mediates the envelopment of herpesviral capsids at the inner nuclear membrane by a yet unknown mechanism. The aim of this study was the biochemical characterization of pUL31, the interaction with pUL34 and the requirements of the viral capsid envelopment mechanism. Therefore, an artificial minimal giant unilamellar vesicles (GUV) membrane model system was employed and further developed. GUVs are spherical membranes consisting of a single lipid bilayer. By reconstitution of the integral membrane protein pUL34 into GUVs the interaction and vesicle formation after pUL31 recruitment, in the absence of other viral and cellular factors, was studied. Furthermore, artificial tethering of the individual NEC components to GUVs was used to dissect the contribution of pUL31 and pUL34 to vesicle formation in the GUV system. Additionally, single point mutations in a conserved stretch of pUL31 were generated in order to separate the binding ability of pUL31 to pUL34 and the ability to mediate membrane deformation in GUVs. Moreover, results obtained in the GUV system were verified in transfection experiments.

Understanding the key process of primary envelopment at the inner nuclear membrane, and as a consequence preventing herpesviral nuclear egress, can contribute to develope antiherpesviral therapies.

2 Results

2.1 Nuclear Membrane budding is induced by complex formation of two herpes viral proteins

2.1.1 Optimized generation of Giant unilamellar vesicles (GUVs)

Giant unilamellar vesicles (GUVs) provide, due to their low complexity, an optimal test system to investigate protein-protein, protein-lipid, or lipid-lipid interactions. Compared to cellular systems this minimal setup ensures highly reproducible conditions. The size of GUVs of up to 150 µm allows microscopic observations of membrane-bound protein-protein interactions that were addressed in this study. In the following the interaction of the recombinantly expressed viral proteins pUL31 and pUL34 were investigated in detail.

GUVs are commonly generated by rehydration of lipid films, a passive and time-consuming method (Meure et al., 2008). To actively assist and improve the formation of unilamellar vesicles, electroformation of lipid films, where an alternating current field is applied, was developed (Angelova & Dimitrov, 1986).

The electroformation method using ITO - (indium-tin-oxide) - coverslips or platinum wire electrodes in non-conductive buffers is commonly performed. The ITO-coverslip-system produces GUVs in large amounts, but these vesicles stay closely attached to the fragile coverslips not usable for single vesicle analysis.

Electroformation on platinum wire electrodes results in high yields of detached vesicles. The surface area where lipid films can be applied is very limited (~8 mm² per electrode) and therefore not suited to dry greater amounts of aqueous proteo-liposomes being the starting point to generate GUVs. Within this study the problem was overcome by increasing the surface area of the platinum wire electrodes by using platinum gauze electrodes (BASinc.) combined with a disposable cuvette system (Fig. 2.1). Thereby, the area to apply lipid films was increased to ~ 35 mm² per electrode.

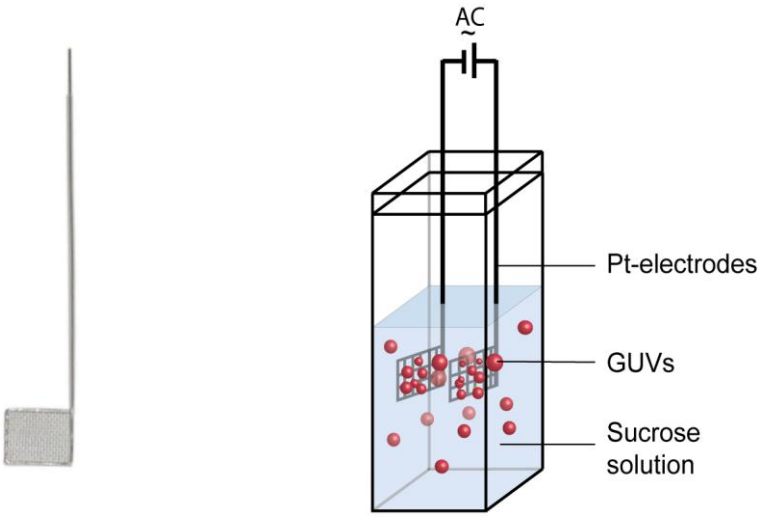

Figure 2.1: Electroformation on platinum gauze electrodes
Electroformation of lipid films was performed on platinum gauze electrodes (left).
Applying an alternating current to platinum electrodes with applied lipid film in a non-conductive sucrose solution results in GUV formation and subsequent vesicle detachment (right).

2.1.2 pUL34 can be reconstituted in GUVs

The viral proteins pUL31 and pUL34 (as well as homologous proteins) are the main factors necessary for nuclear egress of herpes virus capsids from the nucleus (Reynolds et al., 2001). The integral type-II transmembrane protein pUL34 resides in the nuclear envelope, presumably the inner nuclear membrane where it can interact with the nucleoplasmic and actively imported protein pUL31. To investigate and understand their function in more detail, pseudorabies virus (PRV, suHV-1) homologues of both proteins were expressed as full-length proteins in *E. coli* including the C-terminal transmembrane region of UL34. To assist overexpression of this membrane protein, a MISTIC (membrane-integrating sequence for translation of integral membrane protein constructs) protein tag was fused to the N-terminus of pUL34. MISTIC is a membrane protein derived from *Bacillus subtilis* and was found to efficiently increase expression of integral membrane proteins (Deniaud et al., 2011; Roosild et al., 2005; Petrovskaya et al., 2010) by integrating them into the inner membrane of *E. coli,* presumably bypassing the translocon complex (Dvir et al., 2009).

pUL34 was efficiently purified from *E. coli* membranes by detergent mediated solubilisation and subsequent nickel-affinity purification followed by labelling with the

fluorescent dye Alexa-Fluor-546 (see methods, (4.2.18)). The viral protein was efficiently reconstituted into liposomes (proteo-liposomes) with a lipid composition mimicking the nuclear envelope composition (Vollmer et al., 2012; see methods, (4.2.24.1). GUVs were generated by electroformation of dried proteo-liposome layers employing the previously described GUV preparation method. pUL34 was successfully integrated in GUVs and could be visualized by detection of the fluorescent Alexa-Fluor-546 label (Fig. 2.2).

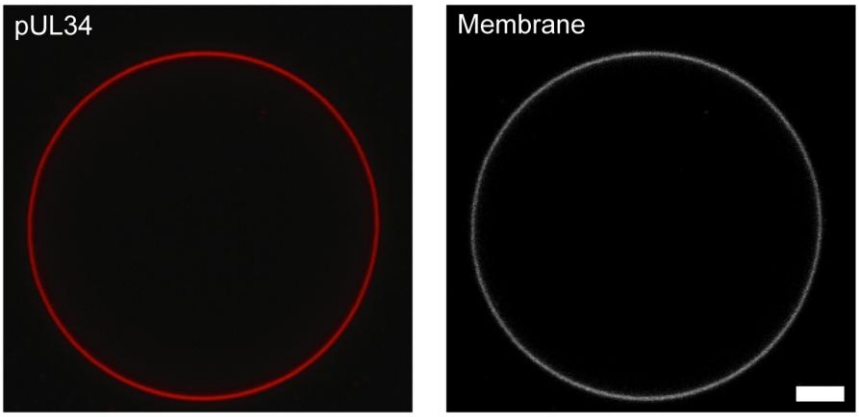

Figure 2.2: Fluorescently labelled pUL34 can be efficiently reconstituted in GUVs
pUL34 was labelled with Alexa-Fluor-546 and reconstituted by gelfiltration in proteo-liposomes. Dried proteo-liposome layers were electroformed and resulting GUVs were imaged by confocal microscopy. Vesicle membrane was visualized using DiD-C_{18}. bar: 10µm

2.1.3 pUL31 and pUL34 are sufficient for membrane budding and scission in giant unilamellar vesicles

pUL31, the interactor of pUL34, was also recombinantly expressed and purified by affinity purification from *E.coli* lysates. The protein was expressed with an N-terminally fused EGFP tag which proved to enhance its solubility. Because of stability issues pUL31 was always purified directly before use.

Employing the GUV system, not only the binding properties of pUL31 to pUL34, but also the functionality of both proteins could be verified.

Therefore, pUL34 GUVs were incubated with a final concentration of 500 nM of EGFP-pUL31 (Fig. 2.3A). This concentration was previously determined by evaluating different concentrations of pUL31 and found to be optimal for fluorescent imaging of GUVs. Thereby 500 nM of pUL31 was used in all experiments unless

differently noted. In this experimental setup pUL31 was recruited to the rim of giant vesicles containing pUL34 within the first five minutes after addition. Most importantly, after recruitment of pUL31 to the GUV membrane, small vesicles started to pinch of from the membrane into the lumen of the vesicles, containing pUL31 and pUL34 . To verify the specific interaction of pUL31 and pUL34 another integral inner nuclear membrane protein, SCL1, used as a control and sharing the same topology as UL34 with a C-terminal transmembrane domain, was reconstituted into GUVs. No recruitment and no invaginations formed in GUV membranes when pUL31 was added to SCL1-GUVs (Fig. 2.3C). Vice versa, also no interaction was observed in pUL34- or SCL1-GUV when EGFP alone was added (Fig. 2.3B). Quantification of three independent experiments under three individual conditions was performed (Fig. 2.4) showing a nearly constant background of GUVs with invaginations of about 20 % (Fig. 2.4A). Only addition of pUL31 to pUL34 GUVs resulted in an increase of intra lumenal vesicles (ILVs) while all other conditions tested resulted in background levels of ILVs (Fig. 2.4B). To verify the size of the UL31/34 induced vesicles, stack images of at least 20 different GUVs containing ILVs were taken in three independent experiments and sizes of individual ILVs were measured (Fig. 2.4C). Data analysis revealed that the majority of the ILVs had a diameter of 1-1.5 µm (39 %) followed by vesicles with greater diameter (23 % Ø 1.5-2 µm) and vesicles with smaller diameter (18 % Ø 0.5-1 µm). Similar amounts were found for vesicles ranging from 1.5-2 µm. Taking this together this demonstrates that both recombinant expressed viral proteins are functional and form a functional complex resulting in vesicle constrictions from GUV membranes into the lumen of the vesicles.

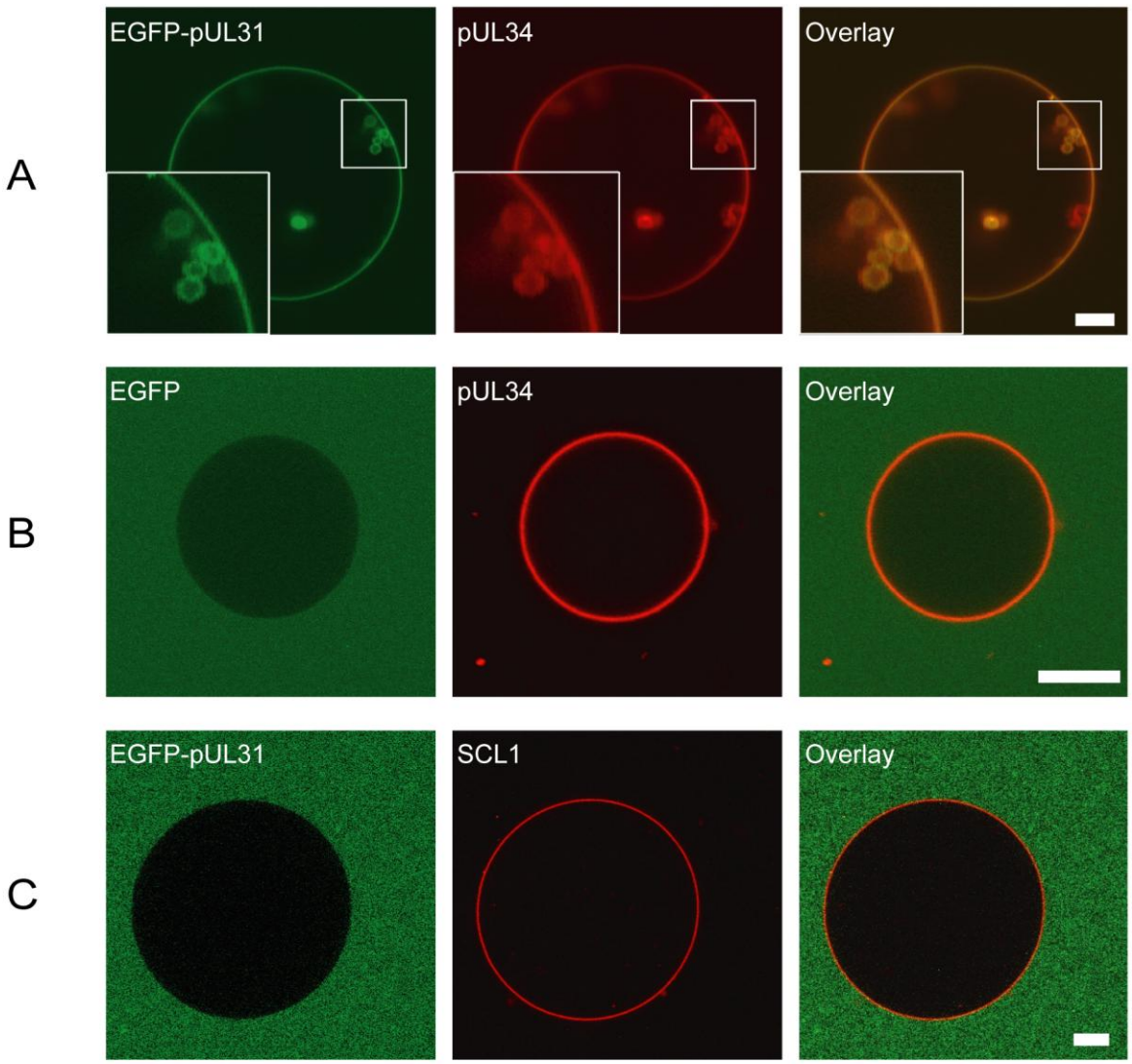

Figure 2.3: pUL34 and pUL31 interact and complex formation is sufficient to induce vesicle formation.
pUL34 or SCL1 was labeled with Alexa-Fluor-546 and reconstituted in proteo-liposomes. Dried proteo-liposome layers were electroformed. Resulting GUVs were imaged using confocal microscopy. Upon addition of EGFP tagged pUL31, pUL31 was efficiently recruited to the GUV membrane and induced vesicle formation into the lumen (A). When EGFP was added no recruitment and vesicle formation was observed (B) or when pUL34 was replaced by another inner nuclear membrane protein SCL1 (C), indicating that the interaction and induction of lumenal vesicles was specific to pUL34/pUL31 complex formation. bars: 5µm

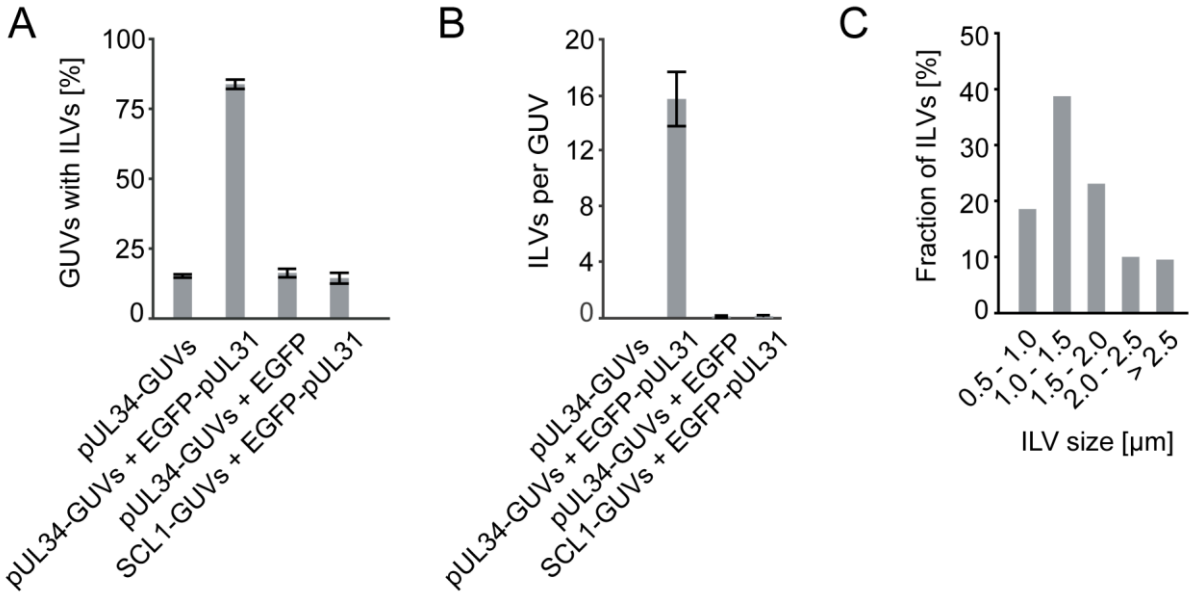

Figure 2.4: Quantification of intralumenal vesicles in pUL34 GUVs
The number of GUVs with intralumenal vesicles (ILVs) was quantified (A). For each condition and experiment at least 70 GUVs were analyzed in three independent experiments. The number of GUVs with detectable ILVs was counted before and after the addition of EGFP-pUL31 to pUL34- or SCL1-GUVs. For each condition and experiment stack images of at least 20 GUVs with detectable ILVs were recorded and the amount (B) as well as the approximately size (C) of the ILVs was measured. As shown in (A) and (B) a significant increase of ILVs could be detected only when EGFP-pUL31 was added to pUL34 GUVs but not when added to SCL1-GUVs. Also no increase was observed when EGFP as control protein was added to pUL34- or SCL1-GUVs. The size distribution of ILVs (C) shows that the most of the ILVs (~ 39 %) was about 1 – 1.5 µm in diameter. Also smaller vesicles < 1 µm (~18 %) and vesicles up to 2 µm (~ 23 %) as well as vesicles larger than 2 µm (~20 %) were detected. Error bars represents the mean (-/+ SEM) of three independent experiments.

2.1.4 pUL31 induces membrane invaginations in pUL34 GUVs

To show that ILVs in GUVs are formed because of membrane constrictions after addition of pUL31 to pUL34 containing GUVs a fluorescent fluid phase marker (Cascade Blue NeutrAvidin, life technologies) was added and should be included as new vesicles invaginate towards the lumen of the GUVs. This uptake is supposed to be visualized by detection of the fluorescence signal in ILVs. Upon adding pUL31 to GUVs ILV formation was induced and the added fluid phase marker was incorporated (Fig. 2.5A). No incorporation was observed when pUL31 was added to SCL1-GUVs (Fig. 2.5B). Also no uptake was visible when the fluid phase marker was added 15 minutes after addition of pUL31 to pUL34 GUVs (Fig. 2.5C) indicating that the vesicles pinched of from the limiting GUV membrane. No effect was observed when

the fluid phase marker was added to GUVs in the absence of additional proteins (Fig 2.6).

This indicates that ILV formation after pUL31 addition to pUL34 GUVs is only induced by complex formation of both proteins. Additionally, vesicles pinched of from the GUV membrane and the bulk formation of ILVs in GUVs is completed within 15 minutes after applying the protein.

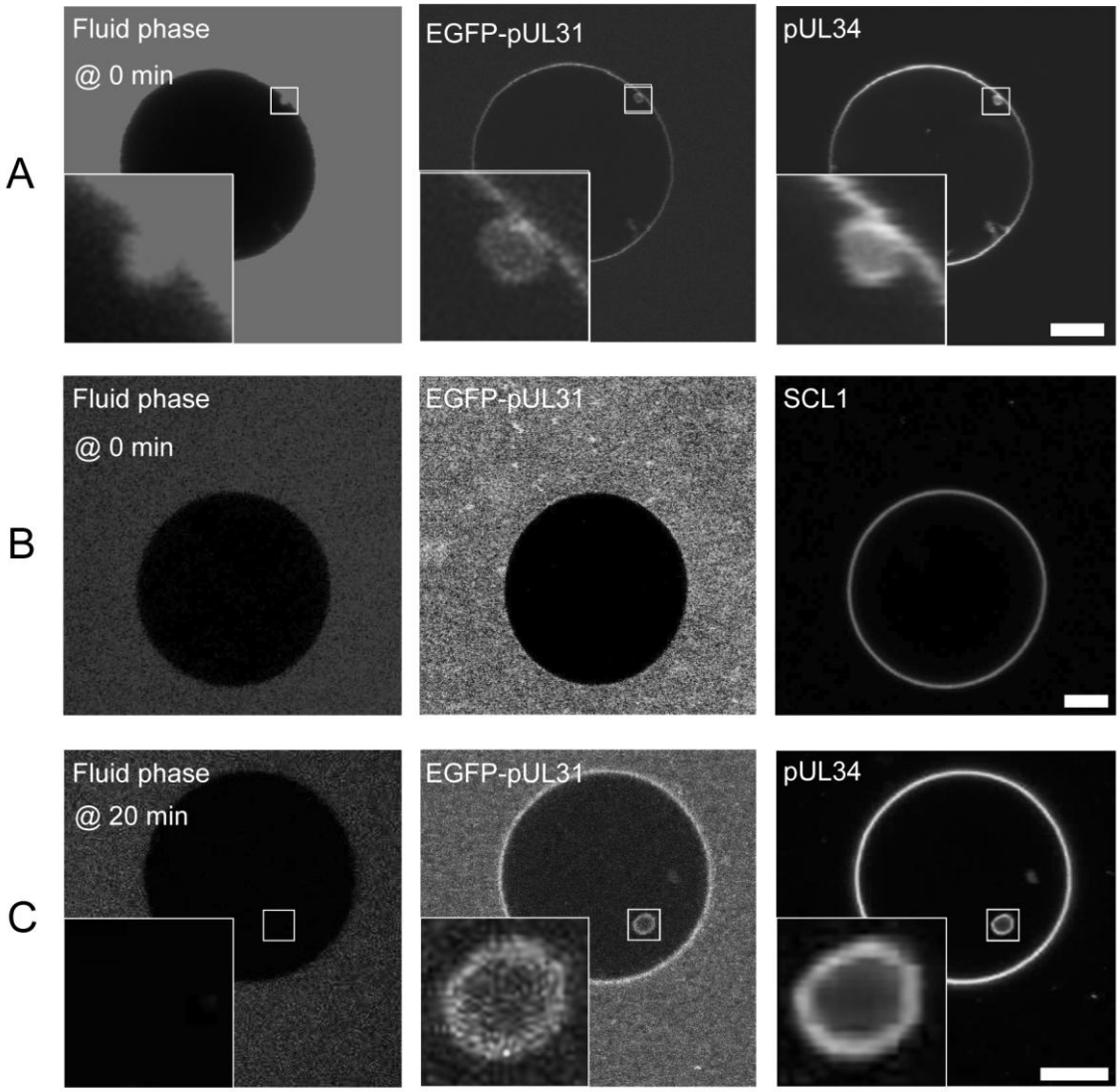

Figure 2.5: Addition of EGFP-pUL31 to pUL34-GUVs initiates vesicle budding
Intralumenal vesicles observed in GUVs are newly formed as a result of the addition of EGFP-pUL31 to pUL34-GUVs and were not present before in the GUVs, as a fluorescently labeled fluid phase marker (Cascade Blue® NeutrAvidin®, life technologies) was added together with EGFP-pUL31. Vesicles budding at the GUV membrane will incorporate detectable amounts of the fluid phase marker (A) but not when added 15 min after EGFP-pUL31 addition to GUVs with reconstituted Alexa-Fluor-546 labeled pUL34 (C) or SCL1 (B).

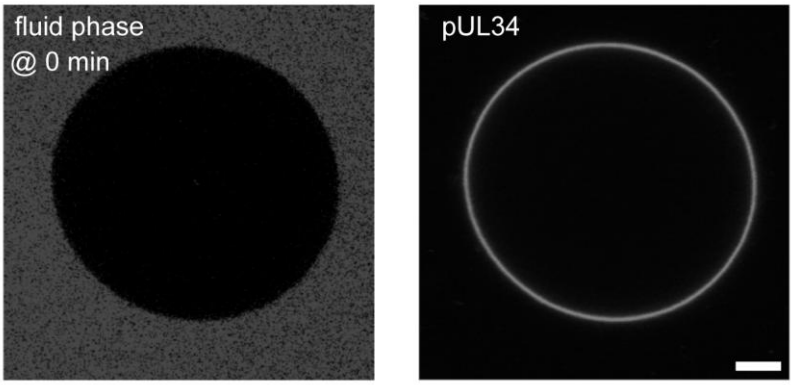

Figure 2.6: Addition of the fluid phase marker to pUL34-GUVs has no effect
To show that the addition of the fluorescently labeled fluid phase marker (Cascade Blue® NeutrAvidin®, life technologies) has no effect, it was added to Alexa-Fluor-546 labeled pUL34 GUVs, indicating that the fluid phase marker has no additional effect on GUVs. bar: 5 µm

2.1.5 pUL31 and pUL34 accumulate in forming buds

Interestingly, when pUL31 is added to pUL34, overlapping fluorescent signals of both proteins appear. The distinct enrichment of both proteins in local spots could represent an early step in vesicle formation. An example of an emerging bud is analyzed (Fig. 2.7A). Fluorescence signals of EGFP-pUL31 and Alexa-Fluor-546 labeled pUL34 were detected by confocal microscopy and analyzed using the straighten function of the image software Fiji. The normalized fluorescence intensity was plotted revealing an increase of pUL31 by 2.5-fold and for pUL34 by 2-fold compared to the basal fluorescence of both proteins in the GUV membranes.
Sequential budding events in GUV membranes were imaged (Fig. 2.8) where local enrichment of pUL31 and pUL34 was be observed, subsequently followed by detachment of small vesicles into the lumen of the giant vesicles containing both proteins. A three dimensional reconstitution of a section of a pUL31 treated pUL34 GUV was generated with IMARIS (v7.7.1) (Fig. 2.7B) showing numerous vesicles detached and mobile in the lumen of the GUV with both proteins present.

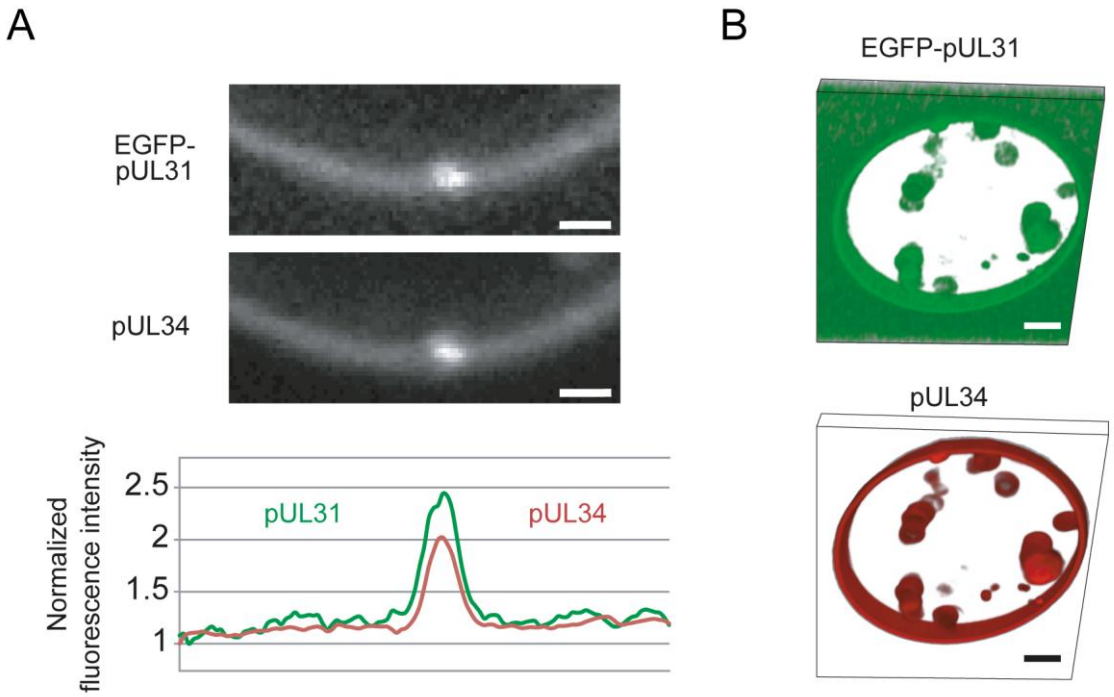

Figure 2.7: pUL31 and pUL34 accumulate in nascent buds and formed vesicles are disconnected from the GUV membrane

pUL31 and pUL34 accumulate at sites were nascent buds in the GUV membrane arise (A). Fluorescent signals of EGFP-pUL31 and pUL34 Alexa-Fluor-546 from a GUV membrane were quantified using the straighten function of Fiji (ImageJ) and the normalized fluorescent intensity for both signal were plotted, indicating an increase of pUL34 in the emerging buds of two-fold and nearly 2.5- fold for pUL31. bars: 1 µm

Three dimensional reconstitution of a pUL34-GUV incubated with pUL31, which shows highly mobile vesicles distant and apparently detached from the limiting GUV membrane (B).

bars: 5 µm

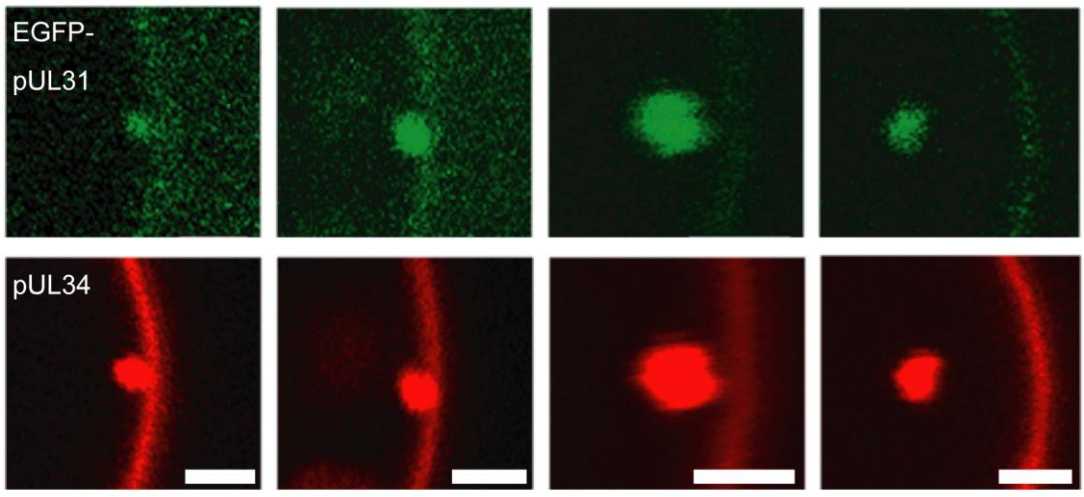

Figure 2.8: pUL31 addition to pUL34-GUVs induces vesicles budding and detachment from the GUV membrane
pUL34-GUVs were incubated with EGFP-pUL31. Confocal pictures were taken from different representative GUVs showing different time points in budding and detaching of an ILV from the GUV membrane. bars: 2 µm

To further characterize the vesicle budding induced by pUL31/pUL34 the influence of the used lipid composition was investigated. The lipid composition (referred to as complete lipid mix) mimics the nuclear envelope ((Vollmer et al., 2012; see methods, (4.2.24.1)) with phosphatidylcholine (PC; 60 mol %) and phosphatidylethanolamine (PE; 20 mol %) as major components. The negatively charged lipids phosphatidylinositol (PI; 10 mol %) and phosphatidylserine (PS; 2.5 mol %) and as well as sphingomyelin (SM; 2.5 mol %) and cholesterol (chol; 5 mol %) were present. Individual lipid types except the main components (PC, PE) were removed from the mixture (marked by Δ) while therefore the amount of PC was increased (Fig. 2.9)

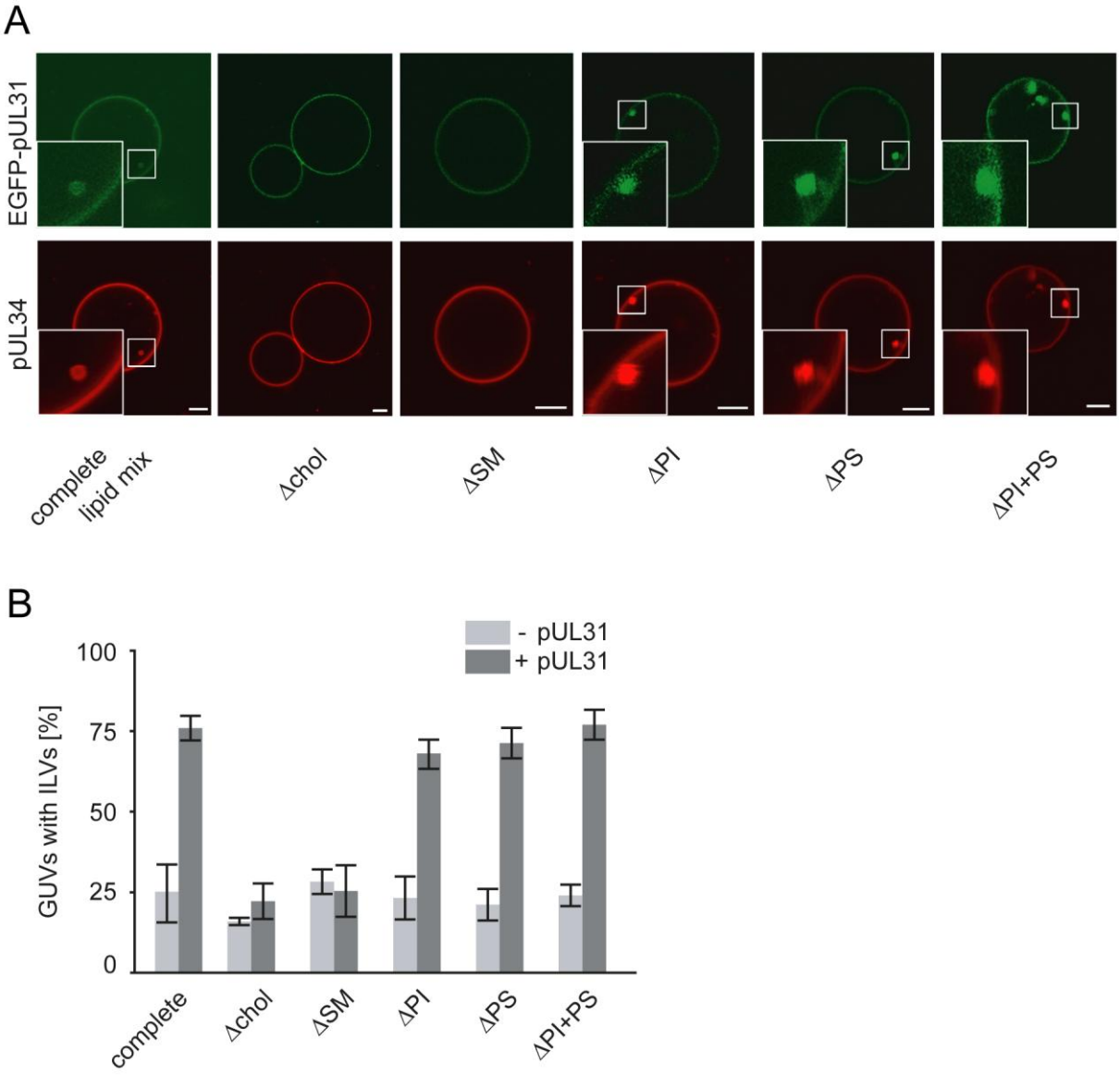

Figure 2.9: Cholesterol and sphingomyelin are required for ILV budding in pUL34-GUVs

pUL34 was labeled with Alexa-Fluor-546 and reconstituted in proteo-liposomes utilizing a lipid mixture mimicking the nuclear envelope composition (complete lipid mixture) or lacking individual lipids (indicated by Δ). Dried proteo-liposome layers were electroformed and GUVs were incubated with EGFP-pUL31 inducing vesicle formation. Recruitment of EGFP-pUL31 was independent of the lipid composition. ILVs were efficiently formed except when GUVs were lacking either cholesterol (chol) or sphingomyelin (SM) indicating that both lipids are needed (A). Quantification of at least 50 GUVs per experiment and condition. Error bars represent mean of three independent experiments (+/- SEM) (B). GUVs were imaged by confocal microscopy. bars: 10 µm, PI - Phosphatidylcholine, PS - Phosphatidylserine

pUL34 was reconstituted into GUVs using these different lipid compositions. In all conditions the recruitment of pUL31 was independent of the used lipid compositions (Fig. 2.9). The complete lipid mix was sufficient to promote vesicle budding from GUV

membranes (Fig. 2.2, 2.5, 2.7, 2.8). Additionally, individual removal of the charged lipids PI and PS or combined removal resulted in no decrease or block in vesicle induction upon pUL31 addition. Interestingly, no invaginations above background levels were observed when the lipid mixture was lacking either cholesterol or sphingomyelin (Fig. 2.9B) indicating that cholesterol and sphingomyelin are required for membrane invagination and scission.
Both lipids are known to modulate membrane fluidity. As cholesterol and sphingomyelin also partition in the liquid ordered phase and are assumed to form lipid rafts in membranes the ability to induce phase separation in giant vesicles upon binding of pUL31 to pUL34 GUVs was investigated.

2.1.6 Phase separation of lipids in GUV membranes.

Biological membranes are composed of a heterogeneous mix of phospholipids and proteins. Some lipids organize themselves because of their physical properties in particular regions of the membrane termed phases. One can define two different fluid phases: the liquid disordered (L_d, also called L_α) and liquid ordered (L_o). Membranes containing high amounts of cholesterol or other sterols are able to form visible L_o domains in membranes (Klymchenko & Kreder, 2014; Baumgart et al., 2007). By using a mixture composed of equimolar amounts of DOPC: cholesterol:sphingomyelin GUVs can be generated having co-existing L_o and L_d domains, which are visible by light microscopy. Therefore fluorescent dyes were employed partitioning into the corresponding domain. Naphthopyrene was used as marker for the liquid ordered domain (L_O) and DiD-C_{18} as marker for the liquid disordered (L_D) domain. Both dyes showed correct phase behavior (Fig. 2.10B). Following the addition of pUL31 ILVs were induced. Visualizing fluorescence signals of naphthopyrene and DiD-C_{18} incorporated in GUV membranes showed no formation of a specific dye enriched phases neither in the giant vesicle membrane nor in the intra luminal vesicles formed employing the nuclear envelope mimicking composition (Fig. 2.10A). This indicates that pUL31/pUL34 interaction does not induce phase separation although it cannot be excluded that sub-resolution domains are formed which promote vesicle budding or ILV are enriched in specific lipids allowing membrane restructuring to vesicles.

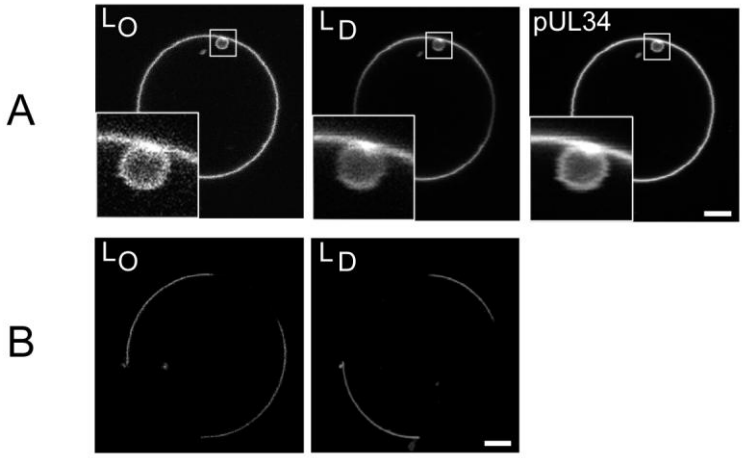

Figure 2.10: pUL31 and pUL34 induce no visible phase separation in GUVs
Alexa-Fluor-546 labeled pUL34 was reconstituted in GUVs and pUL31 was added to induce ILV formation. The used NE lipid mix was supplemented with naphthopyrene as marker for the cholesterol-and sphingomyelin-rich liquid ordered phase (L_O) and the lipophilic dye DiI-C_{18} as marker for the liquid disordered phase (L_D). pUL34 was equally distributed and no phase separation was visible before or after the addition of pUL31 (A). To ensure functionality of the individual phase markers, GUVs comprising of a lipid mixture of DOPC:cholesterol:sphingomyelin (1:1:1), were generated with addition of naphthopyrene and DiI-C_{18} showing functional phase separation and localization of the fluorescent dyes (B). bars: 5 µm

2.1.7 pUL31 is also recruited to the liquid ordered phase in ternary GUV system

The ternary system of DOPC:cholesterol:sphingomyelin was used to assess the phase behavior of pUL31 when added to pUL34 GUVs. pUL34 was partitioning in the liquid disordered phase. Weak signals of pUL34 fluorescence were obtained in the liquid ordered phase and naphthopyrene signal were recorded in the liquid disordered phase resulting from incomplete phase separation (Fig. 2.11). Interestingly, an increased signal in the L_o phase of pUL31 could not be attributed to a binding affinity of pUL31 to either cholesterol or sphingomyelin as no binding was observed to either L_o or L_d phase in the absence of pUL34 (Fig. 2.12).
Additionally, no invaginations could be observed when the ternary lipid composition was used. As high amounts of cholesterol increase the rigidity of the membrane (Rossman et al., 2010; Song & Waugh, 1993) the membrane bending ability of the pUL31/pUL34 complex is probably not high enough to overcome the membrane tension.

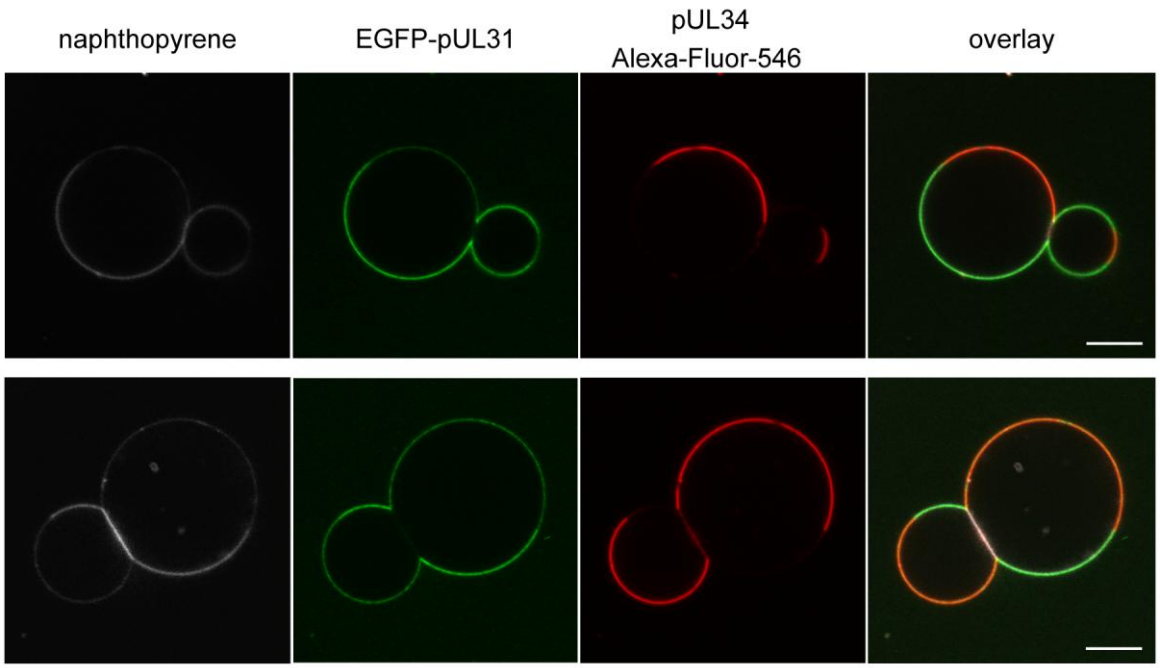

Figure 2.11: pUL31 is also recruited to the liquid ordered phase upon binding to pUL34
GUVs were generated with reconstituted and Alexa-Fluor-546 labeled pUL34 from a lipid mixture of DOPC:cholesterol:sphingomyelin (1:1:1) supplemented with the liquid-ordered-partitioning dye naphthopyrene (gray). EGFP-pUL31 was added to the GUVs leading to recruitment to the vesicle membrane containing pUL34, present in the liquid-disordered phase of the GUV. pUL31 was also strongly recruited to the liquid-ordered phase, almost lacking pUL34 indicating a presumable self-recruiting step. bars: 10 µm

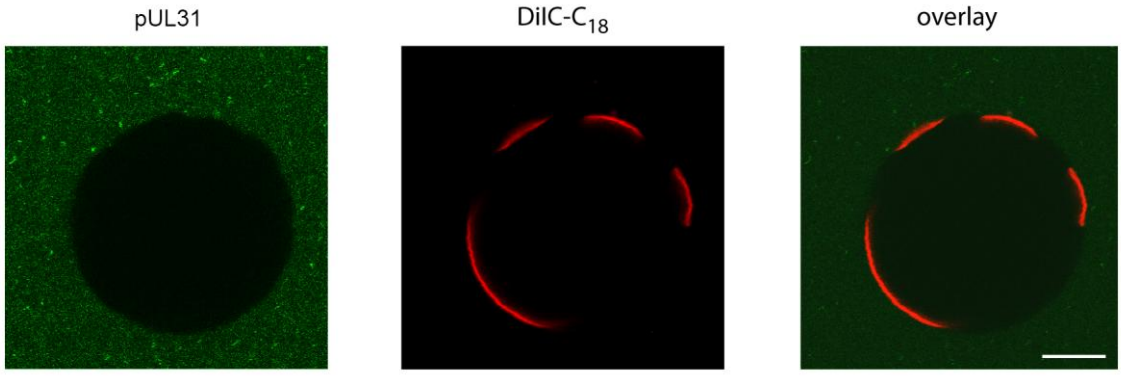

Figure 2.12: pUL31 does not bind ternary GUVs in the absence of pUL34
GUVs were generated from a lipid mixture of DOPC:cholesterol:sphingomyelin (1:1:1) supplemented with the liquid-disordered-partitioning dye with DiI-C_{18} (red). EGFP-pUL31 was added to the GUVs leading to no recruitment to the liquid-disordered or liquid-ordered phase. bar: 10 µm

2.1.8 No energy depending step is involved in vesicle budding

To verify that vesicle budding in GUV membranes involves an energy dependent step pUL34 giant vesicles were generated in a 130 mM glucose / 130 mM sucrose solution. A Hexokinase-glucose-system is commonly used to deplete energy (Magalska et al., 2014; Purich & Allison, 2000; Newmeyer et al., 1986). Prior to the addition of pUL31, both GUVs and pUL31 were incubated with either 10 mM ATP, 10 mM GTP or 10 U / ml Hexokinase for at least 15 minutes. Vesicle formation was induced by adding pUL31 to the GUVs. Vesicle formation was quantified and no difference in efficiency could be observed in either supplying additional energy or depletion of energy (Fig. 2.13).

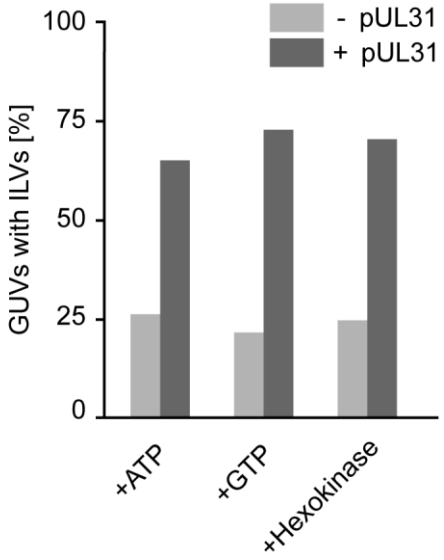

Figure 2.13: Vesicle budding is not depending on provided energy
GUVs were generated with Alexa-Fluor-546 labeled pUL34 in 130 mM glucose / 130 mM sucrose. EGFP-pUL31 was added to induce vesicle formation in presence of 10 mM ATP, 10 mM GTP or an energy depletion system containing 10 U / ml Hexokinase. GUVs with ILVs were counted before and after the addition of EGFP-pUL31. No significant difference was observed in the three different conditions.

Taken together, this data demonstrates that the two viral proteins pUL31 and pUL34 are sufficient to induce membrane perturbations in the minimal GUV system resulting in generating intra-GUV vesicles. The forming buds were enriched in pUL31 and pUL34. Both proteins are therefore also sufficient for scission of budding vesicles. In addition binding, budding and scission do not require additional factors or provided

energy. Moreover, the GUV system is a valuable tool to investigate different aspects of the pUL31-pUL34 interaction mediating vesicle budding and scission.

2.1.9 Determining the importance of the pUL34 transmembrane region

The role of the transmembrane region in vesicle budding was analysed. For this a soluble pUL34 construct was generated lacking the C-terminally predicted transmembrane region. This pUL34 fragment referred to as pUL34ΔTMR consisted of the N-terminal aa 1-240. The fragment was purified in sufficient amounts from *E. coli* lysate by nickel affinity purification and labeled with the Alexa-Fluor-546 fluorescent dye. Soluble proteins are not only recruited to membranes by protein-integral membrane-protein-interactions but also by direct lipid binding. Direct membrane binding is mediated by specific protein domains like e.g. formation of a membrane inserting amphipathic helices, BAR domains or FYVE zinc finger domains. These interactions are mediated by high initial curvature or by electrostatic interactions with special lipid types including phosphoinositide (PIPs), phosphatidic acid (PA), diacyl-glycerol (DAG), Ceramide (van Meer et al., 2008). As no structural predictions indicate for lipid binding domain formation in pUL34 or pUL31 as well as no special lipids are present in the lipid mixture, a head group functionalized lipid was employed. Phosphatidylcholine modified with a chelating Ni-NTA group is capable of efficiently binding His_6-tagged proteins and was added to 1 mol % to the complete lipid mixture and is referred as Ni-DGS. Giant unilamellar vesicles obtained by electroformation of dried chloroform solved lipid films usually result in high yields achieved in less time. Unfortunately due to the use of chloroform no membrane proteins can be reconstituted thereby preventing the use of this technique in the previous assays (see methods, (4.2.27)). When the soluble His_6-tagged fragment of pUL34ΔTMR was added to nickel lipid functionalized GUVs, it was efficiently recruited to the vesicle membrane (Fig. 2.14).

The recruitment was not sufficient to induce ILV formation into GUVs consistent with the observation that full length pUL34 is not sufficient to induce vesicle budding (Fig. 2.2). Verifying if pUL31 can still interact with the soluble pUL34 fragment, pUL31 was added to GUVs previously incubated with pUL34ΔTMR. Additionally, it was verified, if in case of binding, the proteins are still functional to remodel GUV membranes to vesicles. To avoid a direct interaction with the functionalized GUV membranes the

pUL31 added was lacking a His_6-tag. Indeed, pUL31 still bound to the GUV-bound pUL34 fragment and pUL31 recruitment was also sufficient to induce vesicle formation. The vesicle formation was induced independent if pUL31 bound the N-terminally (Fig. 2.14A) or C-terminally (Fig. 2.14B) His_6-tagged pUL34ΔTMR fragment recruited. This gave rise to address the contribution of pUL34 to membrane deformation and vesicle budding in more detail.

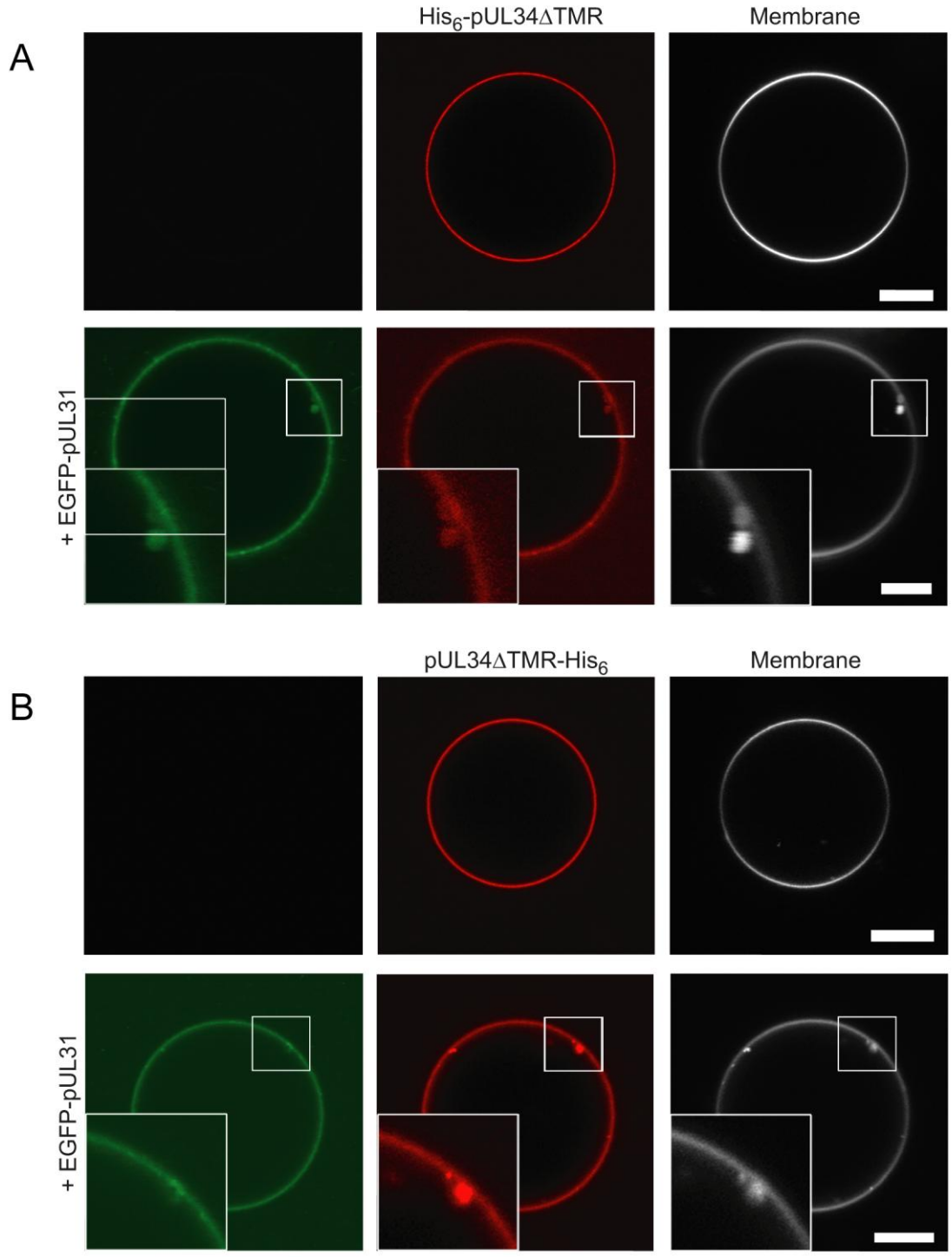

Figure 2.14: The transmembrane region of pUL34 is not important for vesicles budding
Chloroform dissolved lipids (NE-mix) supplemented with 1 mol % Ni-DGS were dried and electroformed. GUVs were incubated with a Alexa-Fluor-546 labelled pUL34 fragment (aa 1-240) lacking the C-terminal transmembrane domain. The either (A) N- or C-terminally (B) His_6-tagged fragment was efficiently recruited to the GUV membrane but was not sufficient to induce vesicle formation. Upon addition of EGFP-pUL31 lacking a His_6-tag was recruited to the limiting membrane indicating that pUL31 was recruited via interaction with pUL34 to the vesicles. Most importantly the pUL31-pUL34 (aa 1-240) interaction was also sufficient to induce vesicle formation suggesting that the transmembrane region is not essential to drive vesicle budding. bars: 5 µm

2.1.10 pUL34 is dispensable and pUL31 is sufficient for vesicle budding

As previously demonstrated, pUL34 alone is not sufficient to induce vesicle budding. Only addition of pUL31 to pUL34 GUVs either harbouring an authentic transmembrane domain (Fig. 2.2) or artificially recruited to membranes (Fig. 2.14) is sufficient for budding and scission of ILVs. Therefore the contribution of pUL31 was determined.

Hence, His_6-EGFP-pUL31 was artificially recruited to Ni-DGS-GUV membranes. Interestingly, the recruitment of pUL31 to the vesicle membranes was already sufficient to induce budding and scission of vesicles from the GUV membranes (Fig. 2.15A). In contrast, no invaginations were observed when His_6-tagged EGFP was recruited to Ni-DGS-GUVs (Fig. 2.15B).

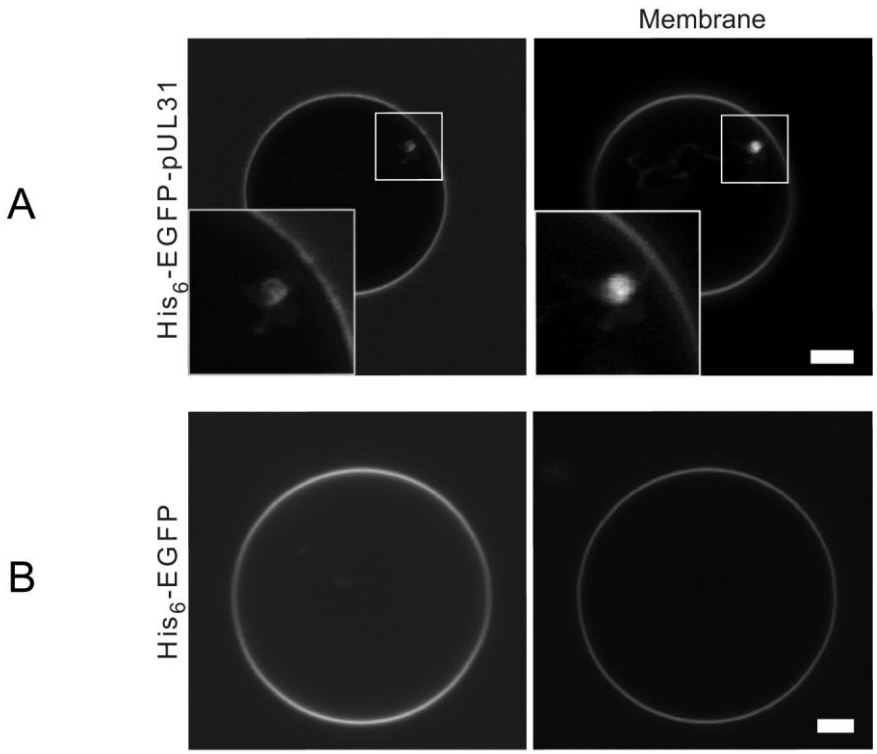

Figure 2.15: Artificial recruitment of pUL31 is sufficient to induce vesicle budding
GUVs from chloroform dissolved lipids (NE-mix) containing 1 mol % Ni-DGS were generated by electroformation. His_6-tagged pUL31 was efficiently recruited to the GUV membrane (A). The recruitment induced vesicle formation and detachment from the GUV membrane visualized by EGFP fluorescence in forming ILVs while recruitment of His_6-tagged EGFP only led to no vesicle formation (B). The GUV membrane was visualized by addition of the lipophilic dye DiD-C_{18}. bars: 5 µm

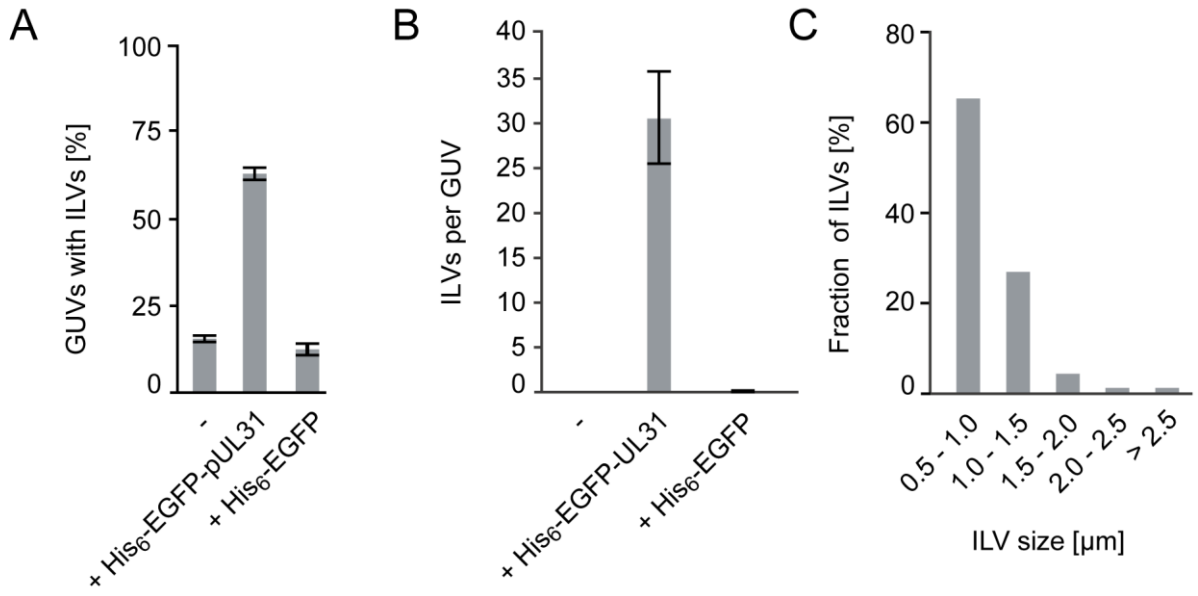

Figure 2.16: The number of GUVs with intralumenal vesicles (ILVs) was quantified.
For each condition and experiment at least 80 GUVs were analysed in three independent experiments. The number of GUVs with detectable ILVs was counted before and after the addition of His_6-EGFP-pUL31 to GUVs originated from chloroform dissolved lipids + 1 mol % Ni-DGS. For each condition and experiment stack images of at least 20 GUVs with detectable ILVs were recorded and the amount (B) as well as the approximately size (C) of the ILVs was measured. A significant increase of ILVs could be detected only when His_6-EGFP-pUL31 was added to the GUVs but not when His_6-EGFP was added (A-B). The size distribution of ILVs (C) shows that the most of the ILVs (~ 67 %) was about 0.5 - 1 µm in diameter. Also vesicles of 1 – 1.5 µm (~25 %) and vesicles larger than 1.5 µm (~8 %) were detected. Error bars represents the mean (-/+ SEM) of three independent experiments.

Quantification of three independent experiments in three different conditions was performed (Fig. 2.16) showing a constant background of GUVs with invaginations of about 15 - 20 % (Fig. 2.16A) as observed previously (Fig. 2.4A, Fig. 2.9B). Only addition of pUL31 to Ni-DGS-GUVs increased ILV levels while recruitment of EGFP did not raise levels above background (Fig. 2.16B). To determine the size of the observed ILVs found in pUL31 treated GUVs stack images of at least 20 different GUVs containing ILVs were taken in three independent experiments. Data analysis, by counting and measuring ILV in each recorded stack, showed that the majority of the ILVs had a diameter of 0.5 - 1.0 µm (65 %) followed by vesicles with a greater diameter (25 % Ø 1.0-1.5 µm). Vesicles with diameter greater than 1.5 µm represented only 10 % (Fig. 2.16C)

2.1.11 pUL31 concentrates in emerging buds formed in GUV membranes

Artificial recruitment of pUL31 resulted in enrichment of the protein in GUV membranes. Upon recruitment vesicle buds were formed and pinched of from the limiting membrane (Fig. 2.15). As pUL31 and pUL34 enrich upon addition of pUL31 in pUL34 GUVs, also pUL31 recruitment to Ni-DGS-GUVs resulted in local enrichments in formed buds (Fig. 2.17A, upper panel). By using the straighten line tool of the image analysis software ImageJ, fluorescent signals in induced buds of EGFP-pUL31 and the membrane, stained by DiD-C_{18} were analyzed. Intensities were normalized and plotted (Fig. 2.17A, lower panel). EGFP-pUL31 is clearly concentrated in the forming buds and as indicated by fluorescence analysis enriched at least two fold compared to average EGFP-pUL31 signals. The membrane fluorescent dye DiD-C_{18} does not seem to increase above background levels indicating a specific enrichment only in EGFP-pUL31. A three dimensional reconstruction of stack images taken was done from a Ni-DGS-GUV incubated with His_6-EGFP-pUL31 showing multiple ILVs in close proximity of inner GUV membrane as well as vesicles detached and floating in the lumen of the giant vesicle (Fig. 2.17B).

Budding steps of vesicles from representative GUV membranes based on the His_6-EGFP-pUL31 signals (Fig. 2.18) indicate that pUL31 is sufficient to induce membrane budding as well as vesicle formation and final scission.

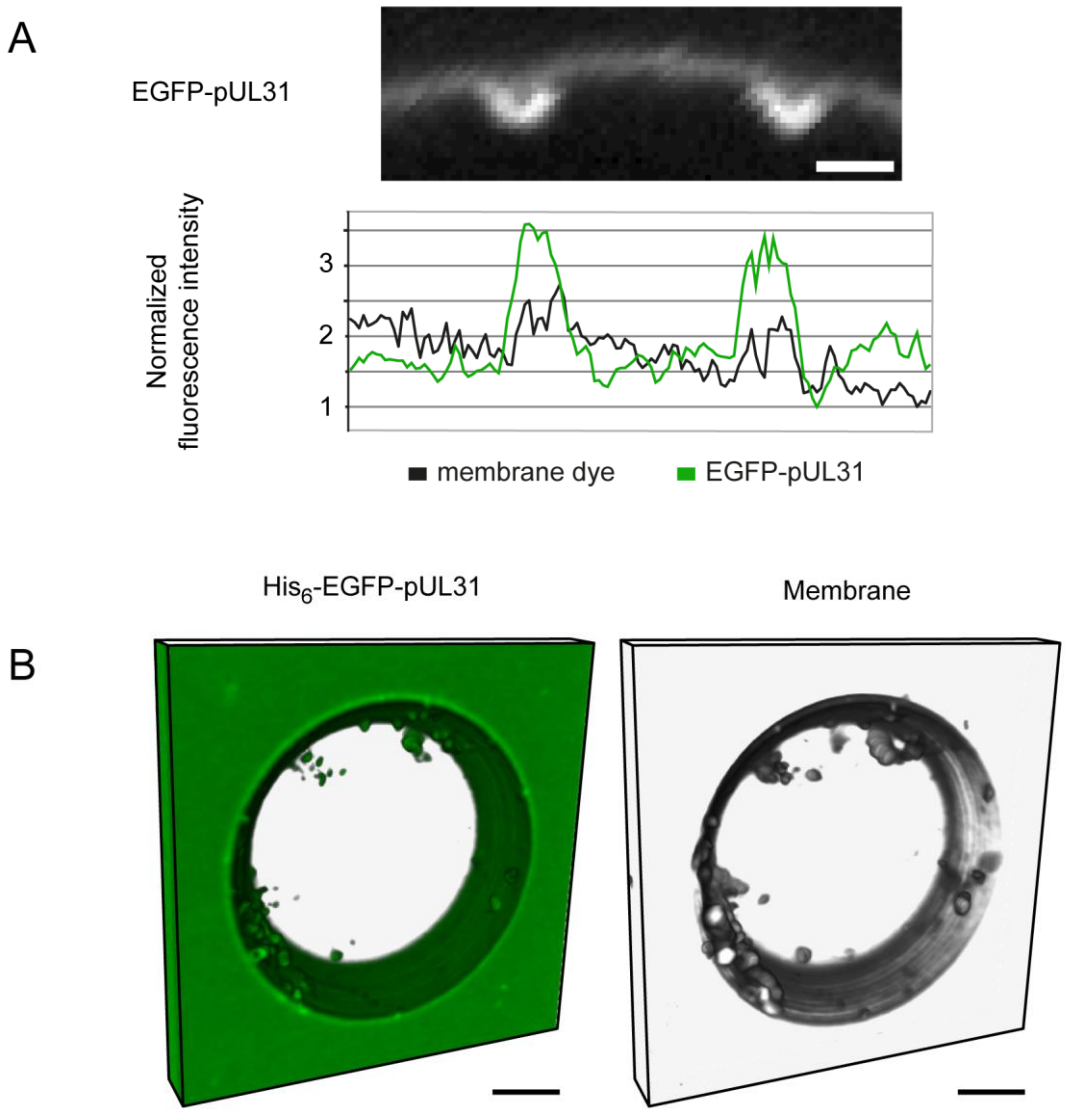

Figure 2.17: pUL31 accumulates in nascent buds and is sufficient to form vesicles which are disconnected from the GUV membrane.
pUL31 accumulates at sites were nascent buds in the GUV membrane emerge. Fluorescent signals of His_6-EGFP-pUL31 and of the lipophilic dye DiD-C_{18} was quantified using the straighten function of Fiji (ImageJ) and the normalized fluorescent intensity for both signal was plotted indicating an accumulation of pUL31 in the emerging buds (A). bars: 1 µm
Three dimensional reconstitution of a GUV with 1 mol % Ni-DGS incubated with His_6-pUL31 which shows efficiently bound His_6-EGFP-pUL31 and highly mobile vesicles distant and apparently detached from the GUV membrane (B). bars: 5 µm

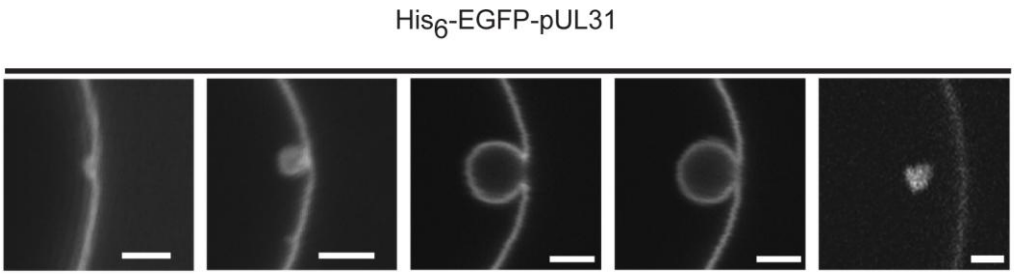

Figure 2.18: Recruiting pUL31 to GUVs is sufficient for vesicles budding and detachment from the GUV membranes
GUVs containing 1 mol % Ni-DGS were incubated with His_6-EGFP-pUL31. Confocal pictures were taken from different representative GUVs showing different time points in budding and detaching of ILVs from the GUV membrane. bars: 2 µm

2.1.12 Determining the influence of lipid compositions in His_6-EGFP-pUL31 induced vesicle budding

One benefit of the GUV system is that lipid compositions used can be varied. Therefore the roles of lipids and their contribution in vesicle budding upon His_6-EGFP-pUL31 can be investigated. Thus, individual lipids were removed from the lipid composition (see methods, (4.2.24.1)) used (indicated by ∆). Removed lipids were replaced by the same amount of PC. The negatively charged lipids phosphatidylinositol (PI; 10 mol %) and phosphatidylserine (PS; 2.5 mol %) as well as sphingomyelin (SM; 2.5 mol %) and cholesterol (chol; 5 mol %) were present in minor quantities (as indicated in mol %).

All used lipid compositions were able to recruit His_6-EGFP-pUL31 to GUV membranes (Fig. 2.19). Removal of the negatively charged lipids PI or PS as well as co-removal of both from the lipid composition had no influence on His_6-EGFP-pUL31 recruitment as well as induction of vesicle budding from the GUV membrane.

Again, as observed before (Fig. 2.9) exclusion of cholesterol and sphingomyelin, or a combination of both, resulted in block of vesicle budding after adding His_6-EGFP-pUL31 (Fig. 2.19). This was also apparent as vesicle amounts in GUVs were not higher than background levels of untreated GUVs indicating a requirement for cholesterol and sphingomyelin to remodel GUV membranes to promote vesicle budding and scission.

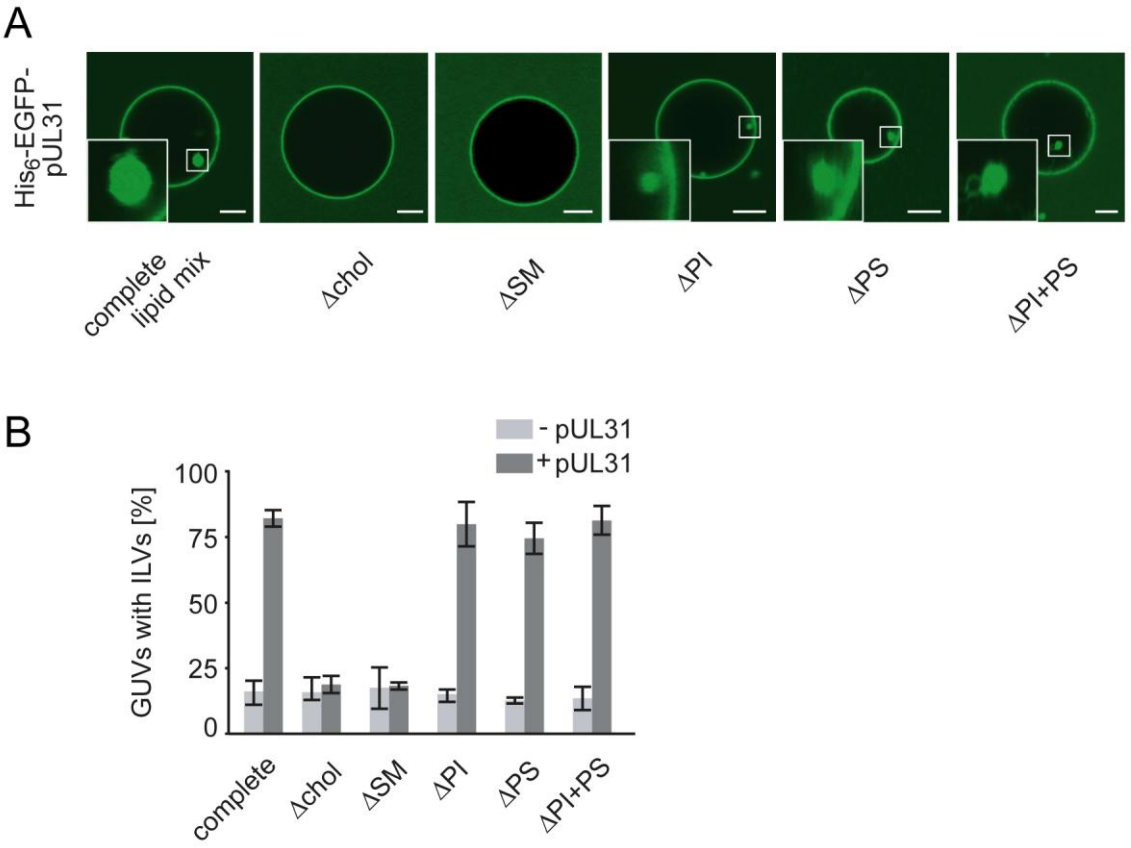

Figure 2.19: Cholesterol and sphingomyelin are required for pUL31 mediated vesicle formation
GUVs were generated from a chloroform dissolved lipid mixture mimicking the nuclear envelope composition (complete lipid mixture) or lacking individual lipids (indicated by Δ) (A). All lipid mixtures contained 1 mol % of the head group modified lipid Ni-DGS. GUVs were incubated with EGFP-pUL31 inducing vesicle formation. Recruitment of EGFP-pUL31 was independent of the lipid composition. ILVs were efficiently formed except when GUVs were lacking either cholesterol (chol) or sphingomyelin (SM) indicating that both lipids are needed. Shown is the quantification of at least 60 GUVs per experiment and condition analysed before and after the addition of EGFP-pUL31 (B). Error bars represent mean of three independent experiments (+/- SEM). GUVs were imaged by confocal microscopy. bars: 10µm, PI - phosphatidylinositol, PS - phosphatidylserine

2.1.13 pUL31 is able to self-interact on GUV membranes

The mechanism of pUL31/pUL34 as well as pUL31-only mediated vesicle budding is still enigmatic. As observed before pUL31 is concentrated in invaginations and budding spots. Many membrane remodelling proteins, such as clathrin or components of the COP I/II or ESCRT machinery can oligomerize on the deforming membrane (McDonald & Martin-Serrano, 2009; Ford et al., 2002). The hypothesis

that pUL31 could form a coat or coat-like structure driving membrane deformation and vesicle budding is tempting. Therefore, giant unilamellar vesicles utilizing the complete lipid mix supplemented with 1 mol % of Ni-DGS were used. His_6-tagged and unlabeled pUL31 was added to GUVs in a 60 nM concentration. This concentration was not sufficient to induce vesicle formation (Fig. 2.20A, first row). Untagged EGFP-pUL31 was then added to pre-treated GUVs or as a control to untreated vesicles (Fig. 2.20A, last row). Indeed, EGFP-pUL31 was recruited to pUL31 pre-treated GUVs but not to untreated vesicles. To verify that soluble proteins were not unspecifically binding to pre-treated GUVs untagged EGFP was added and showed no binding to pre-treated GUVs (Fig. 2.20A, fifth row). Concentrations of 125 nM of EGFP-pUL31 as well as additional 60 nM His_6-UL31 already induced ILV formation (Fig. 2.20A, second row).

This demonstrates that membrane tethered pUL31 can recruit soluble pUL31 by self-interaction to membranes and is sufficient for vesicle formation in the GUV system.

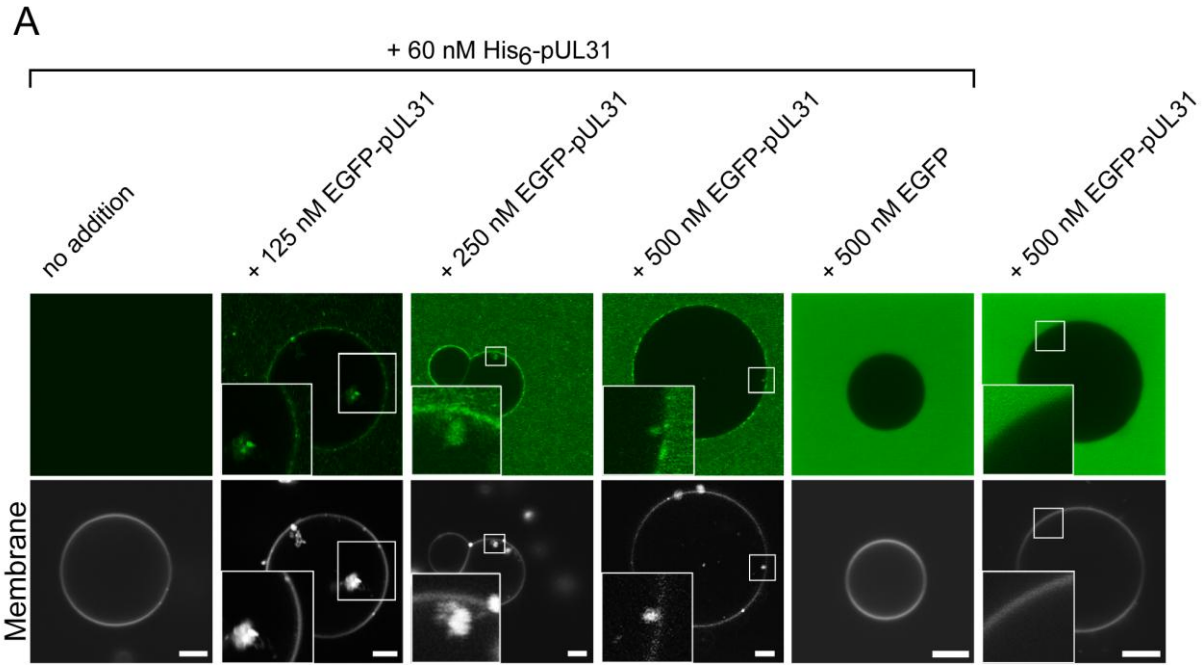

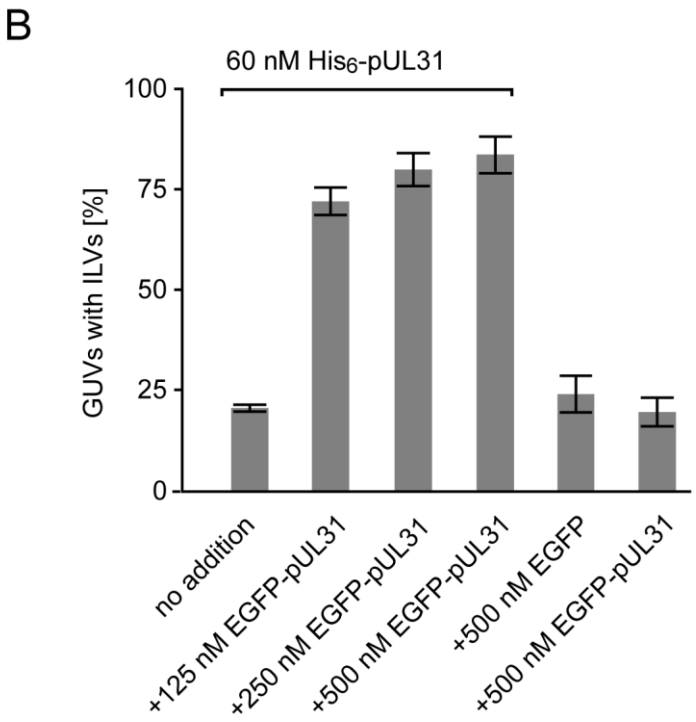

Figure 2.20: pUL31 self-interacts on GUV membranes
GUVs from chloroform dissolved lipids containing 1 mol % Ni-DGS were incubated with 60 nM His_6-pUL31 not sufficient to induce vesicle formation. EGFP-pUL31 lacking a His_6-tag was added in different concentrations. EGFP-pUL31 was recruited in a concentration dependent manner only to pre-incubated vesicles but not in the absence of with His_6-UL31 nor was EGFP recruited to the pre-incubated vesicles (A).
Quantification indicating a drastically increase in ILV formation only when EGFP-pUL31 was added. Error bars represents the mean (-/+ SEM) of three independent experiments (B).

2.1.14 pUL31 does not oligomerize in solution

As pUL31 can oligomerize on GUV membranes (Fig. 2.20A) it was tested for oligomerization in solution. A GST-pull-down assay was employed to test if pUL31 can recruit pUL31 in solution. GST (control), GST-pUL31 and GST-pUL34ΔTMR were bound to GSH sepharose and incubated after blocking with BSA with bacterial lysates expressing either His_6-pUL31 (Fig. 2.21A) or EGFP-UL31 (Fig. 2.21B). Bound proteins were eluted with PreScision protease and subsequently analysed by SDS–PAGE and western blotting. Detection using His_6- and EGFP-antibodies revealed an interaction of His_6-pUL31 as well as EGFP-pUL31 with GST-pUL34ΔTMR demonstration that the interaction between pUL31 and pUL34 is independent of the used protein tag. In addition, no interactions were observed between His_6-pUL31 or

EGFP-pUL31 and GST-pUL31 or with the GST control verifying that pUL31 does not self-interact in solution and the pUL31/pUL34 interaction is specific.

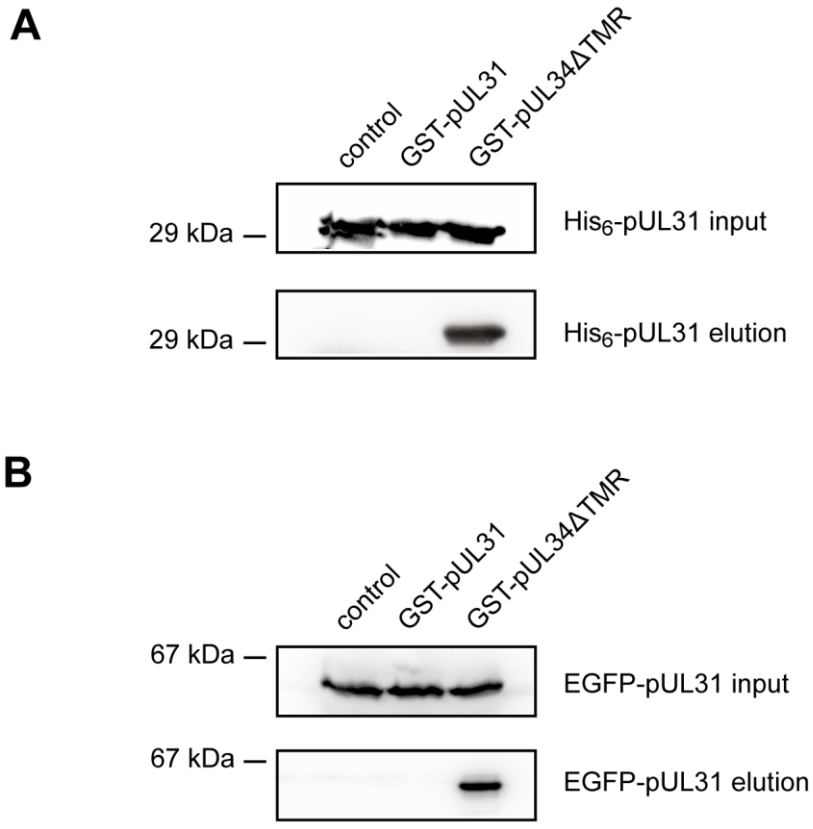

Figure 2.21: pUL31 does not self interact in solution
GST pull down experiments were performed using GST alone (control), GST-pUL31 or GST-pUL34ΔTMR (aa 1-240) as baits. Recombinant proteins were expressed in *E. Coli,* purified and bound to GSH-sepharose. Baits were incubated with bacterial lysates containing recombinant His_6-pUL31 or EGFP-pUL31. Eluates were analysed by western blot analysis using antibodies against His_6 (A) or EGFP (B). pUL31 was pulled down in both cases (A and B) by pUL34, while pUL31 does not pull down pUL31 and also no interaction with pUL31 was observed when using GST as bait.

In addition, size exclusion chromatography coupled with multi-angle laser light scattering (MALLS) was performed, a technique for determining the absolute molar mass and the average size of particles in solution. This revealed that EGFP-pUL31 exists monomeric in solution with a size of 49.2 kDa (calculated size = 58.7 kDa) and does not oligomerize in solution (Fig. 2.22).

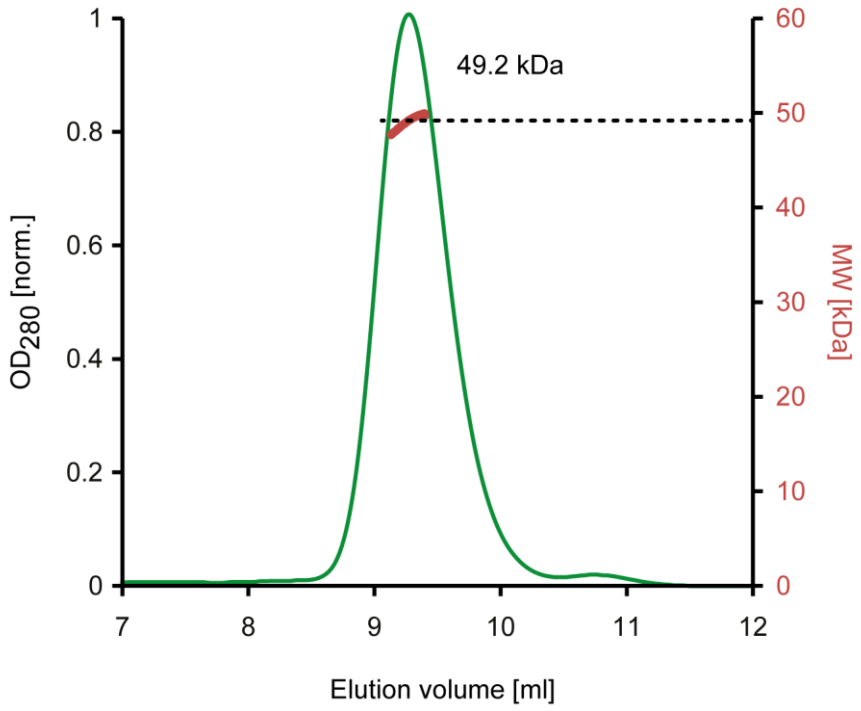

Figure 2.22: EGFP-pUL31 runs monomeric in solution
Size exclusion chromatography was performed on a Superdex 75/300 GL column followed by multiangle static laser light scattering (MALLS) of EGFP-UL31 and shows that it is monomeric in solution (calculated mass 58.7 kDa). The black dots relate to the secondary axis and show the measured molecular weight of the eluting particles.

2.1.15 pUL31 induces oligomerization in supported lipid bilayers

To visualize the pUL31 oligomerization on membrane surfaces and accompanied membrane restructuring, supported lipid bilayers, comprised of the nuclear envelope lipid composition supplemented with Ni-NTA-DGS were employed. His_6-EGFP-pUL31 was recruited to the supported lipid bilayers within seconds where it formed patches of 1.0 ± 0.5 µm in diameter (Fig. 2.23A).

In addition, not only patch formation was induced also recruitment gave rise to the appearance of multiple membrane defects indicating disruption of the lipid bilayer (Fig. 2.23A). Accumulation of membrane defects resulting most likely by increased membrane tension associated with the membrane deforming activity of pUL31. In contrast, His_6-EGFP was also efficiently recruited to the supported lipid bilayers but did not induce patch formation or disruption of the bilayer (Fig. 2.23B).

Formed patches on bilayers were tracked over time (Fig. 2.23C). Subsequently, individual patches fused and were not traceable after 40 seconds.

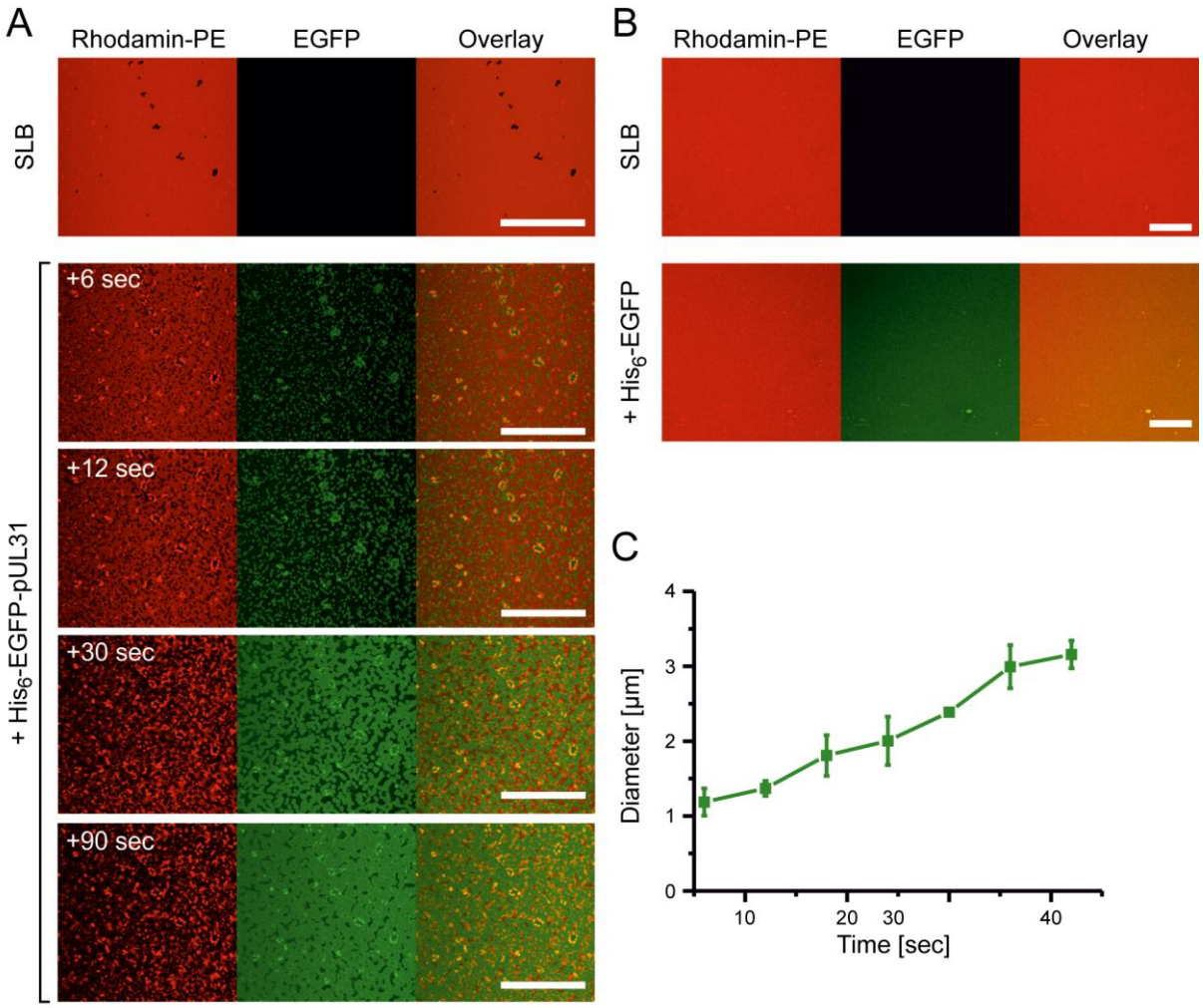

Figure 2.23: pUL31 addition leads to disruption of supported lipid bilayers (SLBs)
SLBs were generated utilizing NE-mix supplemented with 1 mol % Ni-DGS as well as 0.1 mol % Rhodamin-PE. The same areas on SLBs were imaged before and after the addition of His_6-EGFP-pUL31 (A). After only few seconds pUL31 is efficiently recruited to the SLB and forms patches of about 1.2 ± 0.2 µm. Further pUL31 recruitment is observed in a time series leading to disruption of the lipid layer and lipid accumulation (A, lower panels). Addition of His_6-EGFP instead results in recruitment but no observable morphological changes of the SLB (B). The diameter of formed patches was analysed until about 40 seconds. After that time point the majority of patches fuse and can no longer be tracked (C). bars: 50 µm

2.1.16 Atomic force microscopy reveals oligomerization into small protein patches of pUL31 on supported lipid bilayers

Atomic force microscopy (AFM) was performed on supported lipid bilayers incubated with His_6-EGFP-pUL31 or His_6-EGFP, respectively. AFM allows high resolution imaging of lipid surfaces. A cantilever with a small tip is scanning the surface of the sample by lateral movement of the probe or sample. By measuring lateral and vertical deflection of a laser beam by a photo detector high image resolution, with a vertical resolution up to 0.1 nm, is achieved.

Supported lipid bilayers with a nuclear envelope lipid composition including 1 mol % Ni-DGS and 0.1 mol % Rhodamin-PE for fluorescent imaging were generated (Fig. 2.24A). pUL31 was added to the supported bilayer in a concentration of about 150 nM (Fig. 2.24B). Higher resolution images of patches formed showed no clear structure of recruited pUL31 (Fig. 2.24, right panel). Higher concentration added resulted in excessive recruitment to the bilayer and in no general observable structures (not shown), as time between addition of the protein and image acquisition is about five to ten minutes.

Recruitment of His_6-EGFP to supported lipid bilayers followed by atomic force microscopy showed not the patch phenotype but a smooth recruitment to the lipid layer. Additionally no increase in surface height could be noticed (Fig. 2.24C and D) demonstrating no remodeling activity of EGFP. A surface profile was created which is depicted by a yellow line (Fig. 2.24A-D) tracing the height and distance. The diameter and height (roughness) of the patches upon His_6-EGFP-pUL31 addition were analyzed (Fig. 2.24E and F). The majority of patches observed had a diameter of about 1 µm ± 0.5 µm (~ 66 %) while patches with greater diameters (~31 %) and smaller diameter (~ 3 %) were less frequent. Also the average height (roughness) showed a mean patch height of about 2 nm (~75 % of analyzed patches). Atomic force microscopy (AFM) and supported lipid layer (SLB) experiments were performed in collaboration with Prof. Dr. Ana J. García-Sáez and Joseph Unsay at the Interfaculty Institute for Biochemistry (IFIB), University of Tübingen, Germany.

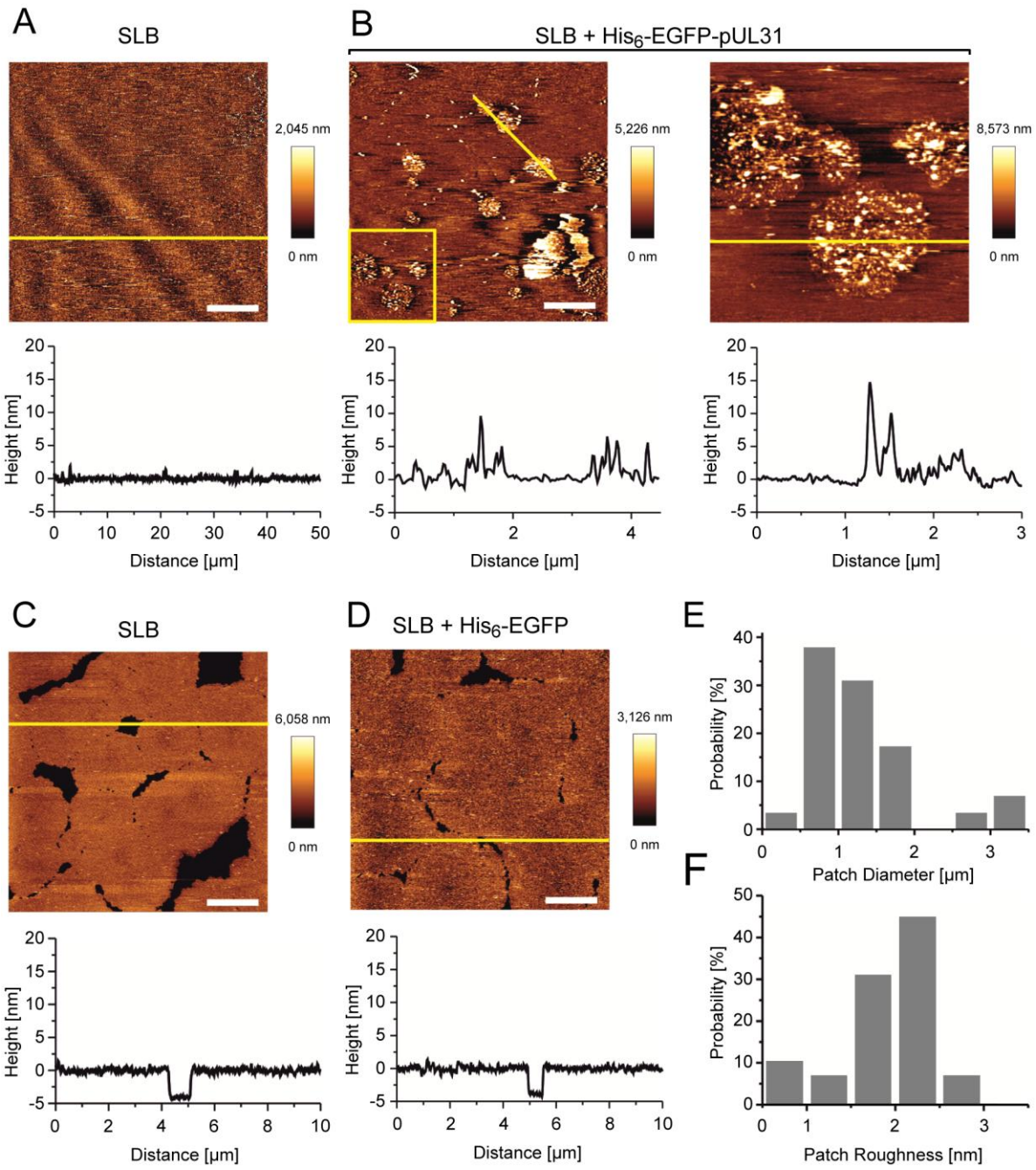

Figure 2.24: Atomic force microscopy (AFM) of supported lipid bilayers (SLBs) reveals patch formation upon addition of pUL31

Supported lipid bilayers were generated by applying SUV (NE mix + 1 mol % of Ni-DGS) in presence of calcium to mica support discs. AFM was performed on SLB before and after addition of His_6-EGFP-pUL31 (A and B) or before and after addition of His_6-EGFP (C and D) revealing patch formation as well as membrane resculpturing upon incubation with pUL31. Incubation of EGFP only with the SLB had no topological effect. The right panel in B is a 3x3 µm magnification of the yellow marked box of the left panel. Graphs below the images are corresponding profiles of the yellow lines in each image. Upon addition of His_6-EGFP-pUL31 the diameter (E) and roughness (average height of the patches) (F) distributions of the observed patches was analysed and plotted. The graphs indicate a peak at 1.0 ± 0.5 µm in diameter (mean ± standard deviation), and 2.0 ± 0.1 nm in roughness (F). bars: (A) 10 µm, (B-D) 2 µm

2.1.17 Mutational analyses of a conserved sequence in UL31

Sequence alignments of pseudorabies virus UL31 and homologues of human pathogenic herpes viruses revealed four constant regions (Loetzerich et al., 2006) with high conservation (Fig. 2.25) indicated by gray boxes. The highest grade of conservation was found in the region comprising aa 56-101 of suid herpes virus-I (PRV, suHV-1) pUL31. The interaction site of homologues of pUL31 with pUL34 in MCMV was mapped to the CR1 of the pUL31 homologue (Loetzerich et al., 2006). To verify if single conserved residues in the CR1 are involved in binding to pUL34 and the remodelling activity of pUL31 a mutational analysis was performed. Using this method it was analyzed if both functions membrane remodeling and pUL34 binding of pUL31 could be separated or if they are located in the same region. Therefore single point mutations of conserved residues were generated.

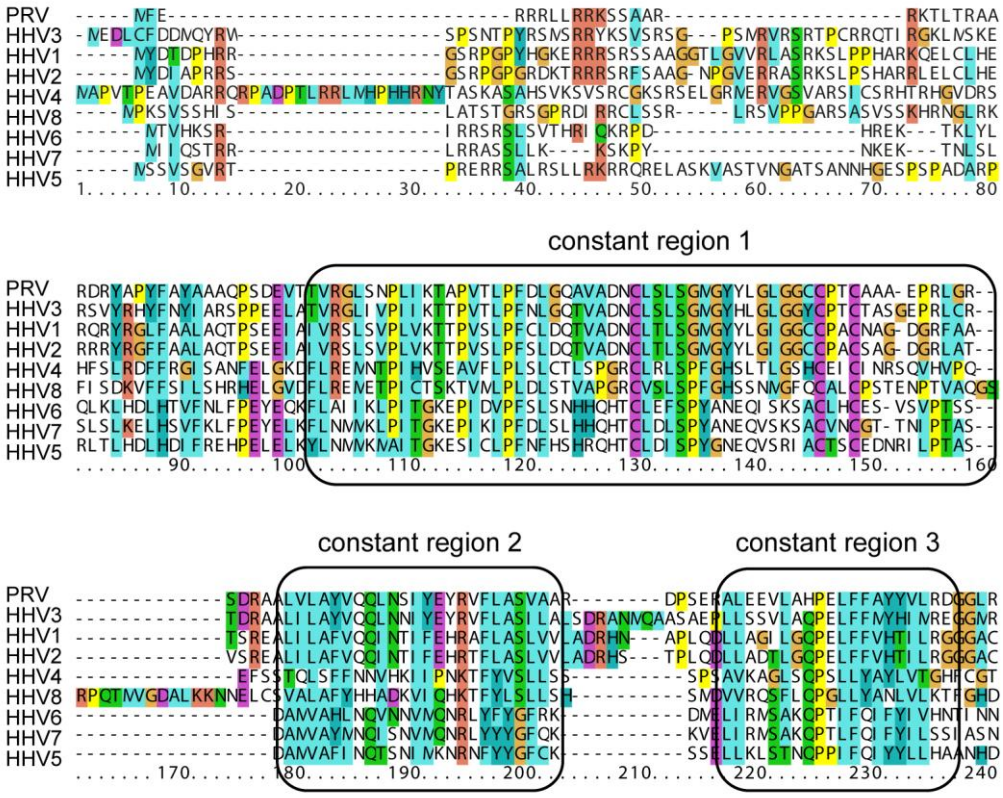

Figure 2.25: Sequence alignments indicate four constant regions
Sequence alignment of PRV pUL31 and homologues of human pathogenic herpes virus subspecies including the N-terminal 240 aa of each protein. Areas with high conservation are indicated by gray boxes. Multiple sequence alignment was created using ClustalX software v.2.1.

Most noticeable were three conserved and one only in herpes HHV-1/2 and Kaposi's sarcoma-associated herpesvirus (HHV-8/KSHV) conserved cysteine residues in the first constant region. Cysteine residues are important for stabilizing protein structures e.g. upon stable formation of disulfide bridges or complexing metal ions such as zinc. To understand the importance of these residues in pUL31 individual point mutants of C73S, C88SC89S and C92S were generated (Fig. 2.26). The cysteine residues may be engaged in disulphide bond formation allowing this conserved stretch of the protein to form an interface for pUL34 interaction and/or to form higher order homo-oligomers/hetero-oligomers.

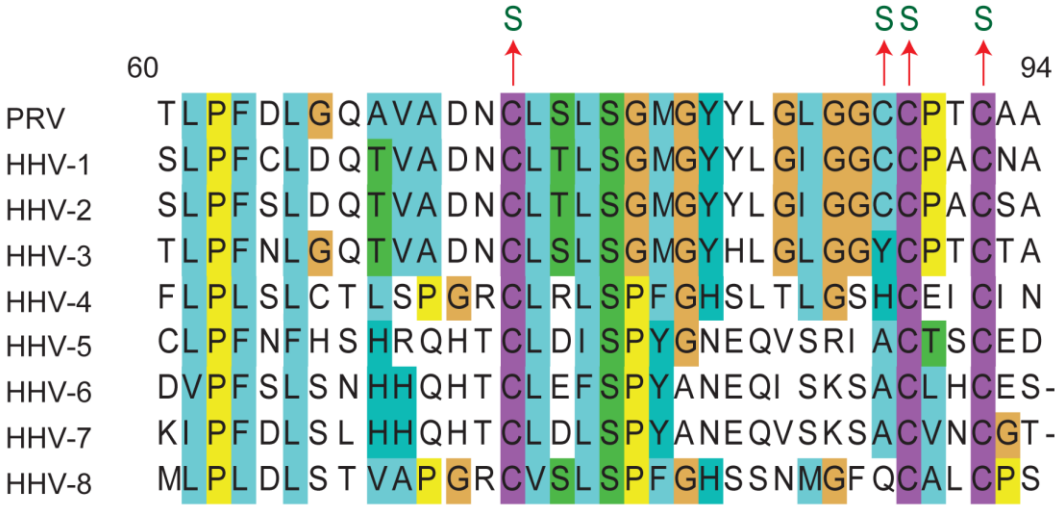

Figure 2.26: Sequence alignment of the first constant region of UL31
Homologous pUL31 sequences among the herpes viruses family are shown. The highly conserved cysteine residues are shown in purple and red arrows indicate cysteines that were substituted by serine residues.

2.1.18 Cysteine mutations block pUL31 interaction with pUL34

Cysteine to serine mutants in pUL31 were expressed in *E. coli* with an EGFP tag as before. When added to UL34 GUVs none of these UL31 mutants were recruited to the membrane surface (Fig. 2.27).

As no interaction with pUL34 was observed it was tested if the ability to induce vesicles upon addition to Ni-DGS containing GUVs was affected.

pUL31 cysteine mutants were added in the same concentration of 500 nM to GUVs. The mutants were efficiently recruited to GUV membranes, but were not able to

induce vesicle formation (Fig. 2.28B-D). Also higher concentrations were tested (not shown) and were not able to restore membrane remodelling ability compared with the wild-type protein (Fig. 2.28A).

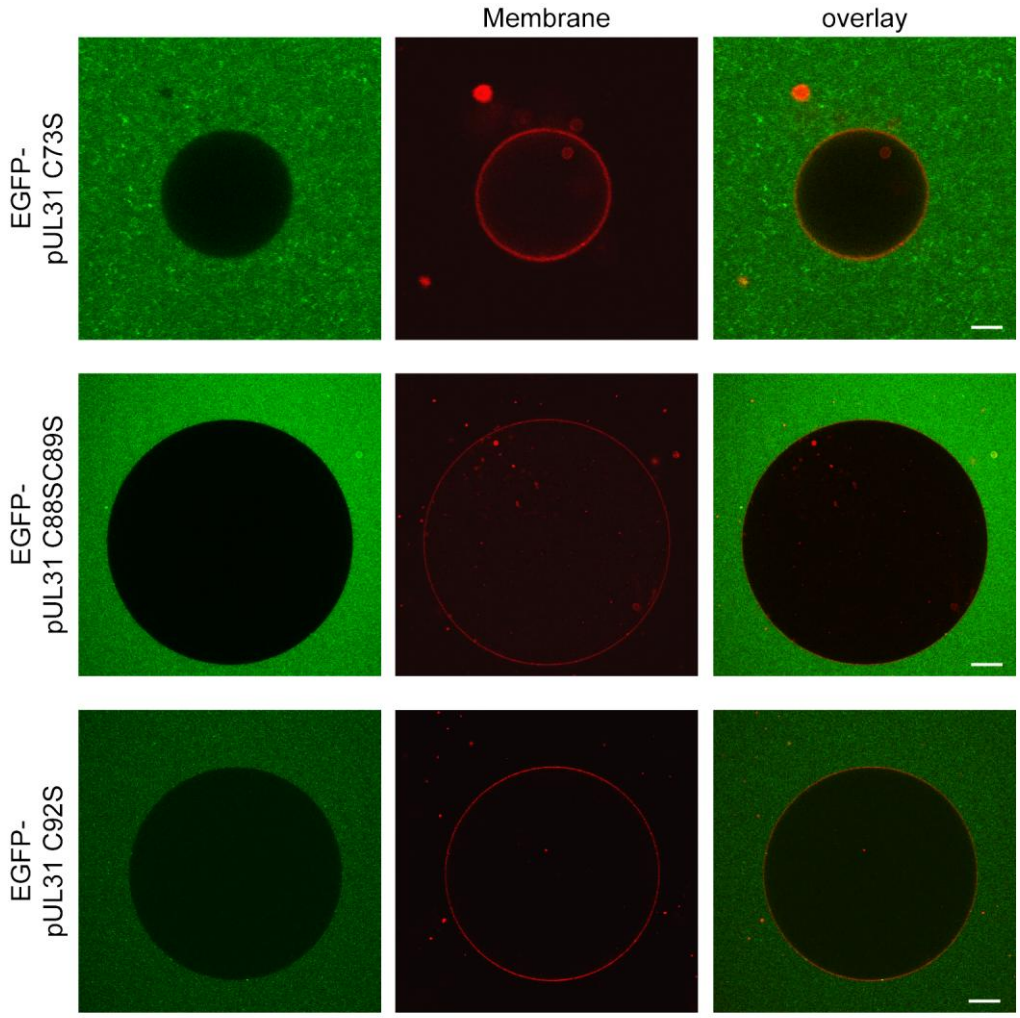

Figure 2.27: pUL34 and pUL31 cysteine mutants do not interact in GUV membranes
pUL34 was labeled with Alexa-Fluor-546 and reconstituted in proteo-liposomes. Dried proteo-liposome layers were electroformed. Resulting GUVs were incubated with EGFP tagged pUL31 cysteine mutants. None of the pUL31 mutants was recruited to the GUV membrane demonstrating a block in pUL34 binding. bars: 10µm

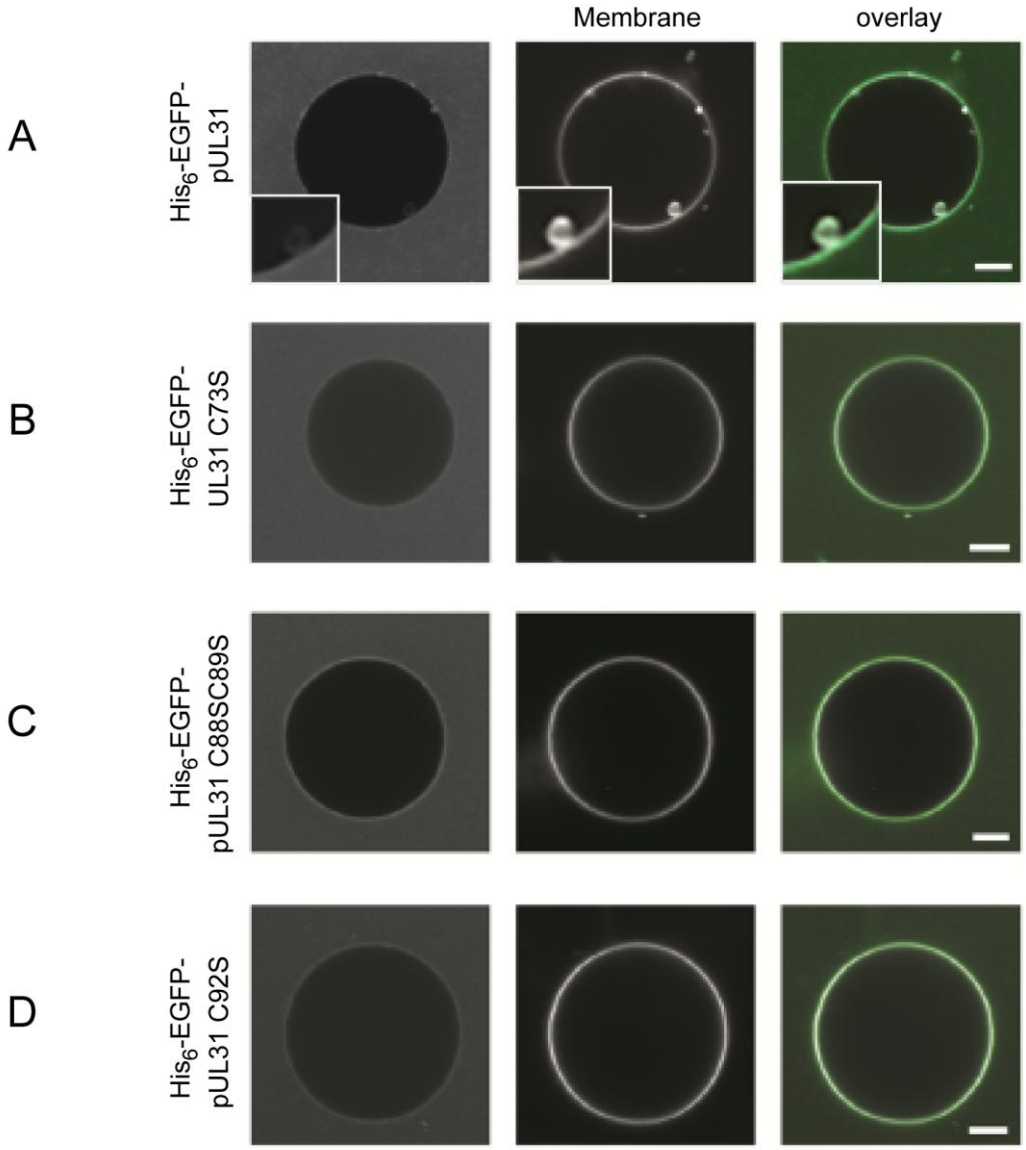

Figure 2.28: Cysteine point mutations also abrogate vesicle formation in GUV membranes
GUVs from chloroform dissolved lipids (NE-mix) containing 1 mol % Ni-DGS were generated by electroformation. His_6-tagged pUL31 was efficiently recruited to the GUV membrane (A). The recruitment induced vesicle formation and detachment from the GUV membrane visualized by EGFP fluorescence in forming ILVs while recruitment of His_6-tagged pUL31 point mutants resulted in no ILV formation (B-D). The GUV membrane was visualized by addition of the lipophilic dye DiD-C_{18}. bars: 5 µm

A GST pull down assay was performed to confirm the observed block in interaction with pUL34 GUVs. Therefore GST only (control) and GST-pUL34ΔTMR (aa 1-240) were used as baits. The baits expressed in *E. coli* and immobilized to GSH sepharose beads were incubated with bacterial lysates containing recombinant His_6-pUL31 or His_6-pUL31 mutants. The eluates were generated by PreScission protease

cleavage of the target sequence in the bait proteins. The elutions were analysed by western blot analysis using antibodies against EGFP (Fig. 2.29). pUL31 was pulled down efficiently by pUL34 but not the pUL31 mutants (Fig. 2.29B) indicating the cysteine mutations abrogated interactions between pUL31 and pUL34.

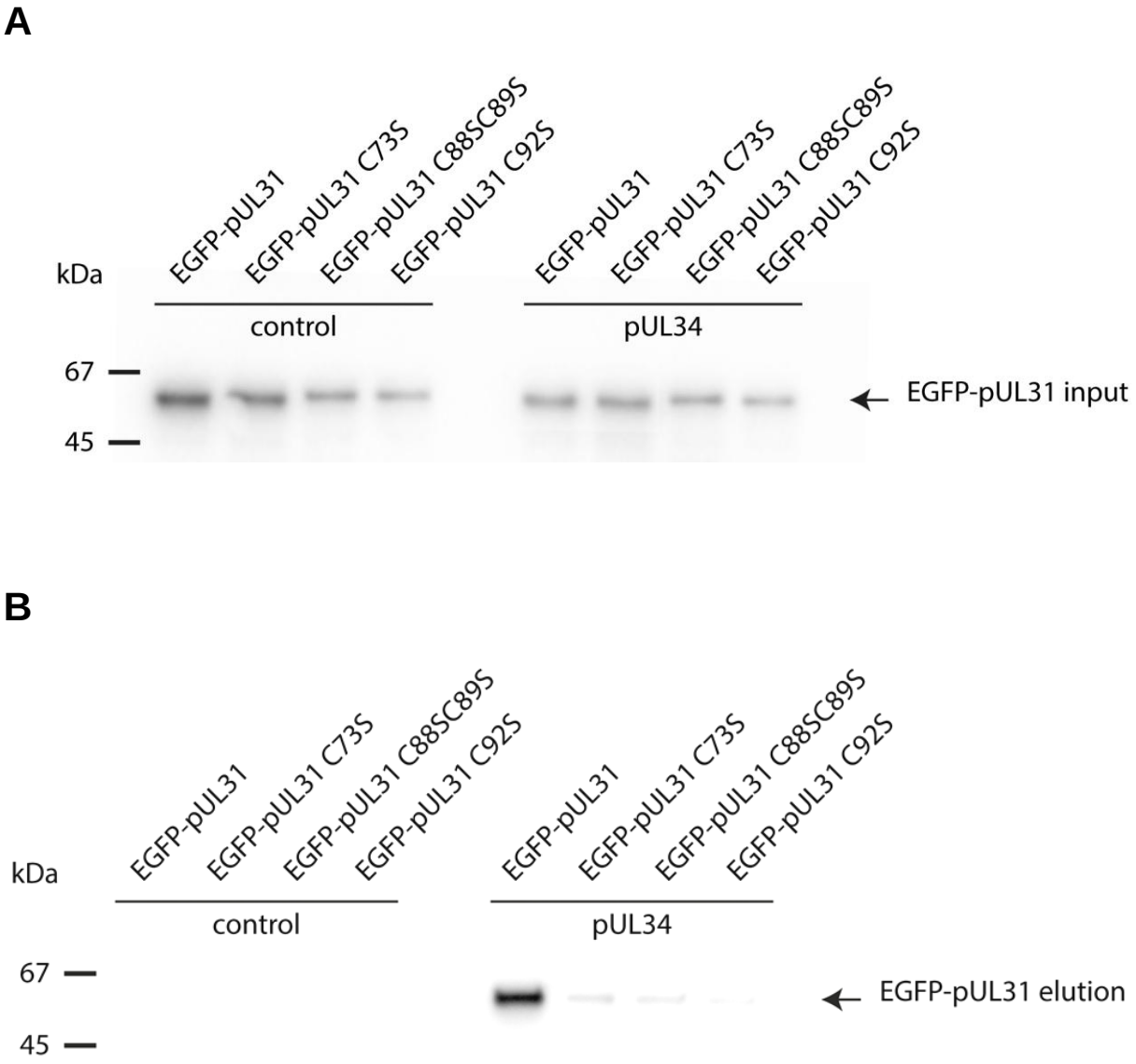

Figure 2.29: GST pull down assays indicate no interaction of pUL31 mutants with pUL34

GST pull down experiments were performed using GST alone (control) and GST-pUL34ΔTMR (aa 1-240) as baits. Recombinant proteins were expressed in *E. coli* purified, bound to GSH-sepharose and blocked with BSA. Baits were incubated with equal amounts of bacterial lysates containing recombinant His_6-pUL31 or His_6-pUL31 mutants (A). Eluates were analysed by western blot analysis using antibodies against EGFP (B). pUL31 was pulled down efficiently by pUL34 but not the pUL31 mutants (B) indicating mutations abrogated interaction between both proteins.

2.1.19 Mutation of conserved amino acids in the first constant region of pUL31 affects pUL34 binding and self-interaction

Mutation of the conserved cysteine residues in the first constant region of pUL31 resulted in a block of pUL34 interaction and membrane remodeling ability upon artificial recruitment to giant vesicle membranes (Fig. 2.27, Fig. 2.28). This indicates that these cysteine residues play an important structural role or are involved in pUL31-pUL31-interaction. Therefore, both functions could not be separated by cysteine mutations.

To further assess if additional mutations in the first constant region could fulfill this requirement further single point mutations were generated (Fig. 2.30). Additionally, the double cysteine mutation C88SC89S in pUL31 was further investigated by the respective individual point mutations verifying if only one or both cysteines are involved in membrane deformation. The membrane remodeling ability of the mutants was determined employing Ni-DGS-GUVs. All mutants expressed with an EGFP tag were efficiently recruited to GUV membranes (Fig. 2.31, Fig. 2.32). Wild type pUL31, the L76A, S77A, G80A and C88S mutations were able to induce vesicle formation from GUV membranes while P62A, L74A and C89S mutations in pUL31 were not sufficient for vesicle formation (Fig. 2.31, Fig. 2.32, summarized in Tab. 2.1). These results further indicate an importance of the first constant region for the membrane remodeling property of pUL31 and pUL34 binding.

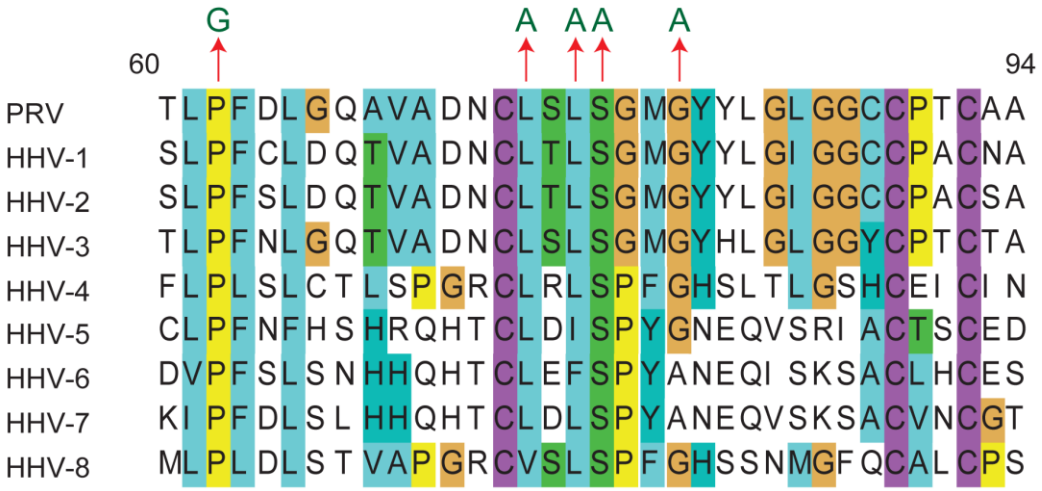

Figure 2.30: Multiple conserved residues in the first constant region were exchanged
Sequence alignment of a part of the first constant region of pUL31 and homologues of human pathogenic herpes virus subspecies are shown. Conserved residues additional to cysteines were mutated and are highlighted. Amino acid exchanges are represented in green letters above the alignment.

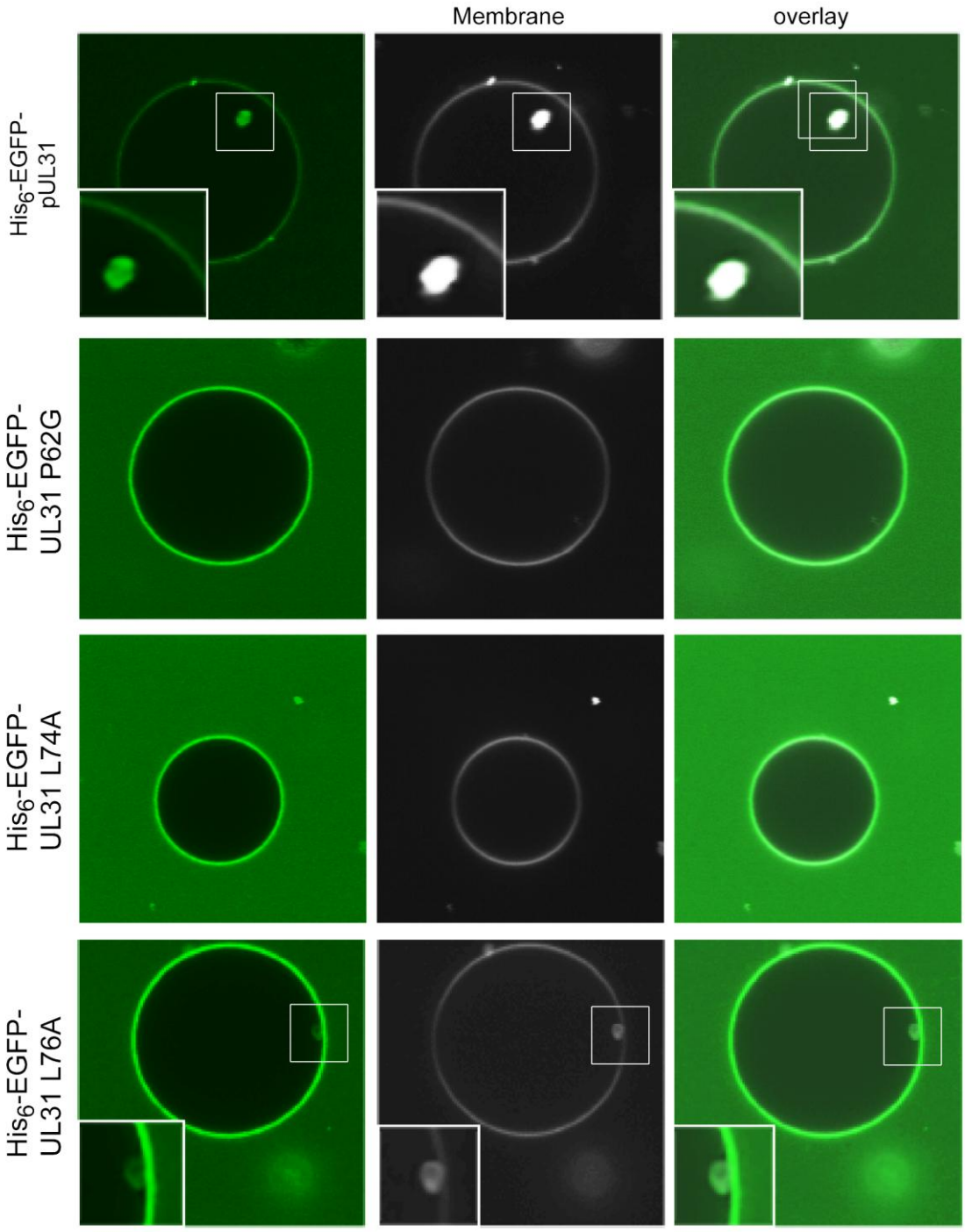

Figure 2.31: Conserved residues in pUL31 are involved in membrane remodelling
The amino acids proline (position 62) and leucine (position 74) in pUL31 appear to be important for membrane remodeling activity of pUL31 in GUV membranes. Amino acid exchange of leucine (position 76 substituted by alanine) is still able to form invaginations in GUV membranes

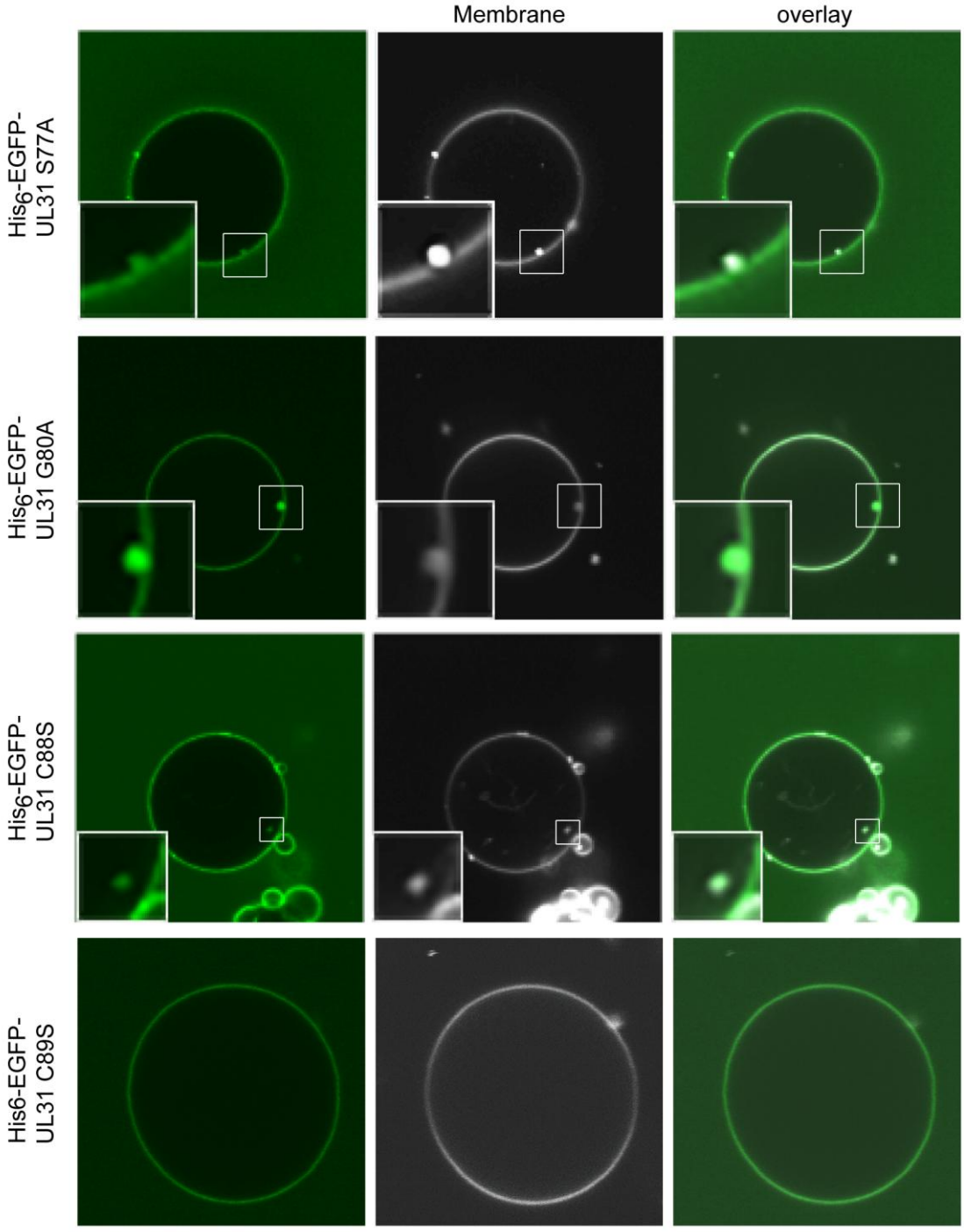

Figure 2.32: Conserved residues in pUL31 are involved in membrane remodeling
The cysteine residue (in position 89) is important for membrane remodeling activity of pUL31 in GUV membranes while cysteine mutation (position 88 to serine) appears not to influence remodeling activity. Single point mutation of serine (position 77 substituted by alanine) and glycine (position 80 substituted by alanine) are still able to induce vesicle budding in GUV membranes.

protein	membrane remodelling activity		protein	membrane remodelling activity
His_6-EGFP-pUL31	yes		His_6-EGFP-pUL31 S77A	yes
His_6-EGFP-pUL31 P62G	no		His_6-EGFP-pUL31 G80A	yes
His_6-EGFP-pUL31 L74A	no		His_6-EGFP-pUL31 C88S	yes
His_6-EGFP-pUL31 L76A	yes		His_6-EGFP-pUL31 C89S	no

Table 2.1: S Summary of mutated conserved residues in pUL31 and their membrane remodeling activity
His_6-EGFP-tagged pUL31 mutants were bound to GUV containing 1 mol % Ni-DGS and analyzed for their membrane remodeling activity.

2.1.20 Coexpression of pUL31 and pUL34 in eukaryotic cells shows remodeling of nuclear membranes

The viral proteins pUL31 and pUL34 are required for primary envelopment at the inner nuclear membrane. Coexpression of pUL31 and pUL34 of *alpha*-herpesvirus pseudorabies virus (PRV) in RK13 cells resulted in the formation and accumulation of vesicles in the perinuclear space between outer and inner nuclear membrane (Klupp et al., 2007). Vesicles present in the perinuclear space are supposed to be similar to viral envelopes. These vesicles contain pUL31 and pUL34 and are derived most likely from the inner nuclear envelope. Thus, coexpression of only these two herpesvirus proteins in the absence of other viral factors is sufficient to remodel nuclear membranes.

To verify results obtained from the giant unilamellar vesicle assay with recombinant proteins a eukaryotic cell system was employed. HeLa cells as well as HEK293T cells were transiently transfected for 24 hours. Cells were fixed with 4 % PFA and subjected to confocal microscopy to verify localization and possible interactions of pUL31 and pUL34.

Upon expression pUL31 localizes in the nucleoplasm while pUL34 is localized in the nuclear membranes and endoplasmic reticulum (Fig. 2.33, upper and middle panel). Coexpression of pUL31/pUL34 resulted in their relocalization. The predominant part of pUL31 was localized to the rim of the nucleus while also pUL34 distribution was altered to be increase in nuclear membranes. Additionally and most noticeable was the appearance of nuclear spots with co-localizations of both proteins (Fig. 2.33, lower panel) consistent with previous observations (Klupp et al., 2007). These spots

were mostly localized at the nuclear rim as well as in the nucleoplasm probably disconnected from the nuclear periphery. The cotransfection of pUL31 with pUL34 did not only result in spot formation, but also showed protrusions forming from nuclear membranes towards the cytoplasm presumably representing membrane proliferation overlapping in pUL31 and pUL34 fluorescent signals (Fig. 2.34). The observed membrane proliferations is consistent with previous studies showing membrane proliferation upon overexpression of pUL31/pUL34 homologs orf67/orf69 of HHV-8 and BFRF1/BFLF2 of HHV-4 (Luitweiler et al., 2013; Gonella et al., 2005; Lake et al., 2004).

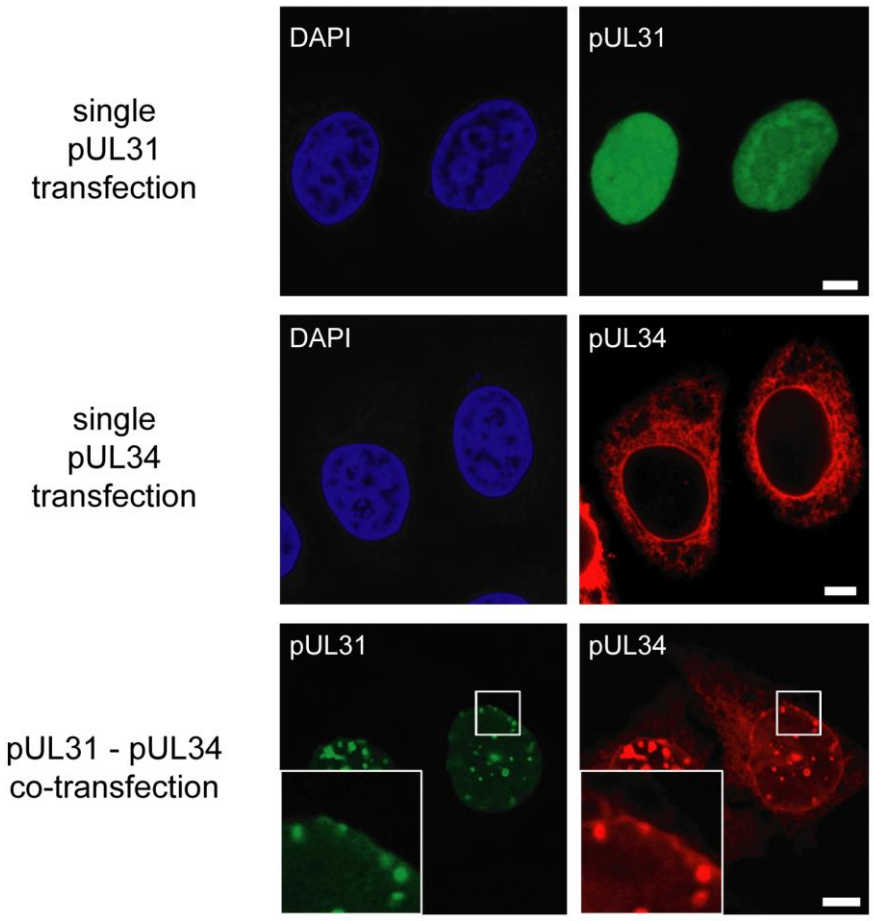

Figure 2.33: Coexpression of pUL31 and pUL34 results in patch formation
HeLa cells were transiently transfected with plasmids expressing either EGFP-pUL31 or mCherry pUL34 for 24 hours. Expression of pUL31 only shows an exclusively nucleoplasmic localisation while expression of pUL34 shows an ER and nuclear membrane localisation. Co-expression of both proteins leads to the recruitment of pUL31 to the nuclear membrane and patch formation showing overlapping signals of both proteins. DNA was stained with DAPI. bars: 5 µm

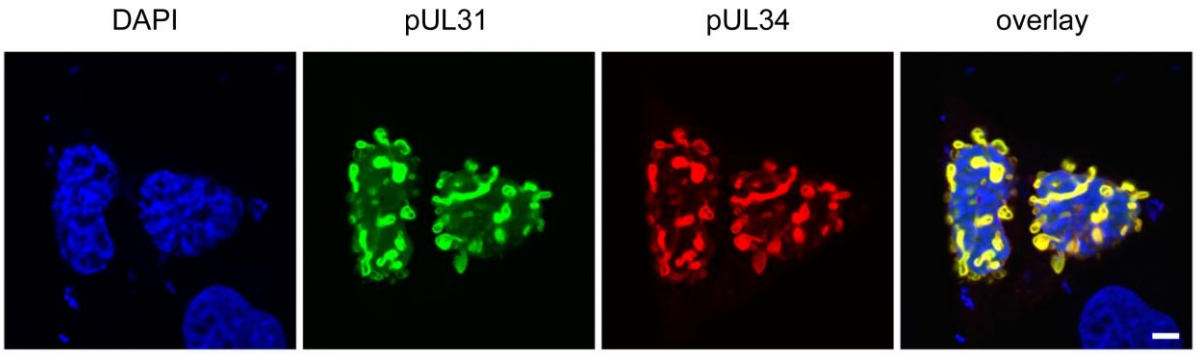

Figure 2.34: Coexpression of pUL31 and pUL34 results in membrane alterations
Transient overexpression of cotransfected pUL31 and pUL34 results in membrane protrusions, presumably forming from the inner nuclear membrane. Chromatin structure appears to be altered at spots colocalizing with putative membrane lobes.

2.1.21 Expression of artificial membrane tethered pUL31 induces patch formation in the nuclear envelope

pUL31 is a soluble protein located in the nucleoplasm due to a nuclear localization signal formed by a basic stretch in the first 20 aa of the protein. As pUL31 is only recruited via pUL34 to the inner nuclear membrane, analyzing pUL31 membrane interaction in the absence of pUL34 requires therefore artificial tethering to nuclear membranes. Therefore constructs were generated expressing full length pUL31 C-terminally fused with the transmembrane domain of pUL34 (aa 241-262) or SCL1 (aa 77-97), an integral membrane protein of the inner nuclear membrane (Fig. 2.38). In addition full length pUL31 fused N-terminally with the N-terminal transmembrane domain of pom121 (aa 1-55), a integral membrane protein of the nuclear pore complex and upstream of the transmembrane domain the construct harbours a inner nuclear membrane signal of rat gp210 also another integral membrane protein of the nuclear pore complex (Fig. 2.38).

Transient transfection of HeLa cells expressing artificial membrane constructs resulted in patch formation lining up at the presumably inner nuclear membrane confirming membrane remodelling activity of pUL31 also in the absence of pUL34 (Fig. 2.35). Additional nucleoplasmic EGFP signal was observed which presumably results from degradation of membrane bound pUL31.

To verify that the observed results are independent of the used cell type HEK293T cells were also transiently transfected with pUL31 and pUL34. The same pattern was observed in HEK293T cells expressing either pUL31 or pUL34 or co-expression of

both (Fig. 2.36), demonstrating that membrane remodelling activity of the pUL31/pUL34 complex or of artificial tethered pUL31 only (Fig. 2.37) is independent of the cell type used.

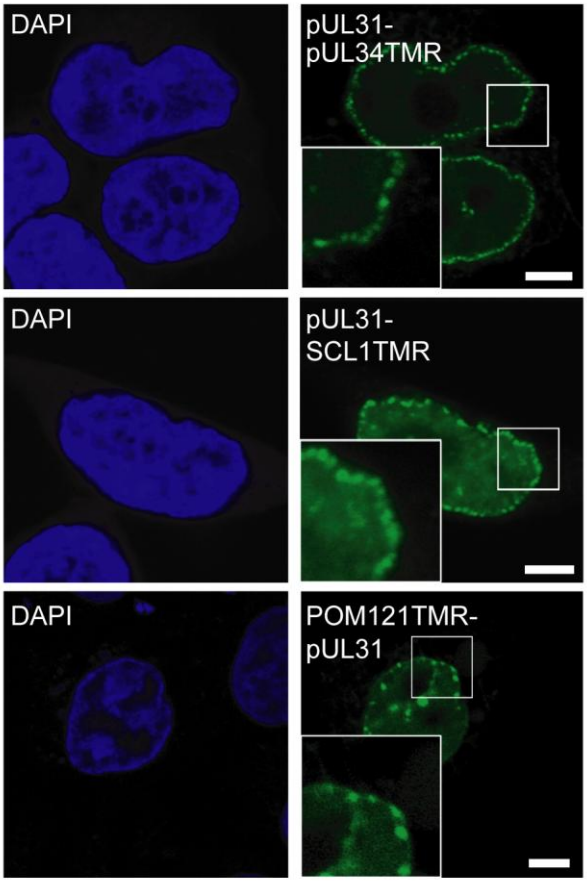

Figure 2.35: Expression of membrane bound pUL31 leads to patch formation.
HeLa cells were transiently transfected with plasmids expressing transmembrane fusion constructs of pUL31 for 24 hours. Expression of constructs with a C-terminally fused transmembrane region (TMR) of pUL34 (aa 241-262) or SCL1 (aa 77-97) as well as a N-terminally fused TMR of Pom121 (aa 1-55) together with an inner nuclear membrane localisation signal of rat gp210 resulted in a mostly nuclear membrane localisation and patch formation. DNA was stained with DAPI. bars: 5 µm

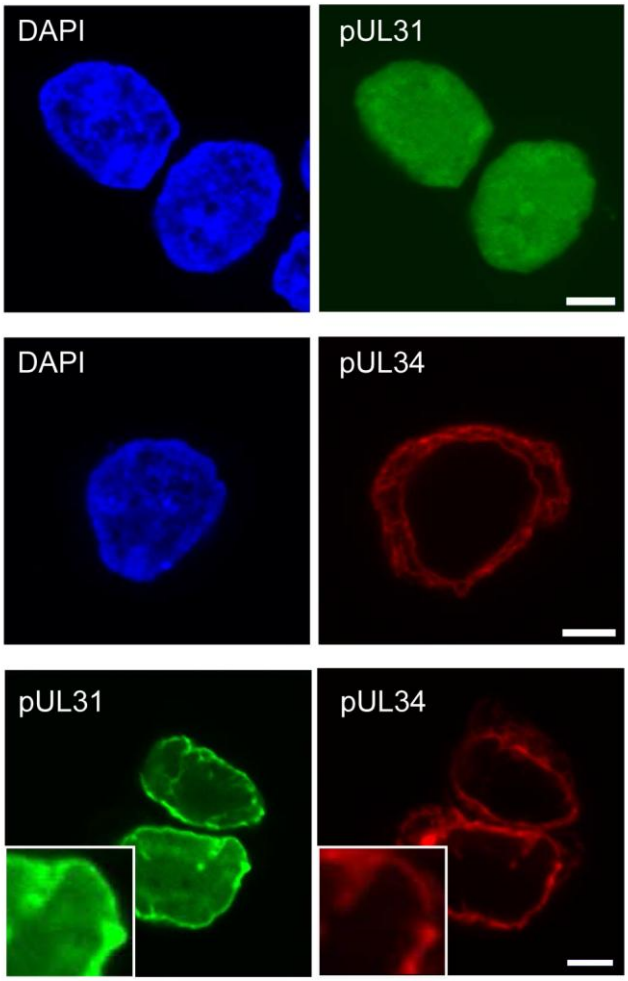

Figure 2.36: Coexpression of pUL31 and pUL34 results in patch formation
HEK293T cells were transiently transfected with plasmids expressing either EGFP-pUL31 or mCherry pUL34 for 24 hours. Expression of pUL31 only shows an exclusively nucleoplasmic localisation while expression of pUL34 shows an ER and nuclear membrane localisation. Co-expression of both proteins recruits pUL31 to the nuclear membrane and patch formation is induced resulting in overlapping signals of both proteins. DNA was stained with DAPI. bars: 5 µm

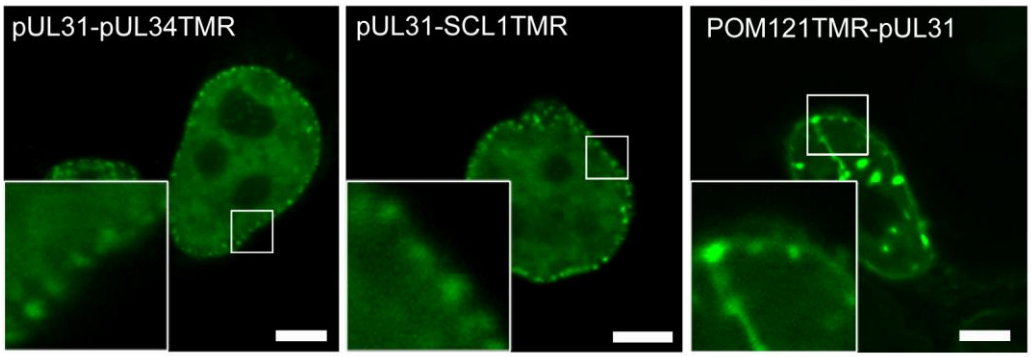

Figure 2.37: Expression of membrane bound pUL31 results in patch formation in HEK293T cells
HEK293T cells were transiently transfected with plasmids expressing transmembrane fusion constructs of pUL31 for 24 hours. Expression of constructs with a C-terminally fused transmembrane region (TMR) of pUL34 (aa 241-262) or SCL1 (aa 77-97) as well as a N-terminally fused TMR of POM121 (aa 1-55) together with an inner nuclear membrane localisation signal of rat gp210 resulted in a mostly nuclear membrane localisation and patch formation. bars: 5 µm

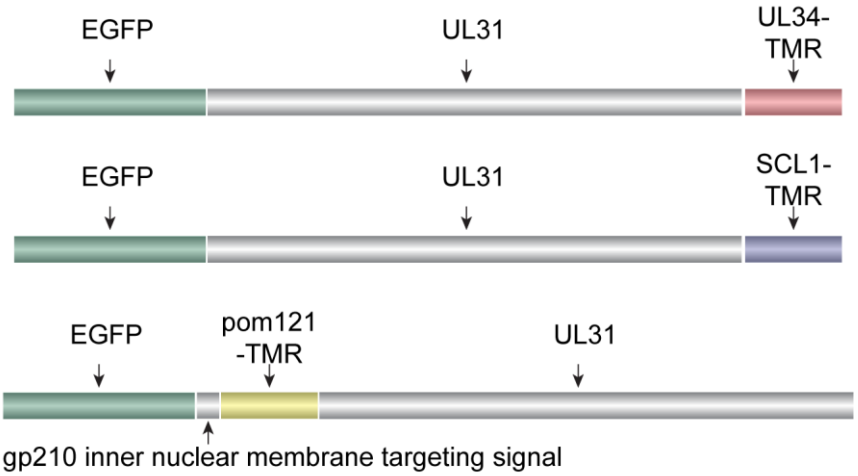

Figure 2.38: Scheme of pUL31 transmembrane constructs
The transmembrane domains (TMR) of pUL34 (aa 241-262) or SCL1 (aa 77-97), an integral membrane protein of the inner nuclear membrane were fused to the C-terminus of full length pUL31. The transmembrane domain of Pom121 (aa 1-55), an integral membrane protein of the nuclear pore complex and the inner nuclear membrane targeting signal of rat gp210, another integral membrane protein of the nuclear pore complex, were fused upstream of the N-terminus of full length pUL31.

2.1.22 Nuclear patches do not contain nuclear pore complexes

To define the observed nuclear patches in more detail the presence of nuclear pore complexes was analysed. If the patches are originating from the nuclear envelope nuclear pore complexes could be present in them. Therefore, HeLa cells were transiently transfected for 24 hours with plasmids encoding pUL31 and pUL34. Cells were fixed with paraformaldehyde and stained with mAB414, an antibody recognizing a subset of FG-repeat proteins. Coupling mAB414 to an Alexa-Fluor-647 labeled secondary antibody revealed that apparently no nuclear pore complexes are present

in nuclear patches (Fig. 2.39). This could indicate a tight packing of proteins thereby excluding other factors and large protein assemblies e.g. nuclear pore complexes.

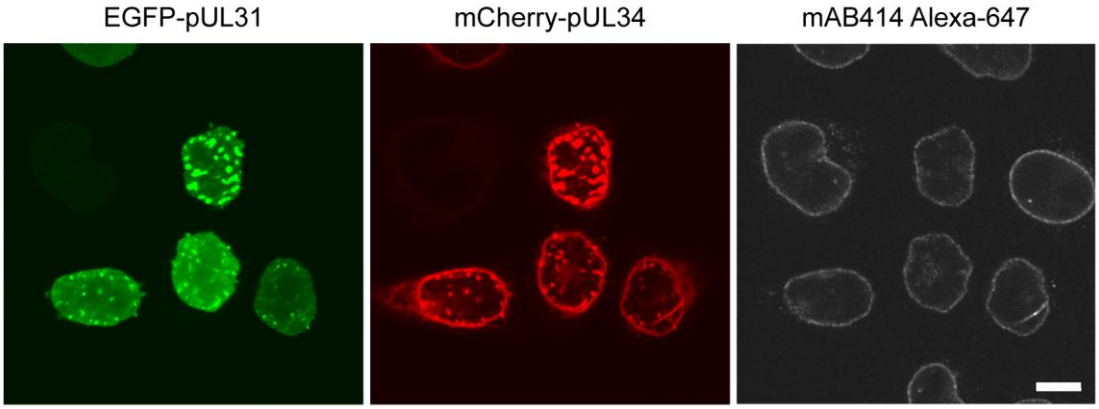

Figure 2.39: Nuclear pore complexes are not present in nuclear membrane patches when coexpressing pUL31 and pUL34
Cells were fixed with 4 % PFA and analysed with mab414 antibody (gray). Fluorescent signals of pUL31 and pUL34 colocalized in formed patches but no mAb414 signal was detected in patches formed, indicating that no NPCs are present. DNA was stained with DAPI. bars: 10 µm

To verify that the patches observed upon artificial transmembrane tethering of pUL31 are also not protein aggregates due to failed import of the proteins at nuclear pore complexes colabelling of NPCs was performed. Therefore, HeLa cells were transiently transfected for 24 hours with plasmids encoding pUL31 and pUL34. Cells were fixed with paraformaldehyde and immunostained again with mAB414. In this case coupling mAB414 to an Alexa-Fluor-546 labelled secondary antibody revealed that apparently no nuclear pore complexes are present in nuclear patches and more importantly most of the nuclear patches do not colocalize with the mAB414 signal indicating that no NPCs are present in nuclear spots at the membrane (Fig. 2.40) and also presumably patches are not formed upon protein aggregation of the pUL31 transmembrane constructs. Consistent with the previous results upon co-transfection with pUL31 and pUL34 (Fig. 2.39) as well as previous observations (Leuzinger et al., 2005) indicate a tight packing of proteins at sites where proteins interact. Thereby excluding large protein assemblies e.g. nuclear pore complexes from budding sites as well as from membrane proliferating sites also in the absence of pUL34 (Fig. 2.40).

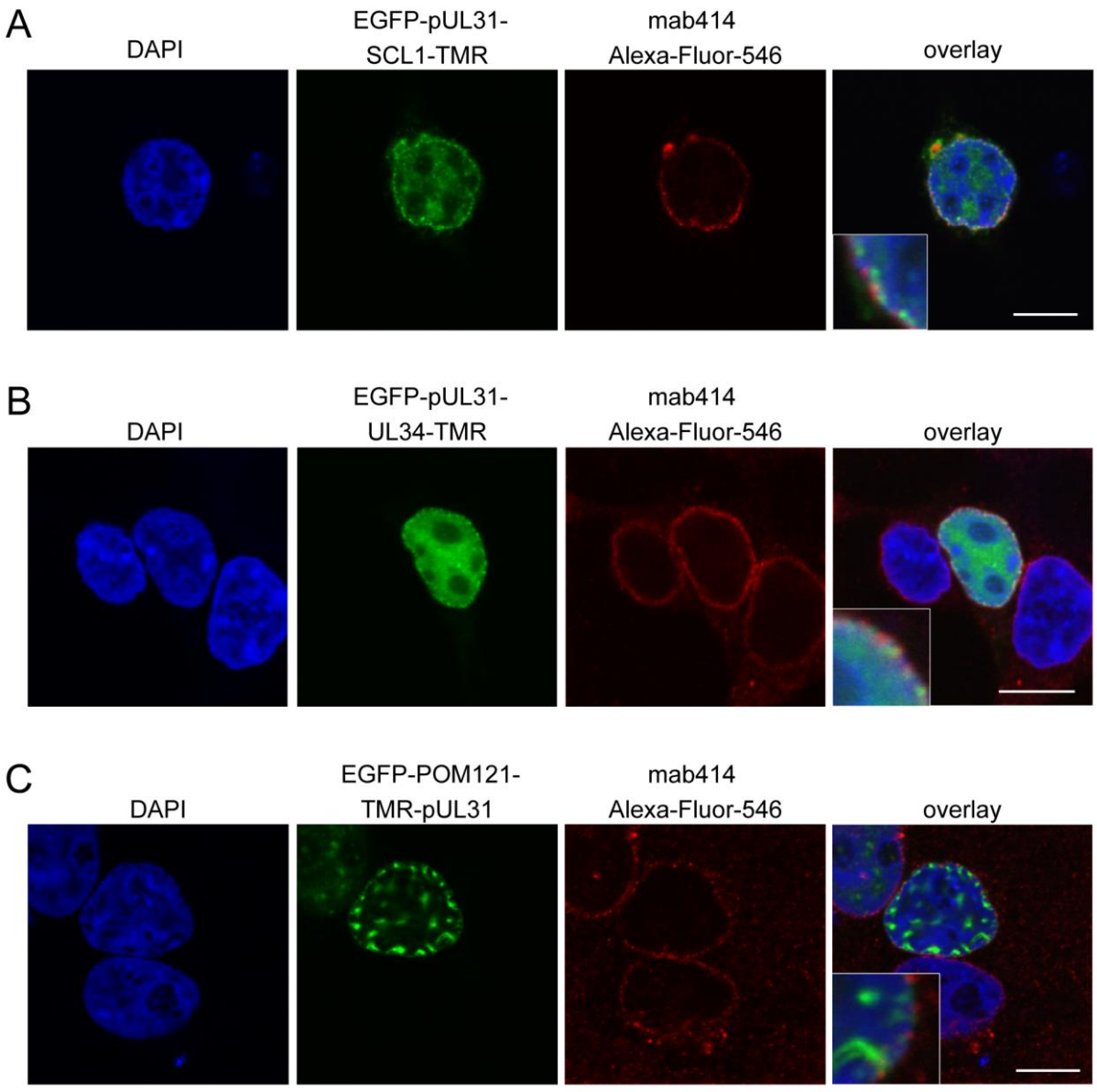

Figure 2.40: Nuclear pore complexes are not present in nuclear membrane patches when expressing chimeric TMR-pUL31 constructs
HeLa cells were transiently transfected with plasmids expressing transmembrane fusion constructs of pUL31 for 24 hours. Expression of constructs with a C-terminally fused transmembrane region (TMR) of pUL34 (aa 241-262) or SCL1 (aa 77-97) (A and B) as well as a N-terminally fused TMR of Pom121 (aa 1-50) together with an inner nuclear membrane localisation signal of rat gp210 (C) resulted in a mostly nuclear membrane localisation and patch formation. Cells were fixed with 4 % PFA and analysed with mab414 antibody (red). Fluorescent signals of the TMR-constructs of pUL31 and mAB414 did mostly not colocalize at the nuclear periphery and no mAb414 signal was detected in patches formed, indicating that no NPCs were present in patches. DNA was stained with DAPI. bars: 10 µm

Nuclear spots observed upon transfection of pUL31/pUL34 or when transmembrane pUL31 fusion constructs were transfected no clear structures or the origin of these spots was definable. Therefore, ultrastructural analyses using transmission electron

microscopy was performed to exclude nuclear spots are protein aggregation. Additional, it was verified that these spots contain membrane vesicles located between the inner and outer nuclear membrane. HEK293T cells were transiently transfected for 24 hours with plasmids expressing pUL31 or pUL34 as well as co-transfection of both. Also plasmids expressing transmembrane fusion constructs of pUL31 were transfected. Cells were fixed and stained with Osmium Tetroxide (OsO_4) and uranyl acetate (UAc) followed by subsequent embedding in EPON. Thin sections of cells were generated and imaged using a Tecnai G20 transmission electron microscope.

Electron microscopy revealed that upon co-expression of pUL31 and pUL34 indeed vesicles form in the perinuclear space between the inner and outer nuclear membrane accompanied by increased spacing between the nuclear membranes (Fig. 2.40A), consistent with previous findings (Klupp et al., 2007). In addition, a strong nuclear membrane proliferation was observed (Fig. 2.43A). A similar membrane proliferation phenotype was shown for homologues of pUL31/pUL34 (Luitweiler et al., 2013; Gonella et al., 2005; Lake et al., 2004). Expression of pUL31 only in HEK293T cells did not result in vesicle formation or increased spacing between the membranes nor does expression of pUL34 alone (Fig. 2.41). Furthermore, pUL34 expression induced stacked membrane arrays probably in response to overexpression (Fig. 2.41).

Interestingly, expression of transmembrane fusion constructs of pUL31 was sufficient to form vesicles between the inner and outer nuclear membrane (Fig. 2.42B-D) confirming that pUL31 alone is sufficient to remodel and induce vesicle formation in nuclear membranes when artificially tethered.

In addition, expressing pUL31 and pUL34 together as well as pUL31 transmembrane constructs induced formation of membrane structures similar to reported *organized smooth ER* (OSER) / karmellae, stacked arrays of proliferated nuclear membrane associated membranes (Fig. 2.43) (Snapp et al., 2003).

These structures were induced due to interactions between transmembrane anchored proteins indicating self-interaction of pUL31 or pUL31/pUL34 complexes in endoplasmic membranes.

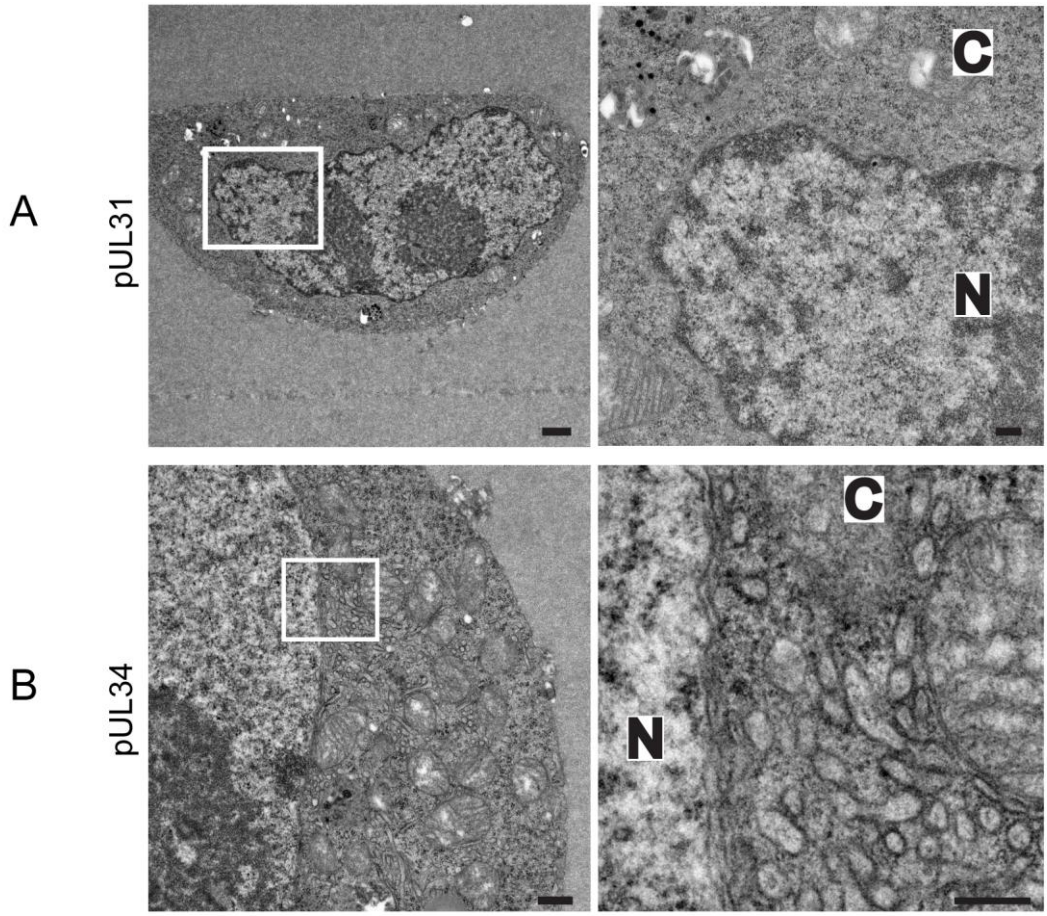

Figure 2.41: Electron microscopy of single transfected HEK293T cells
HEK293T cell were transiently transfected with either pUL31 (A) or pUL34 (B) for 24 hours. No membrane alterations were observed upon single transfection with pUL34. Transfection of pUL34 only in HEK293T induced membrane proliferation upon overexpression of the membrane protein. The nucleus (**N**) and cytoplasm (**C**) are marked. bars: A (left panel) 2 µm, A (right panel) in 200 nm; B (left panel) 0.5 µm, B (right panel) in 250 nm

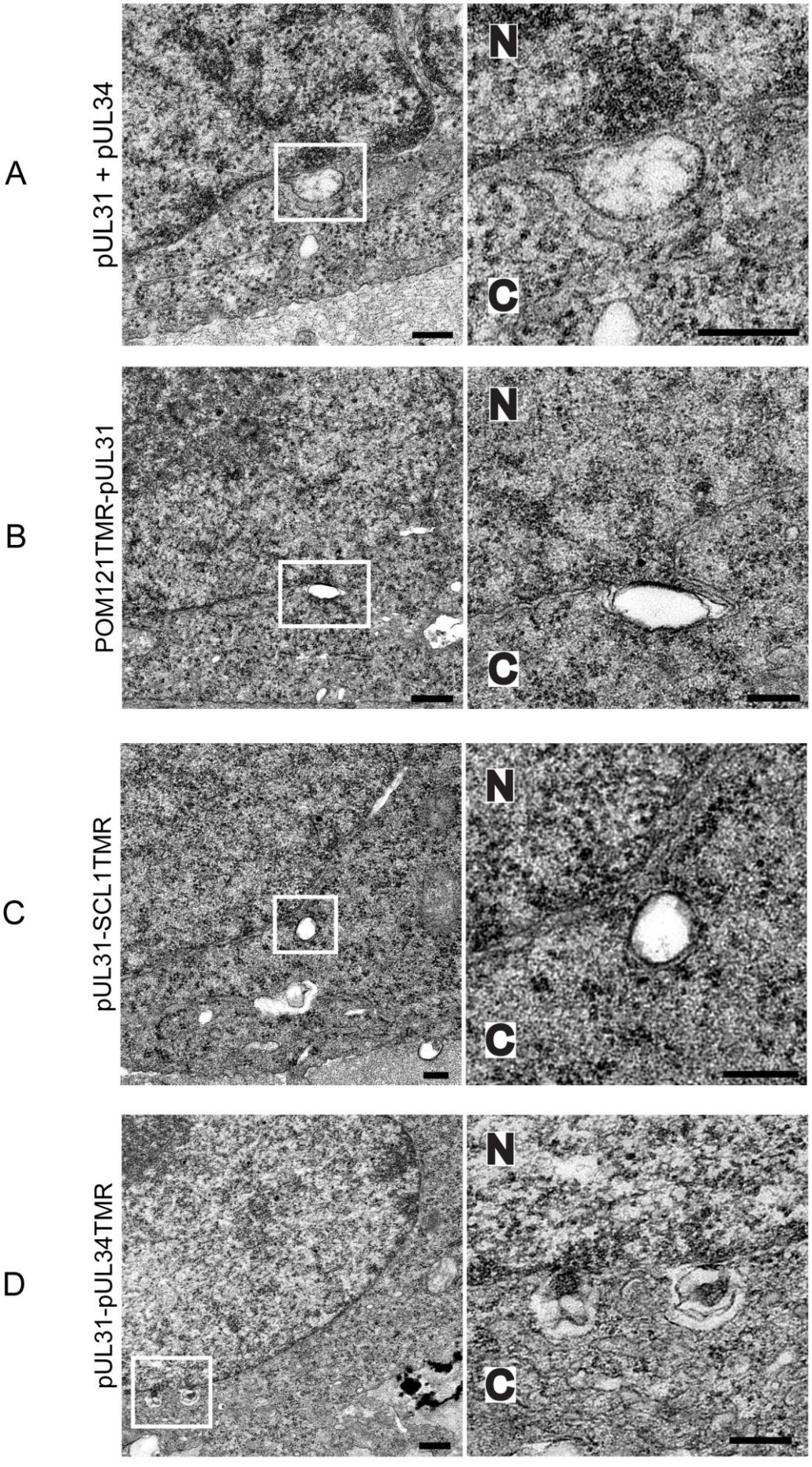
A
pUL31 + pUL34
N
C
B
POM121TMR-pUL31
N
C
C
pUL31-SCL1TMR
N
C
D
pUL31-pUL34TMR
N
C

Figure 2.42: Electron microscopy of transfected HEK293T cells showed vesicle formation upon co-transfection of pUL31 and pUL34 as well as pUL31 transmembrane constructs

HEK293T cell were transiently transfected for 24 hours with either pUL31 or pUL34 or artificial pUL31 transmembrane constructs for 24 hours. Vesicle formation between the inner and outer nuclear membrane was observed in all conditions with the size of about 200 nm (A-D). Right panels are magnifications of the white boxes in the left panel. The nucleus (**N**) and cytoplasm (**C**) are marked. bars: A-D (200 nm), D left panel 500 nm

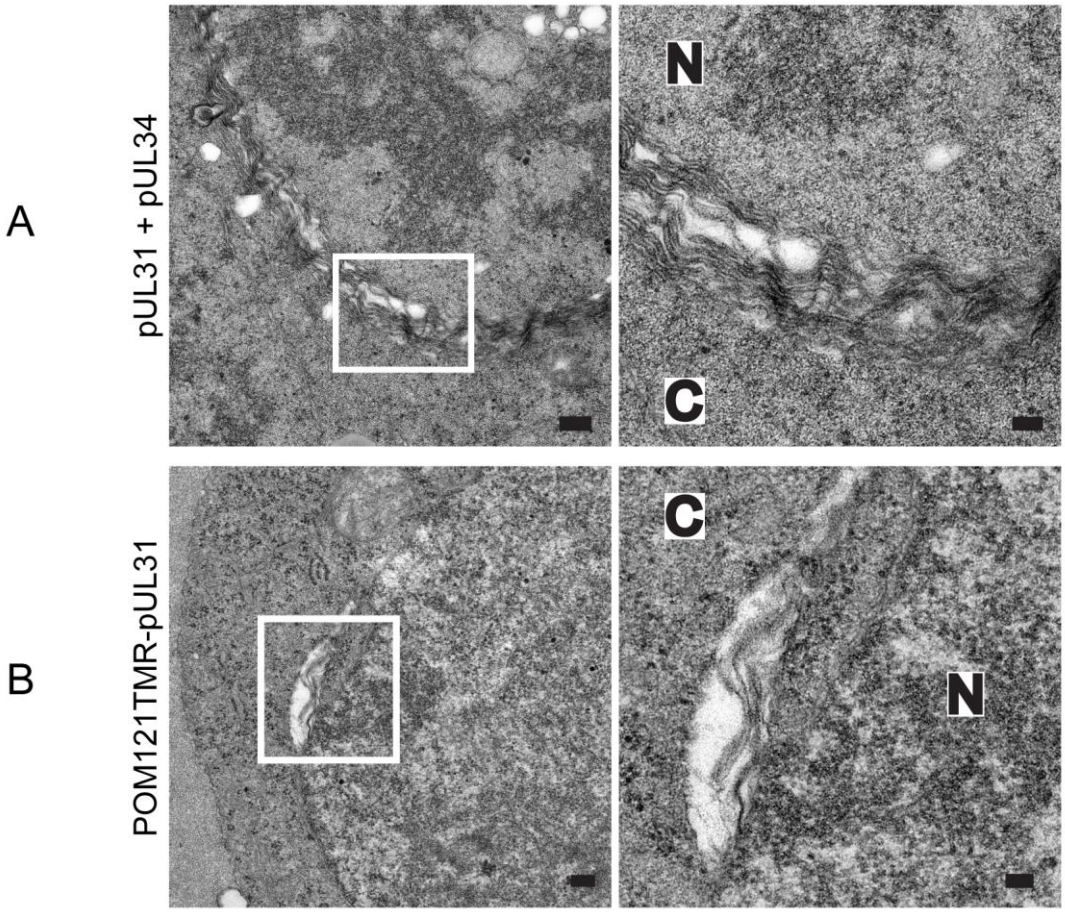

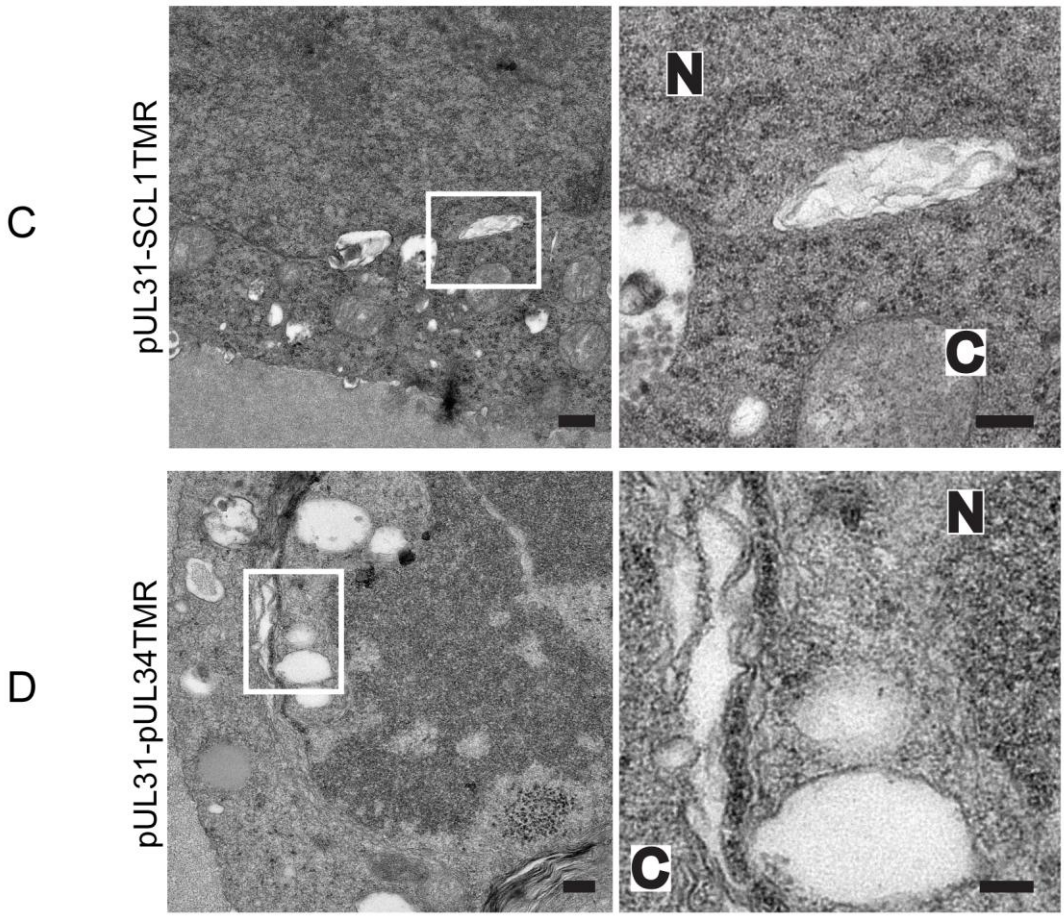

Figure 2.43: Electron microscopy of transfected HEK293T cells showed membrane proliferation upon co-transfection of pUL31 and pUL34 as well as pUL31 transmembrane constructs
HEK293T cell were transiently transfected with either pUL31 or pUL34 or artificial pUL31 transmembrane constructs for 24 hours. Membrane proliferation and increased spacing between the inner and outer nuclear membrane was observed in all conditions (A-D). Right panels are magnifications of the white boxes in the left panel. The nucleus (N) and cytoplasm (C) are marked. Bars: A, B and D (left panel 200 nm, right panel 100 nm), C (left panel 500 nm, right panel 250 nm)

2.1.23 Mutational analysis of conserved residues in pUL31 constant region affects pUL34 interaction in cells

The results obtained from mutational analysis of the first constant region in pUL31 using the GUV system (Fig. 2.27, Fig. 2.31, Fig. 2.32) were verified in a cellular context. Therefore, pUL31 mutants were transfected individually or co-transfected with pUL34 (Fig. 2.45-2.51) and pUL31 recruitment to the nuclear periphery was quantified (Fig. 2.52).

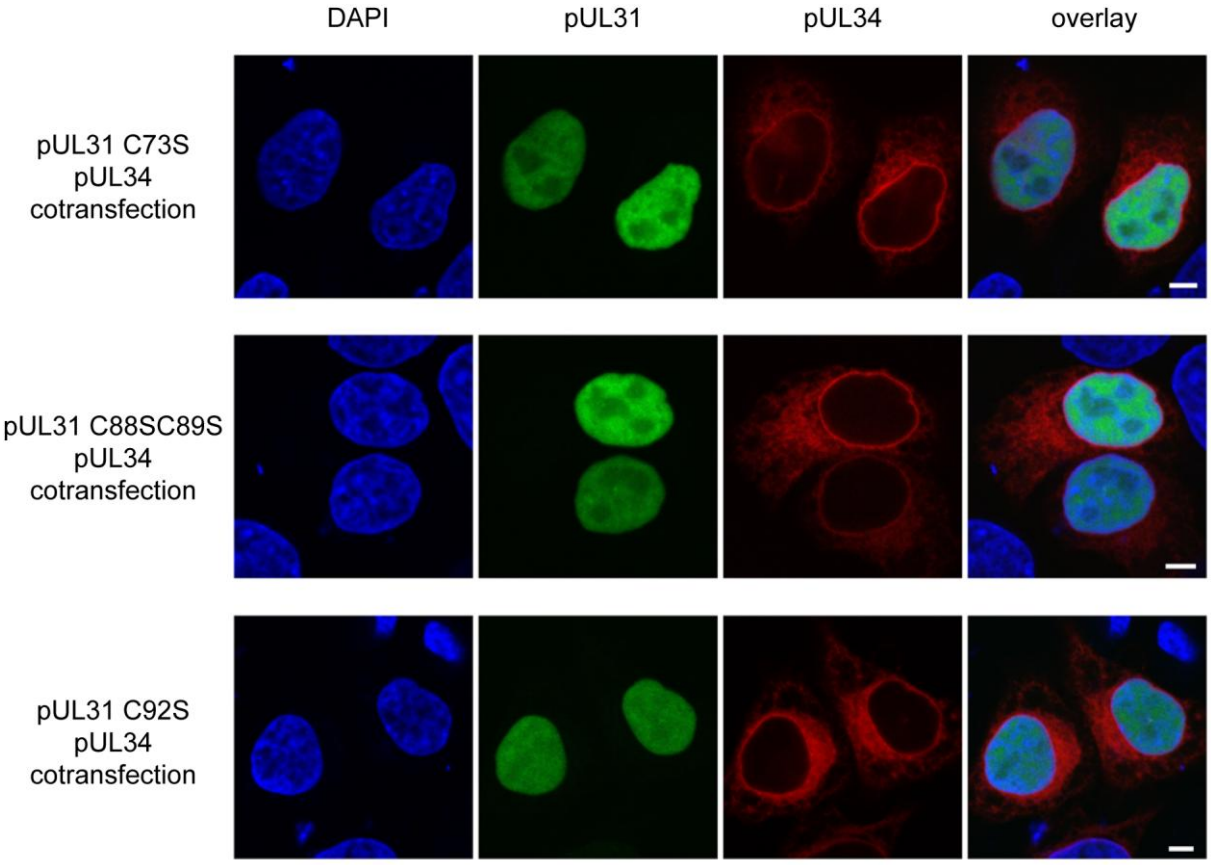

Figure 2.44: pUL34 and the pUL31 cysteine mutants do not colocalize and do not form patches

Hela cells were transiently transfected with plasmids expressing the EGFP-pUL31 cysteine C73S, C88SC89S and C92S mutants cotransfected with mCherry-pUL34. Expression of all pUL31 cysteine mutants together with pUL34 resulted in no recruitment of the pUL31 mutant to the nuclear membrane and no patch formation was observed. DNA was stained with DAPI. bars: 5 µm

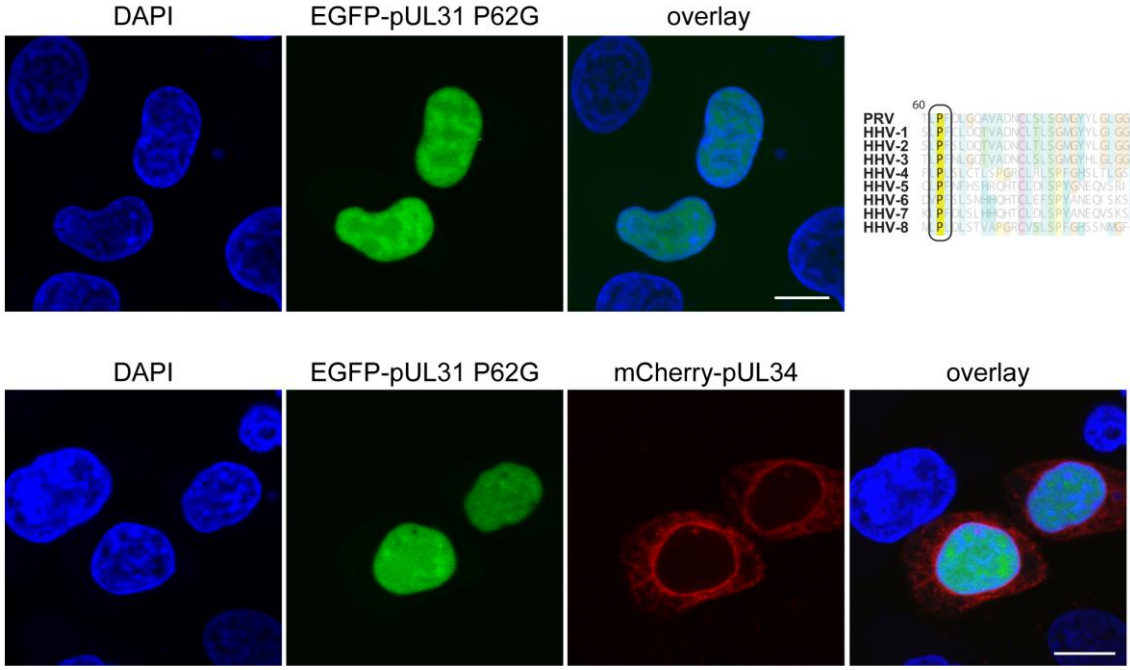

Figure 2.45: pUL34 and the pUL31 mutant P62G do not colocalize and do not form patches

Hela cells were transiently transfected with plasmids expressing either the EGFP-pUL31 P62G mutant alone or cotransfected with mCherry-pUL34. Expression of pUL31 P62G only shows an exclusively nucleoplasmic localisation while expression of pUL34 gives an ER and nuclear membrane localisation as shown before. Coexpression of both proteins leads to no recruitment of the pUL31 mutant to the nuclear membrane and no patch formation was observed. DNA was stained with DAPI. bars: 10 µm

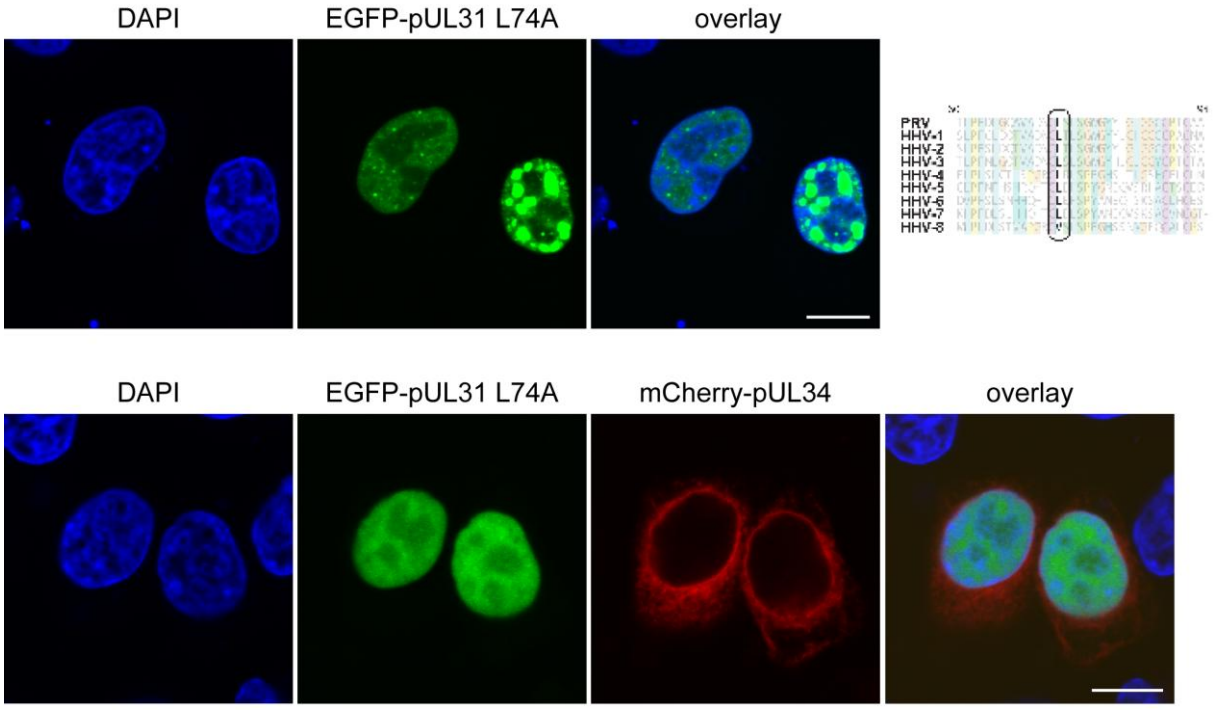

Figure 2.46: pUL34 and the pUL31 mutant L74A do not colocalize and do not form patches

HeLa cells were transiently transfected with plasmids expressing either the EGFP-pUL31 L74A mutant alone or cotransfected with mCherry-pUL34. Expression of pUL31 L74A only shows an exclusively nucleoplasmic localisation with partial protein aggregation while expression of pUL34 gives a ER and nuclear membrane localisation as shown before. Co-expression of both proteins leads to no recruitment of the pUL31 mutant to the nuclear membrane and no patch formation was observed. DNA was stained with DAPI. bars: 10 µm

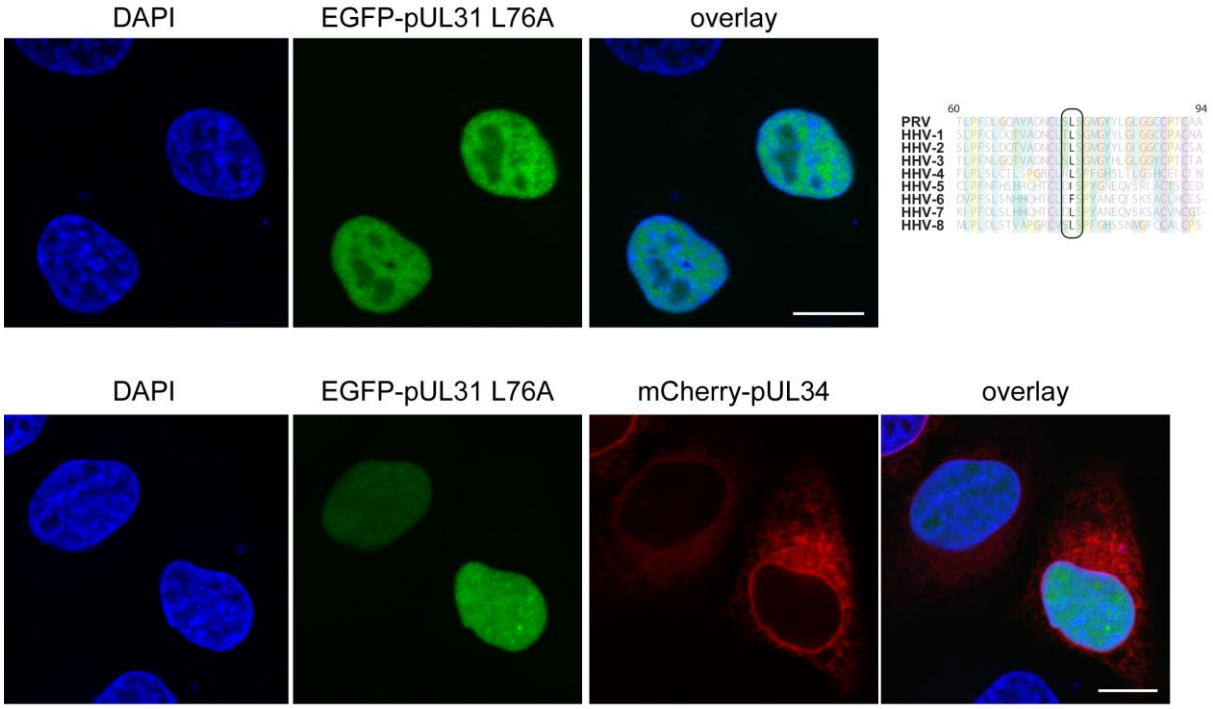

Figure 2.47: pUL34 and the pUL31 mutant L76A do not colocalize and do not form patches

HeLa cells were transiently transfected with plasmids expressing either the EGFP-pUL31 L76A mutant alone or cotransfected with mCherry-pUL34. Expression of pUL31 L76A only shows an exclusively nucleoplasmic localisation with partial protein aggregation while expression of pUL34 gives an ER and nuclear membrane localisation as shown before. Co-expression of both proteins leads to no recruitment of the pUL31 mutant to the nuclear membrane and no patch formation was observed. DNA was stained with DAPI. bars: 10 µm

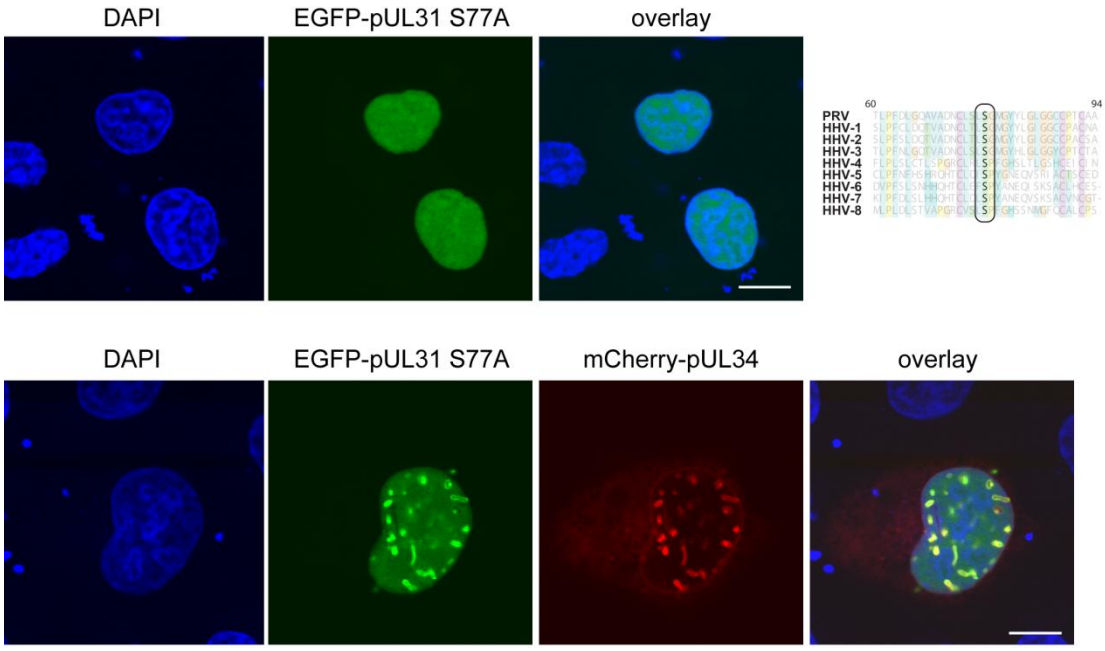

Figure 2.48: pUL34 and the pUL31 mutant S77A do colocalize and form patches
HeLa cells were transiently transfected with plasmids expressing either the EGFP-pUL31 S77A mutant alone or co-transfected with mCherry-pUL34. Expression of pUL31 S77A only shows an exclusively nucleoplasmic localisation while expression of pUL34 gives a ER and nuclear membrane localisation as shown before. Coexpression of both proteins results in recruitment of the pUL31 mutant to the nuclear membrane and patch formation was observed albeit reduced compared to wild-type pUL31. DNA was stained with DAPI. bars: 10 µm

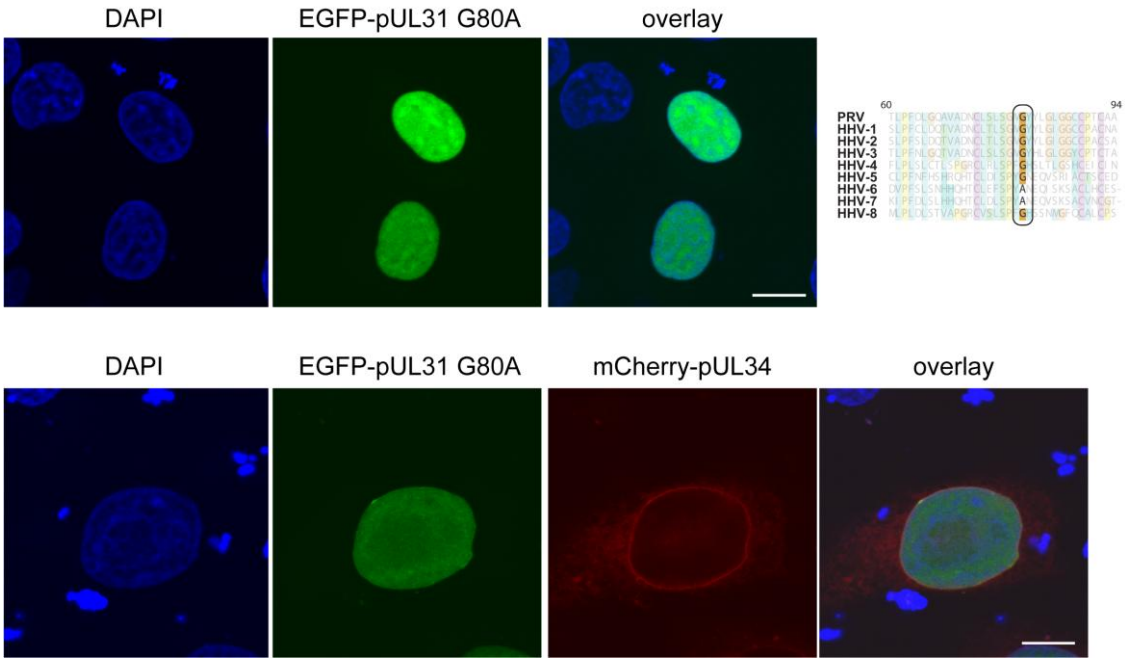

Figure 2.49: pUL34 and the pUL31 mutant G80A do colocalize and not form patches
HeLa cells were transiently transfected with plasmids expressing either the EGFP-pUL31 G80A mutant alone or cotransfected with mCherry-pUL34. Expression of pUL31 G80A only shows an exclusively nucleoplasmic localisation while expression of pUL34 gives a ER and nuclear membrane localisation as shown before. Coexpression of both proteins leads to recruitment of the pUL31 mutant to the nuclear membrane and no patch formation was observed compared to wild-type pUL31. DNA was stained with DAPI. bars: 10 µm

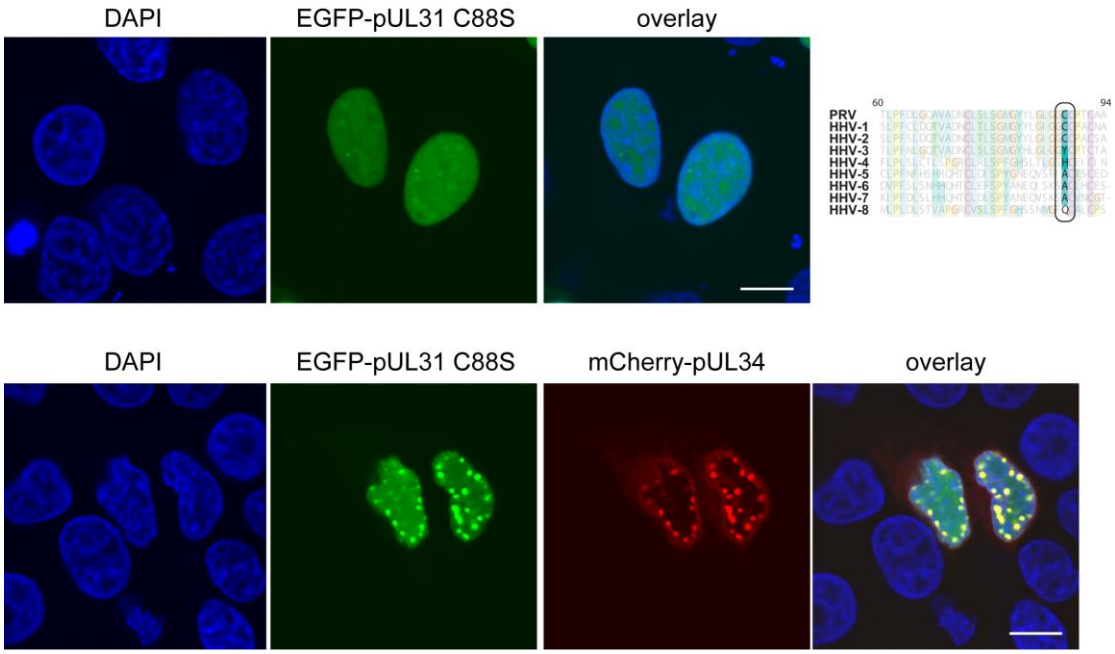

Figure 2.50: pUL34 and the pUL31 mutant C88S do co-localize and form patches
HeLa cells were transiently transfected with plasmids expressing either the EGFP-pUL31 C88S mutant alone or co-transfected with mCherry-pUL34. Expression of pUL31 C88S only shows an exclusively nucleoplasmic localisation while expression of pUL34 gives a ER and nuclear membrane localisation as shown before. Co-expression of both proteins leads to recruitment of the pUL31 mutant to the nuclear membrane and intensive patch formation was observed. DNA was stained with DAPI. bars: 10 µm

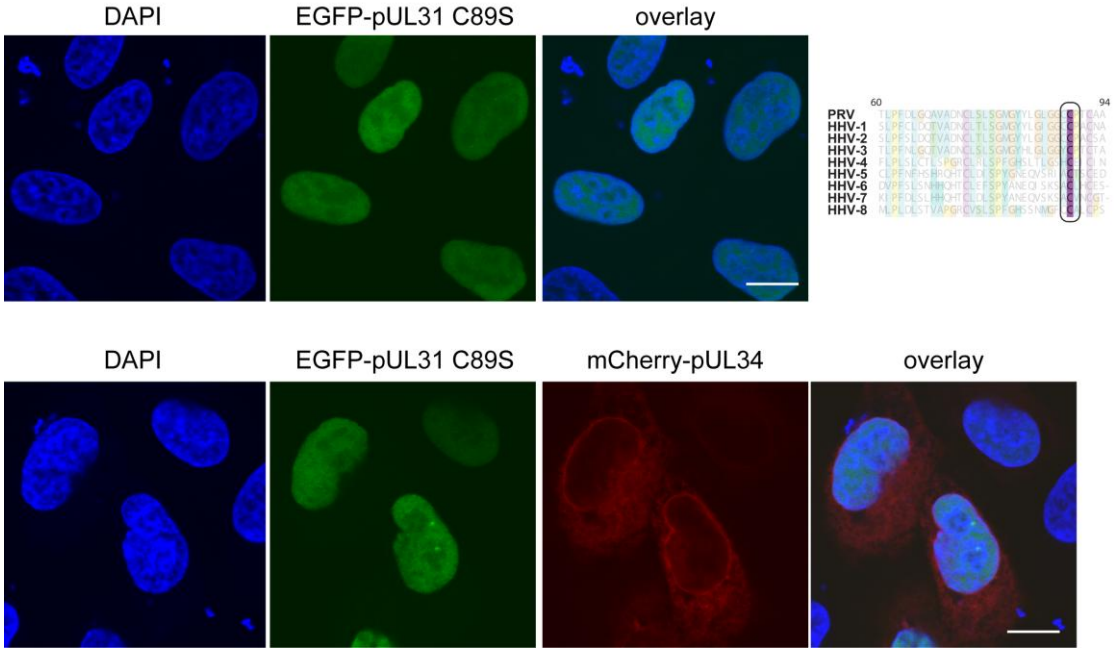

Figure 2.51: pUL34 and the pUL31 mutant C89S do not colocalize and do not form patches
HeLa cells were transiently transfected with plasmids expressing either the EGFP-pUL31 C89S mutant alone or cotransfected with mCherry-pUL34. Expression of pUL31 C89S only shows an exclusively nucleoplasmic localisation while expression of pUL34 gives a ER and nuclear membrane localisation as shown before. Coexpression of both proteins results in no recruitment of the pUL31 mutant to the nuclear membrane and no patch formation was observed. DNA was stained with DAPI. bars: 10 µm

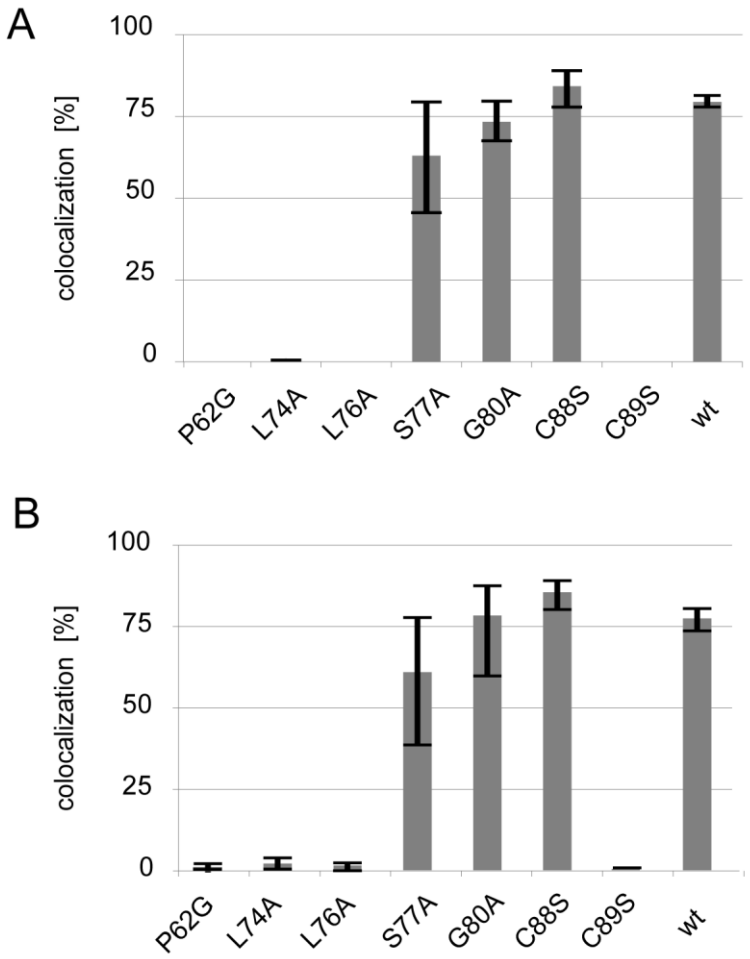

Figure 2.52: Quantification cells expressing pUL34 and pUL31 mutants
HeLa (A) and HEK293T (B) cells were transiently transfected for 24 hours with plasmids expressing mCherry-pUL34 and EGFP-pUL31 single point mutants. Cells expressing both proteins were counted and analysed for membrane recruitment of EGFP-pUL31 to the nuclear membrane. Error bars represents the mean (-/+ SEM) of three independent experiments. For each experiment and condition at least 100 cells were counted.

Mutational analysis of single residues in the first constant region of pUL31 verified the relevance of conserved amino acids, most importantly the conserved cysteine residues in position 73, 88, 89 and 92 of pUL31 appear to be essential in mediating

pUL34 binding (Fig. 2.27, Fig. 2.28, Fig. 2.32) as mutation to serines blocks pUL34 interaction (Fig. 2.44) and membrane remodeling in GUVs (Fig. 2.32). Interestingly, separating the C88SC89S double mutation to individual serine mutations revealed that at least the cysteine in position 89 is crucial for membrane remodelling in GUVs (Fig. 2.32) and pUL34 binding in HeLa cells (Fig. 2.51) while the cysteine in position 88 appears not to be essential to promote membrane remodelling in the GUV system (Fig. 2.32) and pUL34 binding in a cellular context (Fig. 2.50) as mutation to serine to do not result in reduced recruitment to the nuclear envelope (Fig. 2.52).

The results obtained in the GUV system could be confirmed also in a cellular context indicating a functional role of the cysteines in the first constant region for membrane remodelling and pUL34 binding of pUL31. Both functions of pUL31, namely pUL34 binding and membrane remodelling, could not be separated by the cysteine mutations of individual residues in this part of pUL31.

Additional mutations in the first constant region (Table 2.1) were also so far not sufficient to separate these functions. An interesting candidate for further analysis might be the glycine to alanine mutation in position 80 of pUL34 as cotransfection of both proteins results in colocalization but no nuclear membrane spot formation. Artificial recruitment of the G80A mutant to Ni-DGS containing GUVs shows membrane remodelling activity of this mutant (Fig. 2.32). Thus, pUL31 CR1 single point mutants need to be analyzed in further pull down experiments and in the pUL34 GUV binding assay.

2.2. Nup153 recruits the Nup107-160-complex to the inner nuclear membrane

Nuclear pore complexes (NPCs) are large, the inner and outer nuclear membrane-spanning protein complexes. The number of nuclear pores varies depending on the size and metabolic activity of the cell between 3000-5000 per nucleus in vertebrates and about 190 in yeast. In interphase NPCs are doubled in preparation for a new cell division. How these huge protein assemblies are embedded in interphase in an intact nuclear envelope remains largely unknown. However, it is assumed that the outer and inner nuclear membranes are contacted by local deformation and come in close proximity to fuse at these sites. Nucleoporins are inserted in these spots and form ultimately a functional nuclear pore. Factors mediating the curvature of the nuclear membranes and whether components of the nuclear pore complexes are directly involved in this deformation processes are unknown.

Different scenarios can be assumed resulting in approximation of the inner and outer nuclear membrane. This could involve integral membrane proteins inducing membrane curvature and fusion. Furthermore, it can be assumed that cytoplasmic or nucleoplasmic soluble proteins can induce local membrane curvature. Nevertheless, interphasic NPC assembly remains largely enigmatic.

NPC assembly at the end of mitosis and in interphase requires the Nup107-160-complex (Y-complex) as an important structural component of the NPC (Doucet et al., 2010; D'Angelo et al., 2006; Harel et al., 2003; Walther et al., 2003). In postmitotic NPC assembly at the end of mitosis the Y-complex is recruited to the chromatin by MEL28/ELYS (Gillespie et al., 2007; Rasala et al., 2006) while interphasic NPC assembly does not require MEL28/ELYS (Doucet et al., 2010). Most likely NPC assembly in interphase has to begin at the nuclear membranes (Doucet et al., 2010; Dultz & Ellenberg, 2010; Rothballer & Kutay, 2013; Vollmer et al., 2012) but how this is performed remains largely unknown. Here the GUV system was used to analyze the specific role of the nucleoporin Nup153 in interphasic NPC assembly. This was done in collaboration with PD Dr. Wolfram Antonin and Benjamin Vollmer.

2.2.1 Nup153 interacts via its N-terminus directly with membranes

Sequence analysis within Nup153's N-terminus (Fig. 2.53A) identified a, within vertebrates, conserved region that might form an amphipathic helix depicted in the helical wheel presentation (Fig. 2.53B). This amphipathic helix could be responsible for Nup153 recruitment to the nuclear envelope. A point mutation was generated (valine-50 to glutamate, V50E) which predictably disrupts the hydrophobic surface of the helix. So far it is not clear how Nup153 is recruited to the inner nuclear membrane. To test if the membrane interaction is direct, the recombinant and purified N-terminal region of *Xenopus laevis* Nup153 (aa 1-149) was incubated with giant unilamellar vesicles with a nuclear envelope lipid composition. Upon addition of the EGFP-tagged N-terminus of Nup153 to GUVs it was efficiently recruited to the vesicle membrane indicating direct membrane interaction (Fig. 2.53C, left row). The V50E mutant (Fig. 2.53C, right row) did not bind to GUVs confirming that an amphipathic helix is required for membrane binding. Similarly recombinant EGFP as control did not bind the limiting GUV membrane. Additionally when transfected in HeLa cells the EGFP fused N-terminus of *Xenopus laevis (*xl*)* Nup153 localized to the nuclear envelope presumably the inner nuclear membrane (Fig. 2.53E). The expression also induced nuclear envelope proliferation which is typical for membrane interacting proteins (Prufert et al., 2004; Ralle et al., 2004) and has been previously observed when overexpressing full-length Nup153 (Bastos et al., 1996). The V50E mutation abolished nuclear envelope localization and membrane proliferation also in transfected cells (Fig. 2.53E). Instead, the protein localized to the nucleoplasm indicating that also in cells the mutation is sufficient to prevent membrane interaction of Nup153's N-terminus.

Next the direct membrane binding was confirmed for the full-length Nup153. Low expression yield of the *Xenopus laevis* protein resulted in usage of the human orthologue.

When the fluorescently labeled protein was added to nuclear envelope GUVs it was also efficiently recruited to membranes (Fig. 2.53D). The corresponding mutant (valine-47 to glutamate in the human protein, Nup153hs V47E) abrogated Nup153 membrane interaction.

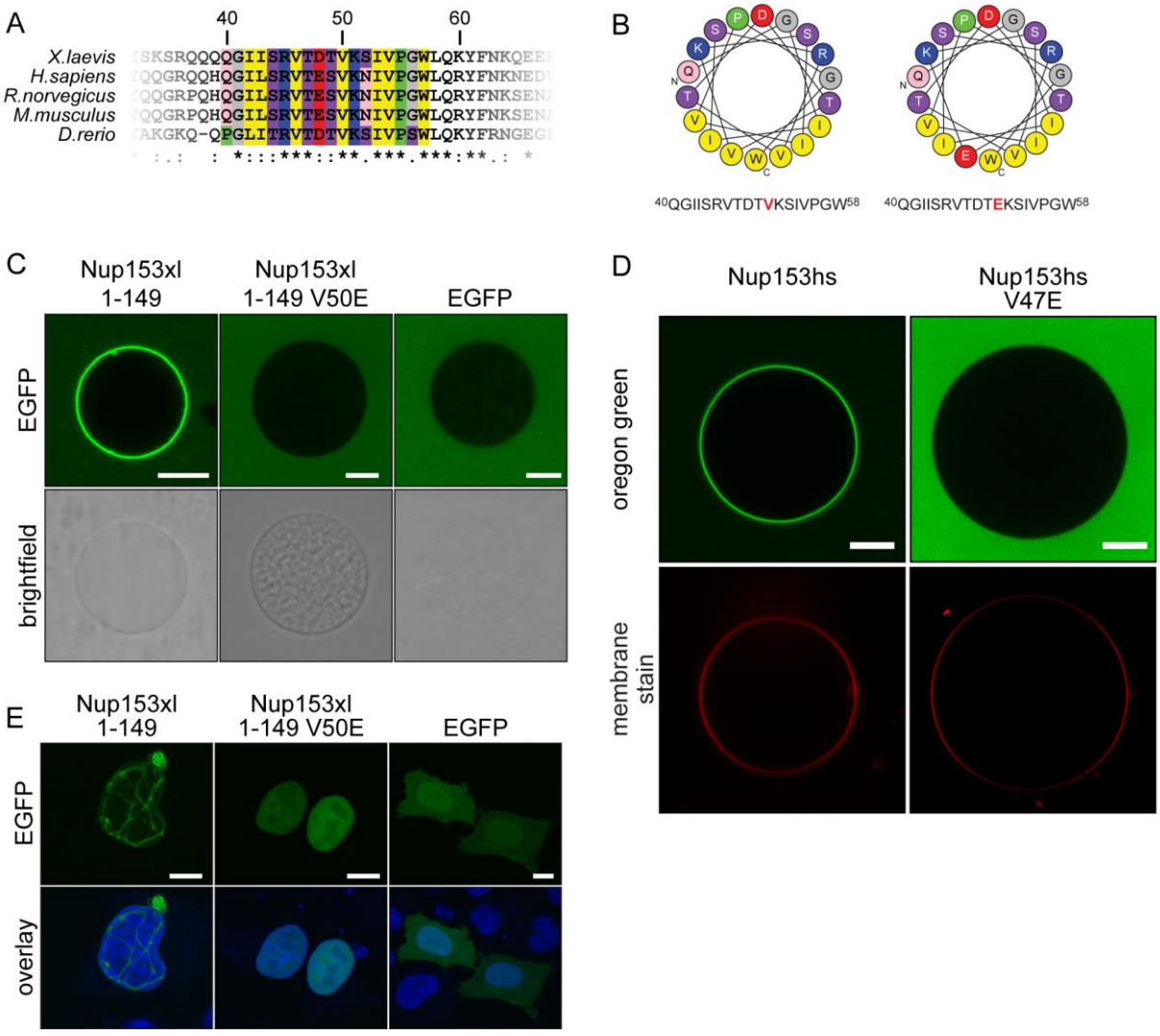
A
40
50
60
X.laevis
H.sapiens
R.norvegicus
M.musculus
D.rerio
B
40QGIISRVTDTVKSIVPGW58
40QGIISRVTDTEKSIVPGW58
C
Nup153xl 1-149
Nup153xl 1-149 V50E
EGFP
EGFP
brightfield
D
Nup153hs
Nup153hs V47E
oregon green
membrane stain
E
Nup153xl 1-149
Nup153xl 1-149 V50E
EGFP
EGFP
overlay

Figure 2.53: Nup153 contains an N-terminal region, directing it to the nuclear membrane
Sequence alignment of vertebrate Nup153 N-terminus (aa 1-149) shows a conserved region presumably forming an amphipathic helix (helical wheel depiction, (A)). A single point mutation (valine-50 to glutamate), disrupts the hydrophobic surface (B). GUVs were generated with a NE lipid composition. EGFP-Nup153xl was added to GUVs and was efficiently recruited to the vesicle membrane indicating direct membrane interaction (C). No binding was observed when the V50E mutant or EGFP was added to the GUVs (C).
The human orthologue of Nup153 was Oregon green 488 labeled and added to GUVs. It was also efficiently bound to GUV membranes (D). The corresponding single point mutation (valine-47 to glutamate) also disrupted membrane interaction.
HeLa cells were transiently transfected with constructs expressing EGFP-Nup153 (of *Xenopus laevis*) for 24 hours. Nup153 showed an almost exclusive NE localization, presumably the inner nuclear membrane and nuclear membrane proliferation (E). Transfection of the V50E mutation results in a blocked NE localization and membrane proliferation. Additionally, the mutant protein shows increased nucleoplasmic localization indicating blocked membrane interaction. bars: 10 µm in C and D, 5 µm in E

2.2.2 Depletion of Nup153 induces NPC clustering

By employing nuclear assembly using *Xenopus laevis* egg extract, a NE forms around the decondensing chromatin in a process resembling the reassembly of the nucleus at the end of mitosis (Gant & Wilson, 1997). Nup153 was depleted from egg extract. When Nup153 was depleted, the protein was absent from the nuclear rim confirming the depletion efficiency. The assembled nuclei contained a closed NE with NPCs that were unevenly distributed. This NPC clustering phenotype upon Nup153 depletion has been previously observed (Walther et al., 2001) and can be visualized by surface rendering of confocal stack images of assembled nuclei (Fig. 2.54, right row). Adding back recombinant Nup153 to endogenous levels rescued the NPC clustering phenotype demonstrating its specificity (Fig. 2.54, left row). NPC clustering was also rescued by the Nup153 membrane-binding mutant (V47E) (Fig. 2.54, left row), which indicates that the Nup153 membrane interaction is not required for proper NPC spacing in the nuclear envelope.

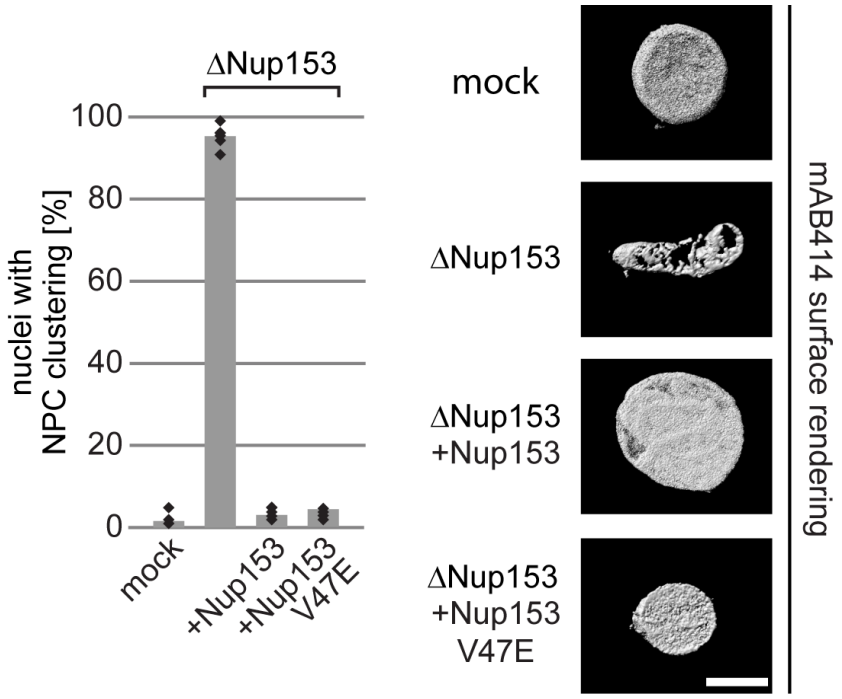

Figure 2.54: Depletion of Nup153 results in NPC clustering.
Nuclei were assembled under mock conditions and using Nup153 depleted *Xenopus* egg extract. Addback of recombinant Nup153 rescued the NPC clustering phenotype. Also addback of the Nup153 membrane-binding mutant (V47E) rescued the NPC clustering phenotype indicating that the membrane interaction is not important for proper NPC spacing. Quantification was done by counting at least 100 randomly chosen chromatin substrates in six independent experiments. The right panel shows surface renderings of confocal stacks of mAB414 labeled nuclei. Bars: 10 µm

2.2.3 Nup153 is necessary for interphasic NPC assembly

To test whether interphasic NPC assembly was affected by Nup153 depletion nuclei were assembled for 120 min and individual NPCs were counted using mAB414 staining (D'Angelo et al., 2006; Vollmer et al., 2012). Addition of 2 µM importin-β, which is known to block interphasic NPC assembly (D'Angelo et al., 2006), to nuclei resulted in a reduction in the number of NPCs per nucleus by about 50 %. Depletion of Nup153 caused a reduction in NPC number, which was not further affected by the addition importin-β. Re-addition of wild type Nup153 but not the membrane binding deficient V47E mutant rescued the reduced number of NPCs formed (Fig. 2.55). This suggests that NPC formation during interphase requires Nup153 and the ability to bind the NE.

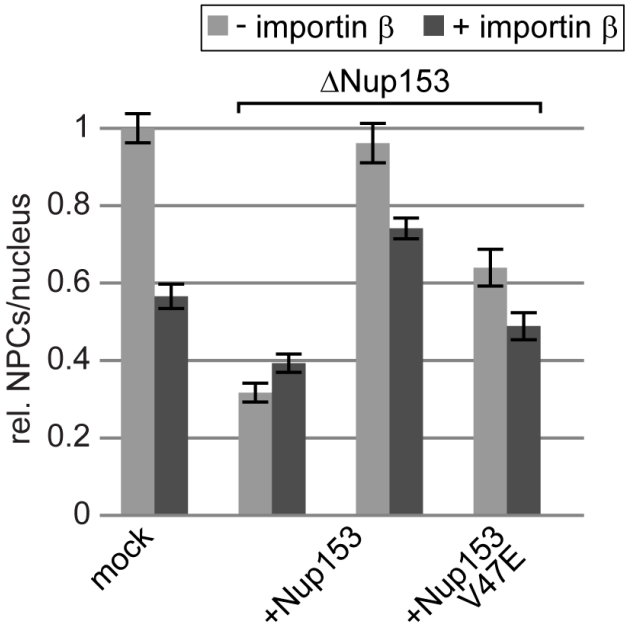

Figure 2.55: Nup153 membrane interaction is important for interphasic NPC assembly
Nuclei assembled were fixed after 120 min and NPC numbers per nucleus counted based on mAB414 staining. Where indicated, interphasic NPC assembly was blocked by importin β addition after 50 min (average from a total of 30 nuclei in 3 independent experiments, normalized to the mock control, error bars are SEM).

2.2.4 Artificial recruitment of the Y-complex to membranes bypasses the presence of Nup153

The membrane binding ability of Nup153 is important for interphasic NPC assembly. As Nup153 binds the Nup107-160 complex (Y-complex) forming the cytoplasmic and nucleoplasmic rings of the NPCs this could point to a recruitment of the Y-complex to the nuclear membranes. Also ran is a known interactor of Nup153 and is required for interphasic NPC assembly (D'Angelo et al., 2006; Doucet et al., 2010). Ran could be important by inducing a release of import receptors from potential targets required for NPC assembly. It was investigated if artificial recruitment of the Y-complex via the Y-complex binding region of Nup153 to membranes can bypass the need of full length Nup153 and results in NPC assembly. Similarly it was assessed if recruitment of ran via the ran-binding site of Nup153 contributes to interphasic NPC assembly.
The Y-complex binding region (aa 210-338) or the ran binding region (aa 658-890) of human Nup153 were each fused N-terminally to EGFP and at the C-terminus with the transmembrane protein SCL1, yielding EGFP-ycBD-SCL1 and EGFP-ranBD-SCL1 (Fig. 2.56A). SCL1 contains a C-terminal transmembrane region and efficiently

targets to the inner nuclear membrane (Theerthagiri et al., 2010). Both constructs were expressed in *E. coli*, purified and reconstituted into small liposomes. To test the functionality of the fusion proteins these liposomes were incubated with Y-complex purified from *Xenopus* egg extracts or recombinant ran and floated through a sucrose gradient. Liposomes containing the EGFP-ycBD-SCL1 protein efficiently bound the Y-complex but not ran and EGFP-ranBD-SCL1 liposomes bound ran but not the Y-complex (Fig. 2.56B). Similarly, when incorporated into GUVs, EGFP-ycBD-SCL1 recruited fluorescently labeled Y-complex to the GUV membrane and EGFP-ranBD-SCL1 recruited ran (Fig. 2.56C). To assess if Y-complex or ran recruitment by these artificial binding constructs restores interphasic NPC assembly, nuclei were assembled in mock or Nup153 depleted extracts supplemented with empty, EGFP-ycBD-SCL1 or EGFP-ranBD-SCL1 containing liposomes. Nuclei were fixed and NPC numbers were determined by mAB414 staining (Fig. 2.56D). When EGFP-yc-SCL1 was incorporated into the nuclear membrane this indeed restored interphasic NPC assembly upon Y-complex recruitment when Nup153 was depleted from the egg extract, while ran binding did not restored interphasic NPC assembly.

Thus, the presumable function of Nup153 in interphasic NPC assembly is to direct the Y-complex to the newly forming NPCs at the NE.

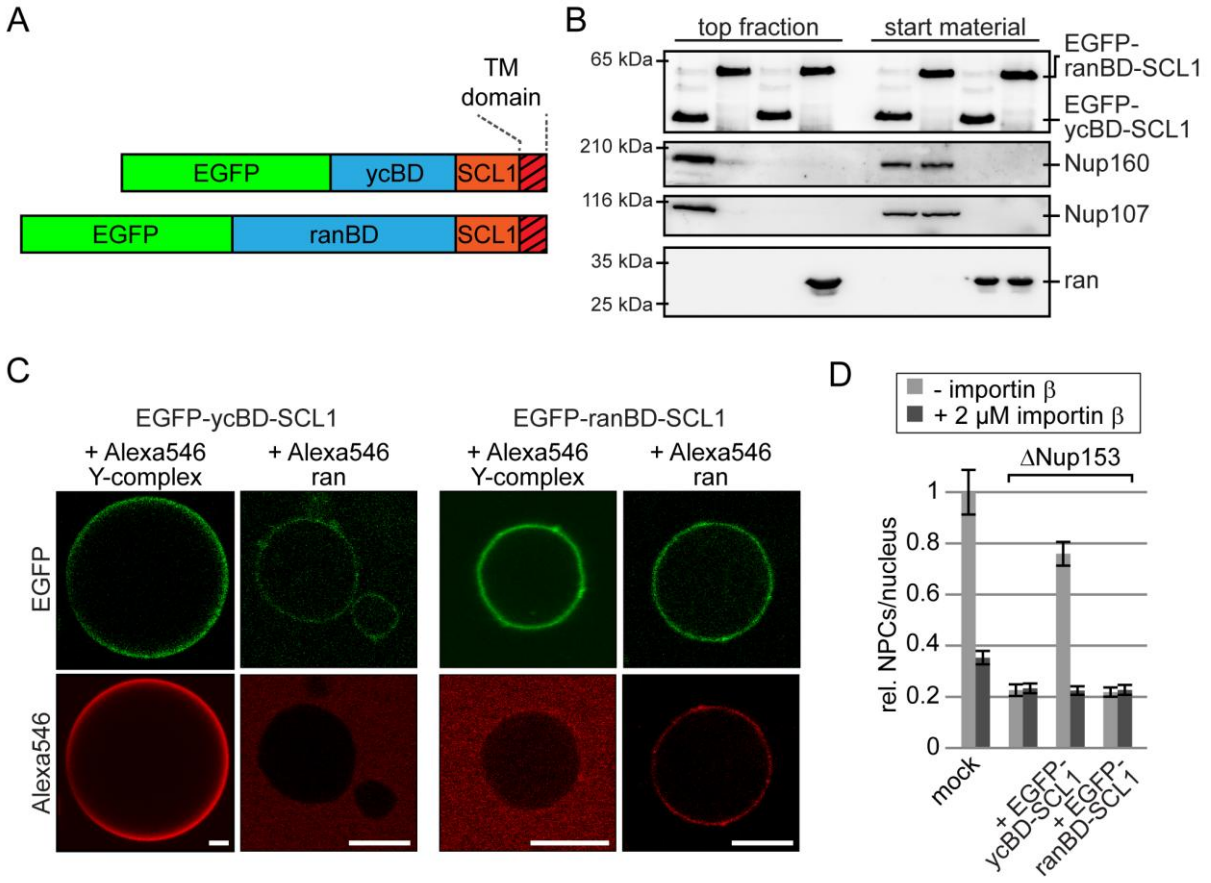

Figure 2.56: Recruitment of the Y-complex to membranes bypasses the presence of Nup153

Schematic representation of Nup153 fusion constructs indicating the Y-complex (aa 210-338) and the ran (aa 658-890) interacting region (blue), an N-terminal EGFP (green), and C-terminal inner nuclear membrane protein SCL1 (orange) yielding EGFP-ycBD-SCL1 or EGFP-ranBD-SCL1, respectively (A). To show binding of ran and the Y complex to the fusion constructs EGFP-ycBD-SCL1 or EGFP-ranBD-SCL1 were reconstituted into small unilamellar liposomes (SUVs) with a nuclear envelope lipid composition. Liposomes were incubated with purified *Xenopus* Y-complex or recombinant ran (start material 50% for the EGFP-ycBD-SCL1 or EGFP-ranBD-SCL1, 30 % for the Y-complex and ran) and top fractions were analyzed by western blotting using EGFP, Nup160, Nup107 and ran antibodies (B).
EGFP-ycBD-SCL1 or EGFP-ranBD-SCL1 were reconstituted into GUVs and Alexa-Fluor-546 labeled Y-complex or ran were efficiently recruited to the GUV membrane (C).
Nuclei were assembled in mock or Nup153 depleted extracts supplemented with empty, EGFP-ycBD-SCL1 or EGFP-ranBD-SCL1 containing liposomes. NPC numbers were determined using mAB414 staining of an average from 30 nuclei from three independent experiments, normalized to the mock control, error bars are SEM (D).

In summary, the data obtained by me and the data generated by PD Dr. Wolfram Antonin and Benjamin Vollmer reveals that Nup153 can bind to the inner nuclear membrane via its N-terminus and recruits the Y-complex to the newly assembling

pores. Thus, it appears that Nup153 is an important factor in interphasic NPC assembly.

.

3 Discussion

3.1 Nuclear membrane budding is induced by complex formation of two conserved herpesviral proteins

3.1.1 Giant unilamellar vesicles as a valuable tool to reconstitute membrane related processes

Cellular membranes are essential key components of living organisms as they are involved in many biological functions like endo- and exocytosis, transport and signaling. The study of membrane related processes is limited by the availability of suitable test systems. Cellular systems are generally employed but the complexity of cellular structures and functions as well as redundancy often prevents a detailed analysis of fundamental biological mechanisms at membranes.

Bottom up approaches come more and more into focus as they can overcome these limitations. Reconstituting cellular behavior by using a minimal set of components enables a new level of controllability in order to dissect their specific functions and requirements. In addition, they mostly enable visualization and tracking on a microscopically scale.

Up to now, many model membrane systems were developed to fulfill these requirements. These systems are therefore perfectly suited to address biochemical and biophysical issues. These artificial membrane systems include spherical vesicles of different sizes, lipid functionalized micro-beads, as well as planar lipids in supported lipid bilayers, nanodiscs or black-lipid-systems (Bayburt & Sligar, 2010; Heimburg, 2010; Borch & Haman, 2009; Castellana & Cremer, 2006; Ries et al., 2004). The selection of suitable systems depends on the issue and availability of the needed components.

Giant unilamellar vesicles (GUVs) are used here to mimic the nuclear envelope and to monitor membrane associated processes. As GUVs are vesicles consisting of one lipid bilayer and, due to their enormous size of up to 150 µm, they can be visualized by light microscopy. The generation of GUVs is straightforward and allows a large

variability in composition. In addition, these vesicles provide the unique opportunity to observe global and local membrane bilayer restructuring.
Many protocols are available to generate giant vesicles but the main drawback of most of them is the incapability to include integral membrane proteins.
Biological membranes are complex structures composed of lipids, proteins and carbohydrates. Many biological functions at membranes are attributed to integral membrane- or membrane-associated proteins. Thus, it is crucial to include these proteins and mimic their environment in order to understand their involvement in membrane associated processes.
Proteo-liposomes obtained by gel filtration are used to generate giant unilamellar vesicles by alternating current assisted electroformation (Angelova & Dimitrov, 1986) on conductive electrodes (Fig. 2.1). Electroformation using ITO-(indium-tin-oxide)-coverslips is commonly performed but the majority of vesicles stays attached to the fragile coverslips. This not only impedes single vesicle visualization but also the addition of soluble factors. Furthermore, the amount of formed vesicles is mostly uncontrollable and large amounts of vesicles can create dense meshwork's which are inaccessible for the bulk solution. Electroformation employing platinum electrodes is more robust in vesicle formation and results in mostly detached vesicles. The main drawback is the limited surface to apply lipid films. Combining the advantages of both electroformation methods resulted in higher reproducibility and yield of vesicles. Employing platinum meshes instead of single platinum wires drastically increased the surface providing enough space to distribute membrane material. The amount of vesicles used in each approach is more adjustable and can be distributed more equally in order to set the same start conditions.

3.1.2 Heterologous expression of pUL31 and pUL34 results in functional proteins

Membrane proteins in artificial membrane systems can purified from natural sources, if possible at all, but are mostly not abundant enough. In addition, isolation of endogenous proteins always bears the risk of co-purifying interaction partners which may result in false positive results and interferes generally with the idea of bottom up approaches. Therefore, to investigate membrane associated processes it is desirable to reconstitute pure, individual components thereby, minimizing the possibility of

artifacts. Heterologous expression of membrane proteins with subsequent extraction is a valuable way to overcome the issues of amount and purity. Still, expression of membrane proteins is a challenging task and depends on the expression system as well as the properties of the individual protein. Furthermore, successful membrane protein expression is not linked to functionality as proteins can become post-translationally modified in order to function.

The issue of insufficient expression was overcome by using the MISTIC protein tag derived from *B.subtilis*. This efficiently enhances expression of integral membrane proteins (Roosild et al., 2005). Employing MISTIC and its self membrane integrating property was therefore well suited to express the herpesviral membrane protein pUL34 in *E.coli* to obtain sufficient amounts of integral membrane proteins.

Extraction of expressed membrane proteins is a demanding task. Membrane proteins are usually extracted by detergent-mediated solubilisation of membranes. Determining the detergent of choice as well as the correct concentration is an important factor to retain functional membrane proteins (Eisenhardt et al., 2014).

Generation of lipid layers with incorporated membrane proteins on the other hand is straightforward. Detergent solubilised lipids or lipid mixtures are combined with solubilized membrane proteins and undergo subsequent detergent removal either slow by dialysis or fast by gel filtration. Advantages of fast removal by gel filtration are a higher functionality of the reconstituted proteins as well as a higher detergent removal rate. This is especially important for the here used detergent CTAB, as this has a very low cmc (critical micelle concentration) value of about 1 mM making it unfavorable for dialysis assisted removal. In addition, the reconstitution rate of the protein is higher using gel filtration.

3.1.3 The viral proteins pUL31 and pUL34 are sufficient for membrane budding and scission in the GUV system

Recombinant expression, purification and subsequent fluorescently labeling of pUL34 (see methods) was efficiently done by detergent solubilisation from *E. coli* membranes. Interaction and recruitment of the other is presumably one function of either pUL31 or pUL34 but not meaningful to predict potential membrane remodeling activity of the formed complex. In order to test for functionality of pUL34, electroformation of proteo-liposome films containing the integrated pUL34 was done.

This reconstitution and electroformation resulted in sufficient amounts of individual giant vesicles containing the pUL34 protein. Recruitment of EGFP tagged pUL31 to pUL34 after the addition indicates that pUL34 comprises an integral membrane region as well as the interacting region with pUL31 is functional. This was indicated by membrane remodeling upon addition of pUL31 (Fig. 2.3A).

In case of no interaction and if no membrane deformation can be observed addition of a protein rich source could overcome the potential lack of cellular interacting or modifying proteins. The source could be either *Xenopus laevis* egg extract or cell lysates e.g. HeLa cell lysates.

Moreover, as budding at the inner nuclear membrane is a locally confined process added cell lysates comprising factors from diverse compartments could initiate misleading interactions. But this could hint to potential interactions and regulations of both viral proteins beyond their role in primary envelopment, as pUL31 and pUL34 were shown to be phosphorylated by the viral kinase pUS3 (Mou & Baines, 2009; Yamauchi et al., 2001; Chang & Roizman, 1993; Purves et al., 1992). Regulation might also involve direct phosphorylation of pUL31 or pUL34 by cellular kinases, as well as indirect by other cellular factors, targeting the individual proteins or the formed complex. Thus, this might reveal that cellular factors are involved in the budding mechanism of the viral capsid at the inner nuclear membrane.

Addition of pUL31 to GUVs showed recruitment of pUL31 to the GUV membrane only in the presence of pUL34. Small vesicles were formed towards the lumen of the giant vesicle with pUL31 and pUL34 integrated, indicating that both proteins are functional and sufficient in the GUV system to remodel membranes in the absence of other viral or cellular proteins (Fig. 2.3A). Furthermore, it appears that both proteins mediate not only membrane deformation but also scission of vesicles from the originating membrane as vesicles were found detached floating in the GUV lumen and detached in close proximity to the GUV membrane (Fig. 2.3A). Budding and scission of vesicles were shown to be independent of provided energy (Fig. 2.13). The bending force applied to the lipid bilayer by the pUL31/pUL34 complex appears to be sufficient for inward directed budding. The needed bending force might result from conformational changes upon binding of pUL31 to pUL34 or pUL31 oligomerization after recruitment and, thus, a rigid coat induces curvature to the GUV membrane. However, membrane deformation is strictly dependent on the presence of pUL31

while pUL34 alone is not sufficient to induce membrane remodeling indicative for a recruiting function of pUL34 (Fig. 2.2).

3.1.4 Defining the requirements for vesicle budding

By assessing the requirements for budding at GUV membranes the transmembrane region of pUL34 was demonstrated to be dispensable for budding and scission of formed vesicles (Fig. 2.14). The reconstitution of the full length pUL34 in GUVs but also the artificial recruitment of a soluble fragment of pUL34 lacking the predicted C-terminal transmembrane region is not able to induce remodeling in GUV membranes (Fig. 2.2, Fig. 2.14). Furthermore, only the addition of pUL31 restored membrane deformation leading to vesicle budding. Interestingly, vesicle formation and subsequent scission was induced independently of the orientation of pUL34 bound to GUVs, prior to addition of pUL31. This indicates even more that the transmembrane region of pUL34 is not important for vesicles budding and scission (Fig. 2.14). This is consistent with the observation that the C-terminal transmembrane region can be replaced by integral membrane regions of cellular inner nuclear membrane proteins, suggesting that the essential role of pUL34 depends on its soluble domain (Schuster et al., 2012). Moreover, these results gave rise to the question of the general function and contribution of pUL34 in vesicle budding.

Therefore, the effect of direct tethering of pUL31 to membranes was determined. Interestingly, artificial tethering of pUL31 was sufficient for vesicle budding in GUV membranes. Vesicles pinched of from the GUV membrane into the lumen of the giant vesicles while recruitment of other soluble proteins did not. This observation indicates that pUL31 combines both functions: budding and scission in the absence of other viral and cellular proteins (Fig. 2.15). These minimal requirements could be a result of the used artificial membrane system. Nevertheless, transfection experiments followed by electron microscopy demonstrated that employing an artificial pUL31 transmembrane construct to recruit pUL31 to the nuclear membrane in HeLa and HEK293T cells was also sufficient to induce vesicle formation at the inner nuclear membrane, even though these events are not very abundant (Fig. 2.42B-D). This could be explained by structural constraints posed by the nuclear lamina. Interestingly ribonucleoprotein (RNP) granules were shown to exit the nucleus in a process, similar to herpesviral mediated nuclear egress (Rose & Schlieker, 2012;

Speese et al., 2012). These specific RNP granules in Drosophila larval neuromuscular junctions are predicted to have approximately the same size as viral capsids und thus exceed the pore size limit of the NPC. It was found that nuclear localized granules are transported in a similar way from the nucleoplasm into the cytoplasm as subpopulations are found on the outside of the outer nuclear membrane. Also in this process an atypical protein kinase C (PKC) isoform, as well as LamC, a Drosophila lamin, are required for this formation. However, the precise mechanism and involvement of factors needs to be elucidated. Interestingly, in both processes the cellular kinase PKC is needed and both include membrane vesicles residing in the PNS followed by subsequent fusion with the outer nuclear membrane. Thus, herpesviruses may highjack a jet unknown cellular pathway to transport viral capsids through the nuclear membrane.

3.1.5 The functions of pUL34 in passing the nuclear envelope

Artificial pUL31 recruitment to GUV membranes is sufficient for vesicle budding induction and scission in the absence of pUL34. These experiments indicate that pUL34 is only functioning as a stalk to recruit pUL31 to membranes.
Nevertheless, it is likely that pUL34 is involved in regulation or definition of the induced membrane curvature as vesicles are smaller upon artificial pUL31 tethering compared to vesicles formed in the presence of pUL34 (Fig. 2.4, Fig. 2.16). It should be mentioned, that the presence of sub-resolution vesicles in both cases cannot be excluded. It appears unlikely that pUL34 only fulfills a recruiting and potential regulatory role in primary envelopment. In the absence of pUL34 viral capsids accumulate at the inner nuclear membrane as a result of impaired primary envelopment. Thus, the involvement of the pUL31/pUL34 egress complex in de-envelopment at the outer nuclear membrane cannot be tested. Expression of artificial transmembrane tethered pUL31 might be a possible way to elucidate the role of the pUL31/pUL34 complex for the de-envelopment process. Both proteins are located inside in perinuclear vesicles and the transmembrane region of pUL34 is predicted to extend only three amino acids into the PNS. Therefore, it is unlikely that these proteins are involved directly in the fusion of vesicles with the outer nuclear membrane. It is more likely, however, that interplay of the pUL31/pUL34 coat disassembly and cellular/viral factors could drive fusion of both membranes.

Phosphorylation of the pUL31/pUL34 by cellular or viral kinases might weaken interactions between both proteins and could give rise to fusogenic potentials of NEC or vesicle-interacting factors. The viral U_S3 kinase directly phosphorylates the viral proteins UL34 and pUL31 (Kato et al., 2005; Purves et al., 1992) but however, phosphorylation of pUL34 appears not involved in vesicle fusion with the outer nuclear membrane as a not phosphorylatable mutant of pUL34 results in normal viral growth behavior. This indicates that pUL31, but not pUL34 phosphorylation might affect perinuclear vesicle fusion. In addition, pUS3 is phosporylated by the viral pUL13 kinase which might provide an extra level of modulating phosphorylation patterns. Deletion of the pUS3 kinase or its catalytical activity results in accumulation of enveloped perinuclear virions and, thus, pUS3 kinase activity effects virion fusion with the outer nuclear membrane (Schumacher et al., 2005; Ryckman & Roller, 2004; Wagenaar et al., 1995).

Interestingly, a pUL34 and pUS3 kinase relationship is also implied to regulate lamina disruption as expression of either pUL34 or pUS3 proteins alone disrupted lamin A/C and lamin B localization while expression of pUL34 and pUS3 together had only little effect on lamin A/C localization (Bjerke et al., 2006).

However, a function of pUL34 involves the previously mentioned dissolution of the nuclear lamina (Bjerke et al., 2006; Reynolds et al., 2004; Simpson-Holley et al., 2004). The presence of pUL34 only or in complex with pUL31 appears to be crucial for that. Bending rigidity of the inner nuclear membrane might be too high to induce membrane deformation in presence of the nuclear lamina. Artificial tethering of pUL31 results in vesicle formation into the PNS as well as membrane proliferation (Fig. 2.43B-D) in transfected cells. The necessity of pUL34 was therefore overcome to recruit pUL31 to the membrane. The lack of pUL34 may result in reduced or no recruitment of the cellular kinases to pUL31 necessary to inducing local lamina softening. As a consequence, this would result in a need of higher bending strength to deform the inner nuclear membrane and, thus, explain the observed low abundance of perinuclear vesicles (Fig. 2.42B-D).

In contrast, in the GUV system no lamina is present and, therefore, artificial tethered pUL31 has to overcome a less prominent membrane rigidity to induce vesicle formation.

3.1.6 Contribution of perinuclear factors to herpesviral nuclear egress

The perinuclear space is continuous with the lumen of the endoplasmic reticulum, and known to be a calcium reservoir (Xu et al., 2005). Measurements of resting calcium concentrations of the endoplasmic reticulum revealed concentrations of 250 to 600 µM (Demaurex & Frieden, 2003) complexed with ER chaperones, acting as Ca^{2+} buffers (Coe & Michalak, 2009; Papp et al., 2003; Lievremont et al., 1997). Divalent cations like calcium or magnesium play a role in fusion processes. They bind to negatively charged lipids (Papahadjopoulos et al., 1990) shielding the overall negative charge of the bilayer. This reduces the electrostatic repulsion of vesicle membranes and target membranes and, thus, contributes to vesicle fusion. Thereby, the endoplasmic calcium in combination with viral glycoproteins could contribute to perinuclear vesicle fusion with the outer nuclear membrane in a process which could be envisioned similar to the SNARE mediated vesicle fusion (Jena, 2011).

It is still unclear, and it was not yet examined, if the perinuclear calcium also contributes to vesicle formation at the inner nuclear membrane. Furthermore, fusion between perinuclear vesicles might be envisioned but the presence and relevance of such effects is questionable.

Interestingly, calcium is known to be a key factor involved in herpesviral entry and cell to cell spreading (Bandyopadhyay et al., 2014; Cheshenko et al., 2013). However, as calcium is essential for countless of cellular processes dissecting a potential contribution of calcium in cellular systems without affecting other processes is difficult.

Furthermore, the contribution of torsinA, a cellular AAA+ ATPase residing in the lumen of the endoplasmic reticulum and implied to be involved in nuclear envelope maintenance and HSV-1 egress (Maric et al., 2011; Ozelius et al., 1997) as well as perinuclear proteins in general is not clear and might provides a new and interesting field of research.

3.1.7 The role of pUL31 and lipids in vesicle coat formation

pUL31 is crucial for vesicle budding and scission at GUV membranes. It mediates membrane remodeling when bound to membranes via pUL34 (Fig. 2.3) or upon

artificial recruitment (Fig. 2.15, Fig. 2.20, Fig. 3.1). While pUL31 does not self interact in solution (Fig. 2.21, Fig. 2.22) it was self recruiting when bound to membranes and resulted in vesicle formation into the GUV lumen (Fig. 2.20), presumably by oligomerization and rigid coat formation on the GUV surface. Interestingly, electron microscopy revealed dense proteinaceous structures at budding sites and vesicles upon pUL31/pUL34 cotransfection (Klupp et al., 2007), presumably representing tightly packed pUL31/pUL34 complexes at the inner nuclear membrane. Tight packing of pUL31/pUL34-complexes or artificial tethered pUL31 would result in a gapless, rigid coat assembly engulfing incoming capsids. Furthermore, exclusion of inner nuclear membrane proteins as well as large protein structures like NPCs would be a plausible explanation for the lack of NPCs in nuclear spots in transfected cells (Fig. 2.39, Fig. 2.40).

How pUL31 mediates its own recruitment in presence of membranes (Fig. 2.20) is a puzzling question as no direct preference for specific lipids was observed when only pUL31 was incubated with GUVs (Fig. 2.19). Additionally, no block in pUL31 recruitment as well as vesicle budding and scission was observed when specific lipids were removed from the used lipid mixture. Also in the absence of the negative charged lipids phosphatidylserine and phosphatidylinositol pUL31 was sufficient to induce vesicle budding and scission in GUV membranes (Fig. 2.9, Fig. 2.19). This indicates, that no electrostatic interactions between lipids and pUL31 and pUL34 mediate membrane remodeling.

Conditions either lacking cholesterol or sphingomyelin resulted in blocked vesicle formation. Both lipids are known to alter membrane fluidity and thus, pUL31 oligomerization, in presence or absence of pUL34, seems not sufficient to overcome the membrane rigidity (Fig. 2.9, Fig. 2.19).

The same also applies to unnaturally increased amounts of both lipids (Fig. 2.11) as high concentrations counteract vesicle formation in presence of pUL34 due to the increased rigidity of membranes (Fig. 2.11) (Rossman et al., 2010).

Lipids can also induce membrane curvature as a result of shape and insertion in the lipid bilayer mostly by conical or cone shaped lipids e.g. DHPC (1,2-Dihexanoyl-sn-glycero-3-phosphocholine) or DPPC (1,2-dipentadecanoyl-sn-glycero-3-phospho-choline). None of these special lipids were used in this work.

However, membrane deformations induced by protein crowding, demonstrate an opposite topology: away from the vesicle membrane and not into the lumen

(Stachowiak et al., 2012) and thus, cannot be an explanation for vesicle budding observed upon direct tethering of pUL31 (Fig. 2.15).

Also asymmetries in the bilayer can promote membrane deformation by affecting lipid packing. Such restructuring involves lipid transporters (flippases) (Devaux et al., 2008) resulting in redistribution of lipids in bilayers. Neither pUL31 nor pUL34 are predicted to have a lipid transport activity. Additional, budding and scission of pUL31 and pUL34 do not depend on provided energy (Fig. 2.13). Lipid transport activity across a lipid bilayer is also not inevitably energy dependent. Thus, it cannot be excluded that a local redistribution of lipids by the viral proteins induces membrane curvature or at least contributes to it. Furthermore, the headgroup modified lipid Ni-DGS (Avanti polar lipids) is commonly used for artificial tethering of factors to membranes (Kubalek et al., 1994; Krogsgaard et al., 2005) and was shown not to effect membrane rigidity (Settles et al., 2010).

pUL31 is sufficient to promote membrane curvature towards the lumen of giant vesicles (Fig. 2.15). It enriches at membranes upon seeding of untagged pUL31 (Fig. 2.20) and is enriched in formed buds in GUV membranes pointing to the center of the vesicle (Fig. 2.17A). pUL31 and pUL31/pUL34 mediated budding have a reverse topology compared to most other cellular budding processes e.g. COP-I/-II vesicle transport or clathrin mediated endocytosis. In contrast, the endosomal sorting complexes (ESCRT) mediate budding away from the cytoplasm as the pUL31/pUL34 mediated primary envelopment bud away from the nucleoplasm but involves numerous proteins compared to two, here described, viral proteins. Thus, both budding processes share the same topology. Interestingly, many viruses, including herpesviruses (Pawliczek & Crump, 2009; Tandon et al., 2009) recruit the hosts ESCRT machinery in order to facilitate their escape from the cell. So far, there is no evidence that the ESCRT machinery participates in primary envelopment and de-envelopment at the nuclear membranes.

Artificial recruitment of pUL31 to supported lipid layers results in rupturing of the lipid layer (Fig. 2.23A) accompanied by an increase in surface height by pUL31 (Fig. 2.24B). This is topologically contradicting but the surface attached lipid layer is incapable to promote inwarded budding but additional points to the membrane remodeling and coat forming ability of pUL31.

Curvature in membranes can be induced by proteins in several ways (Farsad & De Camilli, 2003). Structural predictions of pUL31 or pUL34 do not indicate special

properties of the proteins like membrane inserting amphipathic helices (Drin & Antonny, 2010) or other lipid interacting domains e.g. FYVE domains or Bar domains. This is consistent with observations that pUL31 cannot interact with membranes in the absence of pUL34 or artificial tethers (Fig. 2.3C, Fig. 2.5B, Fig. 2.12). Although an amphipathic helix formation upon pUL31 and pUL34 interaction cannot be excluded.

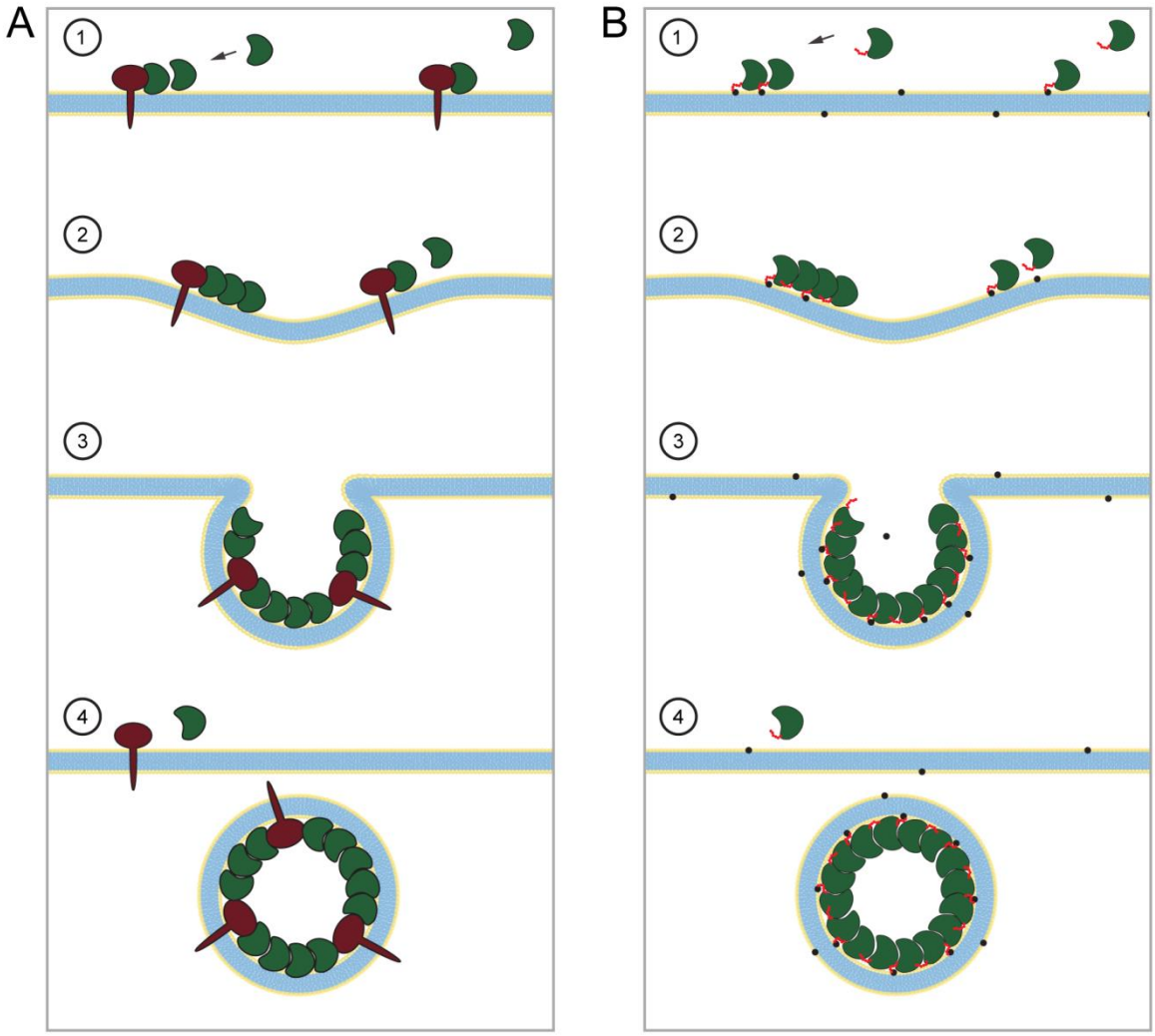

Figure 3.1: Model of budding steps in GUV membranes
(A) Membrane-bound pUL34 (red) recruits pUL31 (green) to the membrane. Subsequent recruitment of pUL31 by pUL34 and pUL31 itself leads to accumulation of both proteins in certain spots at the membrane. (1) Because of presumably structural changes in pUL31 and/or pUL34 accumulation of proteins results in membrane deformation (2) accompanied by more recruitment of pUL31 and pUL34 (3). This results in increased membrane deformation and finally scission of vesicles from the originating membrane. (B) The same sequence of events (1-4) is assumed for vesicles containing the Ni-chelating lipids (Ni-DGS, black dots), which fulfills artificially the initial and subsequent role of pUL34.

3.1.8 The influence of membrane domain organization in reconstituting membrane budding by pUL31 and pUL34

Lipids are organizing themselves according to their physical properties in particular regions of the membrane termed phases. These membrane phases have specific properties and thereby specify the orientation and mobility of membrane lipids and proteins. Beside the solid ordered phase (S_O, gel phase, L_β), where lipids are highly ordered, two different fluid phases are defined: the liquid disordered phase (L_D, L_α) and liquid ordered phase (Lo), the latter one enriched in the sphingolipid sphingomyelin and the sterol cholesterol.

The thickness of the individual lipid phase depends on the chain length of the lipids. Thus, the liquid ordered phase tends to be thicker as saturated hydrocarbon chains of sphingolipids are more extended (van Meer, 2008; Brown, 2006).

Using GUVs comprised of a minimal set of components lipid separation and thus separation of phases can be visualized (Baumgart et al., 2007). GUVs composed of only two or three lipid components can be used to mimic lipid raft formation *in vitro* (Garg et al., 2007). Cholesterol and sphingomyelin rich phases can act as local functional domains by concentrating proteins (Lingwood & Simons, 2010). Additionally, these phases can be stabilized by proteins e.g. calveolin interacts with cholesterol and oligomerizes forming caveolae (Pelkmans et al., 2004). Thus, a potential mechanism how the pUL31/pUL34 complex mediates membrane curvature and budding can be envisioned by inducing lipid separation and subsequent coat formation. Experiments testing this hypothesis by using adequate lipid phase markers (Sezgin et al., 2012; Baumgart et al., 2007) in GUVs, employing the nuclear envelope mimicking lipid mixture revealed no indication for a phase separation (Fig. 2.10A). Interestingly, employing the ternary lipid GUV system resulted in a recruitment of pUL31 to pUL34, which is localized in the liquid disordered phase (Fig. 2.11). Moreover, also a strong pUL31 signal was detected in the liquid ordered phase. This result might imply an interaction of pUL31 with cholesterol but pUL31 does not interact with the liquid ordered phase in the absence of pUL34 (Fig. 2.12).

An explanation could be that the cholesterol affinity changes upon interaction of pUL31 and pUL34 which might be a reason for the observed interaction of pUL31 with cholesterol. In addition, insufficient separation of lipids and, thus, separation of pUL34 in GUV membranes might be a more reasonable explanation for the observed

pUL31 interaction. The presence of small amounts of pUL34 in the formed liquid ordered phase might function as a recruiting platform for pUL31 and, in agreement with the self interaction ability of pUL31, results in oligomerization on the GUV membrane. Interestingly, a dependency of cholesterol and sphingomyelin was reported for the formation of nano-rafts, enriched in cholesterol and sphingomyelin, in the outer leaflet of bud-necks of budding vesicles (Ryu et al., 2014). This might contribute to the budding process by stabilizing the local membrane curvature and thereby lowering the energy required for budding (McMahon & Gallop, 2005). As cholesterol and sphingomyelin enrichment occurs in the outer leaflet of the bud-necks it is not accessible by the cholera-toxin-GM1, which was used there as a marker for the ordered phase, as a result of the inward budding in the GUV system.
However, no phase separation was detectable employing adequate membrane markers (Fig. 2.10) but so far one cannot exclude the formation of sub-resolution nano-domains induced by pUL31 and pUL34.

3.1.9 The vesicle size discrepancy in the GUV system

The intralumenal vesicles (ILVs) formed upon pUL31/pUL34 interaction as well as when pUL31 was artificially recruited to GUV membranes are at least ten times bigger compared to the perinuclear vesicles in infected cells of about 150 nm (Klupp et al., 2007). Upon addition of pUL31 to pUL34 GUVs, the majority of intralumenal vesicles (ILVs) showed an average size of 1 -1.5 µm (Fig. 2.4C). In comparison the ILVs in the artificial pUL31 tethered GUV system were found to have an average size of 0.5 – 1 µm (Fig. 2.16C). This might indicate a role of pUL34 in regulating vesicle size. Consistent with that, a recent publication (Bigalke et al., 2014) demonstrates a hexagonal meshwork of pUL31/pUL34 complexes on vesicles. In the absence of pUL34, pUL31 recruitment is still able to remodel vesicle and cellular membranes but the regularity of the coat or the spacing might be affected, resulting in the observed smaller vesicles. An indication might be that no detectable regular structure formation was observed upon artificial pUL31 recruitment to supported bilayers and subsequent atomic force microscope analysis (Fig. 2.24B). In order to resolve potential structures on membranes, high resolution analysis e.g. electron microscopy needs to be performed in further experiments.

The overall increase of vesicles formed in the GUV system can only be in part attributed to the presence of the bulky EGFP tag fused to the N-terminus of pUL31. Due to the topology of the budding reaction the coat assembly by pUL31/pUL34 or pUL31 alone is formed at the inside of the vesicle. In contrast, an increase in vesicle size upon coat assemblies on the outside of vesicles e.g. by clathrin or COP-I/-II components are not reported and might be due to sufficient space for bulky proteins tags. The presence of a spacious protein tag may result in sterical hindrances for coat assembly thereby inducing an increase in vesicle size. Although, fluorescently tagging of ESCRT components or the retroviral gag protein (Serrano & Neil, 2011; Pincetic & Leis, 2009), both sharing the same budding direction as herpesviruses, resulted in no increased vesicle size in cell transfection experiments. Correct sized herpesviral vesicles were also found in cell transfection experiments, cotransfecting pUL31 and pUL34 (Klupp et al., 2007) (Fig. 2.42A) as well as artificial pUL31 transmembrane constructs (Fig. 2.42B-D).
However, increases in vesicle size might be of intrinsic nature when employing the GUV system (Bigalke et al., 2014; Im et al., 2009; Wollert et al., 2009; Solon et al., 2005). This indicates that overcoming the high surface tension of the GUV membrane might be an additional plausible cause or at least contributes to increased vesicle sizes.
Furthermore, it cannot be excluded that sub-resolution ILVs, formed by either pUL31 or pUL31/pUL34, are present as they are smaller than the resolution limit of confocal microscopy or are exposed to fast photo bleaching upon analysis.
An indication for this, are the reported correct sized vesicles in GUVs revealed by electron microscopy (100 nm - 150 nm) (Bigalke et al., 2014).

3.1.10 Uncoupling the pUL34 binding and membrane remodeling activity of pUL31

pUL31 and pUL34 mediate budding and scission of vesicles in the absence of other viral and cellular proteins in the GUV system (Fig. 2.3A). pUL31 was sufficient to fulfill both tasks when artificially recruited to membranes (Fig. 2.15A). It was investigated whether the binding ability of pUL31 to pUL34 and the membrane remodeling activity of pUL31 were part of the same region within pUL31.

Sequence analyses of pUL31 indicated several regions with greater conservation and were classified as constant regions 1-4 (CR1-4) (Fig. 2.25) (Schnee et al., 2006). The first constant region is assumed to contain the pUL34 binding region (Schnee et al., 2006). Secondary structure predictions indicated that CR1 is mostly unstructured (http://toolkit.tuebingen.mpg.de/). Thus, CR1 may provide an interface for pUL34 interaction and folds upon pUL34 binding. Therefore, the first constant region of pUL31 was investigated in more detail in terms of pUL34 binding and membrane remodeling activity. Several amino acids within CR1 were conserved throughout all analyzed pUL31 homologues (Fig. 2.26, Fig. 2.30). These include three cysteine residues in position 73, 89 and 92 as well as one proline residue in position 62 and one serine residue in position 77 of pUL31. Several residues highly conserved within the *alphaherpesviridae* and in part within the *betaherpesviridae* or *gammaherpesviridae* were also included in the analysis (leucine in position 74, leucine in position 76, glycine in position 80, cysteine in position 88).

Mutation of the highly conserved cysteines (C73S, C89S, C92S) in pUL31 to serines, containing a hydroxyl group in the position of the thiol group of cysteine, abolished not only interaction with pUL34 (Fig. 2.27) but also the pUL31 membrane deformation ability upon artificial membrane recruitment in the GUV system (Fig. 2.28). Employing the cysteine mutants upon cotransfection with pUL34 in HeLa cells also revealed a block in nuclear membrane recruiting presumably by blocked pUL34 interaction and thus, nuclear membrane deformation was impaired (Fig. 2.44). Also in the HeLa cells system separation of the C88SC89S double mutation indicated that only the highly conserved cysteine residue in position 89 is involved in pUL34 interaction, while the less conserved cysteine residue in position 88 appears not to be involved in mediating pUL34 interaction (Fig. 2.50, Fig. 2.51).

This might indicate that the conserved cysteines are involved in potential disulfide bond formation thereby stabilizing the secondary structure of pUL31. Thus, mutation of these cysteine residues could affect folding and therefore results in non functional proteins.

However, it is unlikely that disulfide bonds form in the reducing cellular environment. Additional, protein disulfide-isomerases can catalyze formation and breakage of disulfide bonds but are residing in the oxidative environment of the endoplasmic reticulum, thus, not accessible for pUL31.

Cysteines can also play a structural key role, as they can coordinate heavy metal ions e.g. iron or zinc. The three conserved cysteines in pUL31 as well as histidines could form a cluster coordinating heavy metal ions in order to stabilize the folding thereby maintaining protein functionality (Giles et al., 2003).
Furthermore, they also could be involved in the formation of putative zinc finger motifs binding to DNA, RNA and mediating protein-protein interaction. So far no nucleic acid binding of pUL31 or homologues is reported. Nevertheless, pUL31 could be actively involved in displacing not only the nuclear lamina but also chromatin or chromatin interacting factors from potential budding sites and, thus, contribute to access the inner nuclear membrane. However this potential novel function remains to be determined. Also the function and precise involvement of cysteine and histidine residues in pUL31 in the proposed metals chelating needs to be addressed in future experiments. In addition, mutations of residues different than cysteine in the CR1 of pUL31 revealed that substitution of the proline residue in position 62 by glycine (P62G), leucine in position 74 to alanine (L74A) and leucine in position 76 to alanine (L76A) (Fig. 2.45, Fig. 2.46, Fig. 2.47) resulted in loss of pUL34 interaction in HeLa cells. However, the L76A and the G80A mutation within pUL31 were still sufficient to induce vesicle formation upon artificial recruitment to Ni-DGS-GUVs (Fig. 2.31, Fig. 2.32). Interestingly, the G80A mutation in pUL31 was not able to induce nuclear patch formation in the nuclear envelope in Hela cells although it was recruited to the nuclear envelope upon cotransfection (Fig. 2.49). These residues in pUL31 might be involved in forming a binding platform for pUL34. Thus, mutation of these could result in structural changes of the binding region of pUL31 unable to bind pUL34 and/or to self interact. A general unfolding upon mutation of single residues cannot be completely excluded but still present membrane remodeling activity of several mutants in the GUV system (Fig. 2.31, Fig. 2.32) and in transfected HeLa cells, there in part with pUL34 binding (Fig. 2.48-50), speaks against this hypothesis.
Taking together, these results indicate that both functions of pUL31, binding to pUL34 and membrane remodeling, are most likely located in the first constant region. A consistent loss of functions after mutations of individual cysteines in pUL31 indicates a particular importance of these residues in pUL31. So far, mutations of the cysteine residues in the CR1 do not allow the separation of both functions. This might also be an indication that both functions are structurally linked within pUL31. Also the binding ability of pUL31 mutants other than cysteines to pUL34 containing GUVs was

yet not examined and remains to be elucidated. The pUL31 G80A mutant appears to be an interesting candidate for further dissection of pUL34 binding and membrane remodeling activity. To further dissect the influence of mutations in the first constant region for both functions of pUL31 as well as for the pUL31/pUL34-complex future biochemical and biophysical experiments must be employed.

After fusion of periplasmic vesicles with the outer nuclear membrane the fate of pUL31 and pUL34 is unknown. Presumably, pUL31 is rapidly degraded, if not interacting with pUL34 (Ye & Roizman, 2000), consistent with the instability of the protein when purified without pUL34 pUL34 and pUL31 might be reimported into the nucleus to perform another round of vesicle budding.

Whether, and, if yes, how the NEC is disassembled upon or before vesicle fusion with the outer nuclear membrane is unknown.

Herpesviruses evolved a two component system, mediating budding, scission and potential fusion of vesicles with membranes. This might represent the driving force for the vesicle transport of capsids through the nuclear envelope and, thus, impose the directionality of the process.

3.2 Nup153 recruits the Nup107-160-complex to the inner nuclear membrane

3.2.1 Nup153 is targeted to membranes by its N-terminus

NPC assembly at the end of mitosis is a well coordinated and regulated assembly process. By employing cell free assays like the *Xenopus leavis* egg extract system the stepwise fashion of this self assembly was intensively studied. The chromatin binding nucleoporin MEL28/ELYS is known to be crucial for post-mitotic NPC assembly and initiates NPC assembly on the decondensing chromatin (Franz et al., 2007; Rasala et al., 2006).

The requirements for interphasic NPC assembly into the intact nuclear envelope are yet poorly defined. Most likely, NPC assembly in interphase is directly performed at the nuclear envelope as MEL28/ELYS is dispensable (Doucet et al., 2010).

In order to target structural components to the nuclear envelope a factor similar to MEL28/ELYS must perform initial recruitment steps of nuclear pore components. Experiments shown here suggest that Nup153 provides a building platform thereby allowing recruitment of nuclear pore building blocks in interphase. Sequence analysis of vertebrate Nup153 (Fig. 2.53A) revealed a predicted amphipathic helix (Segrest et al., 1990) in the N-terminus of Nup153 (Fig. 2.53B) (http://heliquest.ipmc.cnrs.fr/). Additionally, a single point mutation of the valine residue in position 50 to glutamate (V50E) was predicted to disrupt this potential amphipathic helix. The N-terminus of *Xenopus laevis* Nup153 (aa 1-149) was recombinantly expressed with an EGFP tag, fused to the N-terminus. Employing GUVs composed of the nuclear envelope mimicking lipid mixture demonstrated that indeed the N-terminus of Nup153 is able to interact with membranes confirming that the N-terminus of Nup153 mediates membrane binding (Fig. 2.53C). The binding of the N-terminal fragment was also confirmed by transfection experiments in HeLa cells. Overexpression of this fragment induced nucleoplasmic membrane proliferation (Fig. 2.53E) known for membrane interacting proteins like lamin B (Ralle et al., 2004). Furthermore, the predicted amphipathic helix disrupting mutation V50E impaired interaction with GUV membranes (Fig. 2.53C). The human orthologue of Nup153 was fluorescently labeled and employed in the GUV system. Consistent with the previous result, human

Nup153 was also efficiently recruited to GUVs while the corresponding V47E mutation was unable to interact with GUV membranes (Fig. 2.53D).
These results indicate that indeed Nup153 contains an at least in vertebrates conserved amphipathic helix in the N-terminus and, thus, can directly interact with membranes.
In order to define the exact role of Nup153 in nuclear pore assembly, Nup153 was depleted from *Xenopus laevis* egg extract, which was employed in nuclear assembly reactions. Interestingly, the NPCs were unevenly distributed in the assembled nuclei (Fig. 2.54, right panel). This NPC clustering phenotype upon Nup153 depletion has been previously observed (Walther et al., 2001). The NPC clustering phenotype was rescued when recombinant Nup153 was added back to the assembly reaction and, thus, confirmed the functionality of recombinant Nup153 and the specificity of the depletion (Fig. 2.54). NPC clustering was also rescued by the Nup153 membrane-binding mutant (V47E), although the nuclei formed appeared smaller in size compared to the wildtype addback.
This indicates that the Nup153 membrane interaction is not required for proper NPC spacing in the nuclear envelope.

3.2.2 Nup153 membrane binding is necessary for interphasic NPC assembly

The role of Nup153 in interphasic NPC assembly was assessed by individual NPC counting in assembled nuclei under Nup153 depletion conditions. Addition of 2 µM importin-β is known to block interphasic NPC assembly (D'Angelo et al., 2006). When added to forming nuclei this resulted in a reduction in the number of NPCs per nucleus by about 50 % demonstrating that half of the final number of NPCs are formed by interphasic NPC assembly (Fig. 2.55). The depletion of Nup153 from egg extract caused a reduction in NPC number, which was not further affected by the addition importin-β, suggesting that Nup153 is necessary for interphasic NPC assembly. While the re-addition of wild type Nup153 resulted in similar NPC numbers compared to the mock-depleted sample addback of the membrane binding deficient V47E mutant did not restore NPC levels (Fig. 2.55). This again indicates that interphase NPC assembly requires Nup153 but, furthermore, that the crucial function of Nup153 is that of a membrane binding factor necessary to target NPC components to the nuclear envelope.

Thus, unlike to its dispensable role in NPC assembly after mitosis, the here presented results indicate that Nup153 functions as a crucial building platform for NPC assembly during interphase.

Nup153 binds the Nup107-160 complex (Y-complex) forming the cytoplasmic and nucleoplasmic rings of the NPCs (Enarson et al., 1998). As membrane binding of Nup153 is required for interphasic NPC assembly this could point to a recruitment role for the Y-complex to the nuclear membranes by Nup153.

In addition, the small GTPase ran is also known to interact with Nup153 and is required for interphasic NPC assembly (Doucet et al., 2010; D'Angelo et al., 2006; Walther et al., 2003). To test if the essential function of Nup153 is to recruit one of these two interaction partners to the membrane artificially membrane tethered, EGFP tagged constructs containing the Y-complex binding site or the ran binding site of Nup153 were generated. The synthetic Y-complex binding construct was able to bind purified and labeled *Xenopus laevis* Y-complex, as demonstrated by liposome floatation assays (Fig. 2.56B) and when reconstituted in GUVs (Fig. 2.56C). In contrast, the Y-complex was not able to bind the ran-binding construct (Fig. 2.56B-C). The opposite pattern was seen for the ran binding construct as ran was efficiently recruited but not by the Y-complex (Fig. 2.56B-C).

This demonstrates that the generated constructs, containing the individual binding regions, were sufficient to recruit the Y-complex or ran to membranes, respectively.

Recruitment of the Y-complex but not ran by the corresponding binding region of Nup153 to membranes was sufficient for subsequent interphasic NPC assembly when employed in NPC assembly reactions after depletion of endogenous Nup153 (Fig. 2.56D). Thus, the Y-complex as a crucial structural component of the NPC must be recruited by Nup153 to membranes in order to mediate NPC assembly in interphase (Fig. 3.2). This to Nup153 previously not assigned function still poses several unanswered questions. Nup153 is located at the inner nuclear membrane. Nevertheless, formation of new NPCs in interphase is initiated from the nuclear as well as the cytoplasmic side (D'angelo et al., 2006). This could indicate that Nup153 is only necessary for the membrane attachment of the Nup107-160 inside the nucleus, acting as an enhancer of membrane binding. Consistent with this view is the fact that the inner nuclear membrane is coated by the lattice of the nuclear lamina and therefore less accessible than the ONM (Gruenbaum et al., 2005). The Nup107-160 complex contains several proteins with an intrinsic membrane binding capability

like Nup133 (Drin et al., 2007). Nevertheless, this membrane interaction seems not to be sufficient for membrane attachment during interphasic NPC assembly. Consistent with this, Nup107-160 complex purified from *Xenopus laevis* did not show an interaction with GUVs and LUVs on its own (Fig. 2.56B-C. Therefore, Nup153 would provide an interaction platform on the membrane in order to recruit the Nup107-160 complex for the formation of new NPCs. This function seems to be taken over by ELYS/MEL28 during the process of NPC assembly after mitosis. As this mode of assembly is most likely initiated on the chromatin, a recruitment factor for the Nup107-160 complex needs to interact with DNA. ELYS/MEL28 contains an AT-hook that allows an interaction with DNA (Gillespie et al., 2007) providing the interaction platform for the Nup107-160 complex, thereby making Nup153 in this respect obsolete. Vice versa in NPC assembly during interphase Nup153 takes over this role, making ELYS/MEL28 dispensable.

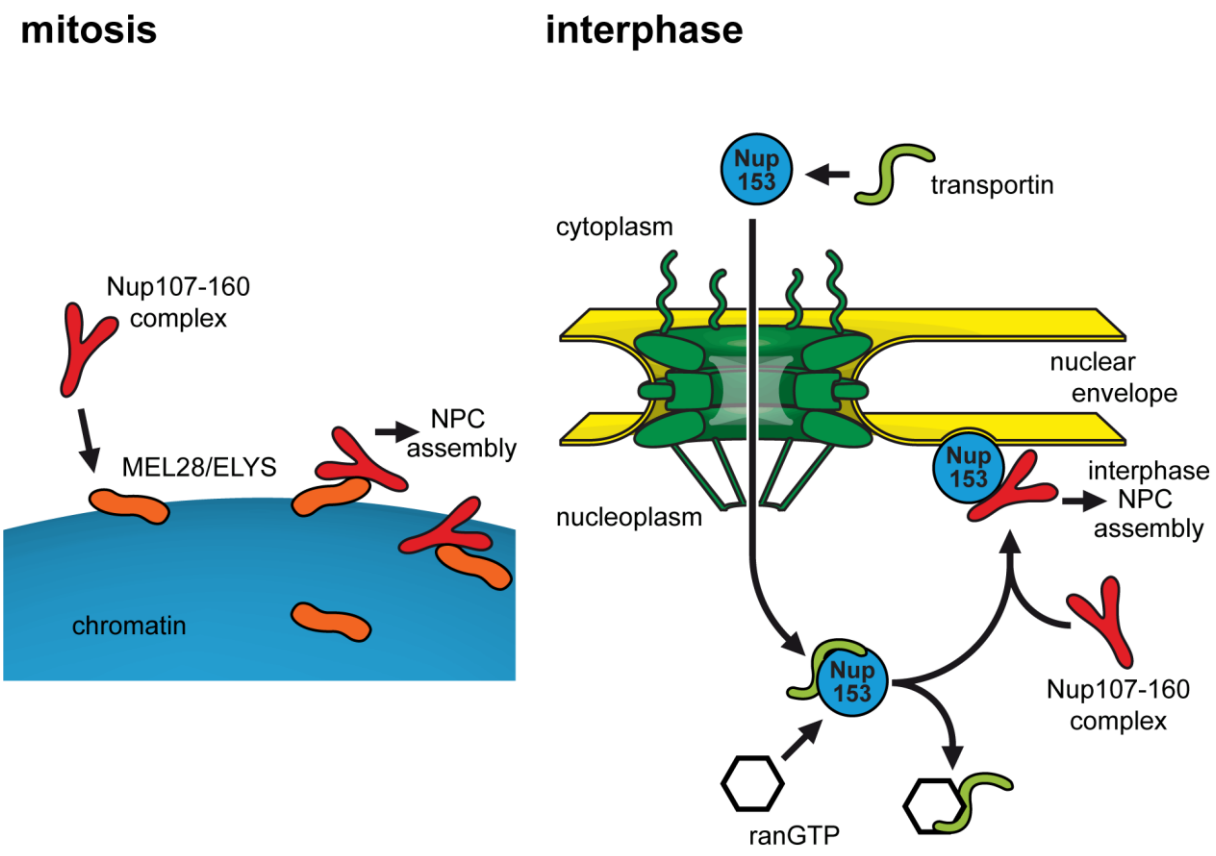

Figure 3.2: Model of post-mitotic and function of Nup153 in interphasic NPC assembly

NPC assembly at the end of mitosis is dependent on y-complex recruitment of MEL28/ELYS, interacting with chromatin. For interphasic NPC assembly, transportin is binding and preventing thereby membrane interaction of Nup153, facilitating import into the nucleus. The high concentration of ranGTP in the nucleus results in release of the Nup153 cargo and can thereby interact and recruit the Y-complex to the inner nuclear membrane for interphasic NPC assembly.

4 Material and Methods

4.1 Materials

4.1.1 Devices

CP2201 balance	Satorius AG, Göttingen, Germany
Dri-Block DB-2A – heating block	Bibby Scientific Limited, Staffordshire, UK
EmulsiFlex-C3	Avestin Inc., Ottawa, Canada
BioPhotometer	Eppendorf, Hamburg, Germany
FluoView FV1000	Olympus Europa Holding GmbH, Hamburg, Germany
GelAir Drying System	Biorad Laboratories, Hercules, USA
Gel-Logic-1500 Imaging Systems	Carestream Health, Inc., Rochester, USA
HT Multitron	Infors-HAT Inc. Bottmingen, Switzerland
Haake DC10-P5/U	Thermo Fisher Scientific, Waltham, USA
Heraeus Fresco-17	Thermo Fisher Scientific, Waltham, USA
Heraeus Pico-17	Thermo Fisher Scientific, Waltham, USA
MR 3000	Heidolph Instruments GmbH & Co. KG, Schwabach, Germany
Mettler AE240	Mettler Toledo, Gießen, Germany
Mini-PROTEAN-3 Electrophoresis Cell	Biorad Laboratories, Hercules, USA
Mini-PROTEAN Tetra System	Biorad Laboratories, Hercules, USA
Multifuge	Thermo Fisher Scientific, Waltham, USA
MultiImage Light Cabinet	Alpha Innotech, Santa Clara, USA
Nanodrop ND-1000	Thermo Fisher Scientific, Waltham, USA
NeoBlock - Heizer Duo 2-2504	NeoLab,Heidelberg, Germany
Optima L-60	Beckmann-Coulter, Krefeld, Germany
Optima TLX	Beckmann-Coulter, Krefeld, Germany
Peltier Thermal Cycler PTC-200	Biorad Laboratories, Hercules, USA
Polymax 2040	Heidolph Instruments GmbH & Co. KG, Schwabach, Germany
PowerPac Basic	Biorad Laboratories, Hercules, USA
Seven Easy	Mettler Toledo, Gießen, Germany
Sorvall Evolution RC	Thermo Fisher Scientific, Waltham, USA
Stuart SB2	Keison Products, Essex, UK
TG315 Function Generator	AIM-TTI Instruments, Huntingdon, UK
Thermomixer comfort 5355	Eppendorf, Hamburg, Germany
Thermomixer compact 5250	Eppendorf, Hamburg, Germany
Vortex Genie 2	Scientific Industries Inc., New York, USA

4.1.2 Reagents and consumables

α-lactose	Carl Roth GmbH + Co. KG - Karlsruhe, Germany
1,4-dithiothreitol	Carl Roth GmbH + Co. KG - Karlsruhe, Germany
agarose	Carl Roth GmbH + Co. KG - Karlsruhe, Germany
ammonium peroxydisulfate	Carl Roth GmbH + Co. KG - Karlsruhe, Germany
ammonium sulfate	Merck KGaA, Darmstadt, Germany
boric acid	Carl Roth GmbH + Co. KG - Karlsruhe, Germany
bromophenol blue (3',3",5',5"-tetrabromophenolsulfonphthalein)	Carl Roth GmbH + Co. KG - Karlsruhe, Germany
bovine serum albumin	Calbiochem, Merck KGaA, Darmstadt, Germany
calcium chloride	AnalaR Normapur, VWR International, Radnor, USA
chloroform	Thermo Fisher Scientific, Waltham, USA Scientific
coomassie R-250	Carl Roth GmbH + Co. KG - Karlsruhe, Germany
cetyltrimethylammonium bromide	Calbiochem, Merck KGaA, Darmstadt, Germany
dimethyl sulfoxide	SERVA Electrophoresis GmbH, Heidelberg, Germany
disodium hydrogen phosphate	Merck KGaA, Darmstadt, Germany
Dulbecco´s modified Eagle medium	Life Technologies,Carlsbad, USA
Disodium-ethylenediamine-tetraacetic acid	Merck KGaA, Darmstadt, Germany
acetic acid	Sigma-Aldrich, St. Louis, USA
ethanol	Carl Roth GmbH + Co. KG - Karlsruhe, Germany
fetal calf serum	Life Technologies,Carlsbad, USA
formaldehyde	Sigma-Aldrich, St. Louis, USA
ethidium bromide	Sigma-Aldrich, St. Louis, USA
glucose	Carl Roth GmbH + Co. KG - Karlsruhe, Germany
glycerine	Sigma-Aldrich
glycine	Carl Roth GmbH + Co. KG - Karlsruhe, Germany
yeast extract	Carl Roth GmbH + Co. KG - Karlsruhe, Germany
4-(2-hydroxyethyl)-1-piperazine-ethanesulfonic acid (HEPES)	Carl Carl Roth GmbH + Co. KG - Karlsruhe, Germany Roth GmbH + Co. KG - Karlsruhe, Germany
hydroxylamine	Alfa Aesar, Ward Hill,USA
imidazole	Carl Roth GmbH + Co. KG - Karlsruhe, Germany
isopropyl-β-D-thiogalacto-pyranoside	Carl Roth GmbH + Co. KG - Karlsruhe, Germany
potassium dihydrogen phosphate	Merck KGaA, Darmstadt, Germany
kanamycin sulfate	Carl Roth GmbH + Co. KG - Karlsruhe, Germany
magnesium chloride	Fluka, Sigma-Aldrich, St. Louis, USA
magnesium sulfate	Novagen, Merck KGaA, Darmstadt, Germany
nonfat dried milk powder	AppliChem GmbH, Darmstadt, Germany
methanol	Thermo Fisher Scientific, Waltham, USA

sodium azide	Carl Roth GmbH + Co. KG - Karlsruhe, Germany
sodium chloride	Merck KGaA, Darmstadt, Germany
sodium carbonate	Merck KGaA, Darmstadt, Germany
sodium hydrogen carbonate	Carl Roth GmbH + Co. KG - Karlsruhe, Germany
sodium dihydrogen phosphate	Merck KGaA, Darmstadt, Germany
sodium dodecyl sulfate	Carl Roth GmbH + Co. KG - Karlsruhe, Germany
sodium thiosulfate	Merck KGaA, Darmstadt, Germany
octyl glucoside	Calbiochem, Merck KGaA, Darmstadt, Germany
phenylmethylsulfonyl fluoride	Biochemica, AppliChem GmbH, Darmstadt, Germany
Ponceau-S	Fluka, Sigma-Aldrich, St. Louis, USA
Rotiphorese® Gel 30 (37.5:1) solution	Carl Roth GmbH + Co. KG - Karlsruhe, Germany
sucrose	Carl Roth GmbH + Co. KG - Karlsruhe, Germany
hydrochloric acid	Sigma-Aldrich, St. Louis, USA
silver nitrate	Merck KGaA, Darmstadt, Germany
tetramethylethylenediamine	Carl Roth GmbH + Co. KG - Karlsruhe, Germany
tricine	Carl Roth GmbH + Co. KG - Karlsruhe, Germany
Tris-HCl	Carl Roth GmbH + Co. KG - Karlsruhe, Germany
Tween®-20	Carl Roth GmbH + Co. KG - Karlsruhe, Germany

4.1.3 Kits used

QIAquick Gel Extraction Kit	Qiagen N.V., Venlo, Netherlands
QIAquick PCR Purification Kit	Qiagen N.V., Venlo, Netherlands
QIAquick Plasmid Mini Kit	Qiagen N.V., Venlo, Netherlands
QIAquick Plasmid Midi Kit	Qiagen N.V., Venlo, Netherlands
Western Lightning Plus ECL Kit	PerkinElmer, Waltham, USA

4.1.4 Enzymes used

DNase I, RNase-free, recombinant 10 U/µl (bovine pancreas)	Roche
KOD DNA polymerase 1 U/µl (*Thermococcus kodakaraensis*)	Novagen
Nde I, 20 U/µl, recombinant (*Neisseria denitrificans*)	NewEngland Biolabs
T4 DNA Ligase, 400 U/µl, recombinant (T4 bacteriophage, Myoviridae)	NewEngland Biolabs

Taq DNA Polymerase, recombinant (*Thermus aquaticus* YT-1)	
Xho I, 20 U/µl, recombinant (*Xanthomonas holcicola)*	NewEngland Biolabs

4.1.5 Bacterial strains used

XL1 blue (Stratagene)	recA1 endA1 gyrA96 thi-1 hsdR17 supE44 relA1 lac [F' proAB lacIqZDeltaM15 Tn10 (Tetr)]
Bl21 (DE3)	F– *omp*T *hsd*SB(rB–, mB–) *gal dcm* lambda(DE3)
Bl21 gold (DE3)	F– omp T *hsd*S(rB mB) dcm+ Tetr gal lambda(DE3) endA Hte
Bl21 star (DE3)	F– *omp*T *hsd*SB(rB–, mB–) *gal dcm rne*131 lambda(DE3)

4.1.6 Cell lines used

HeLa S3	human negroid cervix carcinoma cell line	ATCC nr. CCL-2.2
293T	human primary embryonal kidney cell line 293	ATCC nr. CRL-3216
U-2 OS	human osteosarcoma cell line	ATCC nr. HTB-96
RK13	rabbit kidney cell line	ATCC nr. CCL-37

4.1.7 Primary antibodies used

α-His6	mouse	Roche	1:500 dilution
mAb414	mouse	covance	1:2000 dilution
α-EGFP	mouse	Roche	1:2000 dilution

4.1.8 Secondary antibodies used

Cy3 goat α-mouse IgG	life technologies	1:2000 dilution
Alexa-Fluor-488 goat α-mouse IgG	life technologies	1:2000 dilution

Alexa-Fluor-546 goat α-mouse IgG	life technologies	1:2000 dilution
Alexa-Fluor-647 goat α-mouse IgG	life technologies	1:2000 dilution
goat α-mouse IgG linked horseradish peroxidase	Calbiochem	1:5000 dilution

4.1.9 Oligonucleotides used

Oligonucleotides used in this study were purchased from Sigma-Aldrich and are listed in 5’ - 3’ orientation.

UL31COXhoINS	GGCGGCTCGAGCGGACGCGGAGGACGAAAATC
UL31CONdeI	GGCGGCATATGTTTGAACGTCGTCGTC
UL31COBamHI	CCGCCGGATCCGATGTTTGAACGTCGTCGTCTGC
UL31COXhoI	GGCGGCTCGAGTTATTACGGACGCGG
UL31COC92Sfw	GGGTCTGGGTGGTTGTTGTCCGACCAGCGCAGCA GCAGAACCGCGTC
UL31COC92Srev	GACGCGGTTCTGCTGCTGCGCTGGTCGGACAACA ACCACCCAGACCC
UL31COC73Sfw	GGTCAGGCAGTTGCAGATAATAGCCTGAGCCTGAG CGGTATGG
UL31COC73Srev	CCATACCGCTCAGGCTCAGGCTATTATCTGCAAC TGCCTGACC
UL31COC88SC89Sfw	TATTATCTGGGTCTGGGTGGTAGCAGCCCGACCT GTGCAGCAGCA
UL31COC88SC89Srev	TGCTGCTGCACAGGTCGGGCTGCTACCACCCAG ACCCAGATAATA
UL31COBamHIpGEX6P	GGCGCGGATCCATGTTTGAACGTCGTCGTCTG
EGFPBamHIpGEX6P	GGCGCGGATCCATGGTGAGCAAGGGCGAGG
UL31COP62Gfw	AACCGCACCGGTTACCCTGGGTTTTGATCTGGGT CAGGCAGTT
UL31COP62Grv	AACTGCCTGACCCAGATCAAAACCCAGGGTAAC CGGTGCGGTT
UL31COL74Afw	TCAGGCAGTTGCAGATAATTGTGCAAGCCTGACG GTATGGGTTA
UL31COL74Arv	TAACCCATACCGCTCAGGCTTGCACAATTATCTG CAACTGCCTGA
UL31COL76Afw	AGTTGCAGATAATTGTCTGAGCGCAAGCGGTATG GGTTATTATCTGG
UL31COL76Arv	CCAGATAATAACCCATACCGCTTGCGCTCAGAC AATTATCTGCAACT

UL31COS77Afw	GCAGATAATTGTCTGAGCCTGGCAGGTATGGGTTATTATCTGGGTC
UL31COS77Arv	GACCCAGATAATAACCCATACCTGCCAGGCTCAGACAATTATCTGC
UL31COG80Afw	CTGAGCCTGAGCGGTATGGCATATTATCTGGGTCTGGGTGGT
UL31COG80Arv	ACCACCCAGACCCAGATAATATGCCATACCGCTCAGGCTCAG
UL31COC88Sfw	TATTATCTGGGTCTGGGTGGTAGCTGTCCGACCTGTGCAGCAG
UL31COC88Srv	CTGCTGCACAGGTCGGACAGCTACCACCCAGACCCAGATAATA
UL31COC89Sfw	ATCTGGGTCTGGGTGGTTGTAGCCCGACCTGTGCAGCAGCAG
UL31COC89Srv	CTGCTGCTGCACAGGTCGGGCTACAACCACCCAGACCCAGAT
UL31COH188Afw	GTGTTTCCGGAAAAAAGCGTGGCAGTTCATCATCGTGTTCTGGATC
UL31COH188Arv	GATCCAGAACACGATGATGAACTGCCACGCTTTTTTCCGGAAACAC
UL31CONheI	CCGCCGCTAGCATGTTTGAACGTCGTCGTCTG
UL34CONdeI	GGCGGCATATGAGCGGCACCCTGG
UL34COXhoI	GGCGGCTCGAGCTATTAACGACGCAGACCCAGCAGG
UL34CO240XhoINS	GGCGGCTCGAGACGACGCAGACCCAGCAGG
UL34COstopXhoI	GGCGGCTCGAGTCATCAGCGCATATTCAGAATAATCACAAT
UL34COTMRSalIfw	GGCGGGTCGACCTGCGTCGTCTGGCAGGTT
UL34COnsXhoI	GGCGGCTCGAGGCGCATATTCAGAATAATCACAAT
Nup153xlNdeI	GGCGGCATATGGCAGCAGCCGGTG
Nup153xl149AseI	GGCGGATTAATCAGGCTTGCACGATGCAGG
Nup153xlSalI	GGCGGGTCGACATGGCAGCAGCCGGTG
Nup153xl149XhoI	GGCGGCTCGAGTTATTACAGGCTTGCACGATGCAGG

4.1.10 Used buffers and solutions

0.2 M PMSF	3.5 g PMSF were dissolved in 100 ml ethanol
0.259 M Sucrose	8.9 g sucrose were dissolved in 100 ml double-distilled water filtered aliquoted and stored at -20 °C
1 M $CaCl_2$	55.5 g $CaCl_2$ were dissolved in 1 l double-distilled water filtered and autoclaved
1 M DTT	15.45 g DTT were dissolved in 1 l double-distilled water aliquoted and stored at -20 °C
1 M HEPES-KOH	238.1 g HEPES were dissolved in 800 ml double-distilled water adjusted with KOH to pH 8, filtered autoclaved and filled up to 1 l
1M Imidazol	68.08 g were dissolved in 800 ml in double-distilled water adjusted with NaOH to pH=7.5 autoclaved and filled up to 1 l
1 M IPTG	2.38 g were dissolved in 10 ml double-distilled water and stored at-20 °C
1 M $MgCl_2$	47.6 g $MgCl_2$ were dissolved in 1 l double-distilled water filtered and autoclaved
1 M $MgSO_4$	246.5 g $MgSO_4$ were dissolved in 1 l double-distilled water and autoclaved
1 M Tris	121.1 g were dissolved in 800 ml double-distilled water and adjusted with hydrochloric acid to the desired pH value and filled up to 1 l with double-distilled water, filtered and autoclaved
1.5 M Tris pH 8.8	181.7g were dissolved in 800 ml double-distilled water ajusted with hydrochloric acid to pH=8.8 , filled op to 1 l with double-distilled water, filtered an autoclaved
2 M KCl	149.1g KCL were dissolved in 1 l double-distilled water filtered and autoclaved
5 % BSA	5 g BSA were dissolved in 100 ml 1x PBS and stored at 4 °C
1x PBS-Tween (0.1%)	2 ml Tween-20 were dissolved in 2 l 1x PBS
3x gel buffer	36.3g Tris-HCl and 0.3 g SDS were dissolved in 100 ml double-distilled water
6x DNA-loading buffer	5 ml Glycerin 1 ml 10x TBE 1 ml 10 % Orange G were dissolved in double-distilled water and filled up to 10 ml and aliquoted
6x SDS-sample buffer	18.75 ml 1 M Tris pH 6.8 30 g sucrose 9 g SDS 1 ml 10 % bromophenol blue were dissolved in double-distilled water and filled up to 90 ml. Before use DTT was added to a final concentration of 100 mM
10x Anode-buffer	242.2 g Tris-HCl were dissolved in 800 ml double-distilled water adjusted with hydrochloricacid to pH 8.9 and filled up to 1 l .
10x Cathode-buffer	121.1g Tris-HCl 179.2 g Tricine and 10 g SDS were dissolved in 1 l double-distilled water
10x Laemmli-buffer	50 g SDS 721 g glycine and 150 g Tris-HCl were dissolved in 5 l double-distilled water

10x PBS	10 g KCL 400 g NaCl 89 g Na_2HPO_4 12 g KH_2PO_4 were dissolved in 4 l double-distilled water adjusted to pH 7.4 with hydrochloric acid filled up to 5 l double-distilled water and autoclaved
10x TBE	540 g Tris-HCl 275 g boric acid and 46.5 g of disodium ethylenediaminetetraacetic acid were dissolved in 5 l double-distilled water
10x Tris-glycin-buffer	151.5 g Tris-HCl and 720.5 g glycine were dissolved in 5 l double-distilled water
20x NPS	66 g $(NH_4)_2SO_4$ 136 g KH_2PO_4 178 g Na_2HPO_4 were dissolved in 1 l double-distilled water and autoclaved
50x 5052	250g glycerole (87%w/v) 25g glucose and 100g α-lactose were dissolved in 1l double-distilled water and autoclaved
Blocking buffer	50 g nonfat dried milk powder and 1 ml Tween-20 were dissolved in 1 l 1x PBS and stored at 4 °C
Coomassie stain	2.5 l methanol 0.5 l acetic acid and 10 g Coomassie R-250 were dissolved in 5 l double-distilled water and filtered through Whatman filter paper
Coomassie destain I	2.5 l methanol and 0.5 l acetic acid were filled up to 5 l with double-distilled water
Coomassie destain II	0.5 l ethanol 0.25 l acetic acid were filled up to 5 l with double-distilled water
Developer solution	12 g Na_2CO_3 100 µl formaldehyd (37 wt. % in H_2O) and 4 ml of postfix solution were filled up to 200 ml with double-distilled water
Fixing solution	100 ml methanol 24 ml acetic acid and 100 µl formaldehyd (37 wt. % in H_2O) were filled up to 200 ml with double-distilled water
Kanamycin (25 mg/ml)	2.5 g kanamycin was dissolved in 100 ml double-distilled water, aliquoted and stored at -20 °C
Lysogeny Broth (modified Lennox)	10 g thryptone, 5 g yeast extract and 5 g NaCl were dissolved in 1 l double-distilled water, adjusted to pH 7 with NaOH and autoclaved
Nickel wash buffer	58.44 g NaCl 40 ml 1 M Tris-HCl pH 7.5 and 60 ml 1 M Imidazol pH 7.5 were filled up to 2 l with double-distilled water
Nickel wash buffer + 1 % CTAB	58.44 g NaCl 40 ml 1 M Tris-HCl pH 7.5 60 ml 1 M Imidazole pH 7.5 and 20 g CTAB were filled up to 2 l with double-distilled water and stored up to 6 month at room temperature
Nickel elutions buffer + 1 % CTAB	14.6 g NaCl 10 ml 1 M Tris-HCl pH 7.5 200 ml 1 M imidazole, 5 g CTAB and 57 ml glycerol (87 % w/w) were dissolved in 500 ml double-distilled water and stored at room temperature
Nickel elution buffer	14.6 g NaCl 10 ml 1 M Tris-HCl pH 7.5 200 ml 1 M imidazole and 57 ml glycerol (87 % w/w) were dissolved in 500 ml double-distilled water and stored at 4 °C
Ponceau staining solution	1 g Ponceau S, 10 ml acetic acid (99 %) were dissolved and filled up to 1 l in double-distilled water
Postfix solution	0.1 g $Na_2S_2O_3$ was dissolved in 500 ml double-distilled water

S0-Puffer	50 mM KCl 2.5 mM $MgCl_2$ and 10 mM HEPES pH 7.5 were dissolved in 1 l double-distilled water
S2100 solution	71.88 g sucrose was dissolved in 100 ml S0 buffer
Silverstain solution	0.2 g $AgNO_3$ was dissolved in 100 ml double-distilled water
Lysogeny Broth (modified Luria)	20 g thryptone 5 g yeast extract and 0.5 g NaCl were dissolved in 1 l double-distilled water and autoclaved
STOPP II solution	18.6 g Na_2-EDTA was dissolved in 1 l double-distilled water
Blocking buffer (IF)	3 g BSA were dissolved in 99.5 ml 1x PBS, 500 µl of 20 % Triton X-100 solution (w/v) was added
4 % Paraformaldehyde	20 g paraformaldehyde was dissolved in 450 ml 1x PBS and adjusted with NaOH to pH 7.5, aliquoted and stored at -20 °C
Sodium cacodylate	4.28 g sodium cacodylate was disolved in 90 ml double-distilled water, adjusted to pH 7,4 and filled up to 100 ml
Fixation buffer	50 ml of 0.2 M sodium cacodylate and 5 ml glutaraldehyde (50 % wt. % in in H_2O) was filled up to 100 ml double-distilled water and stored at 4 °C
SLB buffer	10 mM HEPES, pH 7.4, 150 mM NaCl

4.2 Methodes

4.2.1 Polymerase chain reaction (PCR)

All PCR reactions were performed in the DNA Engine - Peltier Thermal Cycler PTC-200 (Biorad). Each reaction was composed of 5 µl 10x KOD Buffer (Novagen), 2.5 µl 25 mM MgSO4 (Novagen), 5 µl dNTP mix (2 mM) (Stratagene),1 ng of the DNA template and 10 µl of 0.5 µM forward and reverse primer.
The mixture was brought if necessary to a volume of 49 µl double-distilled water and 1 µl of KOD polymerase (1 U/ul, Novagen) was added to a final volume of 50 µl. The KOD polymerase has a high elongation rate of 106-138 bases per second (Taq polymerase 61 bases per second) and has in contrast to the Taq polymerase a 3' to 5' exonuclease activity (Takagi et al., 1997).
For difficult reactions a mixture of 0.8 µl KOD polymerase and 0.2 µl Taq polymerase (5 U/µl, Novagen) was used. The commonly used PCR program consisted of usual 30 cycles starting with an initial denaturing step for 30 seconds at 95 °C.
This step was followed by 5 cycles each with 30 seconds denaturing at 95 °C and the annealing temperature was set to 58 °C. Elongation temperature was set to 75 °C for 50 seconds. The following 25 cycles were carried out as before but the annealing temperature was increased to 62 °C. The final step is an elongation step for five minutes at 75 °C.
After completion of the PCR program the 5 µl of the PCR mixture was mixed with 5 µl of 6x DNA loading buffer an analysed according to the size of the PCR product on 0.8 % - 2 % agarose gel.
The remaining PCR product was purified using the QIAquick PCR Purification Kit (Qiagen) following manufacturer's instruction. The amplified PCR product was eluted subsequently in 100 µl EB buffer (Qiagen).

4.2.2 Agarose gel electrophoresis for separation of DNA fragments

The separation of DNA fragments was carried out on 0.8 % - 2 % agarose gels. Therefore 8 g/l – 20 g/l agarose (Invitrogen) were boiled with one liter of 1x TBE buffer and poured hot in a flat chamber custom made chamber with inserted comb and spacers. Additionally 2 µl of ethidium bromide (10 mg/ml) was mixed with the

solution. After solidification of the agarose, the spacer and excess agarose was removed. Subsequently, the chamber was filled with 1x TBE buffer and the comb could be drawn. Prior to the application of the samples they were mixed with 6x DNA loading buffer and applied into the respective pockets. Electrophoresis was performed by applying a voltage of 90 $V_{constant}$ until the sample buffer band reached the end of the agarose gel. As DNA standard a DNA size standard marker (GeneRuler® DNA Ladder Mix, Fermentas) was applied to determine the size of the separated DNA fragments. The analysis was performed on the visualization of the intercalated ethidium bromide between the basespairs of the DNA. Ethidium bromide has absorption maxima at 210 nm and 285 nm and emits light at 605 nm after excitation. Excitation was recordet using a MultiImage Light Cabinet (AlphaImager HP System 1.4 Megapixel camera, motorized 8-48 mm, F1.2 zoom lens with +2 diopter close-up lens, white light table, EPI white lights, Orange filter and UV transilluminator (Alpha Innotech)) and analysed using the included AlphaView Image Analysis Software v.6.0.

4.2.3 Restriction digestion of DNA

4.2.3.1 Restriction digestion of PCR products

Restriction enzymes recognize specific DNA sequences and can cut out specific parts of the DNA. Restriction enzymes are categorizes in five different subclasses according to the site they recognize and the site they can cleave as well as the dependency cofactors. For double digestion approaches the corresponding buffer was chosen in which both enzymes have their highest activity.

Therefore 100 µl of the elution from the purification using the PCR purification Kit (Qiagen) were mixed with 13 µl of 10x buffer 4 (NewEngland Biolabs) and mixed with 1 µl Nde I (NewEngland Biolabs) and 1 µl Xho I (NewEngland Biolabs). The reaction mix was was filled up to 130 µl with double-distilled water and incubated for 2 h at 37 °C. Thereafter 0.5 µl of each enzyme was added and incubated for an additional hour.

The restriction digest was purified using the QIAquick PCR Purification Kit (Qiagen) following the manufacturer's instructions and the digested DNA fragment was eluted with 30 µl of EB buffer.

4.2.3.2 Restriction digest of vector fragments

The vector with the desired DNA fragment was incubated with the desired restriction enzymes. The fragment thereby is flanked by the corresponding cleavage sites. The appropriate 10x buffer was chosen in which the used enzymes have the highest activity. By default, a reaction volume of 30 µl was used. For this purpose 1 µg of being cut vector and 3 µl of the appropriate 10x buffer (NewEngland Biolabs) as well as 1 µl of each enzyme was mixed.
The mixture was brought to a final volume of 30 µl with double-distilled water and incubated for two hours at 37 °C. After 1 h each of the enzymes used was added freshly and incubated for an additional hour at 37 °C. The complete digest was then analyzed on an appropriate agarose gel at 90 $V_{constant}$ containing 2 µl ethidium bromide (10 mg/ml). After the separation the expected DNA fragment (Vetter GmbH Contact Lamp Type Chroma 42) was determined using a DNA size standard GeneRuler DNA Ladder Mix (Fermentas). Ethidium bromide was excited at 210 nm and 285 nm and emission was collected at 605 nm using a Vetter GmbH Contact Lamp Type Chroma 42. The correct band was excised from the gel using a scalpel and transferred to an Eppendorf 1.5 ml tube. The fragment was purified by QIAquick Gel Extraction Kit (Qiagen) according to manufacturer's instructions from the isolated gel slice. The elution of the fragment was carried out in 30 µl Buffer EB (Qiagen).

4.2.4 Ligation von DNA fragments

The vectors used for ligations were already cutted using appropriate restriction enzymes and dephosphorylated. Always following approach was used for the ligation of DNA fragments.
5 µl of the cutted and purified DNA fragment was mixed with 0.5 µl of the desired vector. 1 µl of 10x T4-ligase buffer (NewEngland Biolabs) and 1 µl of T4 ligase (400 U/µl, NewEngland Biolabs) was added to the mixture and filled up with 2.5 µl to a final volume of 10 µl. The mixture was mixed well and the ligation was carried out for at least 6 h in a DNA Engine - Peltier Thermal Cycler PTC-200 (Biorad). A DNA fragment excised from a DNA vector and should be ligated to another DNA vector, all volumes of the ligation mixture were reduced by half.

4.2.5 Heat shock transformation of Vector DNA in competent *E. coli* XL-1

For multiplication of the ligated DNA fragments the vector plasmids were heat-shock transformed into competent *E. coli* XL-1 bacteria (Stratagene) were added. Therefor an aliquot (200 ml) was thawed on ice and 3.4 µl β-mercaptoethanol (1.42 M, Stratagene) was added. The mixture was gently shaken every two minutes for ten minutes. For each transformation mixture 50 µl of competent bacteria were mixed with 10 µl of the ligation reaction of a PCR product and incubated for 30 min on ice. The heat shock was performed by incubation of the mixture for 45 seconds at 42 °C in a water bath (Haake DC10-P5 / U) and subsequent incubation on ice for additional two minutes. To each transformation 500 µl of preheated 42 °C SOC medium was added followed by one hour incubation at 37 °C and gently shaking at 600 rpm. LB (modified Luria) medium was previously complemented with 20 µl of a sterile-filtered 20 % glucose solution (w/v) and 10 µl of 1M $MgCl_2$ solution. Each transformation mixture was plated onto prewarmed agar plates containing the appropriate antibiotic and incubated overnight at 37 °C.

4.2.6 Analysis of cloned PCR fragments

After plating the transformed XL-1 bacteria (Stratagene) on antibiotic-containing agar plates and overnight overnight at least three grown colonies were picked and inoculated in each 5 ml of LB medium supplemented with the appropriated antibiotic using sealable test tubes. Further incubation was carried out overnight at 37 ° C and and gently shaking at 300 rpm in an incubator (HT Multitron Infor, Infor AG). 2 ml each overnight culture were placed in a 2 ml Eppendorf tube and centrifuged at 13,000 rpm 1 min and the supernatant was discarded. Remaining overnight cultures were stored temporarily at 4 °C. The resulting pellets were resuspended in 250 µl per P1 buffer (Qiagen). Then 250 µl buffer P2 (Qiagen) were added, mixed by repeated inversion and 350 µl N3 buffer (Qiagen) was added. The mixtures were centrifuged several times for ten minutes at 13,000 rpm and 4 °C (Heraeus Fresco 17, Thermo Fisher Scientific). In parallel spin columns (Qiagen 50) were washed with 800 µl of distilled water by centrifugation. The supernatant prepared by alkaline lysis of bacteria was added to the centrifugation column and purified by centrifugation for one minute at 13,000 rpm. The centrifuged supernatant was discarded and the columns

were washed by centrifugation with 800 µl PE buffer (Qiagen). PE buffer was discarded again and the remaining buffer removed by an additional washing step for one minute at 13,000 rpm. Spin columns were set on top of 1.5 ml Eppendorf tubes and incubated for one to two minutes with EB buffer (Qiagen). The plasmid DNA was eluted from the spin column matrix by centrifugation with 30 µl EB buffer. 10 µl of each elution was mixed with 5 µl of a previously prepared mastermix in a 96-well microtiter plate (Nalge Nunc International Corp.) and sealed with Parafilm (Alcan Packaging) followed by a 2 h incubation at 37 °C. The enzyme mastermixed for one reaction was composed of 0.3 µl each of the appropriate enzymes (NewEngland Biolabs), 1.5 µl of the corresponding 10x NEB buffer and was brought to 5 µl with double-distilled water. Subsequently each reaction was mixed well with 5 µl of 6x DNA sample buffer directly in the microtiter plate and 10 µl each were separated on an appropriate agarose gel at 90 $V_{constant}$ .The result was verified by comparison with the applied DNA standard (GeneRuler DNA Ladder Mix, Fermentas), whether a DNA fragment of the correct size was. Documentation was performed using the Multi Image Light Cabinet (Alpha Innotech). In case of a positive match 15 ml LB medium with the appropriate antibiotic was inoculated using the temporarily stored overnight culture followed by further incubation overnight at 37 °C and 300 rpm in a shaking incubator (HT Multitron Infors, Infors AG). The overnight culture was further processed by pelleting the bacteria in 15 ml centrifugation tubes (BD Falcon) and subsequent centrifugtion for 5 minutes at 4,000 rpm 4 °C.

The plasmid isolation as then performed using the Plasmid Mini Kit (Qiagen) according to manufacturer's instructions. Deviating from the manufacturer's protocol were the increased volumes of the used P1, P2 and P3 buffers from 300 µl to 600 µl. Furthermore, a second centrifugation step to remove genomic DNA was added directly after the first centrifugation to remove any residual genomic DNA. Additionally to precipitate the eluted plasmid DNA each reaction was mixed with isopropanol but the incubation was performed at -20 °C room temperature and not as indicated at room temperatur. Finally plasmid DNA was air-dried resuspended in 50 µl TE buffer for two hours at 37 °C and shaking at 1400 rpm in a thermo mixer compact 5250 (Eppendorf). The DNA concentration was determined by measuring the absorbence at 260 nm using a NanoDrop 1000 spectrophotometer (peqlab GmbH). The plasmid DNA was then sequenced in the in house sequencing facility and stored at -20 °C.

The analysis of cloned vector fragements was analogous to the analysis of cloned PCR fragements with the difference that only 5 µl of the elution was analyzed and filled up with double distilled water to 10 µl.

4.2.7 Generation of chemically competent *E. coli* BL21 (DE3)

Bacterial stocks stored at -80 °C were used to plate the *E. coli* strain BL21 (DE3) containing the λ DE3 lysogen carrying the gene for T7 RNA polymerase under the control of the lac UV5 promoter.

4.2.8 Heat shock transformation of competent *E. coli* BL21 (DE3)

The heat shock method was used to introduction the desired vector DNA in competent *E. coli* BL21 (DE3). Therefor an aliquot of about 200 µl competent *E. coli* BL21 (DE3) was thawed on ice. For one batch 50 µl competent bacteria were mixed with 50 ng – 100 ng the corresponding vector DNA in prechilled Eppendorf tubes and incubated for 20 minutes on ice. Each transformation was heat shocked for 30 seconds at 42 °C using a water bath (Haake DC10-P5 / U) followed by incubation for 2 minutes on ice. 350 µl of preheated LB medium was added without antibiotic and incubated for additional 30 minutes at 37 °C and 600 rpm (Thermo Mixer compact 5250, Eppendorf). The plating was carried out using agar plates containing the appropriate antibiotics and subsequent incubating at 37 °C overnight.

4.2.9 Affinity purification of His-tagged fusion proteins

Affinity purification of His-tagged fusion proteins is the most commonly used technique to purify recombinant proteins expressed in *E. coli*. Therefor proteins were designed to be expressed with a polyhistidine, usually six subsequent Histidines fused to the N- or C-terminus of the desired protein. This His tag binds specifically to bivalent metal ions, mostly nickel ions. The Ni^{2+} ions are bound by nitrilotriacetic acid (Ni-NTA), a chelating agent conjugated to a supportive material, mostly agarose. The Ni^{2+} ions can interact with two histidine residues of the protein and ensures that only the fusion protein binds to the used resin. To remove unspecifically bound proteins from the resin low Imidazole containg buffers are commonly used. The Imidazol

competes for the binding to Ni^{2+} ions and is thereby displacing the His-tagged proteins from the used resin in high concentrations (200 – 500 mM). Because of the higher binding affinity of the poly histidine, buffers with low concentrations of Imidazol (5 - 50 mM) can be used to remove proteins binding with their endogenous Histidines to the resin.

4.2.10 Test expression by affinity purification of His-tagged fusion proteins

To determine the optimal expression conditions of the used recombinant proteins test expressions were performed. Therefor 4x 50 ml LB medium containing each 1 mM $MgSO_4$, 1 ml of 50x 5052 and 2.5 ml 20x NPS as well as the appropriate antibiotics were placed in 200ml flasks. Each batch was inoculated with 1:100 of the respective overnight culture and incubated at 37 °C and 300 rpm in a shaking incubator (HT Multitron Infor, Infor AG). After the cultures had reached an OD_{600} of 1.5 each approach was separately incubated overnight at 18 °C, 25 °C, 30 °C and 37 °C.
The following day, the cultures should have reached OD_{600} of at least 5. Subsequently, the bacteria were harvested.

4.2.11 Purification of test expressions by affinity purification of His-tagged fusion proteins

Each of the bacterial cultures grown overnight was transferred in 50 ml centrifugation tubes (BD Falcon) and centrifugation for at least 5 minutes at 4,000 rpm and 4 °C using a Multifuge 1L-R, (Thermo Fisher Scientific). The LB medium was discarded and the bacterial pellet was resuspended in 15 ml cold nickel wash buffer with the addition of 200 µl of 0.2 M PMSF .The bacterial suspension was then homogenized using a high pressure homogenizer EmulsiFlex-C3 (Avestin). Each crude cell lysate was then supplemented were 1 M $MgCl_2$ to a final concentration of 1 mM $MgCl_2$, 10 µl DNAse I (Roche, 10 mg/ml in PBS) and 0.1 ml of 0.2 M PMSF, subsequently incubated for 10 minutes on ice. Bacterial cell debris was the removed by centrifugation in 50 ml containers (Sorvall) for 15 minutes at 15,000 rpm and 4 °C in a F21-8x50y rotor (Sorvall) centrifuged (Sorvall Evolution RC, Thermo Fisher Scientific). The supernatants after centrifugation were filtered through a piece of cheesecloth (Holthaus Medical) and 200 µl a 50 % slurry Ni-NTA-agarose resin

(Qiagen) was added followed by 2 h incubation at 4 °C rotating. The Ni-NTA-agarose was collected by centrifugation for 2 min at 1000 rpm using a Multifuge 1L-R (Thermo Fisher Scientific). The remaining supernatant was discarded. The centrifugation concentrated Ni-NTA-agarose was mixed with 2 ml of nickel wash buffer and transferred to 5 ml column (Pierce Centrifuge Columns, Thermo Scientific). The column was washed twice with 10 ml cold nickel wash buffer and afterwards sealed at the bottom end. 200 µl of nickel elution buffer was added to the resin with occasional brief shaking. The eluates were collected in 1.5 ml Eppendorf tubed and stored on ice. Small quantities of supernatants, cell debris and eluates as well as standard dilutions of BSA were subsequently analyzed by SDS gel electrophoresis to determine the optimal expression temperature.

4.2.12 Expression His_6-tagged fusion proteins

4.2.12.1 Expression by autoinduction

The expression by autoinduction was the commonly used method to express recombinant proteins. As the used LB media is supplemented with glucose and lactose, glucose is the preferred carbon source for rapid growing of *E. coli*. In presence of glucose uptake of lactose is prevented by inactivation of the lactose permease. The glucose present in the media blocks the enzyme adenylate cyclase which synthesizes cyclic adenosine monophosphate (cAMP) from ATP. Due to the lack of cAMP, complex formation of cAMP and CAP (catabolite activator protein) is prevented. Subsequently the required binding of the complex to the promoter to activate the transcription of the lac operon is not possible. This regulation is termed catabolite repression.

When most the glucose is metabolized, lactose is becoming the preferred carbon source. Thereby lactose is metabolized to preferentially glucose and galactose by β-galactosidase but also to allolactose, which binds to the tightly bound lac repressor. Binding leads to a conformational change and ultimately to a release of the repressor from the DNA. The RNA polymerase can now access the lac promoter leading to transcription of the lac genes. The used pET28 vector in this study contains the gene of the T7 polymerase under the control of a lac Operon. Upon activation of the lac

operon, expression of the T7 polymerase leads to transcription and translation of the desired gene construct.
For the expression of larger amounts of protein the amount of reagents was scaled up. One liter of LB media supplemented with 1 mM $MgSO_4$, 20 ml of 50x 5052 and 20 ml 50 ml NPS as well was the appropriate antibiotics and divided equally among two 2 l flask. Each 500 ml batch was inoculated with 5 ml of the same overnight culture and incubated at 37 °C and 300 rpm in a shaking incubator (HT Multitron Infor, Infor AG) incubated. After the cultures had reached an OD_{600} of 1.5, the flasks were incubated overnight the atcertain temperature, determined from the previously performed test expression. The following day, the cultures should have reached an OD_{600} ≥5. The bacteria were then harvested and further processed.

4.2.12.2 IPTG-Induction

For the expression of toxic and difficult to express proteins IPTG induction was used. IPTG as a synthetic analogue of allolactose can also induce the expression of genes under the control of a lac operon but is in comparison of allolactose not hydrolysable.
To express large quantities of proteins by IPTG induction LB media containing the appropriated antibiotics was distributed equally at 500 ml among 2 l flasks. Each 500 ml batch was inoculated with 5 ml of the same overnight culture, incubated at 37 °C and 300 rpm in a shaking incubator (HT Multitron Infor, Infor AG) and grown to an OD_{600} of 0.4. Subsequently, all reactions were further incubated at the defined temperature and grown to an OD_{600} of 0.8. Protein expression was induced by addition IPTG to a final concentration of 200 µM and further incubated for three hours.

4.2.13 large scale purification of His6-tagged fusion proteins

The IPTG-induced cultures were pooled and equally distributed on 1 l centrifugation tubes (Sorvall) and centrifuged at 5,000 rpm and 4 °C in a SLC-4000 rotor (Sorvall) (Sorvall Evolution RC, Thermo Fisher Scientific). The medium was discarded and the bacterial pellets were resuspended in approximately 200 ml of cold nickel wash buffer with the addition of 0.2 mM PMSF. The bacteria were then further processed using a high-pressure homogenizer (EmulsiFlex-C3, Avestin). The homogenates were

supplemented with 1 mM $MgCl_2$, 400 µl DnaseI (10 U/ml in PBS) and 0.2 mM PMSF and incubated for 10 min on ice. Bacterial cell debris was removed by centrifugation for 15 min at 15,000 rpm 4 °C in 250 ml centrifugation containers (Sorvall) using a SLA-1500 rotor (Sorvall) in a Sorvall Evolution RC (Thermo Fisher Scientific). A small sample of the cell debris was resuspended in approximately 400 µl of distilled water and stored on ice for analysis while the remaining pellets were discarded. The supernatant was filtered through a piece of cheesecloth and 1 ml of Ni-NTA agarose (50 % slurry, Qiagen) was added for two hours at 4 °C rotating incubation. The nickel-NTA-agarose beads were collected using a 10 ml column (Pierce Inc.). About 200 µl of the flowthrough was kept for further analysis on ice, while the remaining supernatant was discarded. The beads were washed with approximately 300 ml of cold nickel wash buffer. The column was sealed at the bottom and 1 ml of nickel elution buffer was added and incubated with occasional brief shaking for at least 10 min. The eluate was collected and stored on ice. The stored samples of each purification step were on 12 % SDS-polyacrylamide gels and for their protein content.

4.2.14 Testexpression of MISTIC fusion constructs

Testexpressions of MISTIC fusion constructs were performed as previously described in test expression by purification of His_6-tagged fusion proteins (4.2.9).

4.2.15 Purification of test expressions of MISTIC fusion constructs

Purification of MISTIC fusion constructs was performed as previously described in purification of test expressions by affinity purification of His-tagged fusion proteins (4.2.10) with the exception that the pellets were taken up in 10 mL of Nickel Wash buffer containing 1 % CTAB (w/v) and 0.2 mM PMSF and brought to a final volume of 80 ml with additional Nickel Wash Buffer + 1 % CTAB. All subsequent steps had to be carried out at room temperature, as CTAB precipitates at temperatures lower than 15 °C. The suspension was incubated for 30 min rotating at room temperature and finally centrifuged utilizing a SLA-1500 rotor for 15 min at 10,000 rpm at 20 °C (Sorvall Evolution RC, Thermo Fisher Scientific). A small amount of cell debris was resuspended in 400 µl of distilled water and not stored on ice due to the presence of CTAB. The centrifugation supernatants were filtered through a piece of cheesecloth

and 400 µl of a 50 % slurry nickel-NTA agarose (Qiagen) was added. After two hours incubation at room temperature the nickel-NTA-agarose beads were pre-concentrated by centrifugation in conical 50 ml centrifugation tubes (BD Falcon) utilizing a Multifuge 1L-R (Thermo Fisher Scientific) A small amount of supernatants were kept as a sample at room temperature while the remaining supernatants was aspirated and discarded. The nickel-NTA-agarose beads were transferred to 5 ml columns (Pierce Centrifuge columns, Thermo Scientific) and washed once with 25 mL of nickel wash Buffer + 0.1 % CTAB. The columns were sealed at the bottom end and 400 µl nickel elution buffer + 1 % CTAB was added to each column and incubated with occasional brief shaking for five minutes. Eluates were collected and further processed. Stored samples of the individual steps were subsequently analyzed on SDS-polyacrylamide gels for their protein content.

4.2.16 Large scale expression of MISTIC fusion constructs

The expression of larger amounts of MISTIC fusion proteins was carried out analogously to large scale expression of His_6-tagged fusion constructs by auto-induction with the exception that expression was performed overnight at 25 °C instead of 18 °C. This was necessary since all MISTIC constructs showed better protein expression at 25 °C.

4.2.17 Large scale expression of MISTIC fusion constructs

Purification of MISTIC fusion constructs were performed as previously described in purification of test expressions of MISTIC fusion constructs (4.2.14). with the exception that the pellets were taken up in 20 mL of Nickel Wash buffer containing 1 % CTAB (w/v) and 0.2 mM PMSF and brought to a final volume of 200 ml with additional Nickel Wash Buffer + 1 % CTAB.

The subsequent removal of CTAB from the elution using an appropriate volume of dialysis membranes (Spectra / Pore Membrane Dialysis, MWCO 12 – 14 kDa, Spectrum Laboratories) against one liter of 1x PBS was followed for one hour on a magnetic stirrer (MR 3000, Heidolph Instruments). The dialysis buffer was exchanged after 1 h followed by an additional dialysis for at least 1 h or overnight.

4.2.18 Fluorescent labelling of proteins

For labeling of proteins with Alexa Fluor fluorescent amine-reactive dyes the desired protein solution was dialyzed against two liters of 0.2 M $NaHCO_3$ in dialysis membranes (Spectra / Pore Dialysis Membrane MWCO 12 – 14 kDa, Spectrum Laboratories) for one hour. After exchanging the buffer a second dialysis step was carried out against 0.2 M $NaHCO_3$ for at least an hour. 1 mg of Alexa Fluor 488-succinimidyl ester (Invitrogen) was dissolved at 30 °C for five minutes and 600 rpm in 100 µl DMSO (Roth) and centrifugated at 13,000 rpm for five minutes at room temperature (Heraeus Pico 17, Thermo Fisher Scientific). The same procedure was carried out for the Alexa Fluor 546-succinimidyl ester (Invitrogen). Subsequently, to each 100 µl of dialyzed protein solution 5 µl of the dissolved fluorescent dye was added and mixed well. Further incubation of the reaction mixture was carried out for two hours at 25 °C and 300 rpm (Thermo Mixer compact 5250, Eppendorf) under exclusion of light. A 1.5 M hydroxylamine pH 8.5 was prepared by mixing 100 µl a 50 % hydroxylamine solution with 900 µl of distilled water and 5 µl 37 % HCl solution. The conjugation reaction was stopped by the addition of 10 µl of the 1.5 M hydroxylamine per 100 µl reaction mixture and further incubation for one hour at 25 °C and 300 rpm (Thermo Mixer compact 5250, Eppendorf) again under light exclusion. The mixture was then aliquoted and stored at -80 °C for further use.

4.2.19 SDS-polyacrylamide gel electrophoresis

For the separation of proteins, the discontinuous SDS polyacrylamide gel electrophoresis according to Laemmli (Laemmli, 1970) was used.
Glass plates with integrated spacers and a small glass plate were assembled. The separating gel was prepared and immediately filled with a pipette into the space between the glass plates to about 1 cm below the top glass plate and carefully covered with about 1 ml of water. When the separation gel was completely polymerized the stacking gel was immediately poured onto the separating gel and a comb was placed. The completely completely polymerized gels was used directly or packaged for long term storage in damp towels at 4 °C.

4.2.19.1 Sample preparation

The samples to be analyzed were mixed with 6x SDS sample buffer in ratio a 1:1, thoroughly mixed and boiled in a heating block at 95 °C for five minutes (neoBlock - Heater Duo 2-2504, neoLab). Subsequently all samples were spun at 13,000 rpm for 15 s (Heraeus Pico 17, Thermo Fisher Scientific) and 10 µl were applied to each lane. As a molecular weight standard 5 µl Unstained Protein Molecular Weight Markers (range 14.4 - 116 kDa (Fermentas) or 5 µl of Unstained SDS PAGE protein marker (range 6.5 - 200 kDa, (Serva) were used per gel.

4.2.19.2 Gel run

The prepared SDS gels were hooked into a electrophoresis tank (Mini-PROTEAN 3 electrophoresis cell or mini-PROTEAN Tetra system, Bio-Rad) and filled with 1x Laemmli running buffer. The comb was removed and the pockets were rinsed with electrophoresis buffer. After the samples were loaded on the gel a constant current of 15 mA per gel was applied. After complete entry of the sample into the stacking gel, the applied current was increased to 25 mA per gel. When the running front reached the bottom of the gel electrophoresis was stopped.

4.2.20 Tricine-SDS-Polyacrylamid-Gelelektrophoresis

To improve the separation of small proteins discontinuous SDS-polyacrylamide-gel electrophoresis was used according to Schägger (Schägger & Jagow, 1987). It is a modified form of the SDS-PAGE. It is based on a Tricine-Tris buffer system and is able to improve the separation of proteins in the range of ~ 1 - 100 kDa. The gel assembly was performed as described in SDS-polyacrylamide gel electrophoresis (4.2.19) with the exception that the separation gel was immediately overlaid with the stacking gel and the comb was placed after pouring the stacking gel. Fully polymerized gels were then used directly or stored in packaged wet wipes for not more than 2-3 days at 4 °C.

separation gel (for 2 gels):

1.66 ml	Rotiphorese Gel A 30 % Acrylamid 37.5:1 (Roth)
1.675 ml	gelbuffer (3 M Tris, 0.3 % SDS, adjusted to pH 8.5)
570 µl	H_2O
1.06 ml	50 % glycerol
3 µl	TEMED
25 µl	10 % APS

stacking gel (for 2 gels):

400 µl	Rotiphorese Gel A 30 % Acrylamid 37.5:1 (Roth)
750 µl	gelbuffer (3 M Tris, 0.3 % SDS, adjusted to pH 8.5)
1.85 ml	H_2O
4 µl	TEMED
20 µl	10 % APS

4.2.20.1 Sample preparation

Sample preparation was performed as previously described in 4.2.19.1

4.2.20.2 Gel run

Gels were hooked in gel electrophoresis systems (Mini-PROTEAN Electrophoresis Cell or Bio-Rad Mini-PROTEAN Tetra system, Biorad). The outer region of the electrophoresis chamber was filled with 1x anode buffer while the part between the gels was filled with 1x cathode buffer. A constant current of 15 mA per gel was applied after applying of the sample and the protein standards. After the sample entered the stacking gel, the applied current was increased to 25 mA per gel.

4.2.21 Staining and destaining of gels

After separation both the SDS gels and modified according to Schägger were incubated for at least one hour at room temperature in Coomassie stain solution.

Subsequently, the staining solution was discarded and briefly washed with water. The destaining of gels was performed by incubation with destaining solution I for at least 30 min followed by incubation with destaining solution II for additional 30 min. Gels were stored in water or dried using the Gelair Drying System (Biorad).

4.2.22 Western Blot

Using the western blotting procedure separated proteins from SDS polyacrylamide gels were transferred to nitrocellulose membranes (Towbin et al., (1979)) utilizing the tank blotting procedure in a Trans-Blot Cell (Biorad). By applying an electric field, proteins are transferred and fixed to nitrocellulose membranes by hydrophobic interactions. The transfer cassettes were assembled in a sandwich process and subsequently mounted in the transfer buffer filled. As a transfer buffer used was a Tris-glycine buffer + 20 % ethanol. The transfer was carried out at 4 °C with an applied constant current of 100 mA for small or 370 mA for large transfer chambers for three hours with constant stirring on a magnetic stirrer (MR 3000, Heidolph Instruments). After transfer, the nitrocellulose membrane was stained with Ponceau S solution (Fluka), an anionic azo dye reversibly binds to amino groups of proteins to verify success of the transfer. Nitrocellulose membranes were blocked with blocking solution for at least one hour at room temperature or better overnight at 4 °C to saturate nonspecific binding sites. Incubation of membranes with primary antibodies was carried out for two hours at room temperature in 10 ml of blocking solution with an antibody dilution of usually 1: 1000 on a rocker (See-Saw Rocker SSL4, Stuart). After incubation membranes were washed. Subsequently the secondary horseradish peroxidase-coupled antibody was added and incubated for one hour in blocking solution with an antibody dilution of usually 1: 5000 rocking (See-Saw Rocker SSL4, Stuart). Non-specifically bound secondary antibodies were largely removed by a series of washing steps (3x 1 min, 5x 5 min, 5x 10 min) with PBS-Tween-20 (0.1 %). Bands were visualized by applying the ECL reagent I + II (Western Lightning, PerkinElmer). The chemiluminescence was recorded using the Gel Logic 1500 Imaging System (Kodak).

4.2.23 GST pulldown assay

Each 2 mg of GST-fusion protein were coupled with 400 µl of a 50 % GSH-Sepharose suspension (Glutathione Sepharose 4 Fast flow, GE Healthcare) overnight rotating (SB2, Stuart) at 4 °C. After incubation GSH-Sepharose beads were centrifuged for five minutes at 5,000 rpm (Heraeus Fresco 17, Thermo Fisher Scientific), the supernatant was discarded and further blocked for 5 % BSA for one hour rotation. Subsequently, the GSH-Sepharose beads were centrifuged, the supernatant was removed and the beads washed with 2 ml cold 1x PBS. The procedure was repeated at least five times. The blocked and washed beads were resuspended in 200 µl 1x PBS and stored until further use at 4 °C.
To perform pull down assays with bacterial lysates bead bound GST proteins were incubated with 500 µl of *E. coli* lysates or from untransformed bacteria. After 1 h of incubation rotating samples were washed six times with 20 mM Tris and 50 mM NaCl, pH 7.4 and eluted by cleavage employing 30 µl of recombinant TEV or PreScission protease (0.5 mg/ml) for an additional hour at 25 °C shaking at 600 rpm. Samples were eluted by centrifugation and analyzed by SDS–PAGE and Western blotting.

4.2.24 Generation of proteoliposomes

4.2.24.1 Preparation

A lipid mixture corresponding to the composition of the inner nuclear membrane was prepared as follows. The lipids were purchased from Avanti Polar Lipids (Alabaster, Alabama, USA).

Quantity in mol %	Lipid (source)	Molar mass g / mol
60	phosphatidylcholine (egg, chicken), powder	770.1
20	phosphatidylethanolamine (egg, chicken), powder	744.1
10	phosphatidylinositole (liver, bovine), powder	909.1
5	cholesterol (ovine wool >98%), powder	286.7
2.5	phosphatidylserine(brain, porcine), powder	812
2.5	sphingomyelin (egg,chicken), powder	703

The weighed amounts of the individual lipid were dissolved for about two hours in 10 % Octyl-β-D-glucopyranoside (w/v) in H_2O with a total lipid concentration of 30 mg/ml at 15 °C and 1000 rpm in Thermo Mixer compact 5250 (Eppendorf). The lipid mixture was aliquoted and stored at -80 °C.

An appropriate amount Sepharose (Sephadex G50 fine, GE Healthcare) was added to a sufficient volume of 1x PBS. The sepharose was allowed to swell for 5 min and was subsequently degased in a Desiccator. Transparent glas gel filtration columns (Econo-Column 0.5 x 20 cm 4 ml, Biorad) were clamped in holder (Roth) and almost completely filled with the swollen and degased sepharose. By connecting the lid of the gel filtration columns they were connected to a higher located buffer reservoir. The sepharose was blocked initally by applying 100 µl BSA (1 mg/ml in 1x PBS. The column was washed for additional 30 min.

4.2.24.2 Procedure

Membrane protein solution was mixed completely with 20 µl of the desired lipid mixture (30 mg/ml) in 100 µl 1x PBS and was completely applied to the column.

Additionally lipophilic fluorescent dyes e.g. DiI-C_{18} (1 mg/ml in DMSO) or DiD-C_{18} (1 mg/ml in DMSO) can be added. After the mixture completely entered the column material, the Sepharose was carefully overlayed with 1 ml of 1x PBS and the column was reconnected to the buffer reservoir. In the subsequent separation of the fastest continuous colored band was collected when fluorescently labeled proteins were used.

4.2.25 Preparation of proteoliposomes lipid film

Platinum gauze electrodes (ALS Co., Ltd, Tokyo Japan) were placed in a custom made lid and attached spacer.The electrodes had a distance of 0.5 cm. The electrodes were washed twice with chloroform followed by washing with 70 % ethanol (v/v) and finally with distilled water.The electrodes were dried on a heating block (Dri-Block DB-2A, Techne) dried at 42 °C. Proteoliposomes were prepared as described before and collected. The mixture was transferred to polycarbonate centrifugation tubes (11 x 34 mm PC tube) suitable for a TLA120 rotor (Beckmann). The proteoliposomes were centrifugated using a TLA120.2 rotor (Beckman Coulter) at 4 °C 100,000 rpm for 30 min.The resulting pellet was resuspended in 60 µl HB100 buffer and 5 µl of the solution was spread evenly on the platinum gauzes. The lipid film was dried on a heating block (Dri-Block DB-2A, Techne) at 42 °C for 5 min and subsequently dried in a desiccator under vacuum for at least one hour at room temperature or at 4 °C overnight.

4.2.26 Electroformation of proteoliposome lipid films

To previously prepared lipid film-covered platinum gauzes were mounted in standard cuvette (UVette routine pack 50 – 2,000 µl, Eppendorf, Hamburg, Germany) filled with 1 ml of 259 mM succrose. A sinoidale alternating voltage of 2.1 V with a frequency of 10 Hz (TG315 function generator, TTi) was applied for 140 min followed by 20 min at 2 Hz. Throughout the electroformation the chamber was placed on a heating block at 42 °C. An 8 well chamber (LabTek) was blocked with 5 % BSA in PBS (w/v) for at least 1 h and washed twice with 1x PBS. After electroformation GUVs were pipetted with open tips (Molecular Bio Products) in the prepared chamber und visualized using a confocal fluorescence microscope (Fluoview FV1000, Olympus).

4.2.27 Prepararion of lipid films from chloroform dissolved lipids

Chloroform dissolved lipids (Avanti Polar Lipids) were mixed according to the composition of the inner nuclear membrane (described in 4.2.24.1). The platinum electrodes were cleaned with chloroform and then thoroughly rinsed with distilled water and dried. For each electroformation approach 7.5 µl chloroform and 2.5 µl of the appropriate chloroform dissolved lipid mixture (10 mg/ml) were mixed and supplemented if needed with 0.25 µl DiD-C18 (0.1 mg/ml) / DiI-C_{18} (0.1 mg/ml (Sigma-Aldrich). The mixture was spread quickly equally on both platinum electrodes and dried by evaporation of the chloroform followed by drying for at least one hour under vacuum in a desiccator at room temperature to remove residual chloroform.

4.2.28 Electroformation of lipid films from chloroform dissolved lipids

Electroformation of lipid films from chloroform dissolved lipids was performed as previously described in 4.2.28. Electroformation time at 10 Hz was decreased from 140 min to 80 min.

4.2.29 Confocal laser scanning microscopy

To image giant unilamellar vesicles a confocal laser scanning microscope Olympus Fluoview FV1000 (Olympus Optical Co.) was utilized. The microscope was equipped with an argon laser emitting light at wavelengths of 458 nm, 488 nm and 515 nm is emitted. Furthermore, a combined laser diode laser emitting light with wavelengths of 405 nm, 440 nm, 473 nm, 559 nm and 635 nm was emitted as a laser combiner FV-10 MCPSU-405-633 used (Olympus). All observations were made using a 60x water immersion objective UPLSAPO 60XW N: performed A 1.20. The confocal pinhole size (pinhole) was set to one airy and thus 140 µm (UPLSAPO 60XW N: A 1.20). For detection of the fluorescent signals is a primary beam splitter SDM405/488/559/635 (Olympus) was used and split the signal into three channels. For the detection of the fluorescence signal of Alexa Fluor 488-labeled proteins or antibodies, a dichroic mirror (beam splitter emission SDM560) was used. For the detection of the

fluorescence signal of Alexa Fluor 546-labeled proteins and the Texas Red-labeled dextran 40 kDa was however a dichroic mirror (beam splitter emission SDM640 (Olympus)) used. The DiD-C_{18} membrane dye was determined using the emission filter BA655-755 (Olympus) detected in the beam path. Fluorescence signals were detected and analyzed with the help of three integrated AOTF - PMTs (acousto-optic tunable filter - photomultiplier tubes), detecting faint light signals, convert them into electrical signals and amplifying them.Signals were analysed with the associated software FV10-ASW FV1000 vers. 4.1.

4.2.30 Atomic Force microscopy

Supported lipid bilayers were imaged using a JPK NanoWizard II system (JPK Instruments, Berlin, Germany) mounted on an Axiovert 200 Inverted Microscope (Carl Zeiss, Jena, Germany). Intermittent contact (IC or tapping) mode images were taken using V-shaped silicon nitride cantilevers (SNL-10) with a typical spring constant of 0.08 N/m and a nominal tip radius of 2 nm. The cantilever oscillation was tuned to a frequency between 3 - 10 kHz, and the amplitude was set between 0.3 - 0.6 V. The amplitude was varied during the experiment to minimize the force of the tip on the bilayer. The scan rate was set to 0.7 - 1 Hz. The height, deflection and phase-shift signals were collected, simultaneously, in both trace and retrace directions. AFM images were acquired before and after adding 150 nM His_6-EGFP-pUL31 or His_6-EGFP on the bilayer. AFM images were analysed using JPK Data Analysis software.

4.2.31 Preparation of supported lipid bilayers

Supported lipid bilayers were prepared as described (Unsay et al., 2013). The nuclear envelope lipid mix with 0.2 mol % Rhodamine-PE was dissolved in SLB buffer (10 mM HEPES, pH 7.4, 150 mM NaCl) at a concentration of 5 mg/ml. 20 µL of the mixture were diluted with 150 µL with SLB buffer. The suspension was then vortexed and bath-sonicated until a clear suspension was obtained, indicating that small unilamellar vesicles were formed. The clear solution was put in contact at 37 °C with freshly-cleaved mica glued to a glas coverslip. $CaCl_2$ was added to a final concentration of 3 mM and incubated at 37 °C for 10 min. The samples were rinsed

several times with SLB buffer to remove $CaCl_2$ and unfused vesicles, and then allowed to equilibrate at room temperature before analysis.

4.2.32 Cell Culture

All cells were cultured under standard cell culture conditions at 37 °C and 5 % CO_2.

4.2.32.1 Cell culture media

- 440 ml DMEM for HeLa S3 cells and HEK 293 T cells, high glucose

(lifetechnologies, Gibco)
50 ml fetal calf serum (lifetechnologies, Gibco)
5 ml Pen/Strep (10,000 mg/ml Streptomycin, 10,000 units/ml Penicillin)
(lifetechnologies, Gibco)
5 ml L-glutamine (200 mM) (lifetechnologies, Gibco)

- 440 ml DMEM for RK13 cells, low glucose (lifetechnologies, Gibco)

50 ml fetal calf serum (lifetechnologies, Gibco)
5 ml Pen/Strep (10,000 mg/ml Streptomycin, 10,000 units/ml Penicillin)
(life technologies, Gibco)
5 ml L-glutamine (200 mM) (lifetechnologies, Gibco)

4.2.33 Transfection of cells

Cells were seeded to 50 - 80 % confluency prior to transfection in 24 well plates (Nunc,Thermo Scientific). At the day of transfection 50 µl of serum and antibiotic free media was incubated with 1.5 µl of Fugene 6 transfection reagent and incubated for 5 min. Subsequently 0.5 µg of DNA was added to the mixture and incubated for 15 min at room temperature. To each well 20 µl were pipetted dropwise to the media. The cells were further incubated for 24 h or 48 h before fixation.

4.2.34 Immunofluorescence

Previously on coverslips seeded cells were fixed for 10 min in 4 % paraformaldehyd (w/v) in PBS) incubated for 5 min with 50 mM $(NH_4)Cl$ to quench autofluoresence and subsequently blocked with blocking buffer.Following the cells were incubated with 1:500 (rabbit antibodies) or 1:1000 for (mouse antibodies) with primary antibodies in blocking buffer for 2 h. The cover slips were washed three times with PBS+ 0.1 % Tween and secondary antibodies goat anti-rabbit IgG Alexa 488 / goat anti-mouse IgG Alexa 488 or goat anti-rabbit IgG Cy3 / goat anti-mouse IgG Cy3 in a dilution of 1:2000 in blocking buffer was added for 2 h. Following it cells were stained with DAPI (1 µg/ml in PBS) for 10 min and washed once with 1x PBS. Coverslip was sealed with nail polish and stored at 4 °C.

4.2.35 Electron microscopy

Cells were washed with 1x PBS and fixed with 2.5 % glutaraldehyd in 100 mM sodium cacodylat pH 7.5. Subsequent treatment was processed by the inhouse EM facility. Fixed cells were removed from the plates, washed twice with 100 mM sodium cacodylat and pelleted for 1 min at 1.500g in 15 ml centrifugation tubes (BD Falcons). The cell pellet were embedded in 1.8 % gelatine in 100 mM sodium cacodylat (w/v) and incubated for 10 min at 37 °C followed by cooling on ice for 30 min. Post-fixation of embedded cells was performed with 1 % OsO_4 in 100 mM sodium cacodylat for 2 h at 4 °C and subsequent contrasting with 1 % UAc (w/v) o/n at 4 °C. Dehydration of cell blocks was done by a series of ethanol washes each time increasing the concentration of ethanol up to 100 %. After exchange of ethanol by propylenoxid cells were embedded in EPON.
Epon-embedded cells were thin sectioned and imaged employing a FEI Tecnai G20 transmission electron microscope.

5 References

1. Aimon, Sophie; Manzi, John; Schmidt, Daniel; Poveda Larrosa, Jose Antonio; Bassereau, Patricia; Toombes, Gilman E S (2011): Functional reconstitution of a voltage-gated potassium channel in giant unilamellar vesicles. In: *PLoS One* 6 (10), S. e25529. DOI: 10.1371/journal.pone.0025529.

2. Angelova, Miglena I.; Dimitrov, Dimiter S. (1986): Liposome electroformation. In: *Faraday Discuss. Chem. Soc.* 81, S. 303. DOI: 10.1039/DC9868100303.

3. Baines, J. D.; Jacob, R. J.; Simmerman, L.; Roizman, B. (1995): The herpes simplex virus 1 UL11 proteins are associated with cytoplasmic and nuclear membranes and with nuclear bodies of infected cells. In: *J Virol* 69 (2), S. 825–833.

4. Baines, Joel D.; Wills, Elizabeth; Jacob, Robert J.; Pennington, Janice; Roizman, Bernard (2007): Glycoprotein M of herpes simplex virus 1 is incorporated into virions during budding at the inner nuclear membrane. In: *J Virol* 81 (2), S. 800–812. DOI: 10.1128/JVI.01756-06.

5. Ball, Jennifer R.; Ullman, Katharine S. (2005): Versatility at the nuclear pore complex: lessons learned from the nucleoporin Nup153. In: *Chromosoma* 114 (5), S. 319–330. DOI: 10.1007/s00412-005-0019-3.

6. Bandyopadhyay, Chirosree; Valiya-Veettil, Mohanan; Dutta, Dipanjan; Chakraborty, Sayan; Chandran, Bala (2014): CIB1 synergizes with EphrinA2 to regulate Kaposi's sarcoma-associated herpesvirus macropinocytic entry in human microvascular dermal endothelial cells. In: *PLoS Pathog* 10 (2), S. e1003941. DOI: 10.1371/journal.ppat.1003941.

7. Banfield, B. W.; Leduc, Y.; Esford, L.; Visalli, R. J.; Brandt, C. R.; Tufaro, F. (1995): Evidence for an interaction of herpes simplex virus with chondroitin sulfate proteoglycans during infection. In: *Virology* 208 (2), S. 531–539. DOI: 10.1006/viro.1995.1184.

8. Bastos, R.; Lin, A.; Enarson, M.; Burke, B. (1996): Targeting and function in mRNA export of nuclear pore complex protein Nup153. In: *J Cell Biol* 134 (5), S. 1141–1156.

9. Batterson, W.; Roizman, B. (1983): Characterization of the herpes simplex virion-associated factor responsible for the induction of alpha genes. In: *J Virol* 46 (2), S. 371–377.

10. Baumgart, Tobias; Hammond, Adam T.; Sengupta, Prabuddha; Hess, Samuel T.; Holowka, David A.; Baird, Barbara A.; Webb, Watt W. (2007): Large-scale fluid/fluid phase separation of proteins and lipids in giant plasma membrane vesicles. In: *Proc Natl Acad Sci U S A* 104 (9), S. 3165–3170. DOI: 10.1073/pnas.0611357104.

11. Baumgart, Tobias; Hunt, Geoff; Farkas, Elaine R.; Webb, Watt W.; Feigenson, Gerald W. (2007): Fluorescence probe partitioning between Lo/Ld phases in lipid membranes. In: *Biochim Biophys Acta* 1768 (9), S. 2182–2194. DOI: 10.1016/j.bbamem.2007.05.012.

12. Bayburt, Timothy H.; Sligar, Stephen G. (2010): Membrane protein assembly into Nanodiscs. In: *FEBS letters* 584 (9), S. 1721–1727. DOI: 10.1016/j.febslet.2009.10.024.

13. Bender, Florent C.; Whitbeck, J. Charles; Lou, Huan; Cohen, Gary H.; Eisenberg, Roselyn J. (2005): Herpes simplex virus glycoprotein B binds to cell surfaces independently of heparan sulfate and blocks virus entry. In: *J Virol* 79 (18), S. 11588–11597. DOI: 10.1128/JVI.79.18.11588-11597.2005.

14. Betaneli, Viktoria; Petrov, Eugene P.; Schwille, Petra (2012): The role of lipids in VDAC oligomerization. In: *Biophys J* 102 (3), S. 523–531. DOI: 10.1016/j.bpj.2011.12.049.

15. Betaneli, Viktoria; Worch, Remigiusz; Schwille, Petra (2012): Effect of temperature on the formation of liquid phase-separating giant unilamellar vesicles (GUV). In: *Chem Phys Lipids* 165 (6), S. 630–637. DOI: 10.1016/j.chemphyslip.2012.06.006.

16. Bigalke, Janna M.; Heuser, Thomas; Nicastro, Daniela; Heldwein, Ekaterina E. (2014): Membrane deformation and scission by the HSV-1 nuclear egress complex. In: *Nat Commun* 5, S. 4131. DOI: 10.1038/ncomms5131.

17. Bjerke, Susan L.; Roller, Richard J. (2006): Roles for herpes simplex virus type 1 UL34 and US3 proteins in disrupting the nuclear lamina during herpes simplex virus type 1 egress. In: *Virology* 347 (2), S. 261–276. DOI: 10.1016/j.virol.2005.11.053.

18. Block, T. M.; Hill, J. M. (1997): The latency associated transcripts (LAT) of herpes simplex virus: still no end in sight. In: *J Neurovirol* 3 (5), S. 313–321.

19. Boehmer, P. E.; Lehman, I. R. (1997): Herpes simplex virus DNA replication. In: *Annu Rev Biochem* 66, S. 347–384. DOI: 10.1146/annurev.biochem.66.1.347.

20. Borch, Jonas; Hamann, Thomas (2009): The nanodisc: a novel tool for membrane protein studies. In: *Biol Chem* 390 (8), S. 805–814. DOI: 10.1515/BC.2009.091.

21. Brown, Deborah A. (2006): Lipid rafts, detergent-resistant membranes, and raft targeting signals. In: *Physiology (Bethesda)* 21, S. 430–439. DOI: 10.1152/physiol.00032.2006.

22. Brown, Jay C.; Newcomb, William W. (2011): Herpesvirus capsid assembly: insights from structural analysis. In: *Curr Opin Virol* 1 (2), S. 142–149. DOI: 10.1016/j.coviro.2011.06.003.

23. Burton, Edward A.; Fink, David J.; Glorioso, Joseph C. (2002): Gene delivery using herpes simplex virus vectors. In: *DNA and cell biology* 21 (12), S. 915–936. DOI: 10.1089/104454902762053864.

24. Cai, W. Z.; Person, S.; Warner, S. C.; Zhou, J. H.; DeLuca, N. A. (1987): Linker-insertion nonsense and restriction-site deletion mutations of the gB glycoprotein gene of herpes simplex virus type 1. In: *J Virol* 61 (3), S. 714–721.

25. Campbell, M. E.; Palfreyman, J. W.; Preston, C. M. (1984): Identification of herpes simplex virus DNA sequences which encode a trans-acting polypeptide responsible for stimulation of immediate early transcription. In: *J Mol Biol* 180 (1), S. 1–19.

26. Cano-Monreal, Gina L.; Wylie, Kristine M.; Cao, Feng; Tavis, John E.; Morrison, Lynda A. (2009): Herpes simplex virus 2 UL13 protein kinase disrupts nuclear lamins. In: *Virology* 392 (1), S. 137–147. DOI: 10.1016/j.virol.2009.06.051.

27. Castellana, Edward T.; Cremer, Paul S. (2006): Solid supported lipid bilayers: From biophysical studies to sensor design. In: *Surface Science Reports* 61 (10), S. 429–444. DOI: 10.1016/j.surfrep.2006.06.001.

28. Chang, Y. E.; Roizman, B. (1993): The product of the UL31 gene of herpes simplex virus 1 is a nuclear phosphoprotein which partitions with the nuclear matrix. In: *J Virol* 67 (11), S. 6348–6356.

29. Chang, Y. E.; van Sant, C.; Krug, P. W.; Sears, A. E.; Roizman, B. (1997): The null mutant of the U(L)31 gene of herpes simplex virus 1: construction and phenotype in infected cells. In: *J Virol* 71 (11), S. 8307–8315.

30. Chen, Ting; Muratore, Tara L.; Schaner-Tooley, Christine E.; Shabanowitz, Jeffrey; Hunt, Donald F.; Macara, Ian G. (2007): N-terminal alpha-methylation of RCC1 is necessary for stable chromatin association and normal mitosis. In: *Nat Cell Biol* 9 (5), S. 596–603. DOI: 10.1038/ncb1572.

31. Cheshenko, Natalia; Trepanier, Janie B.; Gonzalez, Pablo A.; Eugenin, Eliseo A.; Jacobs, William R Jr; Herold, Betsy C. (2014): Herpes simplex virus type 2 glycoprotein H interacts with integrin alphavbeta3 to facilitate viral entry and calcium signaling in human genital tract epithelial cells. In: *J Virol* 88 (17), S. 10026–10038. DOI: 10.1128/JVI.00725-14.

32. Cheshenko, Natalia; Trepanier, Janie B.; Stefanidou, Martha; Buckley, Niall; Gonzalez, Pablo; Jacobs, William; Herold, Betsy C. (2013): HSV activates Akt to trigger calcium release and promote viral entry: novel candidate target for treatment and suppression. In: *FASEB J* 27 (7), S. 2584–2599. DOI: 10.1096/fj.12-220285.

33. CM, Preston: Repression of viral transcription during herpes simplex virus latency. - PubMed - NCBI. Online verfügbar unter http://www.ncbi.nlm.nih.gov/pubmed/10640537, zuletzt geprüft am 10.12.2014.

34. Cockrell, Shelley K.; Huffman, Jamie B.; Toropova, Katerina; Conway, James F.; Homa, Fred L. (2011): Residues of the UL25 protein of herpes simplex virus that are required for its stable interaction with capsids. In: *J Virol* 85 (10), S. 4875–4887. DOI: 10.1128/JVI.00242-11.

35. Coe, Helen; Michalak, Marek (2009): Calcium binding chaperones of the endoplasmic reticulum. In: *Gen Physiol Biophys* 28 Spec No Focus, S. F96-F103.

36. Conway JF,Homa FL in Weller, Sandra K. (©2011): Alphaherpesviruses. Molecular virology. Norfolk, UK: Caister Academic Press.

37. Copeland, Anna Maria; Newcomb, William W.; Brown, Jay C. (2009): Herpes simplex virus replication: roles of viral proteins and nucleoporins in capsid-nucleus attachment. In: *J Virol* 83 (4), S. 1660–1668. DOI: 10.1128/JVI.01139-08.

38. D'Angelo, Maximiliano A.; Anderson, Daniel J.; Richard, Erin; Hetzer, Martin W. (2006): Nuclear pores form de novo from both sides of the nuclear envelope. In: *Science* 312 (5772), S. 440–443. DOI: 10.1126/science.1124196.

39. Davison, Andrew J. (2010): Herpesvirus systematics. In: *Vet Microbiol* 143 (1), S. 52–69. DOI: 10.1016/j.vetmic.2010.02.014.

40. Davison, Andrew J.; Eberle, Richard; Ehlers, Bernhard; Hayward, Gary S.; McGeoch, Duncan J.; Minson, Anthony C. et al. (2009): The order Herpesvirales. In: *Arch Virol* 154 (1), S. 171–177. DOI: 10.1007/s00705-008-0278-4.

41. Demaurex, Nicolas; Frieden, Maud (2003): Measurements of the free luminal ER Ca(2+) concentration with targeted "cameleon" fluorescent proteins. In: *Cell Calcium* 34 (2), S. 109–119.

42. Deniaud, Aurelien; Bernaudat, Florent; Frelet-Barrand, Annie; Juillan-Binard, Celine; Vernet, Thierry; Rolland, Norbert; Pebay-Peyroula, Eva (2011): Expression of a chloroplast ATP/ADP transporter in E. coli membranes: behind the Mistic strategy. In: *Biochim Biophys Acta* 1808 (8), S. 2059–2066. DOI: 10.1016/j.bbamem.2011.04.011.

43. Devaux, Philippe F.; Herrmann, Andreas; Ohlwein, Nina; Kozlov, Michael M. (2008): How lipid flippases can modulate membrane structure. In: *Biochim Biophys Acta* 1778 (7-8), S. 1591–1600. DOI: 10.1016/j.bbamem.2008.03.007.

44. Dohner, Katinka; Wolfstein, Andre; Prank, Ute; Echeverri, Christophe; Dujardin, Denis; Vallee, Richard; Sodeik, Beate (2002): Function of dynein and dynactin in herpes simplex virus capsid transport. In: *Mol Biol Cell* 13 (8), S. 2795–2809. DOI: 10.1091/mbc.01-07-0348.

45. Doucet, Christine M.; Hetzer, Martin W. (2010): Nuclear pore biogenesis into an intact nuclear envelope. In: *Chromosoma* 119 (5), S. 469–477. DOI: 10.1007/s00412-010-0289-2.

46. Doucet, Christine M.; Talamas, Jessica A.; Hetzer, Martin W. (2010): Cell cycle-dependent differences in nuclear pore complex assembly in metazoa. In: *Cell* 141 (6), S. 1030–1041. DOI: 10.1016/j.cell.2010.04.036.

47. Drin, Guillaume; Antonny, Bruno (2010): Amphipathic helices and membrane curvature. In: *FEBS Lett* 584 (9), S. 1840–1847. DOI: 10.1016/j.febslet.2009.10.022.

48. Drin, Guillaume; Casella, Jean-Francois; Gautier, Romain; Boehmer, Thomas; Schwartz, Thomas U.; Antonny, Bruno (2007): A general amphipathic alpha-helical motif for sensing membrane curvature. In: *Nat Struct Mol Biol* 14 (2), S. 138–146. DOI: 10.1038/nsmb1194.

49. Dultz, Elisa; Ellenberg, Jan (2007): Nuclear envelope. In: *Curr Biol* 17 (5), S. R154-6. DOI: 10.1016/j.cub.2006.12.035.

50. Dultz, Elisa; Ellenberg, Jan (2010): Live imaging of single nuclear pores reveals unique assembly kinetics and mechanism in interphase. In: *J Cell Biol* 191 (1), S. 15–22. DOI: 10.1083/jcb.201007076.

51. Dvir, Hay; Lundberg, Matthew E.; Maji, Samir K.; Riek, Roland; Choe, Senyon (2009): Mistic: cellular localization, solution behavior, polymerization, and fibril formation. In: *Protein Sci* 18 (7), S. 1564–1570. DOI: 10.1002/pro.148.

52. Eisenberg, Roselyn J.; Atanasiu, Doina; Cairns, Tina M.; Gallagher, John R.; Krummenacher, Claude; Cohen, Gary H. (2012): Herpes virus fusion and entry: a story with many characters. In: *Viruses* 4 (5), S. 800–832. DOI: 10.3390/v4050800.

53. Eisenhardt, Nathalie; Redolfi, Josef; Antonin, Wolfram (2014): Interaction of Nup53 with Ndc1 and Nup155 is required for nuclear pore complex assembly. In: *J Cell Sci* 127 (Pt 4), S. 908–921. DOI: 10.1242/jcs.141739.

54. Eisenhardt, Nathalie; Schooley, Allana; Antonin, Wolfram (2014): Xenopus in vitro assays to analyze the function of transmembrane nucleoporins and targeting of inner nuclear membrane proteins. In: *Methods in cell biology* 122, S. 193–218. DOI: 10.1016/B978-0-12-417160-2.00009-6.

55. Enarson, P.; Enarson, M.; Bastos, R.; Burke, B. (1998): Amino-terminal sequences that direct nucleoporin nup153 to the inner surface of the nuclear envelope. In: *Chromosoma* 107 (4), S. 228–236.

56. Farnsworth, Aaron; Johnson, David C. (2006): Herpes simplex virus gE/gI must accumulate in the trans-Golgi network at early times and then redistribute to cell junctions to promote cell-cell spread. In: *J Virol* 80 (7), S. 3167–3179. DOI: 10.1128/JVI.80.7.3167-3179.2006.

57. Farnsworth, Aaron; Wisner, Todd W.; Webb, Michael; Roller, Richard; Cohen, Gary; Eisenberg, Roselyn; Johnson, David C. (2007): Herpes simplex virus glycoproteins gB and gH function in fusion between the virion envelope and the outer nuclear membrane. In: *Proc Natl Acad Sci U S A* 104 (24), S. 10187–10192. DOI: 10.1073/pnas.0703790104.

58. Farsad, Khashayar; Camilli, Pietro de (2003): Mechanisms of membrane deformation. In: *Curr Opin Cell Biol* 15 (4), S. 372–381.

59. Ford, Marijn G J; Mills, Ian G.; Peter, Brian J.; Vallis, Yvonne; Praefcke, Gerrit J K; Evans, Philip R.; McMahon, Harvey T. (2002): Curvature of clathrin-coated pits driven by epsin. In: *Nature* 419 (6905), S. 361–366. DOI: 10.1038/nature01020.

60. Forrester, A.; Farrell, H.; Wilkinson, G.; Kaye, J.; Davis-Poynter, N.; Minson, T. (1992): Construction and properties of a mutant of herpes simplex virus type 1 with glycoprotein H coding sequences deleted. In: *J Virol* 66 (1), S. 341–348.

61. Franz, Cerstin; Askjaer, Peter; Antonin, Wolfram; Iglesias, Carmen Lopez; Haselmann, Uta; Schelder, Malgorzata et al. (2005): Nup155 regulates nuclear envelope and nuclear pore complex formation in nematodes and vertebrates. In: *EMBO J* 24 (20), S. 3519–3531. DOI: 10.1038/sj.emboj.7600825.

62. Franz, Cerstin; Walczak, Rudolf; Yavuz, Sevil; Santarella, Rachel; Gentzel, Marc; Askjaer, Peter et al. (2007): MEL-28/ELYS is required for the recruitment of nucleoporins to chromatin and postmitotic nuclear pore complex assembly. In: *EMBO Rep* 8 (2), S. 165–172. DOI: 10.1038/sj.embor.7400889.

63. Furlong, D.; Swift, H.; Roizman, B. (1972): Arrangement of herpesvirus deoxyribonucleic acid in the core. In: *J Virol* 10 (5), S. 1071–1074.

64. Gant, T. M.; Wilson, K. L. (1997): Nuclear assembly. In: *Annu Rev Cell Dev Biol* 13, S. 669–695. DOI: 10.1146/annurev.cellbio.13.1.669.

65. Garg, Sumit; Ruhe, Jurgen; Ludtke, Karin; Jordan, Rainer; Naumann, Christoph A. (2007): Domain registration in raft-mimicking lipid mixtures studied using polymer-tethered lipid bilayers. In: *Biophys J* 92 (4), S. 1263–1270. DOI: 10.1529/biophysj.106.091082.

66. Gerster, T.; Roeder, R. G. (1988): A herpesvirus trans-activating protein interacts with transcription factor OTF-1 and other cellular proteins. In: *Proc Natl Acad Sci U S A* 85 (17), S. 6347–6351.

67. Giles, Niroshini M.; Watts, Aaron B.; Giles, Gregory I.; Fry, Fiona H.; Littlechild, Jennifer A.; Jacob, Claus (2003): Metal and redox modulation of cysteine protein function. In: *Chem Biol* 10 (8), S. 677–693.

68. Gillespie, Peter J.; Khoudoli, Guennadi A.; Stewart, Graeme; Swedlow, Jason R.; Blow, J. Julian (2007): ELYS/MEL-28 chromatin association coordinates nuclear pore complex assembly and replication licensing. In: *Curr Biol* 17 (19), S. 1657–1662. DOI: 10.1016/j.cub.2007.08.041.

69. Girard, Philippe; Pecreaux, Jacques; Lenoir, Guillaume; Falson, Pierre; Rigaud, Jean-Louis; Bassereau, Patricia (2004): A new method for the reconstitution of membrane proteins into giant unilamellar vesicles. In: *Biophys J* 87 (1), S. 419–429. DOI: 10.1529/biophysj.104.040360.

70. Gonnella, Roberta; Farina, Antonella; Santarelli, Roberta; Raffa, Salvatore; Feederle, Regina; Bei, Roberto et al. (2005): Characterization and intracellular localization of the Epstein-Barr virus protein BFLF2: interactions with BFRF1 and with the nuclear lamina. In: *J Virol* 79 (6), S. 3713–3727. DOI: 10.1128/JVI.79.6.3713-3727.2005.

71. Gorlich, D.; Mattaj, I. W. (1996): Nucleocytoplasmic transport. In: *Science* 271 (5255), S. 1513–1518.

72. Grossman, Einat; Medalia, Ohad; Zwerger, Monika (2012): Functional architecture of the nuclear pore complex. In: *Annu Rev Biophys* 41, S. 557–584. DOI: 10.1146/annurev-biophys-050511-102328.

73. Gruenbaum, Yosef; Margalit, Ayelet; Goldman, Robert D.; Shumaker, Dale K.; Wilson, Katherine L. (2005): The nuclear lamina comes of age. In: *Nat Rev Mol Cell Biol* 6 (1), S. 21–31. DOI: 10.1038/nrm1550.

74. Grunewald, Kay; Desai, Prashant; Winkler, Dennis C.; Heymann, J. Bernard; Belnap, David M.; Baumeister, Wolfgang; Steven, Alasdair C. (2003): Three-dimensional structure of herpes simplex virus from cryo-electron tomography. In: *Science* 302 (5649), S. 1396–1398. DOI: 10.1126/science.1090284.

75. Harel, Amnon; Orjalo, Arturo V.; Vincent, Thomas; Lachish-Zalait, Aurelie; Vasu, Sanjay; Shah, Sundeep et al. (2003): Removal of a single pore subcomplex results in vertebrate nuclei devoid of nuclear pores. In: *Mol Cell* 11 (4), S. 853–864.

76. Heimburg, T. (2010): Lipid ion channels. In: *Biophys Chem* 150 (1-3), S. 2–22. DOI: 10.1016/j.bpc.2010.02.018.

77. Heming, Jason D.; Huffman, Jamie B.; Jones, Lisa M.; Homa, Fred L. (2014): Isolation and characterization of the herpes simplex virus 1 terminase complex. In: *J Virol* 88 (1), S. 225–236. DOI: 10.1128/JVI.02632-13.

78. Hetzer, M.; Bilbao-Cortes, D.; Walther, T. C.; Gruss, O. J.; Mattaj, I. W. (2000): GTP hydrolysis by Ran is required for nuclear envelope assembly. In: *Mol Cell* 5 (6), S. 1013–1024.

79. Homa; Brown (1997): Capsid assembly and DNA packaging in herpes simplex virus. In: *Rev Med Virol* 7 (2), S. 107–122.

80. Honess, R. W.; Roizman, B. (1974): Regulation of herpesvirus macromolecular synthesis. I. Cascade regulation of the synthesis of three groups of viral proteins. In: *J Virol* 14 (1), S. 8–19.

81. Hutchins, James R A; Moore, William J.; Hood, Fiona E.; Wilson, Jamie S J; Andrews, Paul D.; Swedlow, Jason R.; Clarke, Paul R. (2004): Phosphorylation regulates the dynamic interaction of RCC1 with chromosomes during mitosis. In: *Curr Biol* 14 (12), S. 1099–1104. DOI: 10.1016/j.cub.2004.05.021.

82. Im, Young Jun; Wollert, Thomas; Boura, Evzen; Hurley, James H. (2009): Structure and function of the ESCRT-II-III interface in multivesicular body biogenesis. In: *Dev Cell* 17 (2), S. 234–243. DOI: 10.1016/j.devcel.2009.07.008.

83. Jena, Bhanu P. (2011): Role of SNAREs in membrane fusion. In: *Adv Exp Med Biol* 713, S. 13–32. DOI: 10.1007/978-94-007-0763-4_3.

84. Johannsen, Eric; Luftig, Micah; Chase, Michael R.; Weicksel, Steve; Cahir-McFarland, Ellen; Illanes, Diego et al. (2004): Proteins of purified Epstein-Barr virus. In: *Proc Natl Acad Sci U S A* 101 (46), S. 16286–16291. DOI: 10.1073/pnas.0407320101.

85. Kato, Akihisa; Yamamoto, Mayuko; Ohno, Takashi; Kodaira, Hiroshi; Nishiyama, Yukihiro; Kawaguchi, Yasushi (2005): Identification of proteins phosphorylated directly by the Us3 protein kinase encoded by herpes simplex virus 1. In: *J Virol* 79 (14), S. 9325–9331. DOI: 10.1128/JVI.79.14.9325-9331.2005.

86. Kelly, Barbara J.; Fraefel, Cornel; Cunningham, Anthony L.; Diefenbach, Russell J. (2009): Functional roles of the tegument proteins of herpes simplex virus type 1. In: *Virus Res* 145 (2), S. 173–186. DOI: 10.1016/j.virusres.2009.07.007.

87. Kerr, Alastair Rw; Schirmer, Eric C. (2011): FG repeats facilitate integral protein trafficking to the inner nuclear membrane. In: *Commun Integr Biol* 4 (5), S. 557–559. DOI: 10.4161/cib.4.5.16052.

88. Kim, Ju Youn; Mandarino, Angelo; Chao, Moses V.; Mohr, Ian; Wilson, Angus C. (2012): Transient reversal of episome silencing precedes VP16-dependent transcription during reactivation of latent HSV-1 in neurons. In: *PLoS Pathog* 8 (2), S. e1002540. DOI: 10.1371/journal.ppat.1002540.

89. Klupp, B. G.; Granzow, H.; Mettenleiter, T. C. (2001): Effect of the pseudorabies virus US3 protein on nuclear membrane localization of the UL34 protein and virus egress from the nucleus. In: *J Gen Virol* 82 (Pt 10), S. 2363–2371.

90. Klupp, Barbara; Altenschmidt, Jan; Granzow, Harald; Fuchs, Walter; Mettenleiter, Thomas C. (2008): Glycoproteins required for entry are not necessary for egress of pseudorabies virus. In: *J Virol* 82 (13), S. 6299–6309. DOI: 10.1128/JVI.00386-08.

91. Klupp, Barbara G.; Granzow, Harald; Fuchs, Walter; Keil, Gunther M.; Finke, Stefan; Mettenleiter, Thomas C. (2007): Vesicle formation from the nuclear membrane is induced by coexpression of two conserved herpesvirus proteins. In: *Proc Natl Acad Sci U S A* 104 (17), S. 7241–7246. DOI: 10.1073/pnas.0701757104.

92. Klymchenko, Andrey S.; Kreder, Remy (2014): Fluorescent probes for lipid rafts: from model membranes to living cells. In: *Chem Biol* 21 (1), S. 97–113. DOI: 10.1016/j.chembiol.2013.11.009.

93. Kristie, T. M.; LeBowitz, J. H.; Sharp, P. A. (1989): The octamer-binding proteins form multi-protein--DNA complexes with the HSV alpha TIF regulatory protein. In: *EMBO J* 8 (13), S. 4229–4238.

94. Krogsgaard, Michelle; Li, Qi-Jing; Sumen, Cenk; Huppa, Johannes B.; Huse, Morgan; Davis, Mark M. (2005): Agonist/endogenous peptide-MHC heterodimers drive T cell activation and sensitivity. In: *Nature* 434 (7030), S. 238–243. DOI: 10.1038/nature03391.

95. Kubalek, E. W.; Le Grice, S F; Brown, P. O. (1994): Two-dimensional crystallization of histidine-tagged, HIV-1 reverse transcriptase promoted by a novel nickel-chelating lipid. In: *J Struct Biol* 113 (2), S. 117–123. DOI: 10.1006/jsbi.1994.1039.

96. Laemmli, U. K. (1970): Cleavage of structural proteins during the assembly of the head of bacteriophage T4. In: *Nature* 227 (5259), S. 680–685.

97. Lake, Cathleen M.; Hutt-Fletcher, Lindsey M. (2004): The Epstein-Barr virus BFRF1 and BFLF2 proteins interact and coexpression alters their cellular localization. In: *Virology* 320 (1), S. 99–106. DOI: 10.1016/j.virol.2003.11.018.

98. Leach, Natalie; Bjerke, Susan L.; Christensen, Desire K.; Bouchard, Jacques M.; Mou, Fan; Park, Richard et al. (2007): Emerin is hyperphosphorylated and redistributed in herpes simplex virus type 1-infected cells in a manner dependent on both UL34 and US3. In: *J Virol* 81 (19), S. 10792–10803. DOI: 10.1128/JVI.00196-07.

99. Leach, Natalie R.; Roller, Richard J. (2010): Significance of host cell kinases in herpes simplex virus type 1 egress and lamin-associated protein disassembly from the nuclear lamina. In: *Virology* 406 (1), S. 127–137. DOI: 10.1016/j.virol.2010.07.002.

100. Lehman, I. R.; Boehmer, P. E. (1999): Replication of herpes simplex virus DNA. In: *J Biol Chem* 274 (40), S. 28059–28062.

101. Leuzinger, Helene; Ziegler, Urs; Schraner, Elisabeth M.; Fraefel, Cornel; Glauser, Daniel L.; Heid, Irma et al. (2005): Herpes simplex virus 1 envelopment follows two diverse pathways. In: *J Virol* 79 (20), S. 13047–13059. DOI: 10.1128/JVI.79.20.13047-13059.2005.

102. Li, Hoi-Yeung; Zheng, Yixian (2004): Phosphorylation of RCC1 in mitosis is essential for producing a high RanGTP concentration on chromosomes and for spindle assembly in mammalian cells. In: *Genes Dev* 18 (5), S. 512–527. DOI: 10.1101/gad.1177304.

103. Liang, Li; Baines, Joel D. (2005): Identification of an essential domain in the herpes simplex virus 1 UL34 protein that is necessary and sufficient to interact with UL31 protein. In: *J Virol* 79 (6), S. 3797–3806. DOI: 10.1128/JVI.79.6.3797-3806.2005.

104. Lievremont, J. P.; Rizzuto, R.; Hendershot, L.; Meldolesi, J. (1997): BiP, a major chaperone protein of the endoplasmic reticulum lumen, plays a direct and important role in the storage of the rapidly exchanging pool of Ca2+. In: *J Biol Chem* 272 (49), S. 30873–30879.

105. Ligas, M. W.; Johnson, D. C. (1988): A herpes simplex virus mutant in which glycoprotein D sequences are replaced by beta-galactosidase sequences binds to but is unable to penetrate into cells. In: *J Virol* 62 (5), S. 1486–1494.

106. Lingwood, Daniel; Simons, Kai (2010): Lipid rafts as a membrane-organizing principle. In: *Science* 327 (5961), S. 46–50. DOI: 10.1126/science.1174621.

107. Liu, Y.; Gong, W.; Huang, C. C.; Herr, W.; Cheng, X. (1999): Crystal structure of the conserved core of the herpes simplex virus transcriptional regulatory protein VP16. In: *Genes Dev* 13 (13), S. 1692–1703.

108. Loret, Sandra; Guay, Ginette; Lippe, Roger (2008): Comprehensive characterization of extracellular herpes simplex virus type 1 virions. In: *J Virol* 82 (17), S. 8605–8618. DOI: 10.1128/JVI.00904-08.

109. Lotzerich, Mark; Ruzsics, Zsolt; Koszinowski, Ulrich H. (2006): Functional domains of murine cytomegalovirus nuclear egress protein M53/p38. In: *J Virol* 80 (1), S. 73–84. DOI: 10.1128/JVI.80.1.73-84.2006.

110. Luitweiler, Eric M.; Henson, Brandon W.; Pryce, Erin N.; Patel, Varun; Coombs, Gavin; McCaffery, J. Michael; Desai, Prashant J. (2013): Interactions of the Kaposi's Sarcoma-associated herpesvirus nuclear egress complex: ORF69 is a potent factor for remodeling cellular membranes. In: *J Virol* 87 (7), S. 3915–3929. DOI: 10.1128/JVI.03418-12.

111. Magalska, Adriana; Schellhaus, Anna Katharina; Moreno-Andres, Daniel; Zanini, Fabio; Schooley, Allana; Sachdev, Ruchika et al. (2014): RuvB-like ATPases Function in Chromatin Decondensation at the End of Mitosis. In: *Dev Cell* 31 (3), S. 305–318. DOI: 10.1016/j.devcel.2014.09.001.

112. Maric, Martina; Shao, Jianqiang; Ryan, Randi J.; Wong, Chun-Shu; Gonzalez-Alegre, Pedro; Roller, Richard J. (2011): A functional role for TorsinA in herpes simplex virus 1 nuclear egress. In: *J Virol* 85 (19), S. 9667–9679. DOI: 10.1128/JVI.05314-11.

113. Martin-Serrano, Juan; Neil, Stuart J D (2011): Host factors involved in retroviral budding and release. In: *Nat Rev Microbiol* 9 (7), S. 519–531. DOI: 10.1038/nrmicro2596.

114. Matis, J.; Kudelova, M. (2001): Early shutoff of host protein synthesis in cells infected with herpes simplex viruses. In: *Acta Virol* 45 (5-6), S. 269–277.

115. McDonald, Bethan; Martin-Serrano, Juan (2009): No strings attached: the ESCRT machinery in viral budding and cytokinesis. In: *J Cell Sci* 122 (Pt 13), S. 2167–2177. DOI: 10.1242/jcs.028308.

116. McGeoch, D. J.; Dalrymple, M. A.; Davison, A. J.; Dolan, A.; Frame, M. C.; McNab, D. et al. (1988): The complete DNA sequence of the long unique region in the genome of herpes simplex virus type 1. In: *J Gen Virol* 69 (Pt 7), S. 1531–1574.

117. McMahon, Harvey T.; Gallop, Jennifer L. (2005): Membrane curvature and mechanisms of dynamic cell membrane remodelling. In: *Nature* 438 (7068), S. 590–596. DOI: 10.1038/nature04396.

118. Mettenleiter, Thomas C. (2002): Herpesvirus assembly and egress. In: *J Virol* 76 (4), S. 1537–1547.

119. Mettenleiter, Thomas C. (2004): Budding events in herpesvirus morphogenesis. In: *Virus Res* 106 (2), S. 167–180. DOI: 10.1016/j.virusres.2004.08.013.

120. Meure, Louise A.; Foster, Neil R.; Dehghani, Fariba (2008): Conventional and dense gas techniques for the production of liposomes: a review. In: *AAPS PharmSciTech* 9 (3), S. 798–809. DOI: 10.1208/s12249-008-9097-x.

121. Miranda-Saksena, Monica; Boadle, Ross A.; Aggarwal, Anupriya; Tijono, Bibing; Rixon, Frazer J.; Diefenbach, Russell J.; Cunningham, Anthony L. (2009): Herpes simplex virus utilizes the large secretory vesicle pathway for anterograde transport of tegument and envelope proteins and for viral exocytosis from growth cones of human fetal axons. In: *J Virol* 83 (7), S. 3187–3199. DOI: 10.1128/JVI.01579-08.

122. Mou, Fan; Forest, Tom; Baines, Joel D. (2007): US3 of herpes simplex virus type 1 encodes a promiscuous protein kinase that phosphorylates and alters localization of lamin A/C in infected cells. In: *J Virol* 81 (12), S. 6459–6470. DOI: 10.1128/JVI.00380-07.

123. Mou, Fan; Wills, Elizabeth; Baines, Joel D. (2009): Phosphorylation of the U(L)31 protein of herpes simplex virus 1 by the U(S)3-encoded kinase regulates localization of the nuclear envelopment complex and egress of nucleocapsids. In: *J Virol* 83 (10), S. 5181–5191. DOI: 10.1128/JVI.00090-09.

124. Muranyi, Walter; Haas, Jurgen; Wagner, Markus; Krohne, Georg; Koszinowski, Ulrich H. (2002): Cytomegalovirus recruitment of cellular kinases to dissolve the nuclear lamina. In: *Science* 297 (5582), S. 854–857. DOI: 10.1126/science.1071506.

125. Naldinho-Souto, Raquel; Browne, Helena; Minson, Tony (2006): Herpes simplex virus tegument protein VP16 is a component of primary enveloped virions. In: *J Virol* 80 (5), S. 2582–2584. DOI: 10.1128/JVI.80.5.2582-2584.2006.

126. Newcomb, W. W.; Homa, F. L.; Thomsen, D. R.; Booy, F. P.; Trus, B. L.; Steven, A. C. et al. (1996): Assembly of the herpes simplex virus capsid: characterization of intermediates observed during cell-free capsid formation. In: *J Mol Biol* 263 (3), S. 432–446. DOI: 10.1006/jmbi.1996.0587.

127. Newmeyer, D. D.; Finlay, D. R.; Forbes, D. J. (1986): In vitro transport of a fluorescent nuclear protein and exclusion of non-nuclear proteins. In: *J Cell Biol* 103 (6 Pt 1), S. 2091–2102.

128. Nogueira, Mauricio L.; Wang, Victoria E H; Tantin, Dean; Sharp, Phillip A.; Kristie, Thomas M. (2004): Herpes simplex virus infections are arrested in Oct-1-deficient cells. In: *Proc Natl Acad Sci U S A* 101 (6), S. 1473–1478. DOI: 10.1073/pnas.0307300101.

129. Ozelius, L. J.; Hewett, J. W.; Page, C. E.; Bressman, S. B.; Kramer, P. L.; Shalish, C. et al. (1997): The early-onset torsion dystonia gene (DYT1) encodes an ATP-binding protein. In: *Nat Genet* 17 (1), S. 40–48. DOI: 10.1038/ng0997-40.

130. Padula, Maryn E.; Sydnor, Mariam L.; Wilson, Duncan W. (2009): Isolation and preliminary characterization of herpes simplex virus 1 primary enveloped virions from the perinuclear space. In: *J Virol* 83 (10), S. 4757–4765. DOI: 10.1128/JVI.01927-08.

131. Pante, Nelly; Kann, Michael (2002): Nuclear pore complex is able to transport macromolecules with diameters of about 39 nm. In: *Mol Biol Cell* 13 (2), S. 425–434. DOI: 10.1091/mbc.01-06-0308.

132. Papahadjopoulos, D.; Nir, S.; Duzgunes, N. (1990): Molecular mechanisms of calcium-induced membrane fusion. In: *J Bioenerg Biomembr* 22 (2), S. 157–179.

133. Papp, S.; Dziak, E.; Michalak, M.; Opas, M. (2003): Is all of the endoplasmic reticulum created equal? The effects of the heterogeneous distribution of endoplasmic reticulum Ca2+-handling proteins. In: *J Cell Biol* 160 (4), S. 475–479. DOI: 10.1083/jcb.200207136.

134. Park, Richard; Baines, Joel D. (2006): Herpes simplex virus type 1 infection induces activation and recruitment of protein kinase C to the nuclear membrane and increased phosphorylation of lamin B. In: *J Virol* 80 (1), S. 494–504. DOI: 10.1128/JVI.80.1.494-504.2006.

135. Pasdeloup, David; Blondel, Danielle; Isidro, Anabela L.; Rixon, Frazer J. (2009): Herpesvirus capsid association with the nuclear pore complex and viral DNA release involve the nucleoporin CAN/Nup214 and the capsid protein pUL25. In: *J Virol* 83 (13), S. 6610–6623. DOI: 10.1128/JVI.02655-08.

136. Pawliczek, Tobias; Crump, Colin M. (2009): Herpes simplex virus type 1 production requires a functional ESCRT-III complex but is independent of TSG101 and ALIX expression. In: *J Virol* 83 (21), S. 11254–11264. DOI: 10.1128/JVI.00574-09.

137. Pelkmans, Lucas; Burli, Thomas; Zerial, Marino; Helenius, Ari (2004): Caveolin-stabilized membrane domains as multifunctional transport and sorting devices in endocytic membrane traffic. In: *Cell* 118 (6), S. 767–780. DOI: 10.1016/j.cell.2004.09.003.

138. Petrovskaya, L. E.; Shulga, A. A.; Bocharova, O. V.; Ermolyuk, Ya S.; Kryukova, E. A.; Chupin, V. V. et al. (2010): Expression of G-protein coupled receptors in Escherichia coli for structural studies. In: *Biochemistry (Mosc)* 75 (7), S. 881–891.

139. Pincetic, Andrew; Leis, Jonathan (2009): The Mechanism of Budding of Retroviruses From Cell Membranes. In: *Adv Virol* 2009, S. 6239691–6239699. DOI: 10.1155/2009/623969.

140. Post, L. E.; Mackem, S.; Roizman, B. (1981): Regulation of alpha genes of herpes simplex virus: expression of chimeric genes produced by fusion of thymidine kinase with alpha gene promoters. In: *Cell* 24 (2), S. 555–565.

141. Preston, C. M. (2000): Repression of viral transcription during herpes simplex virus latency. In: *J Gen Virol* 81 (Pt 1), S. 1–19.

142. Prufert, Kristina; Vogel, Annette; Krohne, Georg (2004): The lamin CxxM motif promotes nuclear membrane growth. In: *J Cell Sci* 117 (Pt 25), S. 6105–6116. DOI: 10.1242/jcs.01532.

143. Purich, Daniel L.; Allison, R. Donald (©2000): Handbook of biochemical kinetics. San Diego, CA: Academic Press.

144. Purves, F. C.; Spector, D.; Roizman, B. (1991): The herpes simplex virus 1 protein kinase encoded by the US3 gene mediates posttranslational modification of the phosphoprotein encoded by the UL34 gene. In: *J Virol* 65 (11), S. 5757–5764.

145. Purves, F. C.; Spector, D.; Roizman, B. (1992): UL34, the target of the herpes simplex virus U(S)3 protein kinase, is a membrane protein which in its unphosphorylated state associates with novel phosphoproteins. In: *J Virol* 66 (7), S. 4295–4303.

146. Radtke, Kerstin; Kieneke, Daniela; Wolfstein, Andre; Michael, Kathrin; Steffen, Walter; Scholz, Tim et al. (2010): Plus- and minus-end directed microtubule motors bind simultaneously to herpes simplex virus capsids using different inner tegument structures. In: *PLoS Pathog* 6 (7), S. e1000991. DOI: 10.1371/journal.ppat.1000991.

147. Ralle, Thorsten; Grund, Christine; Franke, Werner W.; Stick, Reimer (2004): Intranuclear membrane structure formations by CaaX-containing nuclear proteins. In: *J Cell Sci* 117 (Pt 25), S. 6095–6104. DOI: 10.1242/jcs.01528.

148. Rasala, Beth A.; Orjalo, Arturo V.; Shen, Zhouxin; Briggs, Steven; Forbes, Douglass J. (2006): ELYS is a dual nucleoporin/kinetochore protein required for nuclear pore assembly and proper cell division. In: *Proc Natl Acad Sci U S A* 103 (47), S. 17801–17806. DOI: 10.1073/pnas.0608484103.

149. Rasala, Beth A.; Ramos, Corinne; Harel, Amnon; Forbes, Douglass J. (2008): Capture of AT-rich chromatin by ELYS recruits POM121 and NDC1 to initiate nuclear pore assembly. In: *Mol Biol Cell* 19 (9), S. 3982–3996. DOI: 10.1091/mbc.E08-01-0012.

150. Read, G. Sullivan; Patterson, Mary (2007): Packaging of the virion host shutoff (Vhs) protein of herpes simplex virus: two forms of the Vhs polypeptide are associated with intranuclear B and C capsids, but only one is associated with enveloped virions. In: *J Virol* 81 (3), S. 1148–1161. DOI: 10.1128/JVI.01812-06.

151. Reynolds, A. E.; Ryckman, B. J.; Baines, J. D.; Zhou, Y.; Liang, L.; Roller, R. J. (2001): U(L)31 and U(L)34 proteins of herpes simplex virus type 1 form a complex that accumulates at the nuclear rim and is required for envelopment of nucleocapsids. In: *J Virol* 75 (18), S. 8803–8817.

152. Reynolds, Ashley E.; Liang, Li; Baines, Joel D. (2004): Conformational changes in the nuclear lamina induced by herpes simplex virus type 1 require

genes U(L)31 and U(L)34. In: *J Virol* 78 (11), S. 5564–5575. DOI: 10.1128/JVI.78.11.5564-5575.2004.

153. Reynolds, Ashley E.; Wills, Elizabeth G.; Roller, Richard J.; Ryckman, Brent J.; Baines, Joel D. (2002): Ultrastructural localization of the herpes simplex virus type 1 UL31, UL34, and US3 proteins suggests specific roles in primary envelopment and egress of nucleocapsids. In: *J Virol* 76 (17), S. 8939–8952.

154. Ries, Ryan S.; Choi, Hyeon; Blunck, Rikard; Bezanilla, Francisco; Heath, James R. (2004): Black Lipid Membranes: Visualizing the Structure, Dynamics, and Substrate Dependence of Membranes. In: *J. Phys. Chem. B* 108 (41), S. 16040–16049. DOI: 10.1021/jp048098h.

155. Rixon FJ - in: Holzenburg, A.; Bogner, Elke (©2002): Structure-function relationships of human pathogenic viruses. New York: Kluwer Academic/Plenum Publishers.

156. Roberts, Kari L.; Baines, Joel D. (2010): Myosin Va enhances secretion of herpes simplex virus 1 virions and cell surface expression of viral glycoproteins. In: *Journal of virology* 84 (19), S. 9889–9896. DOI: 10.1128/JVI.00732-10.

157. Rodriguez, Nicolas; Pincet, Frederic; Cribier, Sophie (2005): Giant vesicles formed by gentle hydration and electroformation: a comparison by fluorescence microscopy. In: *Colloids Surf B Biointerfaces* 42 (2), S. 125–130. DOI: 10.1016/j.colsurfb.2005.01.010.

158. Roizman B. and Knipe DM: Herpes simplex viruses and their replication. In: *Fields Virology, 4th edn* 2001, S. 2399–2459.

159. Roller, R. J.; Zhou, Y.; Schnetzer, R.; Ferguson, J.; DeSalvo, D. (2000): Herpes simplex virus type 1 U(L)34 gene product is required for viral envelopment. In: *J Virol* 74 (1), S. 117–129.

160. Roller, Richard J.; Bjerke, Susan L.; Haugo, Alison C.; Hanson, Sara (2010): Analysis of a charge cluster mutation of herpes simplex virus type 1 UL34 and its extragenic suppressor suggests a novel interaction between pUL34 and pUL31 that is necessary for membrane curvature around capsids. In: *J Virol* 84 (8), S. 3921–3934. DOI: 10.1128/JVI.01638-09.

161. Romaker, Daniel; Schregel, Vera; Maurer, Katja; Auerochs, Sabrina; Marzi, Andrea; Sticht, Heinrich; Marschall, Manfred (2006): Analysis of the structure-activity relationship of four herpesviral UL97 subfamily protein kinases reveals partial but not full functional conservation. In: *J Med Chem* 49 (24), S. 7044–7053. DOI: 10.1021/jm060696s.

162. Roosild, Tarmo P.; Greenwald, Jason; Vega, Mark; Castronovo, Samantha; Riek, Roland; Choe, Senyon (2005): NMR structure of Mistic, a membrane-integrating protein for membrane protein expression. In: *Science* 307 (5713), S. 1317–1321. DOI: 10.1126/science.1106392.

163. Rose, April; Schlieker, Christian (2012): Alternative nuclear transport for cellular protein quality control. In: *Trends Cell Biol* 22 (10), S. 509–514. DOI: 10.1016/j.tcb.2012.07.003.

164. Rossman, Jeremy S.; Jing, Xianghong; Leser, George P.; Lamb, Robert A. (2010): Influenza virus M2 protein mediates ESCRT-independent membrane scission. In: *Cell* 142 (6), S. 902–913. DOI: 10.1016/j.cell.2010.08.029.

165. Rothballer, Andrea; Kutay, Ulrike (2013): Poring over pores: nuclear pore complex insertion into the nuclear envelope. In: *Trends Biochem Sci* 38 (6), S. 292–301. DOI: 10.1016/j.tibs.2013.04.001.

166. Rozen, Ramona; Sathish, Narayanan; Li, Yong; Yuan, Yan (2008): Virion-wide protein interactions of Kaposi's sarcoma-associated herpesvirus. In: *J Virol* 82 (10), S. 4742–4750. DOI: 10.1128/JVI.02745-07.

167. Ryckman, Brent J.; Roller, Richard J. (2004): Herpes simplex virus type 1 primary envelopment: UL34 protein modification and the US3-UL34 catalytic relationship. In: *J Virol* 78 (1), S. 399–412.

168. Ryu, Yong-Sang; Lee, In-Ho; Suh, Jeng-Hun; Park, Seung Chul; Oh, Soojung; Jordan, Luke R. et al. (2014): Reconstituting ring-rafts in bud-mimicking topography of model membranes. In: *Nat Commun* 5, S. 4507. DOI: 10.1038/ncomms5507.

169. Sachdev, Ruchika; Sieverding, Cornelia; Flotenmeyer, Matthias; Antonin, Wolfram (2012): The C-terminal domain of Nup93 is essential for assembly of the structural backbone of nuclear pore complexes. In: *Mol Biol Cell* 23 (4), S. 740–749. DOI: 10.1091/mbc.E11-09-0761.

170. Sawtell, Nancy M.; Triezenberg, Steven J.; Thompson, Richard L. (2011): VP16 serine 375 is a critical determinant of herpes simplex virus exit from latency in vivo. In: *J Neurovirol* 17 (6), S. 546–551. DOI: 10.1007/s13365-011-0065-y.

171. Schagger, H.; Jagow, G. von (1987): Tricine-sodium dodecyl sulfate-polyacrylamide gel electrophoresis for the separation of proteins in the range from 1 to 100 kDa. In: *Anal Biochem* 166 (2), S. 368–379.

172. Schnee, Margit; Ruzsics, Zsolt; Bubeck, Anja; Koszinowski, Ulrich H. (2006): Common and specific properties of herpesvirus UL34/UL31 protein family members revealed by protein complementation assay. In: *J Virol* 80 (23), S. 11658–11666. DOI: 10.1128/JVI.01662-06.

173. Schumacher, Daniel; Tischer, B. Karsten; Trapp, Sascha; Osterrieder, Nikolaus (2005): The protein encoded by the US3 orthologue of Marek's disease virus is required for efficient de-envelopment of perinuclear virions and involved in actin stress fiber breakdown. In: *J Virol* 79 (7), S. 3987–3997. DOI: 10.1128/JVI.79.7.3987-3997.2005.

174. Schuster, Franziska; Klupp, Barbara G.; Granzow, Harald; Mettenleiter, Thomas C. (2012): Structural determinants for nuclear envelope localization and function of pseudorabies virus pUL34. In: *J Virol* 86 (4), S. 2079–2088. DOI: 10.1128/JVI.05484-11.

175. Scott, E. S.; O'Hare, P. (2001): Fate of the inner nuclear membrane protein lamin B receptor and nuclear lamins in herpes simplex virus type 1 infection. In: *J Virol* 75 (18), S. 8818–8830.

176. Segrest, J. P.; Loof, H. de; Dohlman, J. G.; Brouillette, C. G.; Anantharamaiah, G. M. (1990): Amphipathic helix motif: classes and properties. In: *Proteins* 8 (2), S. 103–117. DOI: 10.1002/prot.340080202.

177. Settles, Edward I.; Loftus, Andrew F.; McKeown, Alesia N.; Parthasarathy, Raghuveer (2010): The vesicle trafficking protein Sar1 lowers lipid membrane rigidity. In: *Biophys J* 99 (5), S. 1539–1545. DOI: 10.1016/j.bpj.2010.06.059.

178. Sezgin, Erdinc; Kaiser, Hermann-Josef; Baumgart, Tobias; Schwille, Petra; Simons, Kai; Levental, Ilya (2012): Elucidating membrane structure and protein behavior using giant plasma membrane vesicles. In: *Nat Protoc* 7 (6), S. 1042–1051. DOI: 10.1038/nprot.2012.059.

179. Simpson-Holley, Martha; Baines, Joel; Roller, Richard; Knipe, David M. (2004): Herpes simplex virus 1 U(L)31 and U(L)34 gene products promote the late maturation of viral replication compartments to the nuclear periphery. In: *J Virol* 78 (11), S. 5591–5600. DOI: 10.1128/JVI.78.11.5591-5600.2004.

180. Snapp, Erik L.; Hegde, Ramanujan S.; Francolini, Maura; Lombardo, Francesca; Colombo, Sara; Pedrazzini, Emanuela et al. (2003): Formation of stacked ER cisternae by low affinity protein interactions. In: *J Cell Biol* 163 (2), S. 257–269. DOI: 10.1083/jcb.200306020.

181. Solon, Jerome; Gareil, Olivier; Bassereau, Patricia; Gaudin, Yves (2005): Membrane deformations induced by the matrix protein of vesicular stomatitis virus in a minimal system. In: *J Gen Virol* 86 (Pt 12), S. 3357–3363. DOI: 10.1099/vir.0.81129-0.

182. Song, J.; Waugh, R. E. (1993): Bending rigidity of SOPC membranes containing cholesterol. In: *Biophys J* 64 (6), S. 1967–1970. DOI: 10.1016/S0006-3495(93)81566-2.

183. Speese, Sean D.; Ashley, James; Jokhi, Vahbiz; Nunnari, John; Barria, Romina; Li, Yihang et al. (2012): Nuclear envelope budding enables large ribonucleoprotein particle export during synaptic Wnt signaling. In: *Cell* 149 (4), S. 832–846. DOI: 10.1016/j.cell.2012.03.032.

184. Stachowiak, Jeanne C.; Schmid, Eva M.; Ryan, Christopher J.; Ann, Hyoung Sook; Sasaki, Darryl Y.; Sherman, Michael B. et al. (2012): Membrane bending by protein-protein crowding. In: *Nat Cell Biol* 14 (9), S. 944–949. DOI: 10.1038/ncb2561.

185. Stannard, L. M.; Himmelhoch, S.; Wynchank, S. (1996): Intra-nuclear localization of two envelope proteins, gB and gD, of herpes simplex virus. In: *Arch Virol* 141 (3-4), S. 505–524.

186. Stern, S.; Tanaka, M.; Herr, W. (1989): The Oct-1 homoeodomain directs formation of a multiprotein-DNA complex with the HSV transactivator VP16. In: *Nature* 341 (6243), S. 624–630. DOI: 10.1038/341624a0.

187. Strambio-De-Castillia, Caterina; Niepel, Mario; Rout, Michael P. (2010): The nuclear pore complex: bridging nuclear transport and gene regulation. In: *Nat Rev Mol Cell Biol* 11 (7), S. 490–501. DOI: 10.1038/nrm2928.

188. Taddeo, Brunella; Roizman, Bernard (2006): The virion host shutoff protein (UL41) of herpes simplex virus 1 is an endoribonuclease with a substrate specificity similar to that of RNase A. In: *J Virol* 80 (18), S. 9341–9345. DOI: 10.1128/JVI.01008-06.

189. Takagi, M.; Nishioka, M.; Kakihara, H.; Kitabayashi, M.; Inoue, H.; Kawakami, B. et al. (1997): Characterization of DNA polymerase from Pyrococcus sp. strain KOD1 and its application to PCR. In: *Appl Environ Microbiol* 63 (11), S. 4504–4510.

190. Tandon, Ritesh; AuCoin, David P.; Mocarski, Edward S. (2009): Human cytomegalovirus exploits ESCRT machinery in the process of virion maturation. In: *J Virol* 83 (20), S. 10797–10807. DOI: 10.1128/JVI.01093-09.

191. Theerthagiri, Gandhi; Eisenhardt, Nathalie; Schwarz, Heinz; Antonin, Wolfram (2010): The nucleoporin Nup188 controls passage of membrane proteins across the nuclear pore complex. In: *J Cell Biol* 189 (7), S. 1129–1142. DOI: 10.1083/jcb.200912045.

192. Thompson, Richard L.; Sawtell, Nancy M. (2010): Therapeutic implications of new insights into the critical role of VP16 in initiating the earliest stages of HSV reactivation from latency. In: *Future Med Chem* 2 (7), S. 1099–1105. DOI: 10.4155/fmc.10.197.

193. Toropova, Katerina; Huffman, Jamie B.; Homa, Fred L.; Conway, James F. (2011): The herpes simplex virus 1 UL17 protein is the second constituent of the capsid vertex-specific component required for DNA packaging and retention. In: *J Virol* 85 (15), S. 7513–7522. DOI: 10.1128/JVI.00837-11.

194. Towbin, H.; Staehelin, T.; Gordon, J. (1979): Electrophoretic transfer of proteins from polyacrylamide gels to nitrocellulose sheets: procedure and some applications. In: *Proc Natl Acad Sci U S A* 76 (9), S. 4350–4354.

195. Turcotte, Sophie; Letellier, Josee; Lippe, Roger (2005): Herpes simplex virus type 1 capsids transit by the trans-Golgi network, where viral glycoproteins accumulate independently of capsid egress. In: *J Virol* 79 (14), S. 8847–8860. DOI: 10.1128/JVI.79.14.8847-8860.2005.

196. Unsay, Joseph D.; Cosentino, Katia; Subburaj, Yamunadevi; Garcia-Saez, Ana J. (2013): Cardiolipin effects on membrane structure and dynamics. In: *Langmuir* 29 (51), S. 15878–15887. DOI: 10.1021/la402669z.

197. van Meer, Gerrit; Voelker, Dennis R.; Feigenson, Gerald W. (2008): Membrane lipids: where they are and how they behave. In: *Nat Rev Mol Cell Biol* 9 (2), S. 112–124. DOI: 10.1038/nrm2330.

198. Vollmer, Benjamin; Schooley, Allana; Sachdev, Ruchika; Eisenhardt, Nathalie; Schneider, Anna M.; Sieverding, Cornelia et al. (2012): Dimerization and direct membrane interaction of Nup53 contribute to nuclear pore complex assembly. In: *EMBO J* 31 (20), S. 4072–4084. DOI: 10.1038/emboj.2012.256.

199. Wagenaar, F.; Pol, J. M.; Peeters, B.; Gielkens, A. L.; Wind, N. de; Kimman, T. G. (1995): The US3-encoded protein kinase from pseudorabies virus affects egress of virions from the nucleus. In: *J Gen Virol* 76 (Pt 7), S. 1851–1859.

200. Walde, Peter; Cosentino, Katia; Engel, Helen; Stano, Pasquale (2010): Giant vesicles: preparations and applications. In: *Chembiochem* 11 (7), S. 848–865. DOI: 10.1002/cbic.201000010.

201. Walther, T. C.; Fornerod, M.; Pickersgill, H.; Goldberg, M.; Allen, T. D.; Mattaj, I. W. (2001): The nucleoporin Nup153 is required for nuclear pore basket formation, nuclear pore complex anchoring and import of a subset of nuclear proteins. In: *EMBO J* 20 (20), S. 5703–5714. DOI: 10.1093/emboj/20.20.5703.

202. Walther, Tobias C.; Askjaer, Peter; Gentzel, Marc; Habermann, Anja; Griffiths, Gareth; Wilm, Matthias et al. (2003): RanGTP mediates nuclear pore complex assembly. In: *Nature* 424 (6949), S. 689–694. DOI: 10.1038/nature01898.

203. White, Colleen A.; Stow, Nigel D.; Patel, Arvind H.; Hughes, Michelle; Preston, Valerie G. (2003): Herpes simplex virus type 1 portal protein UL6 interacts with the putative terminase subunits UL15 and UL28. In: *J Virol* 77 (11), S. 6351–6358.

204. Wisner, Todd W.; Johnson, David C. (2004): Redistribution of cellular and herpes simplex virus proteins from the trans-golgi network to cell junctions without enveloped capsids. In: *J Virol* 78 (21), S. 11519–11535. DOI: 10.1128/JVI.78.21.11519-11535.2004.

205. Wisner, Todd W.; Wright, Catherine C.; Kato, Akihisa; Kawaguchi, Yasushi; Mou, Fan; Baines, Joel D. et al. (2009): Herpesvirus gB-induced fusion between the virion envelope and outer nuclear membrane during virus egress is regulated by the viral US3 kinase. In: *J Virol* 83 (7), S. 3115–3126. DOI: 10.1128/JVI.01462-08.

206. Wollert, Thomas; Wunder, Christian; Lippincott-Schwartz, Jennifer; Hurley, James H. (2009): Membrane scission by the ESCRT-III complex. In: *Nature* 458 (7235), S. 172–177. DOI: 10.1038/nature07836.

207. Xu, Chunyan; Bailly-Maitre, Beatrice; Reed, John C. (2005): Endoplasmic reticulum stress: cell life and death decisions. In: *J Clin Invest* 115 (10), S. 2656–2664. DOI: 10.1172/JCI26373.

208. Yamauchi, Y.; Shiba, C.; Goshima, F.; Nawa, A.; Murata, T.; Nishiyama, Y. (2001): Herpes simplex virus type 2 UL34 protein requires UL31 protein for its relocation to the internal nuclear membrane in transfected cells. In: *J Gen Virol* 82 (Pt 6), S. 1423–1428.

209. Yang, Kui; Baines, Joel D. (2011): Selection of HSV capsids for envelopment involves interaction between capsid surface components pUL31, pUL17, and pUL25. In: *Proc Natl Acad Sci U S A* 108 (34), S. 14276–14281. DOI: 10.1073/pnas.1108564108.

210. Ye, G. J.; Roizman, B. (2000): The essential protein encoded by the UL31 gene of herpes simplex virus 1 depends for its stability on the presence of UL34 protein. In: *Proc Natl Acad Sci U S A* 97 (20), S. 11002–11007.

211. Zhu, Fan Xiu; Chong, Jae Min; Wu, Lijun; Yuan, Yan (2005): Virion proteins of Kaposi's sarcoma-associated herpesvirus. In: *J Virol* 79 (2), S. 800–811. DOI: 10.1128/JVI.79.2.800-811.2005.

6 Publications

THE JOURNAL OF BIOLOGICAL CHEMISTRY VOL. 290, NO. ??, pp. 1–xxx, ???? ??, 2015

A Single Herpesvirus Protein Can Mediate Vesicle Formation in the Nuclear Envelope*

Received for publication, November 21, 2014, and in revised form, January 14, 2015 Published, JBC Papers in Press, January 20, 2015, DOI 10.1074/jbc.M114.627521

Michael Lorenz[‡], Benjamin Vollmer[‡], Joseph D. Unsay[§], Barbara G. Klupp[¶], Ana J. García Sáez[§], Thomas C. Mettenleiter[¶], and Wolfram Antonin[‡1]

From the [‡]Friedrich Miescher Laboratory of the Max Planck Society, 72076 Tübingen, Germany, the [§]Interfaculty Institute of Biochemistry, University of Tübingen, 72076 Tübingen, Germany, and the [¶]Friedrich Loeffler Institute, Federal Research Institute for Animal Health, 17493 Greifswald, Germany

Background: Herpesviruses egress from the nucleus by vesicle trafficking through the nuclear envelope.
Results: Using giant unilamellar vesicles, we reconstitute the function of two viral proteins, pUL31 and pUL34, in nuclear envelope vesicle formation.
Conclusion: pUL34 recruits pUL31 to the membrane, which, on its own, deforms membranes to produce nuclear envelope vesicles.
Significance: pUL31 constitutes a minimal machinery mediating inwardly directed membrane budding and scission.

Herpesviruses assemble capsids in the nucleus and egress by unconventional vesicle-mediated trafficking through the nuclear envelope. Capsids bud at the inner nuclear membrane into the nuclear envelope lumen. The resulting intralumenal vesicles fuse with the outer nuclear membrane, delivering the capsids to the cytoplasm. Two viral proteins are required for vesicle formation, the tail-anchored pUL34 and its soluble interactor, pUL31. Whether cellular proteins are involved is unclear. Using giant unilamellar vesicles, we show that pUL31 and pUL34 are sufficient for membrane budding and scission. pUL34 function can be bypassed by membrane tethering of pUL31, demonstrating that pUL34 is required for pUL31 membrane recruitment but not for membrane remodeling. pUL31 can inwardly deform membranes by oligomerizing on their inner surface to form buds that constrict to vesicles. Therefore, a single viral protein can mediate all events necessary for membrane budding and abscission.

Viruses exploit amazing strategies, overcoming various cellular membranes to realize their complex life cycle, including cell entry, genome replication, and assembly of virus particles as well as their egress. For many viruses that replicate in the cell nucleus, a major barrier is the nuclear envelope, a double membrane structure enclosing the chromatin. It consists of the inner nuclear membrane, which, in animal cells, is underlaid by a tight lamina meshwork that connects and stabilizes the nuclear envelope, and the outer nuclear membrane, which is continuous with the endoplasmic reticulum (for a review, see Refs. 1, 2). The nuclear envelope is perforated by nuclear pore complexes, huge macromolecular assemblies of up to 125 MDa in vertebrates that act as selective gateways between the cytoplasm and the nucleus (3). Nuclear pores are used as entry paths for most viruses that replicate in the nucleus (for a review, see Refs. 4, 5). In many cases, this involves an at least partial disassembly of the viral capsid at the cytoplasmic side or core of the nuclear pore complex because these particles are too large to pass the pore intact.

Although many viruses assemble in the cytoplasm, herpesviruses package their newly replicated genomic DNA into capsids of up to 125 nm within the nucleus. Unlike many other DNA viruses, herpesviruses do not depend on the breakdown of the nuclear envelope during mitosis for their release and can also replicate in non-dividing cells. Therefore, they face the challenge of passing the nuclear envelope a second time, now in the opposite direction. Because herpesvirus capsids are too large for passage through the nuclear pore, they are transported through the nuclear envelope by vesicle-mediated transport, also described as an "envelopment-de-envelopment" pathway (6). Capsids bud at the inner nuclear membrane and, therefore, acquire a (primary) envelope, resulting in a nascent virus located in the lumen between the inner and outer nuclear membranes (for a review, see Refs. 7, 8). Subsequently, the primary envelope fuses with the outer nuclear membrane, resulting in translocation of the capsid to the cytoplasm. Final maturation, including assembly of the tegument and secondary envelopment, follows in the cytoplasm, and mature virions are released at the plasma membrane.

Egress from the nucleus is a multifaceted process. In all herpesviruses studied, it involves the formation of a heterodimeric nuclear egress complex consisting of two viral proteins that are conserved throughout the herpesvirus family. One component is a type II transmembrane protein, tail-anchored in the nuclear envelope and termed pUL34 in herpes simplex virus 1 and pseudorabies virus. It interacts with a soluble component, pUL31, and recruits it to the nuclear envelope (9–15). In the absence of this complex, nuclear egress is blocked, and capsids accumulate in the nucleoplasm. One function of the pUL31-pUL34 complex is the recruitment of viral and cellular kinases that phosphorylate locally and disrupt the nuclear lamina (15–

* This work was supported by funding from the Max Planck Society (to W. A.) and by German Research Foundation Grant DFG Me 854/12-1.
[1] To whom correspondence should be addressed: Friedrich Miescher Laboratory of the Max Planck Society, Spemannstr. 39, 72076 Tübingen, Germany. Tel.: 49-7071-601836; Fax: 49-7071-601801; E-mail: wolfram.antonin@tuebingen.mpg.de.

19), a prerequisite for the access of capsids to the inner nuclear membrane. In addition, the pUL31-pUL34 complex might also contribute to the nuclear membrane restructuring necessary for herpesvirus nuclear egress. Transient or stable transgenic expression of pUL31 and pUL34 is sufficient to drive the formation of correctly sized primary envelopes in the perinuclear space between the outer and inner nuclear membrane in the absence of capsids (10, 20). Therefore, pUL31 and pUL34 are the only two viral proteins required for budding and fission of vesicles at the inner nuclear membrane. Whether this process is additionally dependent on the recruitment and function of cellular factors is currently unknown. Recently, it has been suggested that, *in vitro*, pUL31 and pUL34 are sufficient to drive membrane budding and scission by forming a coat on the surface (21). However, this assay depended on an unnaturally high content (up to 40%) of negatively charged lipid headgroups on the deformed lipid bilayer that is not present on physiological membranes. Therefore, it remains questionable to what extent it reflects the natural situation.

Primary envelopment of herpesvirus capsids requires extensive restructuring of the host inner nuclear membrane to allow envelope formation and vesicle detachment into the lumen of the nuclear envelope. Similar membrane deformations have been investigated intensively because they are at the heart of vesicle-mediated intracellular trafficking in the secretory and endocytic pathways. Many such processes are directed by complex but conceptually straightforward mechanisms in which coat proteins impose a curvature on the cytosolic membrane face, thereby generating buds that ultimately constrict to vesicles. The best known coat proteins are clathrin and the COP I and COP II complexes, which assemble on the outer side of the membrane and are crucial for vesicle formation into the cytosol (22). Membrane deformation in the opposite direction, *i.e.* away from the cytosol, such as the invagination of the endosomal membrane during formation of multivesicular bodies or egress of HIV and other enveloped viruses at the plasma membrane, both mediated by the ESCRT machinery, are less frequent (23). pUL31-pUL34-mediated inner nuclear membrane engulfment, much like the suggested pathway for nuclear egress of large ribonucleoprotein complexes identified recently in *Drosophila* (24), represents one of these exceptional pathways. It involves vesicle budding and scission from the nucleoplasm into the intermembrane space of the nuclear envelope, which is connected and topologically identical to the lumen of the endoplasmic reticulum. The molecular machinery mediating inner nuclear membrane deformation and scission remains largely obscure. It is especially unclear whether it requires proteins within the lumen of the nuclear envelope that could assemble a coat on the outer surface of the nascent vesicles, similar to COP I, COP II, and clathrin coats in the cytoplasm.

We reconstituted the function of pseudorabies virus pUL31 and pUL34 in a simple membrane system by using giant unilamellar vesicles (GUVs)[2] mimicking the lipid composition of the nuclear envelope. We show that the two viral proteins are sufficient for budding and fission of membrane vesicles into the lumen of GUVs, a process that is topologically identical to inwardly directed vesicle formation at the inner nuclear membrane during herpesvirus nuclear egress. Artificial membrane recruitment of pUL31 alone results in the same membrane remodelling and generates intra-GUV vesicles. Therefore, pUL31 and pUL34 are sufficient for vesicle formation without the need for additional (cellular) proteins. Moreover, we can assign distinct functions to pUL31 and pUL34 during herpesvirus nuclear egress. pUL34 recruits pUL31 to the membrane and provides membrane anchorage, whereas pUL31 mediates membrane budding and scission.

EXPERIMENTAL PROCEDURES

1,1′-dioctadecyl-3,3,3′,3′-tetramethylindodicarbocyanine,4-chlorobenzenesulfonate salt ($DiDC_{18}$), Alexa Fluor 546 carboxylic acid succinimidyl ester, and cascade blue-labeled neutravidin were obtained from Invitrogen, naphtopyrene from Sigma, and detergents from Calbiochem. The nuclear envelope lipid mix consisted of 5 mol% cholesterol, 2.5 mol% sphingomyeline, 2.5 mol% sodium phosphatidylserine, 10 mol% sodium phosphatidylinositol, 20 mol% phosphatidylethanolamine, and 60 mol% phosphatidylcholine (all from Avanti Polar Lipids). In lipid mixtures lacking a specific component, the respective lipid was replaced by an equimolar amount of phosphatidylcholine.

Protein Expression and Purification—Constructs for expression of pseudorabies virus pUL31 and pUL34 were generated from a synthetic DNA optimized for codon usage in *Escherichia coli* (Geneart). pUL31 was expressed from a modified pET28a vector with a His_6 tag and a TEV site, followed by an EGFP protein amino-terminal of pUL31. The soluble domain of pUL34 (amino acids 1–240), untagged pUL31, as well as EGFP were expressed from a modified pET28a vector with a His_6 tag followed by a TEV site. For C-terminal His_6 tagging of the soluble domain of pUL34 (amino acids 1–240), the fragment was expressed from a modified pET28a vector lacking the amino-terminal His_6 sequence. GST fusions of pUL31 and pUL34 (amino acids 1–240) were expressed from a modified pET28a vector lacking a His_6 tag but with an N-terminal GST tag followed by a recognition site for precision protease upstream of pUL31 and pUL34. All His_6-tagged proteins were expressed in *E. coli* BL21de3 and purified using Ni-NTA. Where applicable, the His_6 tags were cleaved off. Proteins were purified further by gel filtration (Superdex 200, GE Healthcare). GST fusions were purified using GSH-Sepharose (GE Healthcare).

Full-length pUL34 and SCL1 were expressed from a modified pET28a vector with an N-terminal membrane-integrating sequence for translation of integral membrane protein constructs (MISTIC) fragment (25) followed by a thrombin cleavage site and purified as described previously (26). Proteins were labeled using Alexa Fluor 546 carboxylic acid succinimidyl ester in 200 mM $NaHCO_3$ (pH 8.4) or the same buffer containing 1% (w/v) cetyltrimethylammonium bromide for labeling of trans-

[2] The abbreviations used are: GUV, giant unilamellar vesicle; $DiDC_{18}$, 1,1′-dioctadecyl-3,3,3′,3′-tetramethylindodicarbocyanine,4-chlorobenzenesulfonate salt; EGFP, enhanced GFP; Ni-NTA, nickel-nitrilotriacetic acid; DGS, 1,2-dioleoyl-*sn*-glycero-3-(*N*-(5-amino-1-carboxypentyl)iminodiacetic acid)succinyl; ILV, intralumenal vesicle.

membrane proteins and purified by gel filtration on a Sephadex G50 fine column (GE Healthcare).

Generation of GUVs—Detergent-solubilized and labeled SCL1 and pUL34 were reconstituted in proteoliposomes via gel filtration (27). For this, 20 μl of the nuclear envelope lipid mix (30 mg/ml in 10% octylglucopyranoside) was mixed with 20 μl of 2 μM pUL34 or SCL1 protein and 100 μl of PBS. The sample was applied to a Sephadex G50 fine filled Econo chromatography column (0.5 × 20 cm, Bio-Rad) to remove the detergent. The formed proteoliposomes were collected and pelleted for 30 min at 100,000 rpm in a TLA120.2 (Beckman Coulter) rotor at 4 °C. The pellet was resuspended in 120 μl of 20 mM HEPES (pH 7.4), 100 mM KCl, and 1 mM DTT. 5 μl of resuspended proteoliposomes were dried onto two 5 × 5 mm platinum gauzes (ALS) under vacuum for at least 1 h at room temperature. The gauzes were placed in parallel (5 mm distance) into a cuvette (UVette, Eppendorf) and submerged in 259 mM sucrose solution, and for 140 min an alternating current electric field with 10 Hz, 2.2 V was applied, followed by 20 min at 2 Hz at 42 °C.

Lipid GUVs were generated from chloroform-dissolved lipid mixtures where indicated, supplemented with 1 mol% Ni-NTA-DGS (1,2-dioleoyl-*sn*-glycero-3-(*N*-(5-amino-1-carboxypentyl)iminodiacetic acid)succinyl), Avanti Polar Lipids) and 0.8 nM $DiDC_{18}$ as described previously (28).

GUV Vesicle Budding Reaction—An 8-well glass observation chamber (chambered #1.0 borosilicate coverglass system, Lab-Tek) was blocked with 5% (w/v) BSA in PBS and washed with PBS. For each reaction, 50 μl of freshly prepared GUVs were mixed with 150 μl of PBS and placed into a well. Unless indicated otherwise, all soluble proteins were added to a final concentration of 500 nM (cascade blue-labeled neutravidin at 3.8 μM). The proteins and buffers used for GUV preparation matched the osmotic pressure of the sucrose solution, as measured using an osmometer. The mixture was incubated for 5 min and imaged immediately at room temperature on an inverted Olympus Fluoview 1000 confocal laser-scanning system utilizing an UPlanSApo ×60/1.35 oil objective. The cascade blue-labeled neutravidin was excited by a 405-nm DPSS laser, and emission was collected between 425–475 nm. EGFP and Alexa Fluor 546 were excited by an argon ion laser at 488 and 515 nm, respectively. Emission for EGFP was collected between 500–545 nm and between 570–625 nm for Alexa Fluor 546. DiD was excited by a 635-nm DPSS laser, and emission was collected between 655–755 nm. The pinhole was set to 1 airy unit. Three-dimensional reconstructions were generated using Imaris software (version 7.4, Bitplane). Linescan analysis was performed using FIJI software (Fiji.sc/Fiji). Size quantification was done by stack analysis of GUVs using a stack size of 0.5 μm.

Preparation of Supported Lipid Bilayers—Supported lipid bilayers were prepared as described previously (29). The nuclear envelope lipid mix with 0.2 mol % Rhodamine-PE was dissolved in SLB buffer (10 mM HEPES (pH 7.4) and 150 mM NaCl) at a concentration of 5 mg/ml. 20 μl of the mixture was diluted with 150 μl of SLB buffer. The suspension was then vortexed and bath-sonicated until a clear suspension was obtained, indicating that small unilamellar vesicles had formed. The clear solution was put in contact, at 37 °C, with freshly cleaved mica glued to a coverslip. $CaCl_2$ was added to a final concentration of 3 mM and incubated at 37 °C for 10 min. The samples were rinsed several times with SLB buffer to remove $CaCl_2$ and unfused vesicles and then allowed to equilibrate at room temperature before analysis.

Confocal Microscopy of Supported Lipid Bilayers—Supported lipid bilayers were imaged using a commercial LSM 710 (Carl Zeiss, Jena, Germany) at 22 °C. The excitation light of a DPSS laser at 561 nm and of an argon laser at 488 nm was reflected by a dichroic mirror (MBS 488/561/633) and focused through a Zeiss C-Apochromat ×40, numerical aperture 1.2 water immersion objective onto the sample. The fluorescence emission was collected by the objective and directed by spectral beam guides to photomultiplier tube detectors. Images were acquired before and adding His_6-EGFP-pUL31 or His_6-EGFP at the same areas of the supported lipid bilayers. Images were analyzed using FIJI (particle analysis). Proteins were added to a final concentration of 500 nM.

Atomic Force Microscopy—Supported lipid bilayers were imaged using a JPK NanoWizard II system (JPK Instruments, Berlin, Germany) mounted on an Axiovert 200 inverted microscope (Carl Zeiss). Intermittent contact (or tapping) mode images were taken using V-shaped silicon nitride cantilevers (SNL-10) with a typical spring constant of 0.08 N/m and a nominal tip radius of 2 nm. The cantilever oscillation was tuned to a frequency between 3–10 kHz, and the amplitude was set between 0.3–0.6 V. The amplitude was varied during the experiment to minimize the force of the tip on the bilayer. The scan rate was set to 0.7–1 Hz. The height, deflection, and phase shift signals were collected simultaneously in both trace and retrace directions. Atomic force microscopy images were acquired before and after adding 150 nM His_6-EGFP-pUL31 or His_6-EGFP on the bilayer. Atomic force microscopy images were analyzed using JPK data analysis software.

RESULTS

pUL31 and pUL34 Are Sufficient for Membrane Budding and Scission—Viral pUL31 and pUL34 are necessary for nuclear egress of herpesvirus capsids. To investigate their function in detail, we expressed the transmembrane protein pUL34 in *E. coli* as a full-length protein, including its transmembrane region, and, after purification, labeled it with the fluorescent dye Alexa Fluor 546 before reconstitution into liposomes with a nuclear envelope-like lipid composition (30, 31) (see "Experimental Procedures" for details). GUVs were generated from these proteoliposomes. The GUV membrane contained pUL34 as an integral membrane component, which can be detected by its fluorescent label (Fig. 1*A*). The vast majority of these GUVs were large vesicles with no detectable membrane/vesicle structures in the interior.

When added to pUL34-GUVs, purified recombinant EGFP-pUL31 was efficiently recruited to the membranes (Fig. 1*B*), consistent with a direct pUL31-pUL34 interaction (9, 12, 14). In the presence of pUL31, the GUV membrane was deformed and invaginated, leading to small intralumenal vesicles inside the GUVs that contained both pUL31 and pUL34. In typically sized GUVs with a diameter of 30–40 μm, ~15 intralumenal vesicles were detected, the majority of them 0.5–2 μm in size (Fig. 1, *D–F*). Formation of intralumenal vesicles was specific for

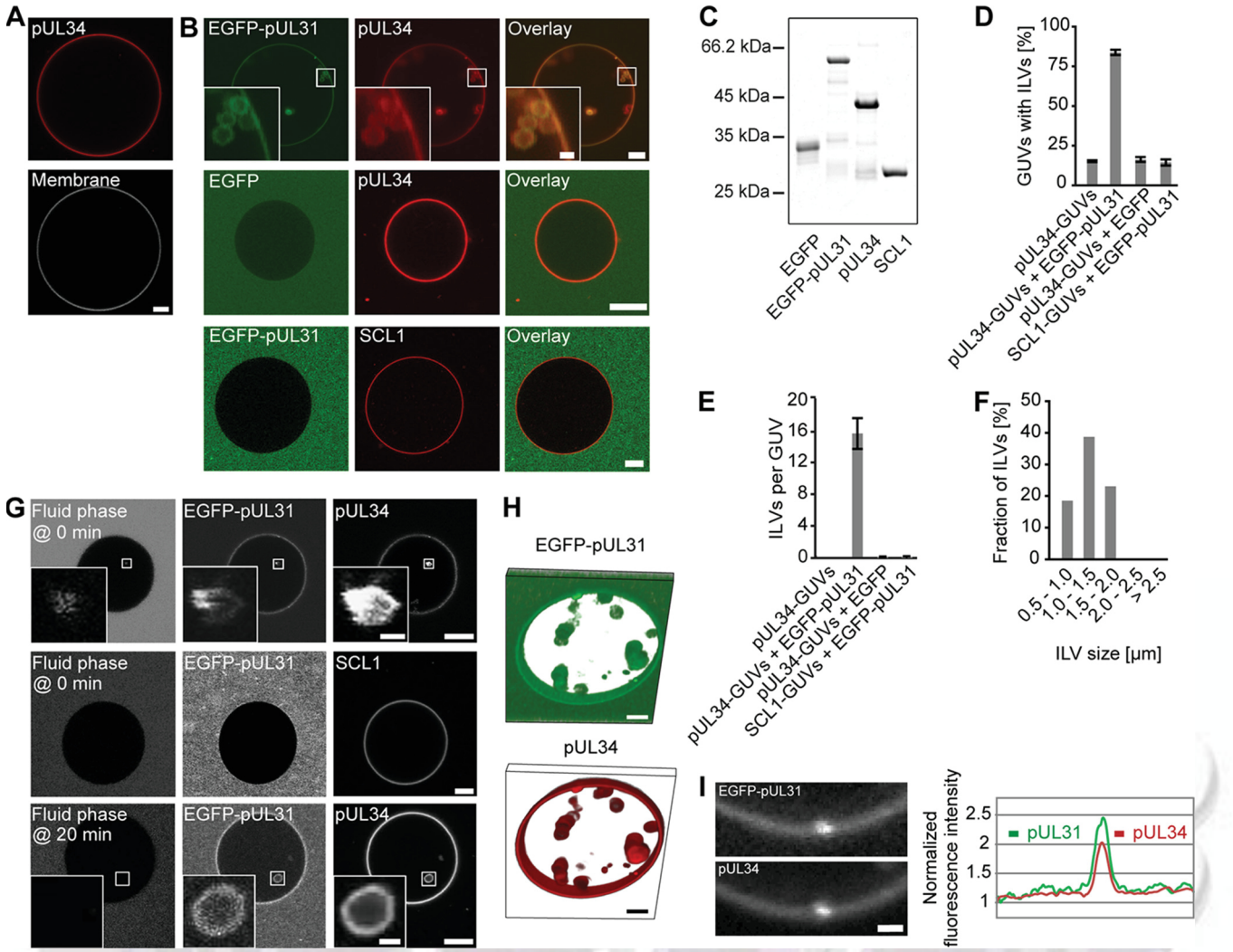

FIGURE 1. **The pUL31-pUL34 complex is sufficient to induce intralumenal vesicles.** *A*, recombinant Alexa Fluor 546-labeled pUL34 (*red*) was reconstituted into GUVs. The GUV membrane was stained with the lipophilic dye $DiDC_{18}$. *B*, Alexa Fluor 546-labeled pUL34 or the inner nuclear membrane protein SCL1 were reconstituted into GUVs (*red*). Addition of EGFP-pUL31 (*green* in *overlay*) induced formation of intra-GUV vesicles on pUL34 but not SCL1 GUVs. *C*, recombinant proteins employed were separated on 12% SDS-PAGE and stained with Coomassie Blue. *D*, quantitation of the number of GUVs with intralumenal vesicles (ILVs) shows the mean ± S.E. of three independent experiments, each including at least 70 GUVs/condition and experiment. *E*, the number of ILVs per GUV was quantified from three independent experiments, each including at least 20 GUVs/condition and experiment. The mean ± S.E. is shown. *F*, the size distribution of ILVs formed in pUL34-GUVs after EGFP-pUL31 addition was analyzed from three independent experiments, each including at least 20 GUVs/condition and experiment. *G*, cascade blue-labeled neutravidin (fluid phase marker) was added together with EGFP-pUL31 (*top row*) or 20 min after EGFP-pUL31 addition to GUVs (*bottom row*) with reconstituted Alexa Fluor 546-labeled pUL34 or SCL1. *H*, three-dimensional reconstruction of an EGFP-pUL31-treated (*green*) pUL34 GUV (*red*). *I*, higher magnification of a budding spot on a pUL34 GUV after EGFP-pUL31 addition. EGFP-UL31 and Alexa Fluor 546-pUL34 was analyzed along the limiting GUV membrane. *Scale bars* = 5 μm (1 μm in *I* and *insets*).

pUL31 because it was not induced by addition of EGFP alone. The same result was observed in different buffer systems and with untagged pUL31, confirming that the EGFP tag did not cause this effect.[3] As a control, we replaced pUL34 with the inner nuclear membrane protein SCL1/BC08 (32). Like pUL34, SCL1 is a type II transmembrane protein with a single membrane-spanning domain at its C terminus. Therefore, the N-terminal region preceding the transmembrane domain of both pUL34 and SCL1 faces the nucleoplasm. EGFP-pUL31 was not recruited to SCL1-GUVs, and membrane invaginations were not observed above background levels, demonstrating that this process specifically requires pUL31 and pUL34 (Fig. 1*B*).

Cascade blue-labeled neutravidin was used as a fluid phase marker to assess permeability between the bulk solution and the pUL31-induced vesicles. When the fluid phase marker was added as a soluble probe, together with pUL31, to pUL34-GUVs, the label was found in intralumenal vesicles (Fig. 1*G*, *top row*). When added 20 min after pUL31 addition, intra-GUV vesicles without the fluid phase marker were detected (Fig. 1*G*, *bottom row*). Therefore, the lumina of vesicles are disconnected from the bulk solution surrounding the GUVs, indicating membrane scission. This is consistent with the three-dimensional reconstitution of an EGFP-pUL31-treated pUL34-GUV that shows highly mobile vesicles distant and apparently detached from the limiting GUV membrane (Fig. 1*H*). When the fluid phase marker was added to SCL1-GUVs together with EGFP-pUL31 or to pUL34-GUVs in the absence of EGFP-pUL31 (Fig.

[3] M. Lorenz, B. Vollmer, J. D. Unsay, B. G. Klupp, A. J. García Sáez, T. C. Mettenleiter, and W. Antonin, unpublished observations.

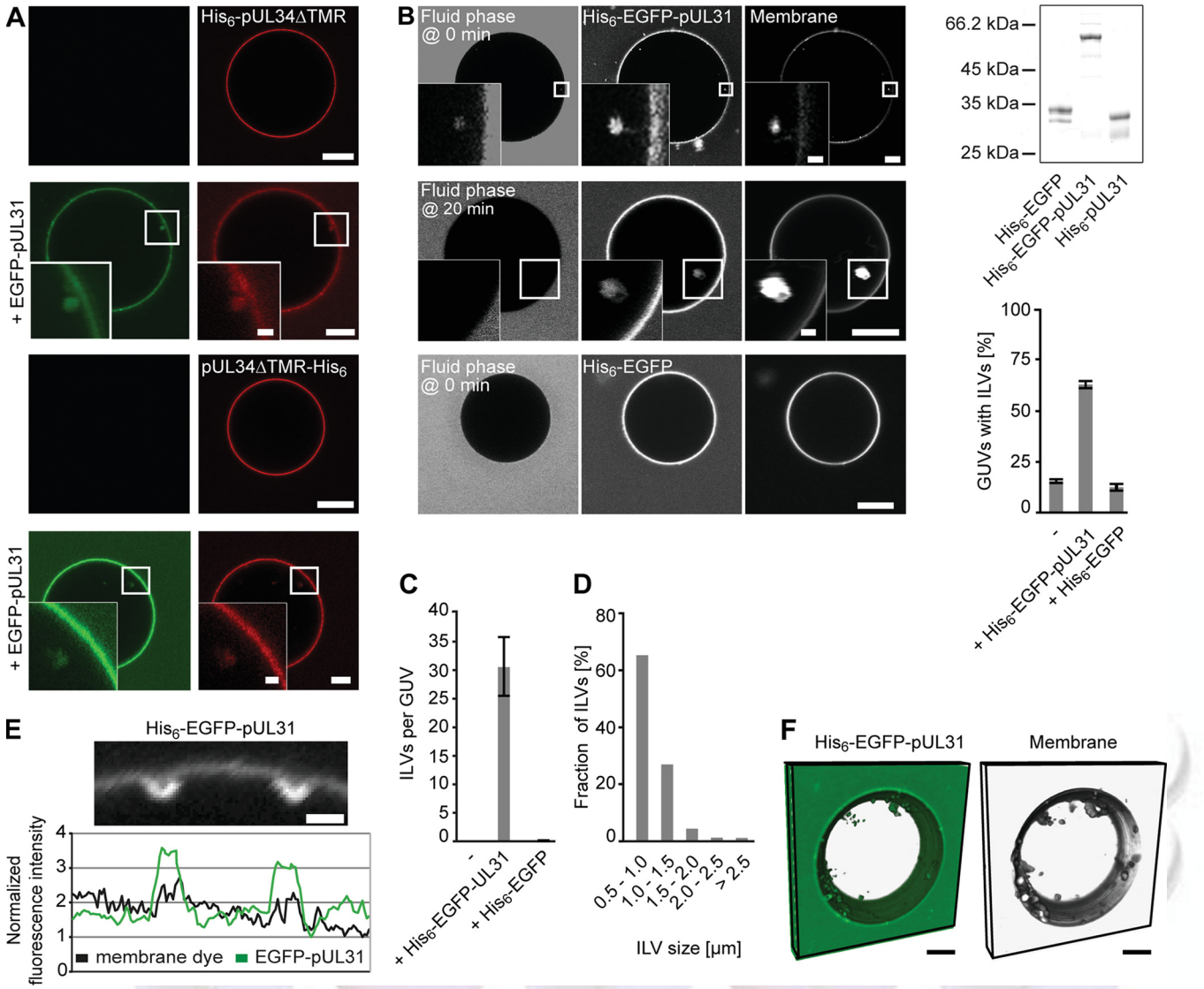

FIGURE 2. **Membrane tethering of pUL31 is sufficient to induce intralumenal vesicles.** *A*, an Alexa Fluor 546-labeled N- or C-terminally His_6-tagged pUL34 fragment (*top* and *bottom rows*, respectively) comprising the soluble domain (amino acids 1–240) was bound to 1% Ni-NTA-DGS-containing GUVs. Addition of EGFP-pUL31 induced intra-GUV vesicles. *B*, His_6-tagged-EGFP or His_6-tagged-EGFP-pUL31 was directly bound to Ni-NTA-DGS-containing GUVs. Membranes were stained with $DiDC_{18}$. Cascade blue-labeled neutravidin as a fluid phase marker was added together with His_6-tagged EGFP-pUL31 or His_6-tagged-EGFP or 20 min after His_6-EGFP-pUL31 addition to GUVs. The purity of the employed recombinant proteins is shown by SDS-PAGE and Coomassie staining. Quantitation shows the mean ± S.E. of three independent experiments, each including at least 80 GUVs/condition and experiment. *C*, the number of ILVs per GUV was quantified from three independent experiments, each including at least 20 GUVs/condition and experiment. The mean ± S.E. is shown. *D*, the size distribution of ILVs formed in Ni-NTA-DGS-containing GUVs after His_6-EGFP-pUL31 addition was analyzed from three independent experiments, each including at least 20 GUVs/condition and experiment. *E*, higher magnification visualizing budding spots on His_6-EGFP-pUL31-tethered Ni-NTA-DGS GUVs. *F*, three-dimensional reconstruction of a His_6-EGFP-pUL31-treated (*green*) GUV containing 1% Ni-NTA-DGS. Membranes were stained with $DiDC_{18}$ (*gray*). *Scale bars* = 5 μm (1 μm in *E* and *insets*).

1*G*),[3] no intra-GUV fluorescence was detected, consistent with the notion that the pUL31-pUL34 interaction specifically induces vesicle budding into the GUV lumen.

These data show that, in a minimal membrane system, the two viral proteins pUL31 and pUL34 are sufficient to induce membrane perturbations generating intra-GUV vesicles. Importantly, in our assay, pUL34 is integrated as a transmembrane protein into the GUV lipid bilayer, mimicking the natural situation at the nuclear envelope membranes. The restructuring of the GUV-limiting membrane is reminiscent of the inwardly directed primary vesicle formation into the lumen of the nuclear envelope during herpesvirus nuclear egress. The emerging buds were enriched in pUL31 and pUL34, indicating that both proteins accumulate at sites of membrane deformation (Fig. 1*I*), consistent with a role in this process. Therefore, this GUV system is a valuable tool to investigate pUL31-pUL34-mediated vesicle budding and scission in detail.

pUL31 Mediates Membrane Budding and Scission—Many membrane-deforming processes, including budding of several viruses at the plasma membrane, specifically involve integral membrane proteins (33–37). To assess whether the membrane-spanning C terminus of pUL34 is required for the formation of intralumenal vesicles, we artificially recruited a pUL34 fragment lacking its transmembrane domain to GUVs (Fig. 2*A*). To this end, the Alexa Fluor 546-labeled soluble domain (amino acids 1–240) of pUL34 fused to an N-or C-terminal His_6 tag was

added to GUVs incorporating the Ni^{2+}-chelating lipid Ni-NTA-DGS. GUVs coated with these tethered pUL34 fragments showed no detectable vesicle structures in their interior. When EGFP-pUL31 was added, it was efficiently recruited to the GUV membranes regardless of whether pUL34 was attached to the membrane via its N or C terminus. This finding is consistent with the fact that the transmembrane region of pUL34 is not required for pUL31 interaction (9, 38). More importantly, pUL34-mediated pUL31 recruitment was sufficient for intralumenal vesicle formation. This indicates that the presence of an authentic transmembrane region is not essential for this process (21).

It should be noted that, in contrast to the experiments presented in Fig. 1, where pUL34, because of its reconstitution as an integral membrane protein, might be present in both orientations in the GUV membrane, the pUL34 fragment is only located on the outer leaflet of the GUVs. Although unlikely in the light of its cellular localization, orienting its non-membrane-spanning region into the nucleoplasm, the experiments shown here exclude that a (wrongly oriented) fraction of pUL34 is causative for *in vitro* vesicle formation.

Next we tested whether pUL34 plays an active role in the invagination process or whether it is merely required for pUL31 recruitment. When His_6-tagged EGFP-pUL31 was bound directly to Ni-NTA-DGS-containing lipid GUVs, intralumenal vesicles were induced efficiently induced (Fig. 2, *B* and *C*). Addition of cascade blue-labeled neutravidin together or 20 min after protein addition indicated that the formed intralumenal vesicles pinched off from the limiting GUV membrane. The size distribution of these intralumenal vesicles was shifted to smaller vesicle diameters (Fig. 2*D*). Although we cannot exclude other scenarios, it is possible that this is due to the absence of pUL34. Three-dimensional reconstitution of a His_6-EGFP-pUL31-treated GUV shows many highly mobile vesicles distant from the GUV membrane, indicating that they have been disconnected (Fig. 2*F*). Therefore, artificial membrane tethering of pUL31 is sufficient for the induction of membrane invaginations and membrane scission. This effect was specific for pUL31 because a His_6-tagged EGFP, despite efficient recruitment to the GUV membrane, did not induce intra-GUV vesicle formation (Fig. 2, *B* and *C*). Therefore, the function of pUL34 in this minimal system is to target pUL31 to the membrane.

pUL31-pUL34-mediated Membrane Resculpting Requires Cholesterol and Sphingomyelin—The GUVs used so far contained a lipid composition resembling the nuclear envelope. We next assessed whether any specific lipid or lipid class in this mixture is required for intralumenal vesicle formation. GUVs were reconstituted with full-length pUL34 in the absence of specific lipid components. EGFP-pUL31 was efficiently recruited to the membrane of pUL34-GUVs regardless of lipid composition (Fig. 3*A*). In fact, efficient formation of intralumenal vesicles was observed in all instances, except when cholesterol or sphingomyelin were absent from the GUV membrane. Also, in the absence of both negatively charged lipid classes, phosphatidylserine and phosphatidylinositol, intralumenal vesicles formed efficiently. Identical results were obtained when His_6-tagged EGFP-pUL31 was directly targeted to Ni-NTA-DGS GUVs (Fig. 3*B*). These data indicate that cholesterol and sphingomyelin are required for pUL31-induced membrane invagination and scission. Both lipids interact and are crucial for lateral segregation of membrane components, leading to membrane subdomain formation, such as rafts (39). However, we did not observe a pUL31-pUL34-induced phase separation of sphingolipid-cholesterol from other membrane components in GUVs (Fig. 3*C*), although we cannot exclude the formation of raft-like nanodomains of a size below the optical resolution of light microscopy. It is possible that cholesterol and sphingomyelin are required for intra-GUV vesicle formation because they permit membrane fluidity (40) and, therefore, might be essential for flexibility of the lipid bilayer, allowing its resculpting to vesicles.

pUL31 Oligomerizes on the Membrane Surface—Our data show that pUL31 membrane recruitment induces vesicle formation on GUVs. Many membrane remodelling proteins, such as clathrin or components of the COP I/II or ESCRT machinery, oligomerize on the deforming membrane (22, 23). His_6-EGFP-pUL31 became enriched at the sites of inwardly directed membrane deformation (Fig. 2*E*). To test for membrane-induced oligomerization, we bound limiting amounts of His_6-pUL31 to Ni-NTA-DGS GUVs. Under these conditions, no intralumenal vesicles were detected (Fig. 4). Addition of increasing amounts of EGFP-pUL31 devoid of a His_6 tag resulted in recruitment of the protein to the membrane and induction of intralumenal vesicle formation. EGFP-pUL31 membrane recruitment was mediated specifically by GUV tethered His_6-pUL31 because EGFP-pUL31 membrane labeling and vesicle formation was not observed in the absence of His_6-pUL31. Interestingly, pUL31 does not self-interact in solution when tested by GST pulldown experiments or gel filtration followed by multiangle laser light scattering (Fig. 4, *B–D*).

To directly observe pUL31 oligomerization on the membrane surface and induction of membrane remodelling activity, we incubated the protein with supported lipid bilayers of nuclear envelope lipid composition supplemented with Ni-NTA-DGS. His_6-EGFP-pUL31 was recruited rapidly to the supported lipid bilayers, where it formed patches of 1.0 ± 0.5 μm in diameter (Figs. 5 and 6) and eventually provoked the appearance of multiple defects, indicating disruption of the lipid bilayer (Fig. 6). This latter effect is likely due to the increase in membrane tension associated with the membrane deformations at the pUL31 assembly sites. In contrast, His_6-EGFP was also recruited efficiently to the supported lipid bilayers but did not induce patch formation or disruption of the bilayer.

Together, these data indicate that pUL31 forms clusters when recruited to membranes. Therefore, our data suggest that when monomeric pUL31 is recruited to membranes in the cellular context by pUL34, it self-interacts to induce membrane deformation, leading to vesicle formation.

DISCUSSION

Nuclear egress is a common mechanism for herpesvirus nucleocapsid translocation through the nuclear envelope (41). Although it has long been thought to be unique to herpesviruses, it has recently been recognized that a similar mechanism also functions in the nuclear export of large ribonucleoprotein

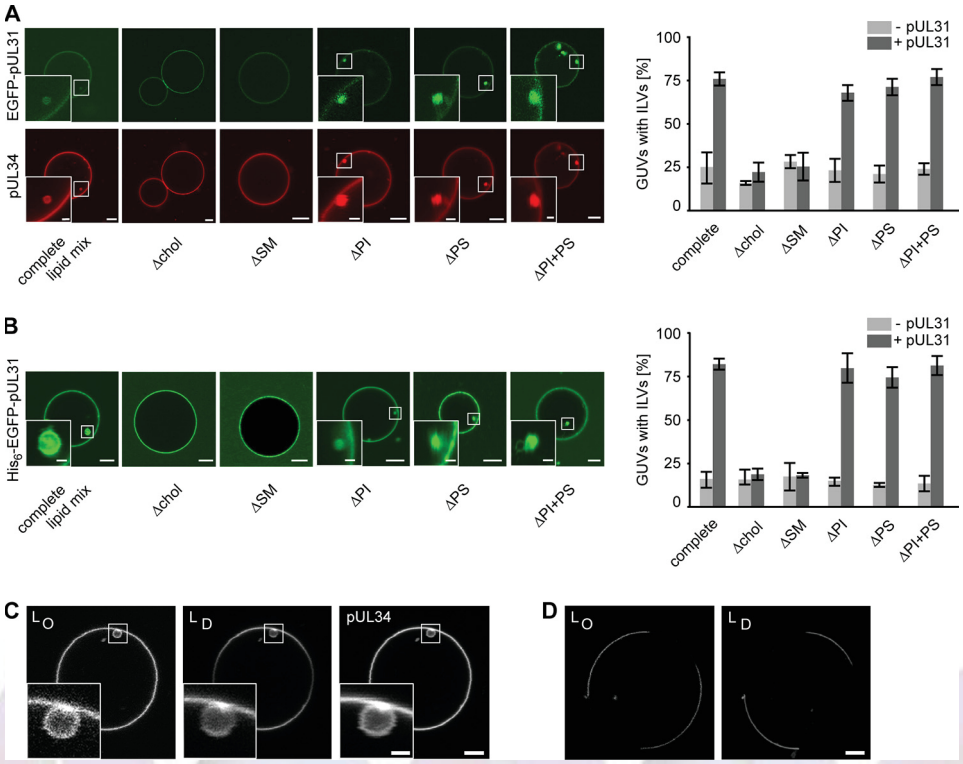

FIGURE 3. **Cholesterol and sphingomyelin are required for pUL31-mediated vesicle formation.** *A*, recombinant Alexa Fluor 546-labeled pUL34 was reconstituted into GUVs containing the nuclear envelope lipid mix (*complete lipid mix*) or the same lipid mix lacking either cholesterol (*chol*), sphingomyelin (*SM*), the negatively charged phospholipids phosphoinositol (*PI*) or phosphatidylserine (*PS*), or both (*PI*+*PS*). Formation of intralumenal vesicles was induced and quantified after EGFP-pUL31 addition (mean ± S.E. of three independent experiments, each including at least 50 GUVs/experiment and condition). *B*, His_6-tagged-EGFP-pUL31 was bound directly to Ni-NTA-DGS-containing GUVs with the same lipid compositions as in *A*, and ILV numbers were quantified (mean ± S.E. of three independent experiments, each including at least 60 GUVs/experiment and condition). *C*, pUL31 was added to pUL34-GUVs loaded with the membrane dyes naphthopyrene and $DiDC_{18}$, which label the liquid ordered (L_O) or liquid disordered phase (L_D), respectively. Although we cannot exclude an enrichment of specific lipids in internal vesicles, there no induction and separation of liquid-ordered and -disordered phases was detectable. *D*, as a control for the functionality of the membrane dyes, their segregation was tested on phase-separating membrane GUVs (33 mol% cholesterol, 33 mol% sphingomyelin, 33 mol% phosphatidylcholine). *Scale bars* = 5 μm (1 μm in *insets*).

particles in *Drosophila* (24), indicating the presence of a general, so far unknown mechanism of vesicular transport through the nuclear envelope. Although the cellular factors involved in this process remain largely enigmatic but may include the AAA+ ATPase torsin (42), all members of the Herpesviridae family analyzed in this respect are dependent on the viral nuclear egress complex, composed of pUL31 and pUL34 homologs, for translocation through the nuclear envelope. In the absence of either complex partner, herpesvirus-induced nuclear envelope breakdown can substitute for pUL31-pUL34-mediated nuclear egress (43). This mode of nuclear escape has, however, only been observed after forced reversion analysis in cell culture. Differing roles for pUL31 and pUL34 in nuclear egress have been demonstrated (7, 8), including recruitment of viral and cellular kinases that locally disrupt the lamina (15–19) as well as functions in herpesvirus replication beyond nuclear egress, including viral DNA binding and packaging (44, 45) or cell-to-cell spread (46).

Here we reconstituted herpesvirus pUL31-pUL34-dependent membrane invagination and scission using a minimal set of protein components and a simple model for the eukaryotic nuclear envelope. The presence of pUL31 at the membrane is sufficient to induce GUV-internal vesicles, a process topologically similar to the formation of primary envelopes, indicating that, in this system, pUL34 is only required to recruit pUL31 to the membrane. In contrast to a recent report (21), we did not observe a dependence on the negatively charged phospholipids phosphatidylserine and phosphatidic acid, which needed to be present in unphysiologically high amounts (up to 40%). In our system, budding and scission also occur in the absence of the comparably low amounts of phosphatidylserine and phosphatidylinositol found in the nuclear envelope. This difference is likely due to the fact that, in the previous report, the negatively charged lipids are required for membrane recruitment by electrostatic interaction of a C-terminally truncated pUL34 lacking the transmembrane region. In contrast, we used either full-length pUL34 containing the C-terminal transmembrane region or directly tethered pUL31 to the GUV membrane. Therefore, our system is less prone to artifacts and mimics the natural situation more faithfully.

The minimal GUV model system provides several fundamental new insights into the process of herpesvirus nuclear egress. First, it shows that pUL31-pUL34-mediated membrane deformation at the inner nuclear membrane can be uncoupled and is, therefore, functionally disconnected from lamina disassembly. It is formally possible that pUL31-pUL34 regulated lamina dynamics are a driving force for restructuring the inner nuclear membrane, similar to other cytoskeleton assembly and disassembly processes that are linked to membrane shape changes of a variety of organelles (47, 48). However, in our min-

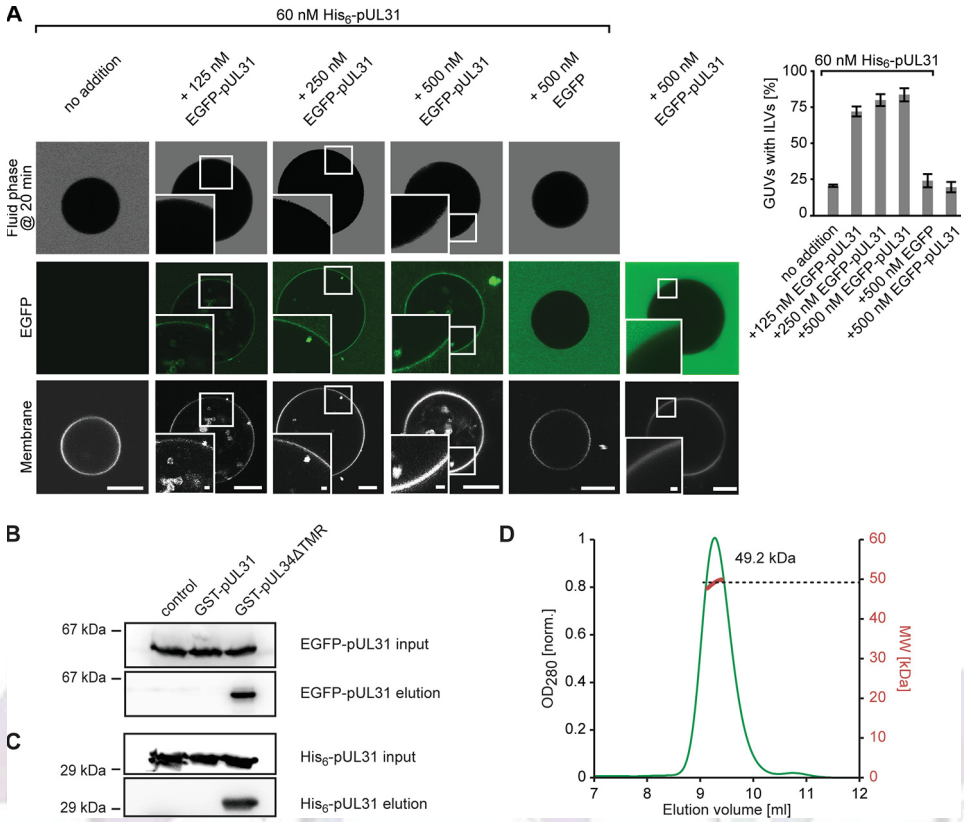

FIGURE 4. **pUL31 self-interacts on membranes but not in solution.** *A*, where indicated, 60 nM His_6-tagged-pUL31 was bound directly to Ni-NTA-DGS-containing GUVs. Increasing amounts of EGFP-pUL31 were added to the GUVs showing a pUL31-mediated membrane recruitment of EGFP-pUL31 and formation of intra-GUV vesicles. Where indicated, cascade blue-labeled neutravidin was added as a fluid phase marker 20 min after protein addition to GUVs to confirm scission of ILVs from the limiting GUV membrane. Quantitation shows the mean ± S.E. of three independent experiments, each including at least 60 GUVs/condition and experiment. *Scale bars* are 10 μm (1 μm in *insets*). *B*, GST pulldown using GST (*control*), GST-pUL31, and GST-pUL34ΔTMR (amino acids 1–240, *i.e.* lacking the transmembrane region) as bait and EGFP-pUL31 as prey. GST-bound EGFP-pUL31 was eluted with precision protease-containing buffer, which cleaves the GST fusions C-terminal of the GST tag, as analyzed by Western blotting using anti-EGFP-antibodies. *C*, GST pulldown as in *B*, but with His_6-pUL31 as prey, detected using anti-His_6 antibodies. *D*, size exclusion chromatography on a Superdex 75/300 GL column followed by multiangle static laser light scattering of EGFP-UL31 shows that it is monomeric in solution (calculated mass, 58.7 kDa). The *red dots* relate to the secondary axis and show the molecular weight of the eluting particle.

imal system, deformation of the GUV membrane leading to vesicle formation occurs in the absence of lamin proteins. Second, pUL31 and pUL34 have well defined and separate functions in the primary envelopment of herpesvirus capsids. pUL31 and pUL34 are both crucial for this process, and coexpression of both proteins in uninfected cells induces the formation and scission of vesicles from the inner nuclear envelope (10, 20). It could be envisioned that cellular proteins participate in the necessary restructuring of the inner nuclear membrane because a similar process occurs during the nuclear export of large ribonucleoprotein particles in *Drosophila* neurons (24). However, our work shows that cellular proteins are not essential to execute the basic membrane restructuring necessary for nuclear egress, including membrane deformation, budding away from the nucleoplasm, and scission to generate vesicles detached from the inner nuclear membrane. In contrast, cellular proteins may be involved in fusion of the intralumenal vesicles with the outer nuclear membrane to complete the transport process. Third, pUL31 membrane recruitment is sufficient for membrane remodelling, resulting in vesicle formation. Therefore, this viral protein is the driving force both for membrane budding and scission in herpesvirus nuclear egress, which constitutes a new archetype of these non-conventional, inwardly directed budding events.

Herpesvirus nuclear egress can be regarded as vesicle-mediated transport through the lumen of the nuclear envelope. In this respect, the process has an inverted topology compared with classical vesicular trafficking pathways through the cytosol. The prime factors inducing membrane deformation and scission in vesicular trafficking localize and act on the outer surface of the exvaginated membrane and/or the vesicle. Our results demonstrate that such an outer membrane coat is not required for vesicle formation during herpesvirus nuclear egress. Rather, formation of the nuclear egress complex on the emerging inner vesicle surface is sufficient to drive membrane bending and scission. Different mechanisms implicated in membrane remodelling might be envisioned to promote vesicle formation (35). First, integral membrane proteins can deform membranes. Well known examples are reticulons and caveolins, which oligomerize and possess unusual hydrophobic segments that might form wedge-shaped hairpins in the membrane (33, 34), and both features can contribute to membrane shaping (35). Similarly, budding of some viruses (*e.g.* coronaviruses) at the plasma membrane is driven by membrane protein

tapraid4/zbc-bc/zbc-bc/zbc01415/zbc1106-15z ZSUBMIT xppws S=5 2/2/15 9:30 | 4/Color Figure(s) F1,2,3,4,5,6 | ARTNO: M114.627521

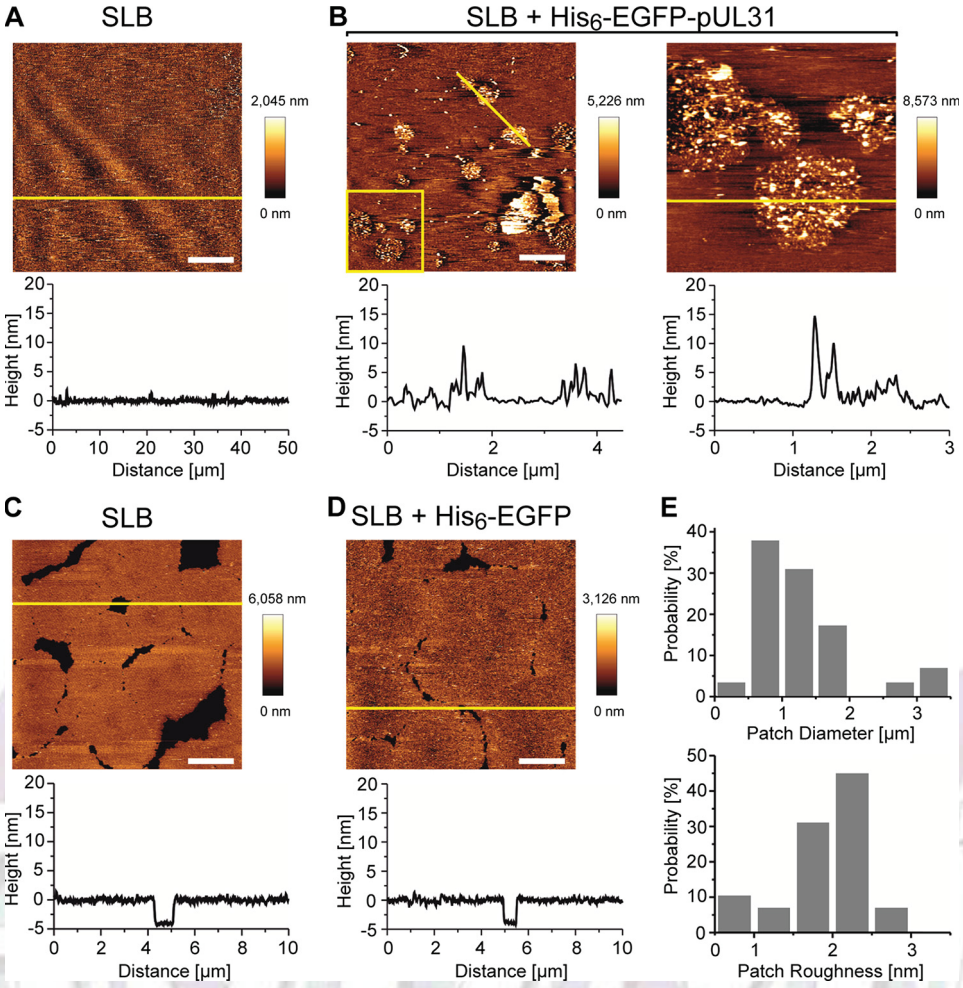

FIGURE 5. **pUL31 forms patches on supported lipid bilayers.** *A*, supported lipid bilayers (*SLB*) mimicking the nuclear envelope lipid composition (supplemented with Ni-NTA-DGS) show a flat topography before protein addition. Graphs below the image are profiles of the *yellow line* in the image. *B*, upon addition of His_6-EGFP-pUL31, patches form with aggregated structures. The right figure is a 3 × 3 μm enlarged image of the *yellow box* within the *left panel*. *C*, supported lipid bilayers before addition of His_6-EGFP. *D*, supported lipid bilayers after addition of His_6-EGFP with no change in topography detectable. *E*, diameter and roughness (average height of the patches) distributions of the patches observed upon addition of His_6-EGFP-pUL31. Gaussian fitting of the histograms shows a peak 1.0 ± 0.5 μm in diameter (mean ± S.D.) and 2.0 ± 0.1 nm in roughness. *Scale bars* = 10 μm for *A* and 2 μm for *B–D*.

oligomerization (49). However, sequence analysis does not suggest such an unusual topology for the pUL34 transmembrane region. Our data rather show that pUL34 is dispensable for membrane restructuring leading to vesicle formation in the nuclear envelope lumen. Furthermore, membrane invaginations can be detected in the GUV system with pUL31 alone, indicating that a transmembrane region does not play a compulsory role in the process.

A second widely discussed mechanism that can contribute to membrane deformation and budding is the insertion of amphipathic helixes into the lipid bilayer (31, 50, 51). However, neither pUL31 nor pUL34 are predicted to form such helixes. More importantly, helix insertion has to take place in the outer lipid leaflet of the nascent vesicle to increase the outer in relation to the inner surface area. pUL31 is localized in the interior of the vesicle, discounting such a mechanism. Similarly, protein crowding generating lateral pressure, which can curve membranes (52), can be excluded for pUL31-mediated membrane budding because this mechanism generates membrane deformation in the opposite direction, *i.e.* outward from the limiting membrane.

In addition to protein-driven processes, lipid-induced changes can restructure membranes. Phase separation can generate membrane curvature and induce budding and scission in simple membrane systems (53–55). The membrane envelope of HIV is highly enriched in the raft-forming lipids sphingomyelin and cholesterol (56, 57), which suggests that budding at the plasma membrane occurs from lipid rafts (58). However, the lipid mixture of the nuclear envelope/endoplasmic reticulum possesses a relatively low amount of cholesterol and sphingomyelin compared with the plasma membrane (30) and does not form detectable lipid rafts (40). Accordingly, we did not observe phase separation between a cholesterol/sphingomyelin-enriched ordered and a disordered phase when pUL31 was added to pUL34-GUVs (Fig. 3*C*). Therefore, there is no indication for a locally induced phase separation, giving rise to the observed invaginations. In addition, changes in lipid composition, especially the localized generation of non-cone shaped lipids or their enrichment, such as the unconventional phospholipid lysobisphosphatidic acid on internal vesicles of multivesicular bodies (59), can contribute to membrane curving. However,

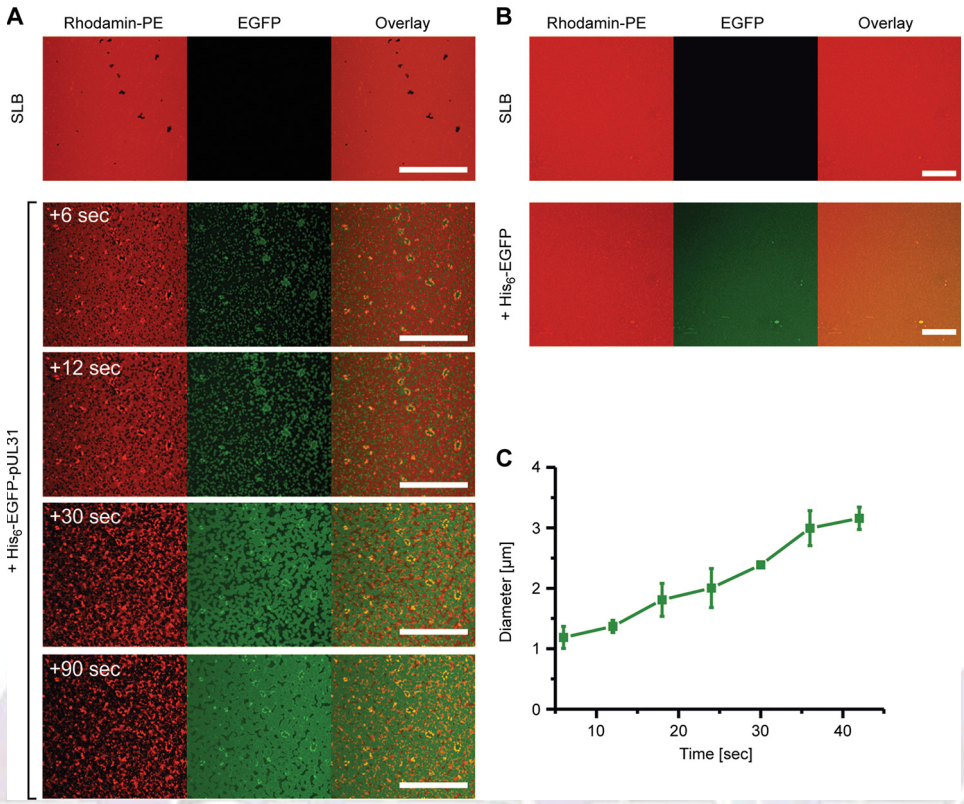

FIGURE 6. **pUL31 disrupts supported lipid bilayers.** *A*, supported lipid bilayers (*SLB*) mimicking the nuclear envelope with rhodamine-PE (*red*) form continuous fluid phase. Bilayers are disrupted upon addition of His6-EGFP-pUL31 (*green*). A few seconds after addition, pUL31 forms 1.2 ± 0.2 μm patches that grow over time until they cover the whole area (around 90 s). The bilayer is destroyed, and lipid aggregation is seen over this period of time. *B*, addition of His_6-EGFP did not change the bilayer. *C*, particle analysis of the patches showing the growth of the particles over time. After 40 s, particles fuse and can no longer be analyzed. *Scale bars* = 50 μm

there is no evidence that pUL31 mediates lipid modifying reactions or has a binding preference for a specific lipid.

Therefore, we prefer a model in which pUL31 acts as a scaffolding protein self-assembling at the inner surface of the forming vesicle. pUL31 is monomeric and does not detectably self-interact in solution (Fig. 4, *B–D*). Artificial membrane tethering of limiting amounts of pUL31 that are not sufficient to promote membrane invaginations can recruit soluble pUL31 (Fig. 4*A*), which, in turn, induces intralumenal vesicle formation. This effect is caused by membrane-induced pUL31 oligomerization, as suggested by confocal and atomic force microscopy on supported lipid bilayers. Consistently, budding sites at the GUV membranes show local enrichment of pUL34-pUL31 or pUL31, respectively (Figs. 1*I* and 2*E*). Although we cannot exclude the contribution of other proteins, in cells, budding sites at the inner nuclear membrane are more electron-dense, an observation that implies high protein density (8, 10). Interestingly, a recent study shows that a pUL31-pUL34 complex lacking the pUL34 transmembrane domain forms ordered assemblies when recruited to membranes (21). Our study suggests that pUL31 alone can oligomerize on membranes and induce vesicle formation. For the Kaposi sarcoma-associated herpesvirus pUL31 homolog ORF69, it has been suggested that it is required for membrane remodelling into circular virion-size vesicles, whereas the pUL34 homolog ORF67 results in membrane proliferation (60). A double point mutation in HSV-1 pUL34 (D35A/E37A) causes a blockage in nuclear envelope vesicle formation without preventing pUL31 membrane recruitment (61). When tethered to GUVs, the corresponding pUL31/pUL34 fails to induce membrane deformation (21). The defect of pUL34 (D35A/E37A) during infection could be overcome by a mutation in pUL31 that restored the ability to induce membrane deformation (61). This indicates that pUL34, in addition to pUL31 recruitment, plays a supportive and regulatory role in the induction of vesicles (62). It is possible that pUL34 undergoes a conformational change upon pUL31 binding that either brings the protein closer to the membrane or triggers multimerization of the complex, features that might be blocked in the D35A/E37A mutation.

The vesicle budding at the nuclear envelope is reminiscent of the invagination processes mediated by the ESCRT machinery during formation of intraendosomal vesicles in multivesicular body formation. In this reaction pathway, ESCRT-I and ESCRT-II complexes direct membrane budding away from the cytosol, and ESCRT-III cleaves the bud necks from their cytosolic faces (23, 63, 64). In a mechanistically related process during HIV egress at the plasma membrane, the viral gag protein assembles and drives initial bud formation but requires the ESCRT complex components for membrane scission (65, 66). Gag protein assembly on the cytoplasmic side of the plasma membrane is thought to be the driving force for bud formation in HIV, and similar roles for membrane-associated proteins are implicated in rhabdovirus, filovirus, arenavirus, and paramyxovirus formation (37). In contrast to the gag/ESCRT machinery,

which mediates HIV release at the plasma membrane (67), the nuclear egress complex requires no energy input for both membrane budding and scission,[3] although we cannot exclude that, in the cellular situation, an energy-dependent step is involved. Interestingly, although, in the case of gag/ESCRT-mediated vesicle formation, several proteins are required and the steps of membrane budding and scission are separated functionally, a single protein, pUL31, can execute this task in herpesvirus nuclear egress. This suggests that pUL31 has the intrinsic ability to oligomerize on the membrane and cleave its own bud neck. How this is achieved mechanistically is an interesting avenue for future research. In contrast to a previous report, we did not detect a regular structural pattern on the membrane surface (Fig. 5), most likely because of the absence of pUL34. This suggest that pUL34 is, in addition to pUL31 recruitment, required for formation of the hexagonal arrangement and drives the otherwise unstructured oligomerization of pUL31 into an ordered pattern.

Although we cannot exclude the presence of smaller-sized vesicles inside the GUVs because of the refraction limit of light microscopy and the rapid vesicle movement, the vesicles observed in the *in vitro* system are considerably larger than the vesicles formed in the nuclear envelope lumen during viral egress (68) but also in the absence of capsids when overexpressing pUL31 and pUL34 (10, 20). Notably, a similar increase in vesicle diameters has been observed when studying budding and/or vesicle formation on GUVs mediated by the ESCRT machinery or other viral proteins, including pUL31/pUL34 (21, 63, 69–71). A number of factors could, in the case of our study, account for the size difference. The inner nuclear membrane is tightly connected to the underlying lamina and the chromatin by integral membrane proteins (1, 2). This could restrain lateral mobility of the membrane and, consequently, impact the size of the vesicles. Moreover, although pUL31 can, on its own, promote vesicle budding and scission, it is conceivable that cellular (and additional viral) factors contribute to the process *in vivo*, which could restrict vesicle size. The fact that a similar vesicle-mediated nuclear export of large ribonucleoprotein particles bypassing nuclear pore complexes is found (24) makes it likely that a cellular machinery exists that mediates membrane budding and scission at the inner nuclear membrane as well as fusion of these vesicles with the outer nuclear membrane and that could participate in herpesvirus nuclear egress.

In summary, our work establishes that pUL34-mediated membrane recruitment of pUL31 drives vesicle budding and constriction in a biochemically well defined system. It shows that a single protein, pUL31, is sufficient to induce inwardly directed membrane deformation and scission. It will be interesting to see whether cellular orthologs of herpesvirus pUL31 exist, especially for the process of RNP egress at the nuclear envelope, which is topologically comparable with herpesvirus nuclear egress. Finally, the methods established and employed here to express and reconstitute pUL34 into GUVs are generally applicable for other single and multiple transmembrane-spanning proteins and, therefore, present a valuable tool for studying these proteins in minimal and well defined membrane systems.

Acknowledgments—We thank C. Liebig (Imaging Facility MPI DevBiol) for help with confocal microscopy and image analysis; V. Betaneli and N. Eisenhardt for the introduction to GUV preparation; V. Ahl for help with the MALLS experiment; C. Sieverding and S. Astrinidis for technical support; and N. Eisenhardt, D. Moreno, K. Schellhaus, and A. Schooley for critical reading of the manuscript.

REFERENCES

1. Hetzer, M. W., and Wente, S. R. (2009) Border control at the nucleus: biogenesis and organization of the nuclear membrane and pore complexes. *Dev. Cell* **17,** 606–616
2. Schooley, A., Vollmer, B., and Antonin, W. (2012) Building a nuclear envelope at the end of mitosis: coordinating membrane reorganization, nuclear pore complex assembly, and chromatin de-condensation. *Chromosoma* **121,** 539–554
3. Adams, R. L., and Wente, S. R. (2013) Uncovering nuclear pore complexity with innovation. *Cell* **152,** 1218–1221
4. Kobiler, O., Drayman, N., Butin-Israeli, V., and Oppenheim, A. (2012) Virus strategies for passing the nuclear envelope barrier. *Nucleus* **3,** 526–539
5. Cohen, S., Au, S., and Panté, N. (2011) How viruses access the nucleus. *Biochim. Biophys. Acta* **1813,** 1634–1645
6. Skepper, J. N., Whiteley, A., Browne, H., and Minson, A. (2001) Herpes simplex virus nucleocapsids mature to progeny virions by an envelopment → deenvelopment → reenvelopment pathway. *J. Virol.* **75,** 5697–5702
7. Johnson, D. C., and Baines, J. D. (2011) Herpesviruses remodel host membranes for virus egress. *Nat. Rev. Microbiol.* **9,** 382–394
8. Mettenleiter, T. C., Müller, F., Granzow, H., and Klupp, B. G. (2013) The way out: what we know and do not know about herpesvirus nuclear egress. *Cell. Microbiol.* **15,** 170–178
9. Fuchs, W., Klupp, B. G., Granzow, H., Osterrieder, N., and Mettenleiter, T. C. (2002) The interacting UL31 and UL34 gene products of pseudorabies virus are involved in egress from the host-cell nucleus and represent components of primary enveloped but not mature virions. *J. Virol.* **76,** 364–378
10. Klupp, B. G., Granzow, H., Fuchs, W., Keil, G. M., Finke, S., and Mettenleiter, T. C. (2007) Vesicle formation from the nuclear membrane is induced by coexpression of two conserved herpesvirus proteins. *Proc. Natl. Acad. Sci. U.S.A.* **104,** 7241–7246
11. Lake, C. M., and Hutt-Fletcher, L. M. (2004) The Epstein-Barr virus BFRF1 and BFLF2 proteins interact and coexpression alters their cellular localization. *Virology* **320,** 99–106
12. Reynolds, A. E., Ryckman, B. J., Baines, J. D., Zhou, Y., Liang, L., and Roller, R. J. (2001) U(L)31 and U(L)34 proteins of herpes simplex virus type 1 form a complex that accumulates at the nuclear rim and is required for envelopment of nucleocapsids. *J. Virol.* **75,** 8803–8817
13. Schnee, M., Ruzsics, Z., Bubeck, A., and Koszinowski, U. H. (2006) Common and specific properties of herpesvirus UL34/UL31 protein family members revealed by protein complementation assay. *J. Virol.* **80,** 11658–11666
14. Sam, M. D., Evans, B. T., Coen, D. M., and Hogle, J. M. (2009) Biochemical, biophysical, and mutational analyses of subunit interactions of the human cytomegalovirus nuclear egress complex. *J. Virol.* **83,** 2996–3006
15. Milbradt, J., Auerochs, S., Sticht, H., and Marschall, M. (2009) Cytomegaloviral proteins that associate with the nuclear lamina: components of a postulated nuclear egress complex. *J. Gen. Virol.* **90,** 579–590
16. Reynolds, A. E., Liang, L., and Baines, J. D. (2004) Conformational changes in the nuclear lamina induced by herpes simplex virus type 1 require genes U(L)31 and U(L)34. *J. Virol.* **78,** 5564–5575
17. Bjerke, S. L., and Roller, R. J. (2006) Roles for herpes simplex virus type 1 UL34 and US3 proteins in disrupting the nuclear lamina during herpes simplex virus type 1 egress. *Virology* **347,** 261–276
18. Mou, F., Forest, T., and Baines, J. D. (2007) US3 of herpes simplex virus type 1 encodes a promiscuous protein kinase that phosphorylates and alters localization of lamin A/C in infected cells. *J. Virol.* **81,** 6459–6470
19. Muranyi, W., Haas, J., Wagner, M., Krohne, G., and Koszinowski, U. H.

(2002) Cytomegalovirus recruitment of cellular kinases to dissolve the nuclear lamina. *Science* **297,** 854–857
20. Desai, P. J., Pryce, E. N., Henson, B. W., Luitweiler, E. M., and Cothran, J. (2012) Reconstitution of the Kaposi's sarcoma-associated herpesvirus nuclear egress complex and formation of nuclear membrane vesicles by coexpression of ORF67 and ORF69 gene products. *J. Virol.* **86,** 594–598
21. Bigalke, J. M., Heuser, T., Nicastro, D., and Heldwein, E. E. (2014) Membrane deformation and scission by the HSV-1 nuclear egress complex. *Nat. Commun.* **5,** 4131
22. Kirchhausen, T. (2000) Three ways to make a vesicle. *Nat. Rev. Mol. Cell Biol.* **1,** 187–198
23. Hurley, J. H., and Hanson, P. I. (2010) Membrane budding and scission by the ESCRT machinery: it's all in the neck. *Nat. Rev. Mol. Cell Biol.* **11,** 556–566
24. Speese, S. D., Ashley, J., Jokhi, V., Nunnari, J., Barria, R., Li, Y., Ataman, B., Koon, A., Chang, Y. T., Li, Q., Moore, M. J., and Budnik, V. (2012) Nuclear envelope budding enables large ribonucleoprotein particle export during synaptic Wnt signaling. *Cell* **149,** 832–846
25. Roosild, T. P., Greenwald, J., Vega, M., Castronovo, S., Riek, R., and Choe, S. (2005) NMR structure of Mistic, a membrane-integrating protein for membrane protein expression. *Science* **307,** 1317–1321
26. Theerthagiri, G., Eisenhardt, N., Schwarz, H., and Antonin, W. (2010) The nucleoporin Nup188 controls passage of membrane proteins across the nuclear pore complex. *J. Cell Biol.* **189,** 1129–1142
27. Eisenhardt, N., Redolfi, J., and Antonin, W. (2014) Interaction of Nup53 with Ndc1 and Nup155 is required for nuclear pore complex assembly. *J. Cell Sci.* **127,** 908–921
28. Angelova, M. I., and Dimitrov, D. S. (1986) Liposome electroformation. *Faraday Discuss.* **81,** 303
29. Unsay, J. D., Cosentino, K., Subburaj, Y., and García-Sáez, A. J. (2013) Cardiolipin effects on membrane structure and dynamics. *Langmuir* **29,** 15878–15887
30. Kleinig, H. (1970) Nuclear membranes from mammalian liver: II: lipid composition. *J. Cell Biol.* **46,** 396–402
31. Vollmer, B., Schooley, A., Sachdev, R., Eisenhardt, N., Schneider, A. M., Sieverding, C., Madlung, J., Gerken, U., Macek, B., and Antonin, W. (2012) Dimerization and direct membrane interaction of Nup53 contribute to nuclear pore complex assembly. *EMBO J.* **31,** 4072–4084
32. Ulbert, S., Platani, M., Boue, S., and Mattaj, I. W. (2006) Direct membrane protein-DNA interactions required early in nuclear envelope assembly. *J. Cell Biol.* **173,** 469–476
33. Voeltz, G. K., Prinz, W. A., Shibata, Y., Rist, J. M., and Rapoport, T. A. (2006) A class of membrane proteins shaping the tubular endoplasmic reticulum. *Cell* **124,** 573–586
34. Walser, P. J., Ariotti, N., Howes, M., Ferguson, C., Webb, R., Schwudke, D., Leneva, N., Cho, K. J., Cooper, L., Rae, J., Floetenmeyer, M., Oorschot, V. M., Skoglund, U., Simons, K., Hancock, J. F., and Parton, R. G. (2012) Constitutive formation of caveolae in a bacterium. *Cell* **150,** 752–763
35. McMahon, H. T., and Gallop, J. L. (2005) Membrane curvature and mechanisms of dynamic cell membrane remodelling. *Nature* **438,** 590–596
36. Garoff, H., and Simons, K. (1974) Location of the spike glycoproteins in the Semliki Forest virus membrane. *Proc. Natl. Acad. Sci. U.S.A.* **71,** 3988–3992
37. Welsch, S., Müller, B., and Kräusslich, H. G. (2007) More than one door: budding of enveloped viruses through cellular membranes. *FEBS Lett.* **581,** 2089–2097
38. Schuster, F., Klupp, B. G., Granzow, H., and Mettenleiter, T. C. (2012) Structural determinants for nuclear envelope localization and function of pseudorabies virus pUL34. *J. Virol.* **86,** 2079–2088
39. Lingwood, D., and Simons, K. (2010) Lipid rafts as a membrane-organizing principle. *Science* **327,** 46–50
40. van Meer, G., Voelker, D. R., and Feigenson, G. W. (2008) Membrane lipids: where they are and how they behave. *Nat. Rev. Mol. Cell Biol.* **9,** 112–124
41. Mettenleiter, T. C. (2002) Herpesvirus assembly and egress. *J. Virol.* **76,** 1537–1547
42. Jokhi, V., Ashley, J., Nunnari, J., Noma, A., Ito, N., Wakabayashi-Ito, N., Moore, M. J., and Budnik, V. (2013) Torsin mediates primary envelopment of large ribonucleoprotein granules at the nuclear envelope. *Cell Rep.* **3,** 988–995
43. Klupp, B. G., Granzow, H., and Mettenleiter, T. C. (2011) Nuclear envelope breakdown can substitute for primary envelopment-mediated nuclear egress of herpesviruses. *J. Virol.* **85,** 8285–8292
44. Chang, Y. E., Van Sant, C., Krug, P. W., Sears, A. E., and Roizman, B. (1997) The null mutant of the U(L)31 gene of herpes simplex virus 1: construction and phenotype in infected cells. *J. Virol.* **71,** 8307–8315
45. Granato, M., Feederle, R., Farina, A., Gonnella, R., Santarelli, R., Hub, B., Faggioni, A., and Delecluse, H. J. (2008) Deletion of Epstein-Barr virus BFLF2 leads to impaired viral DNA packaging and primary egress as well as to the production of defective viral particles. *J. Virol.* **82,** 4042–4051
46. Haugo, A. C., Szpara, M. L., Parsons, L., Enquist, L. W., and Roller, R. J. (2011) Herpes simplex virus 1 pUL34 plays a critical role in cell-to-cell spread of virus in addition to its role in virus replication. *J. Virol.* **85,** 7203–7215
47. Ledesma, M. D., and Dotti, C. G. (2003) Membrane and cytoskeleton dynamics during axonal elongation and stabilization. *Int. Rev. Cytol.* **227,** 183–219
48. Merrifield, C. J. (2004) Seeing is believing: imaging actin dynamics at single sites of endocytosis. *Trends Cell Biol.* **14,** 352–358
49. Vennema, H., Godeke, G. J., Rossen, J. W., Voorhout, W. F., Horzinek, M. C., Opstelten, D. J., and Rottier, P. J. (1996) Nucleocapsid-independent assembly of coronavirus-like particles by co-expression of viral envelope protein genes. *EMBO J.* **15,** 2020–2028
50. Farsad, K., Ringstad, N., Takei, K., Floyd, S. R., Rose, K., and De Camilli, P. (2001) Generation of high curvature membranes mediated by direct endophilin bilayer interactions. *J. Cell Biol.* **155,** 193–200
51. Boucrot, E., Pick, A., Çamdere, G., Liska, N., Evergren, E., McMahon, H. T., and Kozlov, M. M. (2012) Membrane fission is promoted by insertion of amphipathic helices and is restricted by crescent BAR domains. *Cell* **149,** 124–136
52. Stachowiak, J. C., Schmid, E. M., Ryan, C. J., Ann, H. S., Sasaki, D. Y., Sherman, M. B., Geissler, P. L., Fletcher, D. A., and Hayden, C. C. (2012) Membrane bending by protein-protein crowding. *Nat. Cell Biol.* **14,** 944–949
53. Roux, A., Cuvelier, D., Nassoy, P., Prost, J., Bassereau, P., and Goud, B. (2005) Role of curvature and phase transition in lipid sorting and fission of membrane tubules. *EMBO J.* **24,** 1537–1545
54. Baumgart, T., Hess, S. T., and Webb, W. W. (2003) Imaging coexisting fluid domains in biomembrane models coupling curvature and line tension. *Nature* **425,** 821–824
55. Bacia, K., Schwille, P., and Kurzchalia, T. (2005) Sterol structure determines the separation of phases and the curvature of the liquid-ordered phase in model membranes. *Proc. Natl. Acad. Sci. U.S.A.* **102,** 3272–3277
56. Brügger, B., Glass, B., Haberkant, P., Leibrecht, I., Wieland, F. T., and Kräusslich, H. G. (2006) The HIV lipidome: a raft with an unusual composition. *Proc. Natl. Acad. Sci. U.S.A.* **103,** 2641–2646
57. Aloia, R. C., Jensen, F. C., Curtain, C. C., Mobley, P. W., and Gordon, L. M. (1988) Lipid composition and fluidity of the human immunodeficiency virus. *Proc. Natl. Acad. Sci. U.S.A.* **85,** 900–904
58. Ono, A., and Freed, E. O. (2005) Role of lipid rafts in virus replication. *Adv. Virus Res.* **64,** 311–358
59. Matsuo, H., Chevallier, J., Mayran, N., Le Blanc, I., Ferguson, C., Fauré, J., Blanc, N. S., Matile, S., Dubochet, J., Sadoul, R., Parton, R. G., Vilbois, F., and Gruenberg, J. (2004) Role of LBPA and Alix in multivesicular liposome formation and endosome organization. *Science* **303,** 531–534
60. Luitweiler, E. M., Henson, B. W., Pryce, E. N., Patel, V., Coombs, G., McCaffery, J. M., and Desai, P. J. (2013) Interactions of the Kaposi's sarcoma-associated herpesvirus nuclear egress complex: ORF69 is a potent factor for remodeling cellular membranes. *J. Virol.* **87,** 3915–3929
61. Roller, R. J., Bjerke, S. L., Haugo, A. C., and Hanson, S. (2010) Analysis of a charge cluster mutation of herpes simplex virus type 1 UL34 and its extragenic suppressor suggests a novel interaction between pUL34 and pUL31 that is necessary for membrane curvature around capsids. *J. Virol.* **84,** 3921–3934
62. Roller, R. J., Haugo, A. C., and Kopping, N. J. (2011) Intragenic and extragenic suppression of a mutation in herpes simplex virus 1 UL34 that af-

fects both nuclear envelope targeting and membrane budding. *J. Virol.* **85,** 11615–11625
63. Wollert, T., and Hurley, J. H. (2010) Molecular mechanism of multivesicular body biogenesis by ESCRT complexes. *Nature* **464,** 864 – 869
64. Wollert, T., Wunder, C., Lippincott-Schwartz, J., and Hurley, J. H. (2009) Membrane scission by the ESCRT-III complex. *Nature* **458,** 172–177
65. Sundquist, W. I., and Kräusslich, H. G. (2012) HIV-1 assembly, budding, and maturation. *Cold Spring Harb. Perspect. Med.* **2,** a006924
66. Van Engelenburg, S. B., Shtengel, G., Sengupta, P., Waki, K., Jarnik, M., Ablan, S. D., Freed, E. O., Hess, H. F., and Lippincott-Schwartz, J. (2014) Distribution of ESCRT machinery at HIV assembly sites reveals virus scaffolding of ESCRT subunits. *Science* **343,** 653–656
67. Baumgärtel, V., Ivanchenko, S., Dupont, A., Sergeev, M., Wiseman, P. W., Kräusslich, H. G., Bräuchle, C., Müller, B., and Lamb, D. C. (2011) Live-cell visualization of dynamics of HIV budding site interactions with an ESCRT component. *Nat. Cell Biol.* **13,** 469 – 474
68. Mettenleiter, T. C., Klupp, B. G., and Granzow, H. (2009) Herpesvirus assembly: an update. *Virus Res.* **143,** 222–234
69. Shnyrova, A. V., Ayllon, J., Mikhalyov, I. I., Villar, E., Zimmerberg, J., and Frolov, V. A. (2007) Vesicle formation by self-assembly of membrane-bound matrix proteins into a fluidlike budding domain. *J. Cell Biol.* **179,** 627– 633
70. Solon, J., Gareil, O., Bassereau, P., and Gaudin, Y. (2005) Membrane deformations induced by the matrix protein of vesicular stomatitis virus in a minimal system. *J. Gen. Virol.* **86,** 3357–3363
71. Rossman, J. S., Jing, X., Leser, G. P., and Lamb, R. A. (2010) Influenza virus M2 protein mediates ESCRT-independent membrane scission. *Cell* **142,** 902–913

In revision:

Nup153 recruits the Nup107-160 complex to the inner nuclear membrane for interphasic nuclear pore complex assembly

Benjamin Vollmer [1,2], Michael Lorenz [1], Daniel Moreno-Andres, Susanne Astrinidis, Allana Schooley, Matthias Flötenmeyer [3], Wolfram Antonin [4]

Friedrich Miescher Laboratory of the Max Planck Society, Spemannstraße 39, 72076 Tübingen, Germany

[1] both authors contributed equally

[2] present address: Oxford Particle Imaging Centre, Division of Structural Biology, Wellcome Trust Centre for Human Genetics, University of Oxford, Oxford OX3 7BN, UK

[3] Max Planck Institute for Developmental Biology, Spemannstraße 37, 72076 Tübingen, Germany

[4] author for correspondence: wolfram.antonin@tuebingen.mpg.de

54719 characters including spaces

Running Title: Nup153 in interphasic NPC assembly

Abbreviations List:

aa	amino acid
NPC	nuclear pore complex
Nup	nucleoporin
NE	nuclear envelope
AL	annulate lamellae
GUV	giant unilamellar vesicle

Keywords: nuclear pore complex formation, transportin, amphipathic helix, ran, annulate lamellae

Summary

In metazoa, nuclear pore complexes (NPCs) are assembled from constituent nucleoporins by two distinct mechanisms; In the re-forming nuclear envelope at the end of mitosis and into the intact nuclear envelope during interphase. Here, we show that the nucleoporin Nup153 is required for NPC assembly during interphase but not during mitotic exit. It functions in interphasic NPC formation by binding directly to the inner nuclear membrane via an N-terminal amphipathic helix. This binding facilitates the recruitment of the Nup107-160 complex, a crucial structural component of the NPC, to assembly sites. The nuclear transport receptor transportin and the small GTPase ran regulate the interaction of Nup153 with the membrane and in this way direct pore complex assembly to the nuclear envelope during interphase.

Bullet points:

- Nup153 binds membranes via its N-terminus.
- Transportin binding regulates Nup153 membrane interaction.
- Nup153 membrane binding is required for interphasic nuclear pore complex assembly.
- Nup153 recruits the Nup107-160 complex to the inner nuclear membrane.

Introduction

Nuclear pore complexes (NPCs) are gatekeepers of the nucleus. They restrict the diffusion of proteins and nucleic acids between the cytosol and nuclear interior and enable tightly-controlled transport between these compartments (Wente and Rout, 2010). Nuclear import of soluble proteins is mediated by transport receptors that bind cargo proteins in the cytosol. This interaction massively enhances the passage of otherwise inert cargos through NPCs. In the nucleoplasm, transport receptors are detached from cargos by binding to the small GTPase ran in its GTP bound form. The ranGTP-transport receptor complexes then traverse the NPC in the opposite direction. RanGTP hydrolysis at the cytoplasmic site of the NPC frees transport receptors, which are able to act in another round of the cycle.

Despite their enormous size and substantial flexibility with regard to transport substrates, NPCs are composed of only about thirty different proteins, nucleoporins, present in multiple copies (Alber et al., 2007; Bui et al., 2013). They can be roughly categorized into structural nucleoporins, which form the scaffold of the pore, and those responsible for the transport and exclusion functions of the NPC. Nucleoporins of the latter class are characterized by a high number of phenylalanine glycine (FG) repeats that form a meshwork within the pore. A stack of three rings forms the NPC scaffold. The middle ring is laterally linked to the pore membrane and connected to the central transport channel formed mostly by the FG-nucleoporins. The cytoplasmic and nucleoplasmic rings are connected to cytoplasmic filaments and the nuclear basket structure, respectively. Although the dimensions and mass of NPCs varies between different species, the structural arrangement of the three rings is conserved (Grossman et al., 2012).

Most structural nucleoporins are part of one of two evolutionarily conserved subcomplexes within the pore. The Nup93 complex (Nic96 complex in yeast), also known as the inner pore ring module, forms a large part of the inner ring and connects the pore membrane to the central transport channel (Vollmer and Antonin, 2014). The Nup107-160 complex (Nup84 complex in yeast) forms the cytoplasmic and nucleoplasmic rings (Alber et al., 2007; Bui et al., 2013) and is, because of its Y shaped structure (Lutzmann et al., 2002), also referred to as Y-complex. This complex is related to vesicle coats and presumably stabilizes the curved pore membrane of the NPC (Brohawn et al., 2008; Devos et al., 2004; Mans et al., 2004). Connected to the nucleoplasmic ring is the nuclear basket, a fish trap-like structure extending to the nuclear interior. In metazoans, three nucleoporins localize to the basket, Nup153, Nup50 and TPR (Cordes et al., 1993; Cordes et al., 1997; Guan et al., 2000; Sukegawa and Blobel, 1993), the best characterized being Nup153.

Nup153 possesses a tripartite structure (Ball and Ullman, 2005). The N-terminal region is important for NPC targeting (Bastos et al., 1996; Enarson et al., 1998), most likely because it mediates binding to the Y-complex (Vasu et al., 2001). A central zinc-finger containing domain interacts with ran (Nakielny et al., 1999). The C-terminal FG-repeat containing region provides binding sites for a variety of transport receptors (Moroianu et al., 1997; Nakielny et al., 1999; Shah and Forbes, 1998; Shah et al., 1998). Because of its localization at the nucleoplasmic exit site of NPCs as well as its interactions with transport receptors and ran, Nup153 is thought to assist in the dissociation of import cargo-transport receptor complexes and thus facilitate the nuclear import cycles. Indeed, Nup153 depletion reduces importin α/β mediated import (Ogawa et al., 2012; Walther et al., 2001). Nup153 is also important for mRNA export from the nucleus (Bastos et al., 1996; Ullman et al., 1999). Although Nup153 is essential in *C. elegans* and HeLa cells (Galy et al., 2003; Harborth et al., 2001), no

homologues have been found in yeast species. Nonetheless, yeast nucleoporins (such as Nup1 and Nup60 in *S. cerevisiae*, Nup124 in *S. pombe*) might share functional and sequence features with the metazoan Nup153 (Cronshaw et al., 2002; Hase and Cordes, 2003; Varadarajan et al., 2005).

While significant process has been made in understanding how NPCs function in the highly selective transport between cytoplasm and nucleoplasm, elucidating the NPC formation pathway remains a formidable task. The stepwise co-ordinated assembly of NPCs from more than four hundred individual components and their integration into the nuclear envelope (NE) is a fascinating example of molecular self-organisation. In metazoa, NPC assembly occurs at two different stages of the cell cycle: at the end of mitosis and during interphase. During mitotic exit, NPC assembly is concomitant with the formation of a closed NE. The early steps of post-mitotic NPC formation, such as the recruitment of a subset of nucleoporins to the chromatin; are particularly well characterised due to their faithful reconstitution in Xenopus egg extracts. Assembly is initiated by MEL28/ELYS, a chromatin binding nucleoporin, which recruits the Y-complex (Franz et al., 2007; Gillespie et al., 2007; Harel et al., 2003; Rasala et al., 2006; Rasala et al., 2008; Rotem et al., 2009; Walther et al., 2003a). The next step is the establishment of the membrane connection to the assembling NPC by interactions between the transmembrane nucleoporin POM121 and the Y-complex (Antonin et al., 2005; Mitchell et al., 2010; Yavuz et al., 2010). A second transmembrane nucleoporin, NDC1, is also likely to be involved at this step (Mansfeld et al., 2006; Stavru et al., 2006) but its function is less defined. Components of the Nup93 complex subsequently assemble stepwise from the membrane building laterally towards the centre of the NPC (Dultz et al., 2008; Sachdev et al., 2012; Vollmer et al., 2012), which allows for the recruitment of the central channel components, the FG-nucleoporins. The final steps of NPC assembly are the addition of peripheral nucleoporins, which form extensions to the cytoplasmic and nucleoplasmic sides of the pore (Bodoor et al., 1999; Dultz et al., 2008; Hase and Cordes, 2003).

Interphasic NPC assembly in metazoan is relatively poorly characterized. It takes place under fundamentally different conditions. Whereas large numbers of NPCs form in a short time span during mitotic exit, NPC assembly events in interphase are rare and sporadic (D'Angelo et al., 2006; Dultz and Ellenberg, 2010). Both assembly pathways require the Y-complex as an essential structural component of the NPC (D'Angelo et al., 2006; Doucet et al., 2010; Harel et al., 2003; Walther et al., 2003a). However, while the Y-complex is recruited to the chromatin by MEL28/ELYS at the end of mitosis, a feature essential for post-mitotic NPC assembly (Franz et al., 2007; Gillespie et al., 2007; Rasala et al., 2006), MEL28/ELYS is not required for interphasic NPC assembly (Doucet et al., 2010). It is possible that NPC assembly during interphase is rather initiated at the nuclear membranes (Doucet et al., 2010; Dultz and Ellenberg, 2010; Rothballer and Kutay, 2013; Vollmer et al., 2012) but the precise mechanism by which this occurs has not been defined.

Here we show that the nuclear basket component Nup153 is crucially required for NPC assembly during interphase but not at the end of mitosis. Nup153 binds the inner nuclear membrane via its N-terminus, a feature that is fundamental for its function in interphasic NPC assembly as it recruits the Y-complex to the assembling pores. Transportin regulates the interaction of Nup153 with the membrane and thus directs interphasic NPC assembly specifically to the NE from inside the nucleus.

Results

Nup153 interacts via its N-terminus directly with membranes

Nup153 contains a region within its N-terminus that directs it to the inner nuclear membrane (Enarson et al., 1998). It is possible that Nup153 is localized to the NE due to interactions with integral inner nuclear membrane proteins or lamins, proteins that underlay and stabilize the NE by forming a tight meshwork, but it could also bind directly to the lipid bilayer. To test for a direct membrane interaction we incubated the purified recombinant N-terminal region comprising the first 149 aa of *Xenopus laevis* Nup153 with small unilamellar liposomes with a NE lipid composition (Vollmer et al., 2012). Due to their density, lipid vesicles float up through a sucrose gradient. Membrane binding proteins can be identified in the top fraction together with the liposomes. This is indeed the case for Nup153 (Figure 1A) as well as for a Nup133 fragment previously identified as membrane interacting (Drin et al., 2007). The N-terminal region of Nup153 showed preference for small vesicle sizes with high curvature that was independent of lipid composition (Figure 1B).

Sequence analysis of the N-terminus of Nup153 identified a conserved region among vertebrates that might form an amphipathic helix, as depicted in the helical wheel representation (Figure 1C,D). We generated a point mutation (a valine to glutamate exchange in position 50, V50E) that predictably disrupt the hydrophobic surface of the helix. Indeed, the V50E mutation impaired liposome binding in flotation assays (Figure 1A,B). To directly visualize the interaction of Nup153 with membranes we generated giant unilamellar vesicles (GUVs) with sizes up to 50 µm using the NE lipid composition. When the EGFP-tagged N-terminus of Nup153 was added to the exterior of these GUVs it was efficiently recruited to the vesicle membrane indicating a direct membrane interaction (Figure 1E). As a negative control, we employed purified recombinant EGFP, which did not bind the GUV membrane. Importantly, the V50E mutant did not bind to GUVs, confirming that the amphipathic helix is responsible for the membrane binding capacity of Nup153.

The N-terminal fragment of *Xenopus* Nup153 fused to EGFP, when ectopically expressed in HeLa cells, localized to the NE, presumably the inner nuclear membrane (Figure 1F). Overexpression of this fragment induced NE proliferation (Movie S1), as is typical for nuclear membrane interacting proteins (Ralle et al., 2004). Membrane proliferation has previously been observed for the overexpression of full-length Nup153 (Bastos et al., 1996). In our experiments, the V50E mutation abolished NE localization and membrane proliferation. Instead, the protein localized to the nucleoplasm, indicating that the mutation is sufficient to prevent the interaction of the N-terminus of Nup153 with membranes in cells.

In order to confirm the direct membrane binding of full-length Nup153 we turned to the human orthologue, due to the low expression yield of the full length *Xenopus* Nup153. Human Nup153 possesses 42% amino acid identity and 55% similarity with the *Xenopus* protein. The fluorescently labeled human Nup153 efficiently bound GUVs (Figure 1G). The corresponding membrane binding deficient mutation (V47E in the human protein) abrogated the membrane interaction.

Nup153 membrane binding is not required for NPC targeting

To understand the functional implication of the direct membrane interaction we tested whether the inner nuclear membrane targeting of Nup153 is required for its incorporation into NPCs. HeLa cells

were transfected with EGFP-tagged full-length human Nup153 as well as the membrane binding deficient mutant (V47E). Both proteins localized to the nuclear rim and showed a typical punctate pattern (Daigle et al., 2001) on the NE surface (Figure 2A,S1). The pattern overlaps with mCherry-labeled Nup62 but not lamin B, indicating proper NPC localization. Despite its nuclear rim localization, the V47E mutant exhibited increased nucleoplasmic staining consistent with an abolished direct membrane interaction.

Immunoprecipitation from transfected HEK cells demonstrated that the V47E mutation did not impair known interactions, namely to the Y-complex (Nup133 and Nup107) or other nucleoporins (Nup50 and TPR), to A/C and B-type lamins, or to components of the nuclear import machinery, ran, importin α and β, and transportin (Figure 2B). Together these results indicate that membrane binding is not required for the assembly of Nup153 into NPCs. Furthermore, the V47E mutation does not disturb the interaction network of Nup153 but rather specifically affects its direct membrane binding.

Nup153 membrane interaction is not required for NPC assembly at the end of mitosis

We used *Xenopus* egg extracts to assess whether the membrane binding capacity of Nup153 is important for the assembly and function of NPCs. Nup153 can be specifically immuno-depleted from these extracts without affecting the levels of other nucleoporins, including TPR and Nup50 as well as two components of the Y-complex, Nup133 and Nup107, which interact with Nup153 within intact NPCs (Figure 3A). Similarly, the levels of lamin LIII, a B-type lamin found in Xenopus egg extracts, and components of the nuclear transport machinery (ran, importin α and β, transportin) were unchanged.

When de-membranated sperm heads are incubated with egg extracts, a NE forms around the decondensing chromatin in a process resembling the reassembly of the nucleus at the end of mitosis (Gant and Wilson, 1997). The NE contains NPCs visualized with the antibody mAB414, which recognizes several FG-nucleoporins, as seen in the control (mock) depletion (Figure 3B,C). When Nup153 was depleted, the protein was absent from the nuclear rim confirming the depletion efficiency. The assembled nuclei contained a closed NE with NPCs that were unevenly distributed. This NPC clustering phenotype upon Nup153 depletion has been previously observed (Walther et al., 2001) and is best visualized by surface rendering of confocal stacks (Figure 3B). Addition of recombinant Nup153 to endogenous levels (see Figure 3A) rescued the NPC clustering phenotype (Figure 3B-D) demonstrating its specificity. NPC clustering was also rescued by the Nup153 membrane-binding mutant, which indicates that the Nup153 membrane interaction is not required for proper NPC spacing.

Depletion of Nup153 did not affect the localization and regular distribution of lamin B or integral inner nuclear membrane proteins, such as LBR or BC08. Several nucleoporin antibodies including those recognizing the integral pore membrane protein POM121, the Y-complex members Nup133 and Nup107 as well as the Nup93 complex members Nup155 and Nup53 showed a patchy staining (Figure 3E,S2). These observations demonstrate that the structural backbones of NPCs can assemble in the absence of Nup153. Furthermore, the central transport channel (examined by Nup58, Figure S2) is also present at NPCs in the absence of Nup153. Consistent with previous reports, TPR was not detectable at Nup153 depleted nuclei, as it depends on this interaction for NPC localization (Hase

and Cordes, 2003; Walther et al., 2001). Re-addition of recombinant wildtype or membrane binding-deficient Nup153 not only rescued the NPC clustering phenotype but also TPR recruitment. This is consistent with the notion that the V47E mutation does not interfere with TPR binding (Figure 2B).

Taken together, these results suggest that the membrane binding capability of Nup153 is not crucial for NPC assembly at the end of mitosis. The interaction of Nup153 with membranes is not mandatory for proper NPC spacing, as the V47E mutant also rescues the NPC clustering phenotype. However, we observed that the nuclei assembled in the presence of the V47E mutant were smaller in comparison to the wildtype addback (Figure 3B,E,S2). Similarly, nuclei lacking Nup153 were smaller than control nuclei.

Nup153 membrane interaction is not required for efficient nuclear import

The addition of membranes to sperm DNA decondensed in egg extracts results in a fully closed NE containing NPCs within 20 min. After this assembly, which reproduces nuclear reformation at the end of mitosis, the nuclei grow in size - the extent to which depends on the extract quality and an ATP re-generating system - for another 180 min. This nuclear growth requires import of nuclear proteins through NPCs. During this time new NPCs integrate into the growing NE (D'Angelo et al., 2006) in a process reproducing interphasic NPC assembly, which in turn allows for more import and accelerated growth.

Nup153 contributes to the efficiency of nuclear transport cycles (Ogawa et al., 2012; Walther et al., 2001). We therefore tested whether the Nup153 membrane interaction is necessary for its role in nuclear import. We added different nuclear import substrates to in vitro assembled nuclei at a time point when a closed NE had formed. Nuclear import rates for soluble cargos can be determined by the time dependent protection of different import substrates from a cytoplasmic protease as they accumulate in the nucleus (in detail described in (Theerthagiri et al., 2010). The translocation of integral membrane proteins from the endoplasmic reticulum (ER) to the inner nuclear membranes can be assessed in a similar way when the reporter is reconstituted into liposomes, which are then added to the assembly reactions and integrated into the ER. Compared to mock reactions, nuclei depleted of Nup153 exhibited reduced import of a soluble import cargo with a classical bipartite nuclear localization signal (cNLS cargo), which is imported in an importin α/β dependent manner (Figure 4A). In contrast, import of a transportin-dependent cargo (containing an M9 sequence) was not affected by Nup153 depletion. The dependency of the importin α/β import pathway on Nup153 has been previously reported (Walther et al., 2001). Import of the cNLS-containing cargo was rescued by the re-addition of either wildtype or membrane binding-deficient Nup153. Transport of a transmembrane cargo through NPCs was not affected by Nup153 depletion or the addition of either wildtype or membrane binding-deficient Nup153. These results demonstrate that the membrane interaction of Nup153 is not important for efficient nuclear import.

Nup153 is necessary for interphasic NPC assembly

We next tested whether interphasic NPC assembly was affected by Nup153 depletion. Nuclei were assembled for 120 min and individual NPCs were counted using mAB414 staining (D'Angelo et al., 2006; Vollmer et al., 2012). Addition of 2 μM importin β, which blocks interphasic NPC assembly

(D'Angelo et al., 2006), to nuclei formed under control conditions resulted in a reduction in the number of NPCs per nucleus by approximately 50% (Figure 4B). Depletion of Nup153 caused a severe reduction in NPC number, which was not further affected by the addition importin β. Re-addition of wildtype Nup153 but not the membrane binding deficient V47E mutant rescued the reduced number of NPCs formed. These data suggest that NPC formation during interphase requires Nup153, specifically in its capacity to bind the NE.

The antibody mAB414 recognizes several FG-nucleoporins including Nup153 (Sukegawa and Blobel, 1993). Although we did not employ overall staining intensity as readout for NPC numbers but counted individual NPC containing spots on the NE this procedure might be considered as biased due to the loss of a major antigen. Furthermore, counting might also be affected by the NPC clustering observed in Nup153 deficient nuclei. We therefore employed an assay for interphasic NPC assembly that is independent of mAB414 staining. In this setup, interphasic NPC assembly proceeds in the presence of extract depleted of the nucleoporins forming the permeability barrier of the pore. Nuclei with newly integrated NPCs lack this barrier and can be visualized by an influx of fluorescently labeled dextrans (Dawson et al., 2009; Vollmer et al., 2012). It should be noted that each nucleus is counted as either competent or deficient for interphasic NPC assembly. The addition of importin β, for example completely inhibited interphasic NPC assembly monitored by dextran influx. Dextran influx was blocked in nuclei formed in the absence of Nup153, consistent with a block in interphasic NPC assembly (Figure 4C). Wildtype Nup153 but not the V47E mutant rescued interphasic NPC assembly based on dextran influx (Figure 4C).

Having identified an essential role for Nup153 and specifically its membrane interaction in interphasic NPC assembly, we wondered how Nup153 could function in this process. Two known Nup153 interactors are necessary for interphasic NPC assembly, ran and the Y-complex (D'Angelo et al., 2006; Doucet et al., 2010). Ran is most likely required to release import receptors from targets that are crucial for NPC assembly. Meanwhile the Y-complex is a structural component of NPCs. We speculated that Nup153 might recruit these crucial components to the inner nuclear membrane.

Nup153 recruits the Y-complex to the inner nuclear membrane for interphasic NPC assembly

To assess whether Nup153-dependent NE recruitment of ran or the Y-complex is important for interphasic NPC assembly we artificially directed these factors to the inner nuclear membrane thereby bypassing the function of Nup153. The Y-complex binding region (aa 210-338) or the ran binding region (aa 658-890) of human Nup153 were each fused N-terminally to EGFP and at the C-terminus with the transmembrane protein BC08, yielding EGFP-ycBD-BC08 and EGFP-ranBD-BC08 (Figure 5A). BC08 contains a C-terminal transmembrane region and efficiently targets to the inner nuclear membrane (Theerthagiri et al., 2010). Both constructs were expressed in *E. coli*, purified and reconstituted into small liposomes. To test the functionality of the fusion proteins these liposomes were incubated with Y-complex purified from *Xenopus* egg extracts or recombinant ran and floated through a sucrose gradient. Liposomes containing the EGFP-ycBD-BC08 protein efficiently bound the Y-complex but not ran and EGFP-ranBD-BC08 liposomes bound ran but not the Y-complex (Figure 5B). Similarly, when incorporated into GUVs, EGFP-ycBD-BC08 recruited fluorescently labeled Y-complex to the GUV membrane and EGFP-ranBD-BC08 recruited ran (Figure 5C).

When EGFP-ycBD-BC08 or EGFP-ranBD-BC08-containing liposomes where added to nuclear assembly reactions they efficiently targeted to the inner nuclear membrane (Figure 5D) as previously observed for the EGFP-BC08 fusion (Theerthagiri et al., 2010). Interestingly, Nup153 depletion resulted in larger nuclei when EGFP-ycBD-BC08 was incorporated compared to EGFP-ranBD-BC08 nuclei. Most importantly, EGFP-ycBD-BC08 but not EGFP-ranBD-BC08 incorporation into the nuclear membrane restored interphasic NPC assembly when Nup153 was depleted (Figure 5E,F). We conclude that recruitment of the Y-complex to the inner nuclear membrane is sufficient to bypass the requirement for full-length Nup153 in interphasic NPC assembly in vitro. Thus, the crucial function of Nup153 in interphasic NPC assembly is to direct the Y-complex to the newly forming NPCs at the NE.

Annulate lamellae formation depends on Nup153 membrane interaction

NPCs can assemble outside the nucleus in the membranes of the ER forming annulate lamellae (AL). AL form in egg extracts in the absence of chromatin and this process is highly induced upon addition of the constitutively active ran mutant Q69L, which is blocked in the GTP-bound state (Walther et al., 2003b). We wondered whether this NPC assembly mode also depends on Nup153 and specifically on its membrane targeting capability. Membranes were incubated with control or Nup153 depleted cytosol, re-isolated and analyzed by western blotting (Figure 6A,B). As expected, addition of ranQ69L strongly induced AL formation in control extracts, evidenced by an increased presence of Nup62, Nup53 and Nup107 - nucleoporins of the central channel, Nup93 complex or Y-complex, respectively - in the re-isolated membrane fraction. POM121, GP210 and NDC1, transmembrane pore proteins, were found in equal quantities, independent of the presence of ran Q69L. Reticulon 4, an ER marker, was used to control for equal membrane re-isolation efficiency. Nup153 depletion severely reduced the quantity of soluble nucleoporins re-isolated with membranes. Furthermore, the addition of ranQ69L did not result in increased re-isolation of the soluble nucleoporins as was seen in mock-depleted extracts, indicating a block in AL formation. Addition of wildtype Nup153, but not the Nup153 mutant defective for direct membrane binding, to depleted extracts rescued AL formation. Analysis of the re-isolated membrane fraction by electron microscopy showed AL in mock and Nup153 depleted extracts supplemented with the wildtype protein but not in depleted extracts supplemented with the V47E mutant (Figure 6C). Thus, together these data indicate that Nup153 membrane binding is also required for NPC assembly in the ER.

Transportin regulates Nup153 membrane interaction

Having identified a Nup153 membrane interaction that is crucial for both interphasic NPC assembly and AL formation, we wondered why the protein does not localize to cytoplasmic membranes under normal growth conditions but is rather specifically found at the inner nuclear membrane (Figure 1E, 2A). The N-terminal region of Nup153 interacts with transportin and mediates its import to the nucleus, a pre-requisite for its incorporation in NPCs (Bastos et al., 1996; Enarson et al., 1998; Nakielny et al., 1999; Shah and Forbes, 1998), Figure S3). It could be speculated that the rapid transportin-dependent import of Nup153 prevents its membrane association outside of the nucleus. We wondered whether transportin interaction could also directly affect Nup153 membrane binding. To test this, the N-terminus of Nup153 was employed in liposome flotation assays after pre-incubation with transportin. The presence of transportin strongly reduced the ability of Nup153 to

interact with membranes (Figure 7A). Importin β, a related import receptor that does not bind to this region, had no effect on the membrane binding of Nup153. Addition of ranQ69L, which releases import receptors including transportin from their cargos, reversed the inhibitory effect of transportin. Together, these data indicate that transportin inhibits Nup153 membrane binding and that this block is released by ranGTP. As high ranGTP concentrations are found in the nucleus it is conceivable that Nup153 can only function as a membrane interacting protein once it has reached the nucleus.

Discussion

Here we show that Nup153 can directly interact with membranes via an N-terminal amphipathic helix. This membrane interaction is important for interphasic NPC assembly as well as AL formation. During interphasic NPC assembly, Nup153 recruits the Y-complex, a crucial structural component of newly forming pores, to the inner nuclear membrane. Transportin binding to Nup153 inhibits its membrane interaction presumably by masking the membrane interaction surface of Nup153. Taken together our results imply a model in which transportin binding to Nup153, following its synthesis in the cytoplasm, prevents Nup153 from interacting with membranes outside of the nucleus (Figure 7B). After translocation through NPCs, Nup153 is released from transportin due to high nucleoplasmic concentrations of ranGTP. The liberated Nup153 interacts with the inner nuclear membrane and recruits the Y-complex to this locality where it functions in interphasic NPC assembly.

NPC assembly, both at the end of mitosis and in interphase, is regulated by ran and transport receptors (D'Angelo et al., 2006; Walther et al., 2003b). At the end of mitosis, the chromatin binding nucleoporin MEL28/ELYS has been identified as critical ran regulated target (Franz et al., 2007; Rotem et al., 2009). Here we show that Nup153 is during interphasic NPC assembly an important ran target. Both MEL28/ELYS and Nup153, once liberated from the inhibitory effect of importin β or transportin, recruit the Y-complex to NPC assembly sites.

The Y-complex is a basic structural component of the NPC forming a large part of the nucleoplasmic and cytoplasmic rings. It is crucial for NPC formation both at the end of mitosis and during interphase (D'Angelo et al., 2006; Doucet et al., 2010; Harel et al., 2003; Walther et al., 2003a). Nup153 is dispensable for NPC assembly at the end of mitosis (Figure 3) as previously observed (Walther et al., 2001). In this assembly mode the Y-complex is recruited to NPC assembly sites by MEL28/ELYS (Franz et al., 2007; Gillespie et al., 2007; Rasala et al., 2006). This points to an interesting mechanistic difference between NPC assembly at the end of mitosis and in interphase. Post-mitotic NPC assembly is initiated on the decondensing chromatin by MEL28/ELYS as an essential Y-complex targeting factor (Figure 7B). However, MEL28/ELYS has been reported to be dispensable for interphasic NPC assembly (Doucet et al., 2010), most likely because it is initiated at the NE. During interphase, it is Nup153 that acts as the crucial Y-complex recruitment factor at the inner nuclear membrane in a, presumably, chromatin-independent manner. Accordingly, AL formation is Nup153 dependent but does not require MEL28/ELYS, as it is initiated at the membrane in the absence of chromatin. Loss of MEL28/ELYS actually induces AL formation, presumably because it prevents post-mitotic NPC assembly from being initiated on the chromatin (Franz et al., 2007).

Although Nup133, a component of the Y-complex, possess an evolutionary conserved amphipathic helix (Doucet et al., 2010; Drin et al., 2007; Kim et al., 2014), it does not seem to be sufficient to target the Y-complex to the inner nuclear membrane during interphasic NPC assembly. One possible explanation is that the Nup153 and Nup133 membrane interaction motifs need to act together to possess sufficient affinity for the inner nuclear membrane. However, it cannot be excluded that the Nup133 amphipathic helix is non-functional in the intact Y-complex. There is no consensus about the orientation of the Y-complex within NPCs, including whether the Nup133 amphipathic helix could physically interact with the pore membrane (Leksa and Schwartz, 2010). Although a fragment containing this Nup133 motif does bind liposomes (Figure 1A, (Vollmer et al., 2012), the assembled Y-complex does not detectably bind liposomes or GUVs (Figure 5B,C). Other interactions, such as those

occurring between the transmembrane nucleoporin POM121 and the Y-complex (Mitchell et al., 2010; Yavuz et al., 2010) contribute to NPC assembly.

Whether the Nup153 mediated membrane recruitment of the Y-complex is the initial step of interphasic NPC assembly is an open question. Due to the experimental setup of the interphasic NPC formation assay it is difficult to determine the precise assembly order as it was done for the post-mitotic NPC formation pathway (described in (Schooley et al., 2012). The amphipathic helix of Nup133 has been proposed to target the Y-complex to the highly curved pore membrane during interphasic NPC assembly (Doucet et al., 2010). The amphipathic helix of Nup153 shows a similar preference for high curvature (Figure 1B) but it is naturally difficult to distinguish whether that represents a curvature sensing or inducing function. In other words, it is unclear whether Nup153 itself initiates interphasic pore assembly by inducing membrane curvature or whether it binds already curved membranes. If Nup153 only binds highly curved membranes, its recruitment would necessarily be preceded by proteins inducing nuclear pore formation, such as Nup53, reticulons and POM121 (Dawson et al., 2009; Doucet et al., 2010; Dultz and Ellenberg, 2010; Vollmer et al., 2012).

In summary, our work identifies a crucial function for Nup153 in interphasic NPC assembly. We provide insight on an interesting mechanistic difference between NPC assembly at the end of mitosis and during interphase. Whereas post-mitotic assembly is initiated by the MEL28/ELYS-mediated recruitment of the Y-complex to chromatin, interphasic NPC formation crucially requires Nup153 to interact with the inner nuclear membrane to localize the Y-complex to nascent assembly sites. It is currently unclear whether Nup153 recognizes a distinct feature at the site of the newly forming NPC and this will be an interesting avenue for future research.

Experimental Procedures

DiIC18, fluorescently labeled dextrans, and secondary antibodies (Alexa Fluor 488 goat α-rabbit IgG and Cy3 goat α-mouse IgG) were obtained from Invitrogen, detergents from EMD, and lipids from Avanti Polar Lipids.

Membrane binding experiments

Liposome flotations were done as in (Vollmer et al., 2012). GUVs were generated from a chloroform dissolved NE lipid mix (Angelova and Dimitrov, 1986). For the generation of EGFP-ycBD-BC08 or EGFP-ranBD-BC08 containing GUVs, detergent solubilized proteins were reconstituted in proteo-liposomes (Eisenhardt et al., 2014). Proteo-liposomes were dried onto two 5 mm x 5 mm platinum gauzes under vacuum for 1 h at RT. The gauzes were placed in parallel (5 mm distance) into a cuvette, submerged in a sucrose solution with a concentration matching the osmolality of the corresponding buffer used and an AC electric field with 10 Hz, 2.2 V was applied for 140 min followed by 2 Hz at 42°C for 20 min. An 8 well glass observation chamber (Chambered #1.0 Borosilicate Coverglass System, Lab-Tek) was blocked with 5 % (wt/vol) BSA in HEPES buffer (20 mM HEPES pH 7.5, 150 mM NaCl, 1mM DTT) and washed with HEPES buffer. For each reaction 50 µl of freshly prepared GUVs were mixed with 150 µl HEPES buffer and placed into a well. Proteins added and buffers used for GUV preparation matched the osmotic pressure of the sucrose solution. The mixture was incubated for 5 min and imaged immediately at RT on an inverted Olympus Fluoview 1000 confocal laser scanning system utilizing an UPlanSApo 60x/1.35 oil objective.

Miscellaneous

Nuclear assemblies, immunofluorescence, electron microscopy, generation of affinity resins, sperm heads and floated unlabeled or DiIC18-labeled membranes were carried out as described (Eisenhardt et al., 2014). Interphasic NPC assembly using dextran influx was performed as in (Vollmer et al., 2012). Nuclear import assays using EGFP-NPM2 (importin α/β-dependent cargo), EGFP-Nplc-M9-M10 (transportin-dependent cargo) and EGFP-LBR (aa146-258) as well as NPC counting are described in (Theerthagiri et al., 2010). AL were assembled in 15 µl Xenopus egg extract cytosol supplemented with 1.5 µl floated membranes, glycogen and an energy regenerating system (Eisenhardt et al., 2014). After 4 h at 20ºC samples were processed for electron microscopy or diluted in 1 ml sucrose buffer. Membranes were pelleted by centrifugation (10 min at 15.000 g), washed in 1 ml sucrose buffer and analyzed by western blotting. Antibodies, protein expression and purification as well as the transfection experiments are described in detail in the supplemental material section.

References

Alber, F., Dokudovskaya, S., Veenhoff, L.M., Zhang, W., Kipper, J., Devos, D., Suprapto, A., Karni-Schmidt, O., Williams, R., Chait, B.T.*, et al.* (2007). The molecular architecture of the nuclear pore complex. Nature *450*, 695-701.

Angelova, M.I., and Dimitrov, D.S. (1986). Liposome Electroformation. Faraday Discuss *81*, 303-+.

Antonin, W., Franz, C., Haselmann, U., Antony, C., and Mattaj, I.W. (2005). The integral membrane nucleoporin pom121 functionally links nuclear pore complex assembly and nuclear envelope formation. Mol Cell *17*, 83-92.

Ball, J.R., and Ullman, K.S. (2005). Versatility at the nuclear pore complex: lessons learned from the nucleoporin Nup153. Chromosoma *114*, 319-330.

Bastos, R., Lin, A., Enarson, M., and Burke, B. (1996). Targeting and function in mRNA export of nuclear pore complex protein Nup153. J Cell Biol *134*, 1141-1156.

Bodoor, K., Shaikh, S., Salina, D., Raharjo, W.H., Bastos, R., Lohka, M., and Burke, B. (1999). Sequential recruitment of NPC proteins to the nuclear periphery at the end of mitosis. J Cell Sci *112*, 2253-2264.

Brohawn, S.G., Leksa, N.C., Spear, E.D., Rajashankar, K.R., and Schwartz, T.U. (2008). Structural evidence for common ancestry of the nuclear pore complex and vesicle coats. Science *322*, 1369-1373.

Bui, K.H., von Appen, A., Diguilio, A.L., Ori, A., Sparks, L., Mackmull, M.T., Bock, T., Hagen, W., Andres-Pons, A., Glavy, J.S.*, et al.* (2013). Integrated structural analysis of the human nuclear pore complex scaffold. Cell *155*, 1233-1243.

Cordes, V.C., Reidenbach, S., Kohler, A., Stuurman, N., van Driel, R., and Franke, W.W. (1993). Intranuclear filaments containing a nuclear pore complex protein. J Cell Biol *123*, 1333-1344.

Cordes, V.C., Reidenbach, S., Rackwitz, H.R., and Franke, W.W. (1997). Identification of protein p270/Tpr as a constitutive component of the nuclear pore complex-attached intranuclear filaments. J Cell Biol *136*, 515-529.

Cronshaw, J.M., Krutchinsky, A.N., Zhang, W., Chait, B.T., and Matunis, M.J. (2002). Proteomic analysis of the mammalian nuclear pore complex. J Cell Biol *158*, 915-927.

D'Angelo, M.A., Anderson, D.J., Richard, E., and Hetzer, M.W. (2006). Nuclear pores form de novo from both sides of the nuclear envelope. Science *312*, 440-443.

Daigle, N., Beaudouin, J., Hartnell, L., Imreh, G., Hallberg, E., Lippincott-Schwartz, J., and Ellenberg, J. (2001). Nuclear pore complexes form immobile networks and have a very low turnover in live mammalian cells. J Cell Biol *154*, 71-84.

Dawson, T.R., Lazarus, M.D., Hetzer, M.W., and Wente, S.R. (2009). ER membrane-bending proteins are necessary for de novo nuclear pore formation. J Cell Biol *184*, 659-675.

Devos, D., Dokudovskaya, S., Alber, F., Williams, R., Chait, B.T., Sali, A., and Rout, M.P. (2004). Components of coated vesicles and nuclear pore complexes share a common molecular architecture. PLoS Biol *2*, e380.

Doucet, C.M., Talamas, J.A., and Hetzer, M.W. (2010). Cell cycle-dependent differences in nuclear pore complex assembly in metazoa. Cell *141*, 1030-1041.

Drin, G., Casella, J.F., Gautier, R., Boehmer, T., Schwartz, T.U., and Antonny, B. (2007). A general amphipathic alpha-helical motif for sensing membrane curvature. Nat Struct Mol Biol *14*, 138-146.

Dultz, E., and Ellenberg, J. (2010). Live imaging of single nuclear pores reveals unique assembly kinetics and mechanism in interphase. J Cell Biol *191*, 15-22.

Dultz, E., Zanin, E., Wurzenberger, C., Braun, M., Rabut, G., Sironi, L., and Ellenberg, J. (2008). Systematic kinetic analysis of mitotic dis- and reassembly of the nuclear pore in living cells. J Cell Biol *180*, 857-865.

Eisenhardt, N., Schooley, A., and Antonin, W. (2014). Xenopus in vitro assays to analyze the function of transmembrane nucleoporins and targeting of inner nuclear membrane proteins. Methods Cell Biol *122*, 193-218.

Enarson, P., Enarson, M., Bastos, R., and Burke, B. (1998). Amino-terminal sequences that direct nucleoporin nup153 to the inner surface of the nuclear envelope. Chromosoma *107*, 228-236.

Franz, C., Walczak, R., Yavuz, S., Santarella, R., Gentzel, M., Askjaer, P., Galy, V., Hetzer, M., Mattaj, I.W., and Antonin, W. (2007). MEL-28/ELYS is required for the recruitment of nucleoporins to chromatin and postmitotic nuclear pore complex assembly. EMBO Rep *8*, 165-172.
Galy, V., Mattaj, I.W., and Askjaer, P. (2003). Caenorhabditis elegans nucleoporins Nup93 and Nup205 determine the limit of nuclear pore complex size exclusion in vivo. Mol Biol Cell *14*, 5104-5115.
Gant, T.M., and Wilson, K.L. (1997). Nuclear assembly. Annu Rev Cell Dev Biol *13*, 669-695.
Gautier, R., Douguet, D., Antonny, B., and Drin, G. (2008). HELIQUEST: a web server to screen sequences with specific alpha-helical properties. Bioinformatics *24*, 2101-2102.
Gillespie, P.J., Khoudoli, G.A., Stewart, G., Swedlow, J.R., and Blow, J.J. (2007). ELYS/MEL-28 chromatin association coordinates nuclear pore complex assembly and replication licensing. Curr Biol *17*, 1657-1662.
Grossman, E., Medalia, O., and Zwerger, M. (2012). Functional architecture of the nuclear pore complex. Annual review of biophysics *41*, 557-584.
Guan, T., Kehlenbach, R.H., Schirmer, E.C., Kehlenbach, A., Fan, F., Clurman, B.E., Arnheim, N., and Gerace, L. (2000). Nup50, a nucleoplasmically oriented nucleoporin with a role in nuclear protein export. Mol Cell Biol *20*, 5619-5630.
Harborth, J., Elbashir, S.M., Bechert, K., Tuschl, T., and Weber, K. (2001). Identification of essential genes in cultured mammalian cells using small interfering RNAs. J Cell Sci *114*, 4557-4565.
Harel, A., Orjalo, A.V., Vincent, T., Lachish-Zalait, A., Vasu, S., Shah, S., Zimmerman, E., Elbaum, M., and Forbes, D.J. (2003). Removal of a single pore subcomplex results in vertebrate nuclei devoid of nuclear pores. Mol Cell *11*, 853-864.
Hase, M.E., and Cordes, V.C. (2003). Direct interaction with nup153 mediates binding of Tpr to the periphery of the nuclear pore complex. Mol Biol Cell *14*, 1923-1940.
Kim, S.J., Fernandez-Martinez, J., Sampathkumar, P., Martel, A., Matsui, T., Tsuruta, H., Weiss, T., Shi, Y., Markina-Inarrairaegui, A., Bonanno, J.B*., et al.* (2014). Integrative structure-function mapping of the nucleoporin Nup133 suggests a conserved mechanism for membrane anchoring of the nuclear pore complex. Mol Cell Proteomics.
Leksa, N.C., and Schwartz, T.U. (2010). Membrane-coating lattice scaffolds in the nuclear pore and vesicle coats: commonalities, differences, challenges. Nucleus *1*, 314-318.
Lutzmann, M., Kunze R, Buerer, A., Aebi, U., and Hurt, E. (2002). Modular self-assembly of a Y-shaped multiprotein complex from seven nucleoporins. EMBO J *21*, 387-397.
Mans, B.J., Anantharaman, V., Aravind, L., and Koonin, E.V. (2004). Comparative genomics, evolution and origins of the nuclear envelope and nuclear pore complex. Cell Cycle *3*, 1612-1637.
Mansfeld, J., Guttinger, S., Hawryluk-Gara, L.A., Pante, N., Mall, M., Galy, V., Haselmann, U., Muhlhausser, P., Wozniak, R.W., Mattaj, I.W*., et al.* (2006). The conserved transmembrane nucleoporin NDC1 is required for nuclear pore complex assembly in vertebrate cells. Mol Cell *22*, 93-103.
Mitchell, J.M., Mansfeld, J., Capitanio, J., Kutay, U., and Wozniak, R.W. (2010). Pom121 links two essential subcomplexes of the nuclear pore complex core to the membrane. The Journal of cell biology *191*, 505-521.
Moroianu, J., Blobel, G., and Radu, A. (1997). RanGTP-mediated nuclear export of karyopherin alpha involves its interaction with the nucleoporin Nup153. Proc Natl Acad Sci U S A *94*, 9699-9704.
Nakielny, S., Shaikh, S., Burke, B., and Dreyfuss, G. (1999). Nup153 is an M9-containing mobile nucleoporin with a novel Ran-binding domain. EMBO J *18*, 1982-1995.
Ogawa, Y., Miyamoto, Y., Oka, M., and Yoneda, Y. (2012). The interaction between importin-alpha and Nup153 promotes importin-alpha/beta-mediated nuclear import. Traffic *13*, 934-946.
Ralle, T., Grund, C., Franke, W.W., and Stick, R. (2004). Intranuclear membrane structure formations by CaaX-containing nuclear proteins. J Cell Sci *117*, 6095-6104.
Rasala, B.A., Orjalo, A.V., Shen, Z., Briggs, S., and Forbes, D.J. (2006). ELYS is a dual nucleoporin/kinetochore protein required for nuclear pore assembly and proper cell division. Proc Natl Acad Sci U S A *103*, 17801-17806.

Rasala, B.A., Ramos, C., Harel, A., and Forbes, D.J. (2008). Capture of AT-rich chromatin by ELYS recruits POM121 and NDC1 to initiate nuclear pore assembly. Molecular biology of the cell *19*, 3982-3996.
Rotem, A., Gruber, R., Shorer, H., Shaulov, L., Klein, E., and Harel, A. (2009). Importin beta regulates the seeding of chromatin with initiation sites for nuclear pore assembly. Molecular biology of the cell *20*, 4031-4042.
Rothballer, A., and Kutay, U. (2013). Poring over pores: nuclear pore complex insertion into the nuclear envelope. Trends Biochem Sci *38*, 292-301.
Sachdev, R., Sieverding, C., Flotenmeyer, M., and Antonin, W. (2012). The C-terminal domain of Nup93 is essential for assembly of the structural backbone of nuclear pore complexes. Mol Biol Cell *23*, 740-749.
Schooley, A., Vollmer, B., and Antonin, W. (2012). Building a nuclear envelope at the end of mitosis: coordinating membrane reorganization, nuclear pore complex assembly, and chromatin de-condensation. Chromosoma *121*, 539-554.
Shah, S., and Forbes, D.J. (1998). Separate nuclear import pathways converge on the nucleoporin Nup153 and can be dissected with dominant-negative inhibitors. Curr Biol *8*, 1376-1386.
Shah, S., Tugendreich, S., and Forbes, D. (1998). Major binding sites for the nuclear import receptor are the internal nucleoporin Nup153 and the adjacent nuclear filament protein Tpr. J Cell Biol *141*, 31-49.
Stavru, F., Hulsmann, B.B., Spang, A., Hartmann, E., Cordes, V.C., and Gorlich, D. (2006). NDC1: a crucial membrane-integral nucleoporin of metazoan nuclear pore complexes. J Cell Biol *173*, 509-519.
Sukegawa, J., and Blobel, G. (1993). A nuclear pore complex protein that contains zinc finger motifs, binds DNA, and faces the nucleoplasm. Cell *72*, 29-38.
Theerthagiri, G., Eisenhardt, N., Schwarz, H., and Antonin, W. (2010). The nucleoporin Nup188 controls passage of membrane proteins across the nuclear pore complex. The Journal of cell biology *189*, 1129-1142.
Ullman, K.S., Shah, S., Powers, M.A., and Forbes, D.J. (1999). The nucleoporin nup153 plays a critical role in multiple types of nuclear export. Mol Biol Cell *10*, 649-664.
Varadarajan, P., Mahalingam, S., Liu, P., Ng, S.B., Gandotra, S., Dorairajoo, D.S., and Balasundaram, D. (2005). The functionally conserved nucleoporins Nup124p from fission yeast and the human Nup153 mediate nuclear import and activity of the Tf1 retrotransposon and HIV-1 Vpr. Mol Biol Cell *16*, 1823-1838.
Vasu, S., Shah, S., Orjalo, A., Park, M., Fischer, W.H., and Forbes, D.J. (2001). Novel vertebrate nucleoporins Nup133 and Nup160 play a role in mRNA export. J Cell Biol *155*, 339-354.
Vollmer, B., and Antonin, W. (2014). The diverse roles of the Nup93/Nic96 complex proteins - structural scaffolds of the nuclear pore complex with additional cellular functions. Biological chemistry.
Vollmer, B., Schooley, A., Sachdev, R., Eisenhardt, N., Schneider, A.M., Sieverding, C., Madlung, J., Gerken, U., Macek, B., and Antonin, W. (2012). Dimerization and direct membrane interaction of Nup53 contribute to nuclear pore complex assembly. EMBO J *31*, 4072-4084.
Walther, T.C., Alves, A., Pickersgill, H., Loiodice, I., Hetzer, M., Galy, V., Hulsmann, B.B., Kocher, T., Wilm, M., Allen, T*., et al.* (2003a). The conserved Nup107-160 complex is critical for nuclear pore complex assembly. Cell *113*, 195-206.
Walther, T.C., Askjaer, P., Gentzel, M., Habermann, A., Griffiths, G., Wilm, M., Mattaj, I.W., and Hetzer, M. (2003b). RanGTP mediates nuclear pore complex assembly. Nature *424*, 689-694.
Walther, T.C., Fornerod, M., Pickersgill, H., Goldberg, M., Allen, T.D., and Mattaj, I.W. (2001). The nucleoporin Nup153 is required for nuclear pore basket formation, nuclear pore complex anchoring and import of a subset of nuclear proteins. Embo J *20*, 5703-5714.
Wente, S.R., and Rout, M.P. (2010). The nuclear pore complex and nuclear transport. Cold Spring Harb Perspect Biol *2*, a000562.
Yavuz, S., Santarella-Mellwig, R., Koch, B., Jaedicke, A., Mattaj, I.W., and Antonin, W. (2010). NLS-mediated NPC functions of the nucleoporin Pom121. FEBS Lett *584*, 3292-3298.

Figure Legends

Figure 1: Nup153 interacts via its N-terminus directly with membranes

A) 3 µM of the N-terminal domain (aa 1-149) of *Xenopus* Nup153 and the corresponding V50E mutant fragment, as well as a membrane interacting fragment of Nup133 and SUMO as positive and negative controls, respectively, were incubated with 2.5 mg/ml fluorescently labeled NE liposomes and floated through a sucrose gradient. The top gradient fraction and 3% of the starting material were analyzed by SDS-PAGE and silver staining.
B) Binding of the Nup153 N-terminus, the V50E mutant, SUMO and the Nup133 fragment to NE or DOPC liposomes of different sizes were analyzed by flotation experiments and quantified by western blotting (normalized to Nup153 binding to 30 nm liposomes, columns are the average bound quantities of three or four independent experiments, individual data points are indicated).
C) Sequence alignment of the N-terminal region of vertebrate Nup153.
D) Amino acid sequence of *Xenopus* Nup153 with the predicted amphipathic helix, seen in a helical wheel representation (generated with HeliQuest (Gautier et al., 2008)). Valine (V) was exchanged to glutamate (E) in the membrane binding mutant, indicated in red.
E) NE lipid GUVs were incubated with 500 nM EGFP-tagged Nup153 N-terminus, the corresponding V50E mutant or EGFP alone.
F) HeLa cells transfected with the EGFP-tagged Nup153 N-terminus, the V50E mutant or EGFP. Chromatin is stained with DAPI (blue in overlay).
G) NE lipid GUVs were incubated with Oregon green labeled full-length human Nup153 and the corresponding V47E mutant.

Bars: 10 µm.

Figure 2: Nup153 membrane binding is not required for its NPC targeting

A) HeLa cells were co-transfected with triple-EGFP human Nup153 or the corresponding V47E mutant and mCherry-Nup62 or mCherry-laminB and analyzed by live cell imaging. Insets show the nuclear surface at a 1.5 fold higher magnification. Bars: 5 µm
B) HEK293 cells were mock transfected, transfected with triple-EGFP human Nup153 or the V47E mutant. Inputs and immunprecipitates from cell lysates were analyzed by western blotting.

See also Figure S1

Figure 3: Nup153 is not crucial for NPC assembly at the end of mitosis

A) Western blot of mock depleted, Nup153 depleted (ΔNup153), and Nup153 depleted extracts supplemented with recombinant wild type Nup153 or the membrane-binding mutant (Nup153 V47E).

B) Nuclei assembled for 120 min in extracts generated as in (A) were analyzed by immunofluorescence for Nup153 (green) and mAB414 (red). DNA was stained with DAPI (blue) and membranes with DiIC18 (fourth row, red). The fifth row shows the surface rendering of confocal stacks of mAB414 labeled nuclei.
C) Quantification of chromatin substrates with closed NEs. Columns are the average of six independent experiments. The means from individual experiments (each 100 randomly chosen chromatin substrates) are indicated.
D) Quantification of nuclei with NPC clustering identified by mAB414 staining (six independent experiments with 100 chromatin substrates each).
E) Immunofluorescence on nuclei assembled as in (B). Chromatin is stained with DAPI (blue).

Bars: 10 µm. See also Figure S2

Figure 4: Nup153 membrane interaction is not important for nuclear import efficiency but for interphasic NPC assembly

A) Nuclei were assembled in mock, Nup153 depleted extracts or Nup153 depleted extracts supplemented with Nup153 or the V47E mutant. After closed NE formation, import rates for soluble M9 and cNLS cargos as well as for a transmembrane cargo were determined (average of two independent experiments, individual data points are indicated).
B) Nuclei assembled as in (A) were fixed after 120 min and NPC numbers per nucleus counted based on mAB414 staining. Where indicated, interphasic NPC assembly was blocked by importin β addition after 50 min (average from a total of 30 nuclei in 3 independent experiments, normalized to the mock control, error bars are SEM).
C) Nuclei assembled as in (A) were supplemented with cytosol depleted of Nup153 and FG-nucleoporins. After a further 60 min incubation, FITC-labeled 70-kD dextran and Hoechst were added (average of three independent experiments each with 100 nuclei).

Figure 5: Inner nuclear membrane tethering of the Y-complex bypasses the Nup153 necessity for interphasic NPC assembly

A) Schematic representation of the Nup153 fusion constructs. The Y-complex (aa 210-338) and the ran interacting region (aa 658-890) (blue), flanked by EGFP (green) and the inner nuclear membrane protein BC08 (orange) yield EGFP-ycBD-BC08 or EGFP-ranBD-BC08, respectively.
B) EGFP-ycBD-BC08 or EGFP-ranBD-BC08 was reconstituted into NE liposomes and incubated with Y-complex or ran. Start material (50% for the EGFP-ycBD-BC08 or EGFP-ranBD-BC08, 30% for the Y-complex and ran) and top fractions were analyzed using EGFP, Nup160, Nup107, and ran antibodies.
C) EGFP-ycBD-BC08 or EGFP-ranBD-BC08 were reconstituted into NE lipid GUVs and membrane recruitment of Alexa-546 labeled Y-complex or ran was analyzed.
D) Nuclei were assembled in mock or Nup153 depleted extracts supplemented with empty, EGFP-ycBD-BC08 or EGFP-ranBD-BC08 containing liposomes. Samples were fixed after 120

min and visualized using EGFP (green) and immunofluorescence for mAB414 (red). DNA was stained with DAPI (blue).

E) NPC numbers in nuclei assembled as in (D) were determined using mAB414 staining (average from 30 nuclei from 3 independent experiments, normalized to the mock control, error bars are SEM).

F) Nuclei assembled as in (B) and interphasic NPC assembly analyzed by dextran influx as in Figure 4C.

Bars: 10 µm

Figure 6: Nup153 membrane interaction is required for AL formation

A) Mock, Nup153 depleted cytosol or Nup153 depleted cytosol supplemented with Nup153 or the V47E mutant were incubated for 4 h with membranes and where indicated with ranQ69L. 10% of the start material and the re-isolated membranes were analyzed. Reticulon 4 (RTN4) serves as a ER marker.

B) Quantification of Nup62 re-isolated with membranes (average Nup62 intensity value from three independent experiments performed as in (A), normalized to mock control in the absence of ranQ69L).

C) Transmission electron microscopy of re-isolated membranes as in (A) in the presence of 10 µM ranQ69L. Insets show a threefold higher magnification, bar 500 nm.

Figure 7: Transportin regulates Nup153 membrane interaction and function in interphasic NPC assembly

A) 3 µM of the Xenopus Nup153 N-terminus was, where indicated, pre-incubated with 5 µM transportin, 5 µM importin β, or 5 µM transportin along with 15 µM ranQ69L. Proteins were incubated with fluorescently labeled NE liposomes and floated through a sucrose gradient. Top gradient fraction and 3% of the input material were analyzed by western blot (upper panel). For quantification from two independent experiments, liposome binding was normalized to the untreated Nup153 N-terminus.

B) Model for transportin and Nup153 function in interphasic NPC assembly (left panel): Transportin binding to Nup153 in the cytoplasm prevents its membrane interaction and mediates its nuclear import. In the nucleus ranGTP releases transportin from Nup153, which becomes free to interact with the inner nuclear membrane and recruit the Y-complex for interphasic NPC assembly. In contrast, at the end of mitosis (right panel), MEL28/ELYS recruits the Y-complex to chromatin and NPC assembly sites without an essential contribution from Nup153.

See also Figure S3

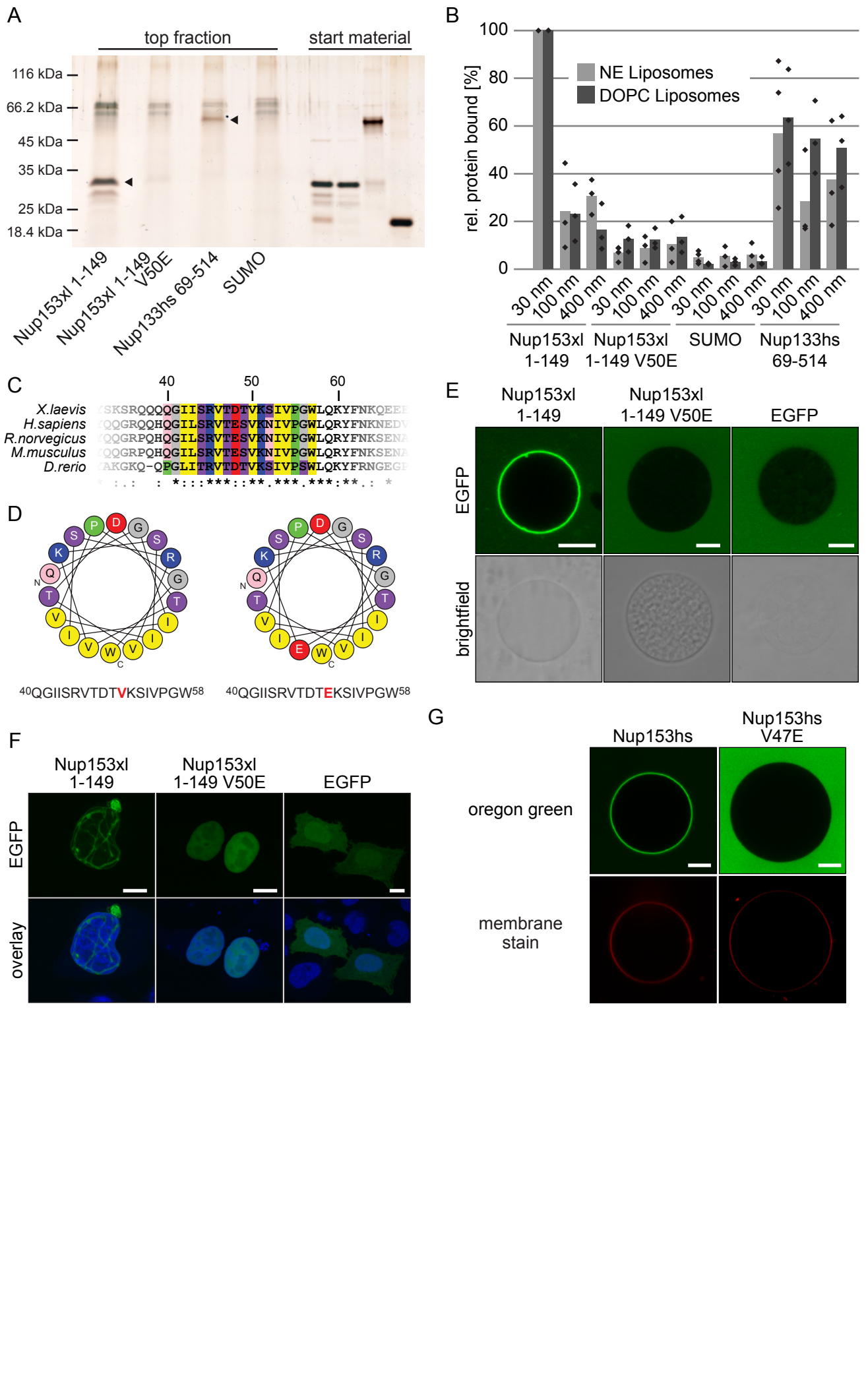
A
top fraction
start material
116 kDa
66.2 kDa
45 kDa
35 kDa
25 kDa
18.4 kDa
Nup153xl 1-149
Nup153xl 1-149 V50E
Nup133hs 69-514
SUMO
B
rel. protein bound [%]
NE Liposomes
DOPC Liposomes
30 nm
100 nm
400 nm
Nup153xl 1-149
Nup153xl 1-149 V50E
SUMO
Nup133hs 69-514
C
X.laevis
H.sapiens
R.norvegicus
M.musculus
D.rerio
D
40QGIISRVTDTVKSIVPGW58
40QGIISRVTDTEKSIVPGW58
E
Nup153xl 1-149
Nup153xl 1-149 V50E
EGFP
brightfield
F
Nup153xl 1-149
Nup153xl 1-149 V50E
EGFP
overlay
G
Nup153hs
Nup153hs V47E
oregon green
membrane stain

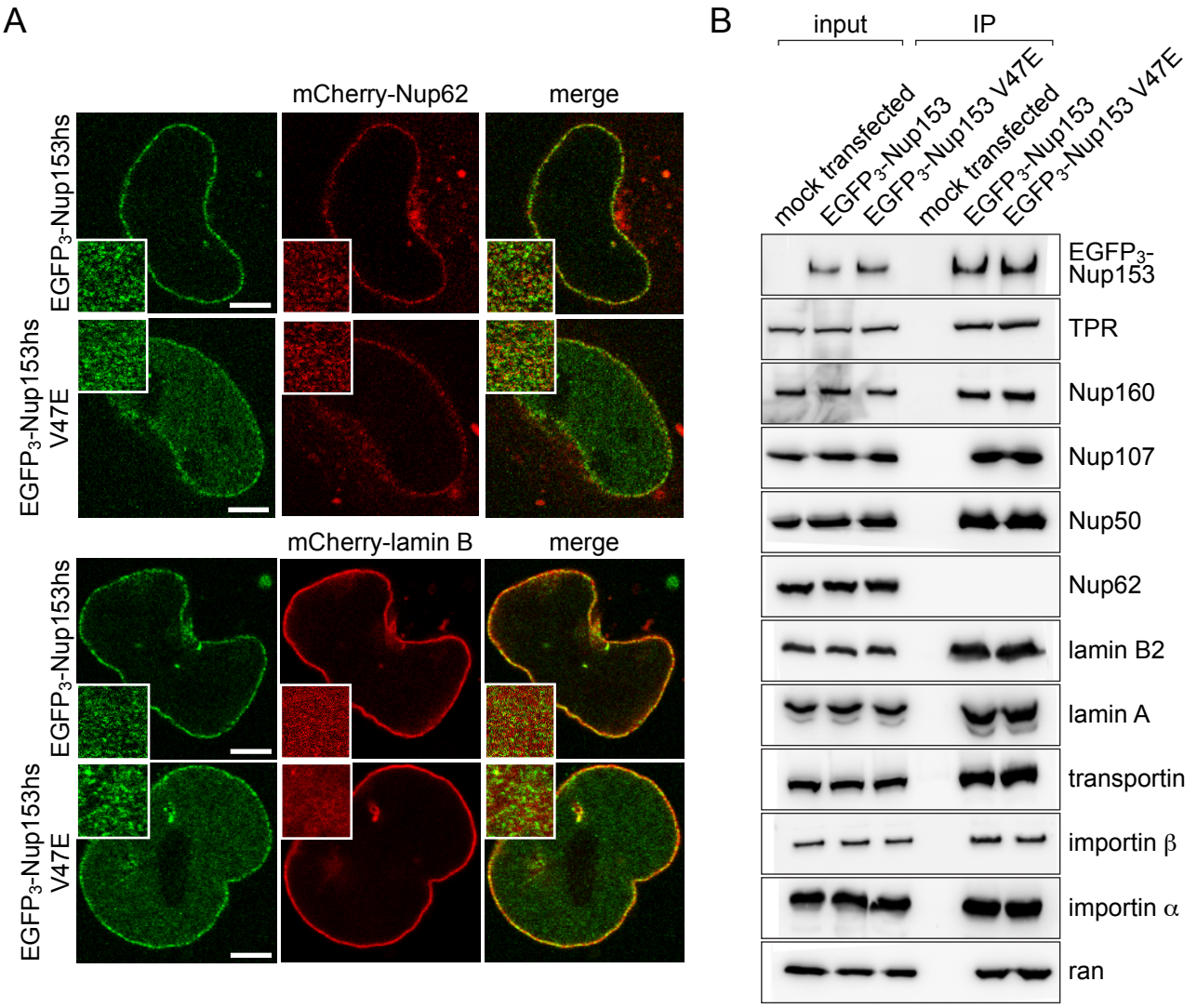
A
mCherry-Nup62
merge
EGFP3-Nup153hs
EGFP3-Nup153hs V47E
mCherry-lamin B
merge
EGFP3-Nup153hs
EGFP3-Nup153hs V47E
B
input
IP
mock transfected
EGFP3-Nup153
EGFP3-Nup153 V47E
mock transfected
EGFP3-Nup153
EGFP3-Nup153 V47E
EGFP3-Nup153
TPR
Nup160
Nup107
Nup50
Nup62
lamin B2
lamin A
transportin
importin β
importin α
ran

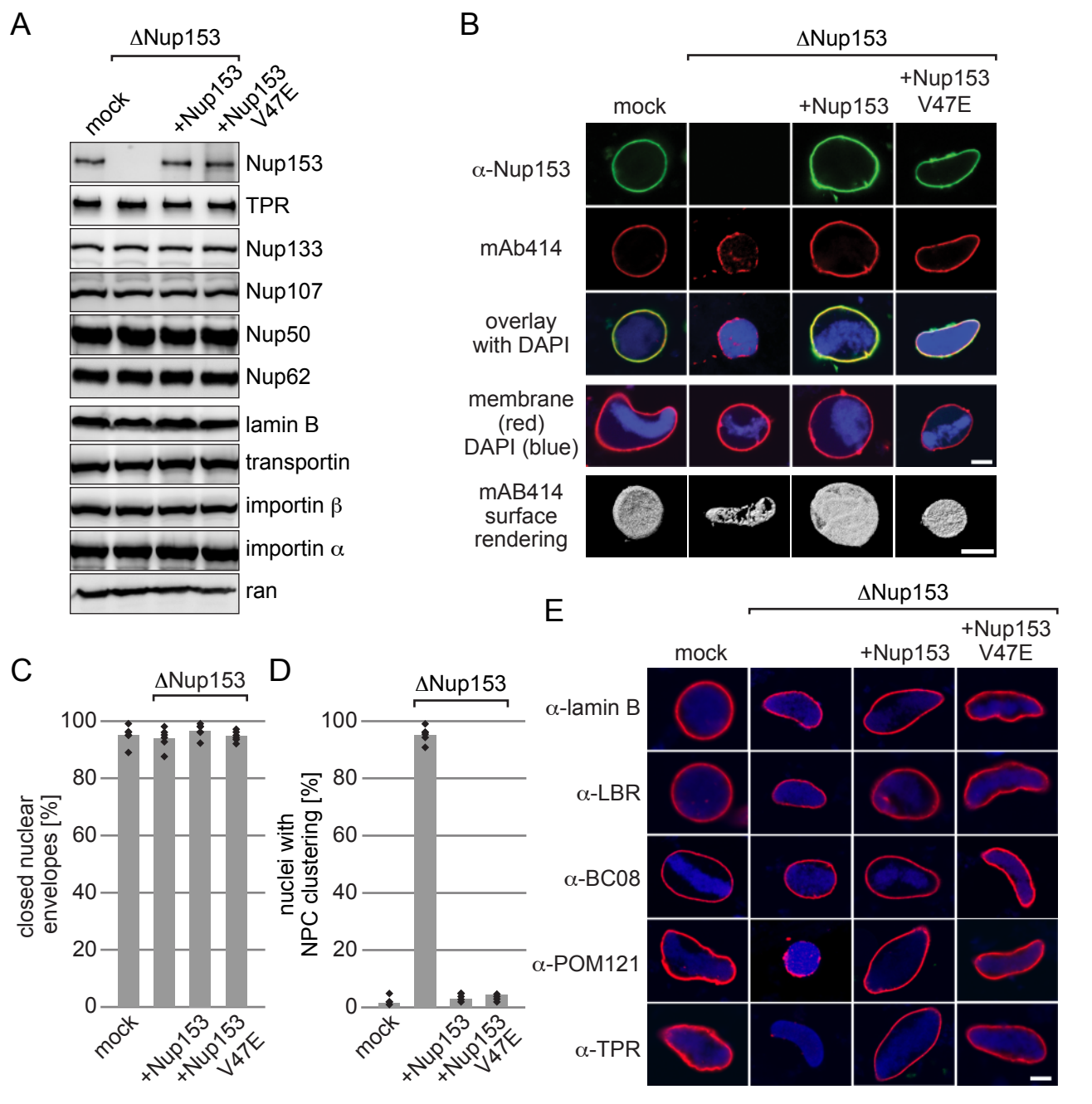
A
ΔNup153
mock
+Nup153
+Nup153 V47E
Nup153
TPR
Nup133
Nup107
Nup50
Nup62
lamin B
transportin
importin β
importin α
ran
B
ΔNup153
mock
+Nup153
+Nup153 V47E
α-Nup153
mAb414
overlay with DAPI
membrane (red) DAPI (blue)
mAB414 surface rendering
C
ΔNup153
closed nuclear envelopes [%]
100
80
60
40
20
0
mock
+Nup153
+Nup153 V47E
D
ΔNup153
nuclei with NPC clustering [%]
100
80
60
40
20
0
mock
+Nup153
+Nup153 V47E
E
ΔNup153
mock
+Nup153
+Nup153 V47E
α-lamin B
α-LBR
α-BC08
α-POM121
α-TPR

A

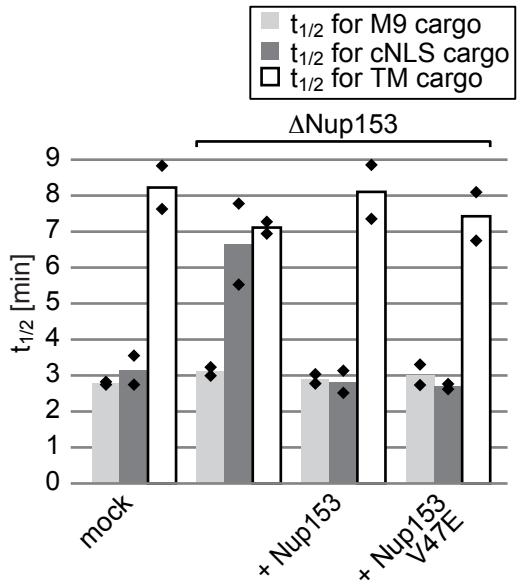
t1/2 for M9 cargo
t1/2 for cNLS cargo
t1/2 for TM cargo
ΔNup153
t1/2 [min]
0
1
2
3
4
5
6
7
8
9
mock
+ Nup153
+ Nup153 V47E

B

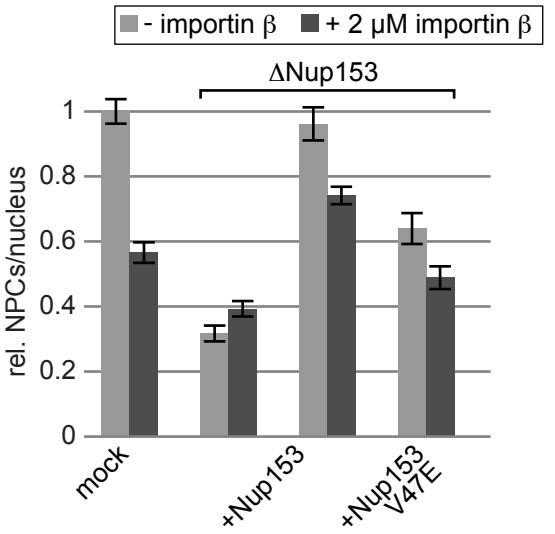
- importin β
+ 2 µM importin β
ΔNup153
rel. NPCs/nucleus
0
0.2
0.4
0.6
0.8
1
mock
+Nup153
+Nup153 V47E

C

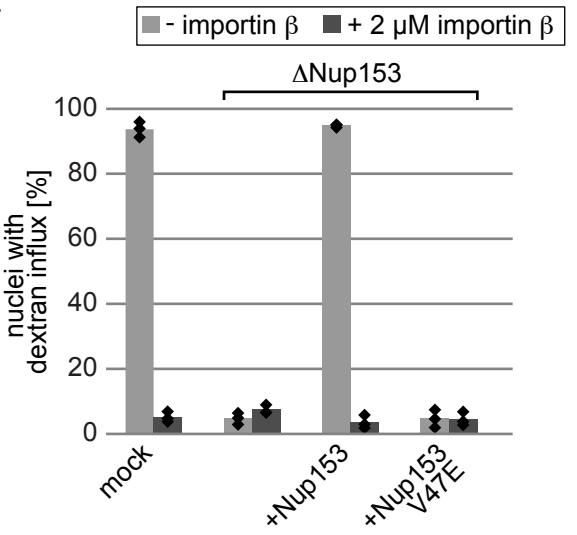
- importin β
+ 2 µM importin β
ΔNup153
nuclei with dextran influx [%]
0
20
40
60
80
100
mock
+Nup153
+Nup153 V47E

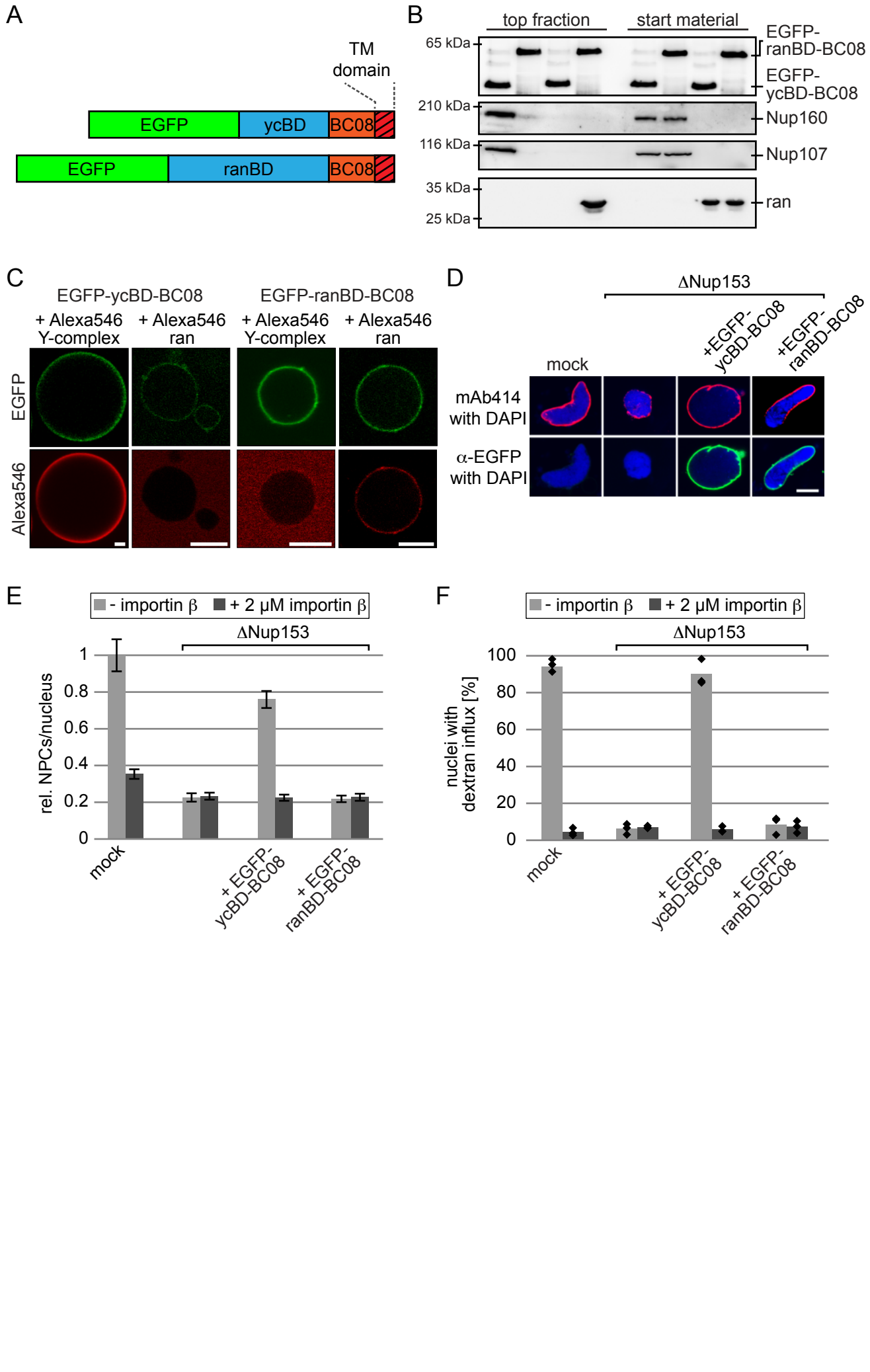
A
TM domain
EGFP
ycBD
BC08
EGFP
ranBD
BC08
B
top fraction
start material
65 kDa
210 kDa
116 kDa
35 kDa
25 kDa
EGFP-ranBD-BC08
EGFP-ycBD-BC08
Nup160
Nup107
ran
C
EGFP-ycBD-BC08
EGFP-ranBD-BC08
+ Alexa546 Y-complex
+ Alexa546 ran
+ Alexa546 Y-complex
+ Alexa546 ran
EGFP
Alexa546
D
ΔNup153
mock
+EGFP-ycBD-BC08
+EGFP-ranBD-BC08
mAb414 with DAPI
α-EGFP with DAPI
E
- importin β
+ 2 μM importin β
ΔNup153
rel. NPCs/nucleus
1
0.8
0.6
0.4
0.2
0
mock
+ EGFP-ycBD-BC08
+ EGFP-ranBD-BC08
F
- importin β
+ 2 μM importin β
ΔNup153
nuclei with dextran influx [%]
100
80
60
40
20
0
mock
+ EGFP-ycBD-BC08
+ EGFP-ranBD-BC08

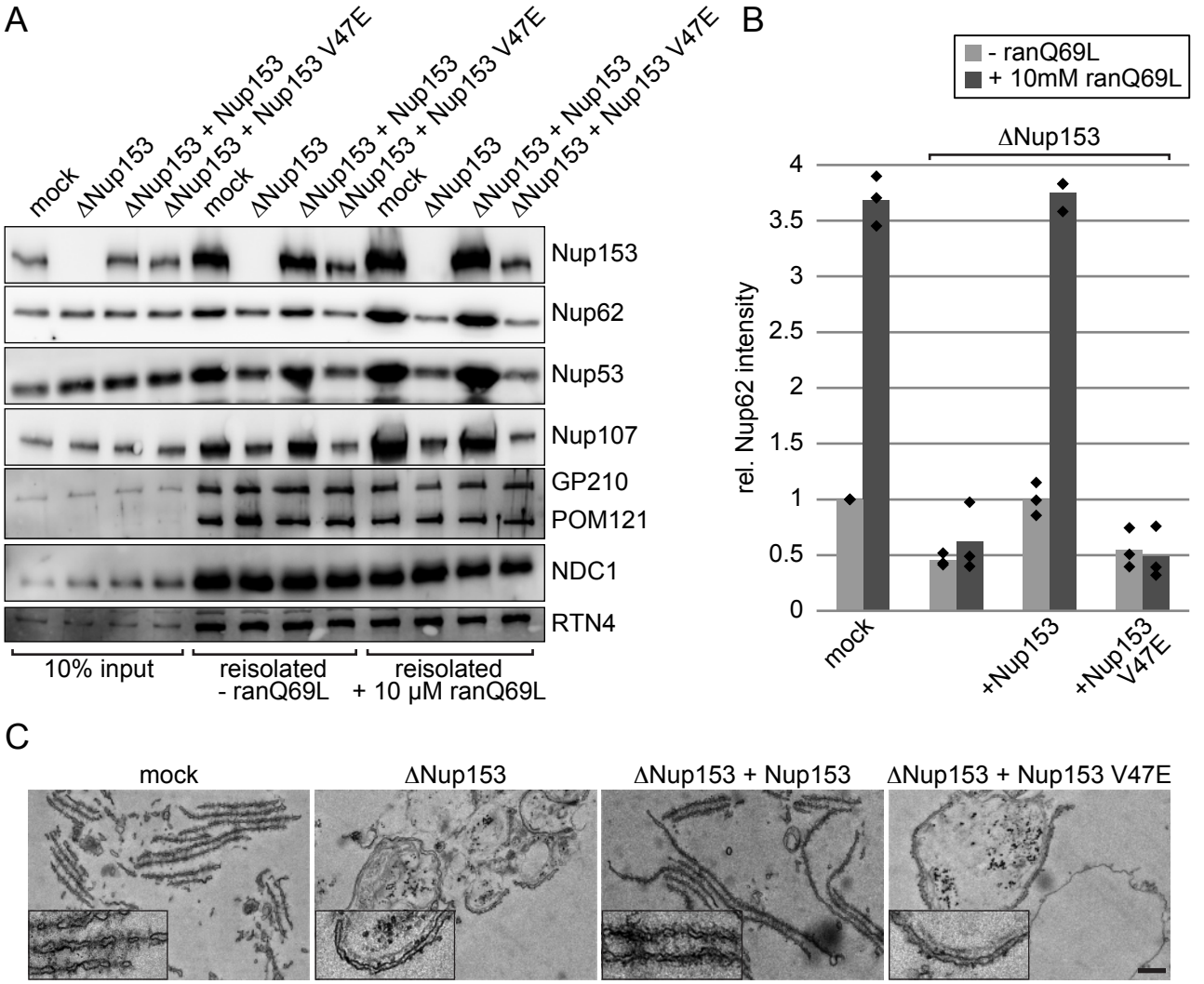
A
mock
ΔNup153
ΔNup153 + Nup153
ΔNup153 + Nup153 V47E
Nup153
Nup62
Nup53
Nup107
GP210
POM121
NDC1
RTN4
10% input
reisolated - ranQ69L
reisolated + 10 μM ranQ69L
B
- ranQ69L
+ 10mM ranQ69L
ΔNup153
rel. Nup62 intensity
0
0.5
1
1.5
2
2.5
3
3.5
4
mock
+Nup153
+Nup153 V47E
C
mock
ΔNup153
ΔNup153 + Nup153
ΔNup153 + Nup153 V47E

A

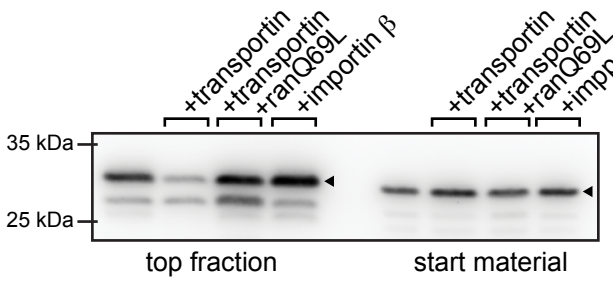
+transportin
+transportin +ranQ69L
+importin β
35 kDa
25 kDa
top fraction
start material

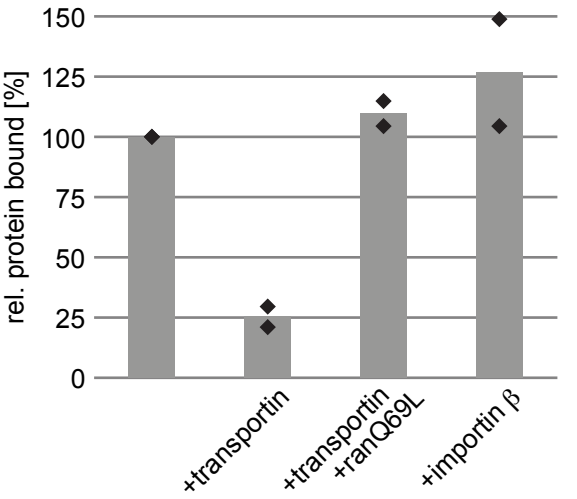
rel. protein bound [%]
150
125
100
75
50
25
0
+transportin
+transportin +ranQ69L
+importin β

B

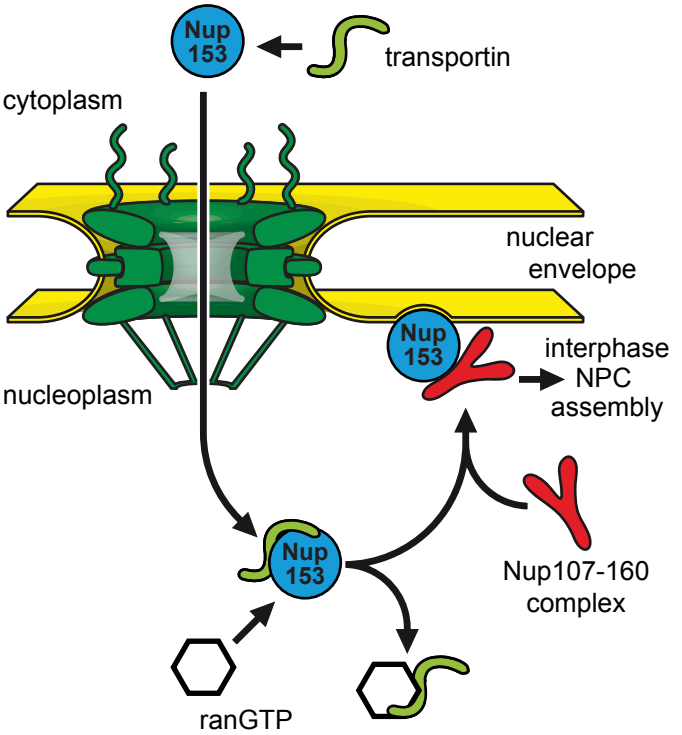
interphase
Nup 153
transportin
cytoplasm
nuclear envelope
Nup 153
interphase NPC assembly
nucleoplasm
Nup 153
Nup107-160 complex
ranGTP

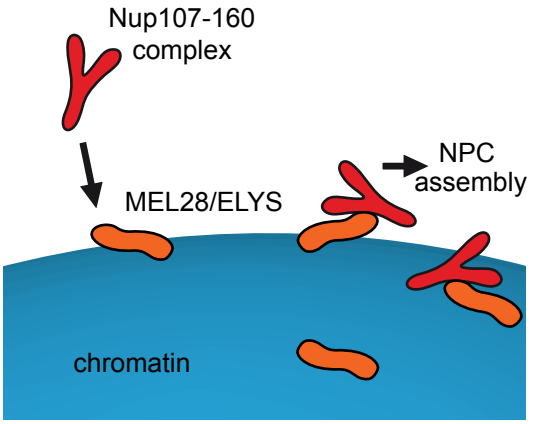
mitosis
Nup107-160 complex
MEL28/ELYS
NPC assembly
chromatin

Supplemental Material to

Nup153 recruits the Nup107-160 complex to the inner nuclear membrane for interphasic nuclear pore complex assembly

Benjamin Vollmer, Michael Lorenz, Daniel Moreno-Andres, Susanne Astrinidis, Allana Schooley, Matthias Flötenmeyer and Wolfram Antonin

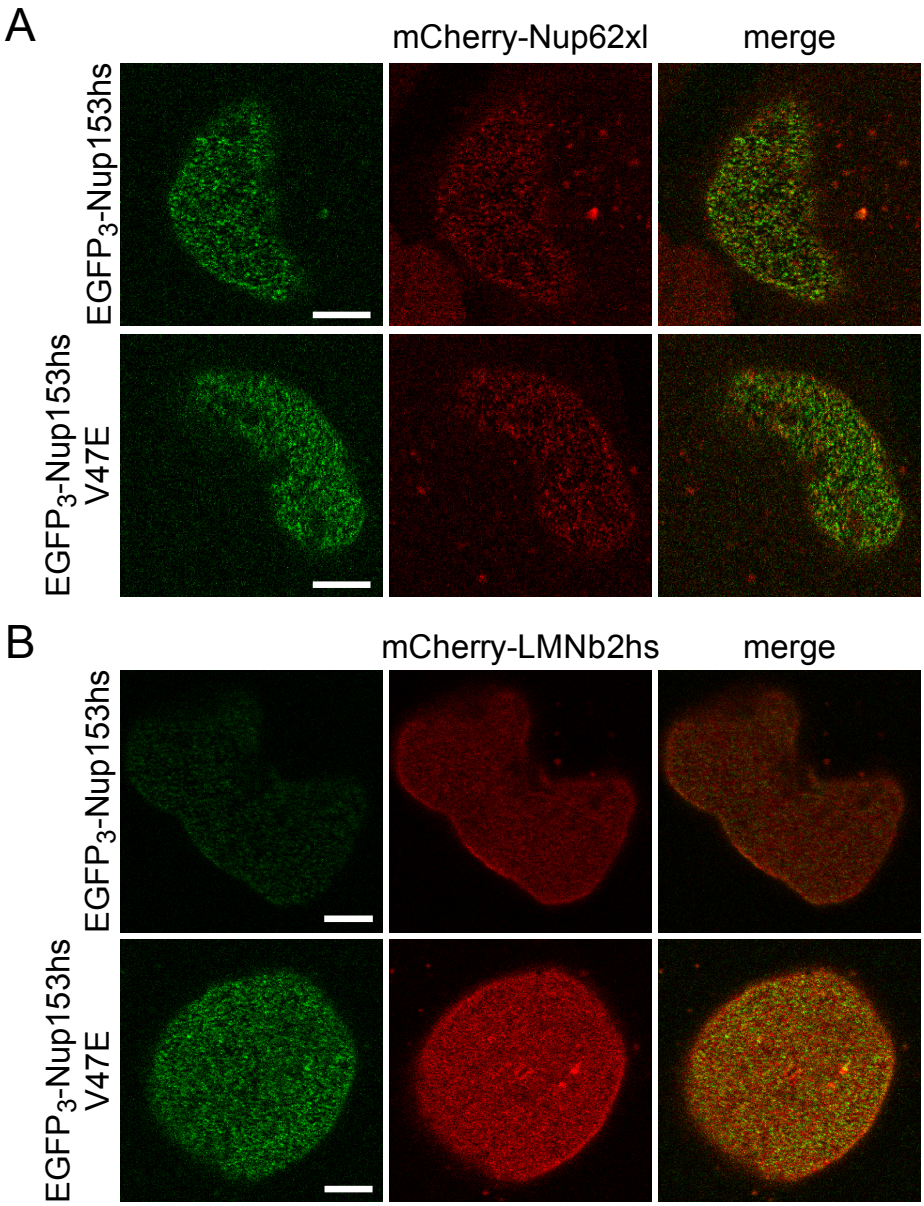

Figure S1, related to Figure 2

Complete images of nuclear surface of HeLa cells co-transfected with triple-EGFP-tagged human Nup153 or the corresponding V47E mutant and mCherry-Nup62 or mCherry-lamin B which are shown as insets in Figure 2A. Bars: 5 µm

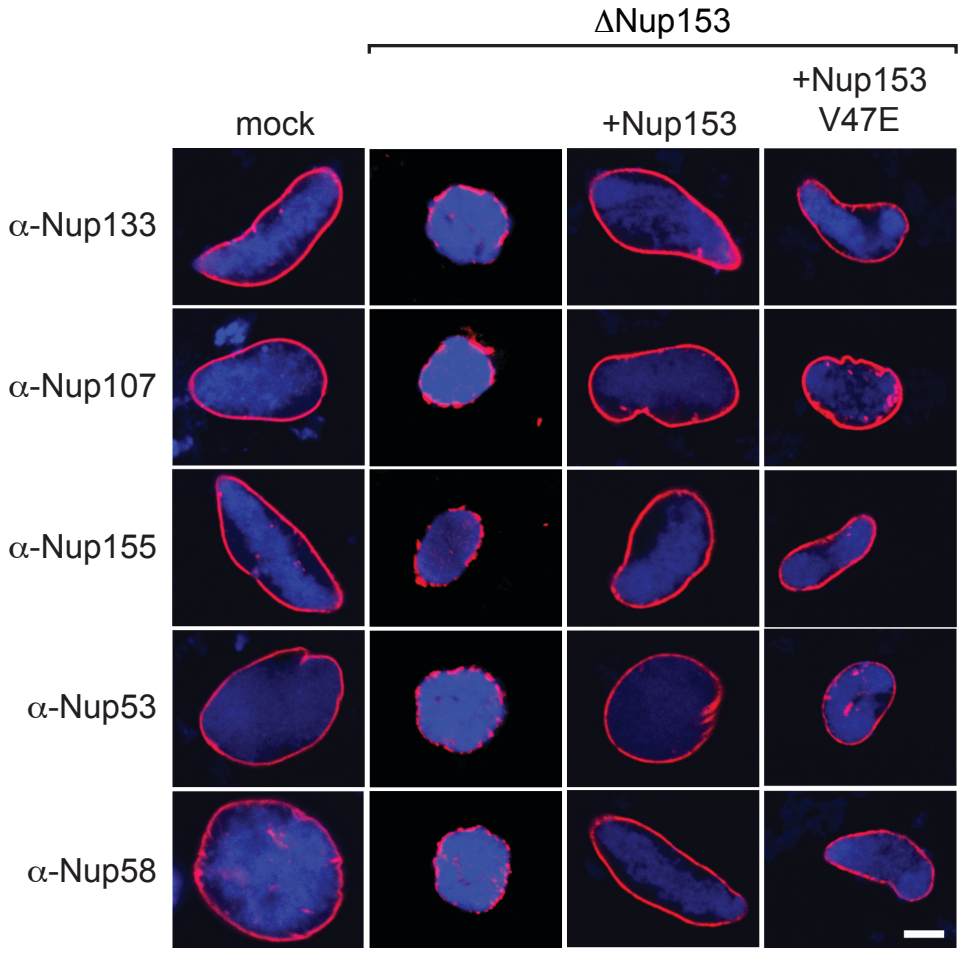

Figure S2, related to Figure 3

Nuclei were assembled for 120 min in mock, Nup153 depleted (ΔNup153) and Nup153 depleted extracts supplemented with recombinant wild type protein (Nup153) or the membrane binding mutant (Nup153 V47E). Samples were analyzed by immunofluorescence for Nup107 and Nup133 (as nucleoporins of the Y-complex), Nup155 and Nup53 (as nucleoporins of the Nup93-complex) and Nup58 (as central channel nucleoporin). DNA was stained with DAPI (blue). Bar 10 µm

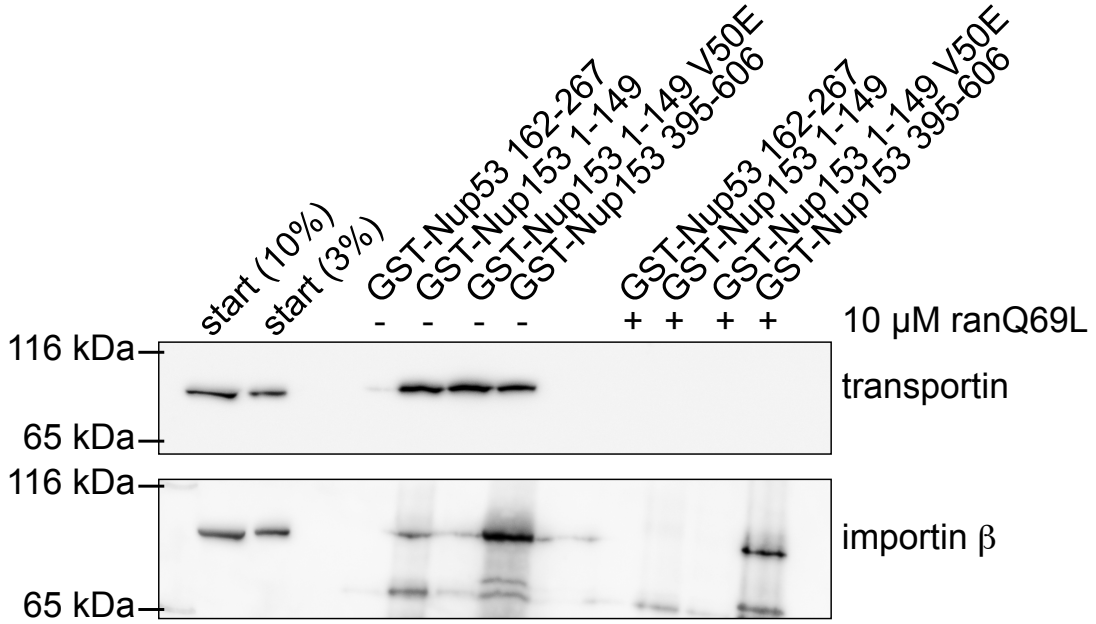

Figure S3, related to Figure 7

GST-fusions of the RRM domain *Xenopus* Nup53 (aa 162-267) (Vollmer et al., 2012) as a control and of *Xenopus* Nup153 (aa-149), the corresponding membrane binding mutant (V50E) as well as *Xenopus* Nup153 (aa 395-608), known to bind Nup50 (Makise et al., 2012), were incubated with cytosol from *Xenopus* egg extracts. Where indicated 10 µM ranQ69L was added to the incubation. Eluates were analyzed by western blotting with antibodies against transportin and importin β. Please note that transportin binding to Nup153 N-terminal fragment is not affected by the V50E mutation. The Nup153 aa 395-608 fragment binds transportin consistent with a previous report which mapped a transportin binding site to a partially overlapping Nup153 fragment (aa 440-720) (Shah and Forbes, 1998)

Supplemental Movie 1

3D reconstruction (generated with IMARIS) of confocal stack images of the HeLa cell transfected with EGFP-Nup153xl 1-149 shown in Figure 1F.

Supplemental Experimental Procedures

Antibodies

Antibodies against Nup107 (Walther et al., 2003), GP210 (Antonin et al., 2005), NDC1 (Mansfeld et al., 2006), Nup160 (Franz et al, 2007), Nup53 and LBR (Theerthagiri et al., 2010) and Nup58 (Sachdev et al., 2012) have been described. mAB414 (Babco), transportin and ran (558660 and 610341, BD Bioscience), EGFP (11814460001, Roche), as well as TPR, human lamin A and B2 antibodies (ab58344, ab26300, ab151735 abcam) were purchased. Antibodies for POM121, RTN4, Nup153 and Nup133, were generated against recombinant fragments of the respective proteins (*Xenopus* POM121 aa 1-314, RTN4 aa 763-1043 and Nup153 aa 1-149, human Nup133 aa 67-514). Antibodies for Nup155, Nup50, importin β, lamin B (expressed as GFP-laminB3, kind gift from Rebecca Heald) are against the *Xenopus* full-length proteins, *Xenopus* importin α and BC08 antibodies are a kind gift from Iain Mattaj.

Protein expression and purification

Constructs for the *Xenopus* Nup153 N-terminus (aa 1-149) were generated from synthetic DNA optimized for codon usage in E. coli (Geneart), human full-length constructs from EGFP3-hNup153 (Rabut et al., 2004) and the corresponding V50E or V47E mutants by mutagenesis using QuikChange site-directed mutagenesis kit (Agilent). The Nup153 N-terminus (wildtype and V50E mutant) was cloned into a modified pET28a vector with a yeast SUMO solubility tag followed by a TEV site or into a modified pET28a vector with EGFP upstream of Nup153. Proteins were expressed in E. coli and purified using Ni-agarose. His_6- and SUMO-tags were cleaved using TEV protease and proteins were concentrated using VIVASPIN columns (Sartorius) and separated by gelfiltration (Superdex200 10/300 GL or Superdex200 PC 3.2/30, GE Healthcare) in HEPES buffer (20 mM HEPES pH 7.5, 150 mM NaCl, 1mM DTT). SUMO and EGFP were expressed and purified from the corresponding empty vectors. Human Nup133 (aa 67-514) was generated as described (Vollmer et al., 2012).
Y-complex was purified from *Xenopus* egg extracts using TAP-tagged Nup98 (Walther et al., 2003) and labelled using Alexa Fluor 546 carboxylic acid succinimidyl ester in 200 mM $NaHCO_3$ pH 8.4. Human ranQ69L was expressed from a modified pET28a vector with a His_6-GST tag, which was cleaved of using TEV protease. The protein was separated from the tag after dialysis using Ni-agarose and further purified by gelfiltration (Superdex200 10/300 GL). Purified ranQ69L was labelled using Alexa Fluor 546 C5 Maleimide in HEPES buffer. Excess dye was removed by gelfiltration (Superdex200 PC 3.2/30).
EGFP-ycBD-BC08 or EGFP-ranBD-BC08 where generated by insertion of human Nup153 fragments (aa 210-338 or aa 658-890) into an BC08 reporter construct (Theerthagiri et al., 2010) between EGFP and BC08. The corresponding constructs were expressed, purified and reconstituted into small unilamellar liposomes with a NE lipid composition previously described (Eisenhardt et al., 2014).

Transfection experiments

Plasmids encoding the *Xenopus* Nup153-N-Terminus and the corresponding V50E mutant (cloned into a modified pEGFP-C3 vector) were transfected into HeLa cells using Fugene 6 (Roche) following the manufacturer's instructions. After 24 h cells were fixed and analyzed by confocal microscopy. For immunoprecipitations, EGFP3-hNup153 constructs were transfected into HEK293 cells. 48 h post-transfection cells were harvested and lysed in lysis buffer (50 mM TRIS-HCl pH 7.5, 150 mM NaCl, 1 mM EDTA 10% glycerol 0.1% Triton X-100 supplemented with protease inhibitors (2 µg/ml leupeptin, 1 µg/ml pepstatin, 2 µg/ml aprotinin, 0.1 mg/ml AEBSF final concentration) for 10 min at 4°C. After centrifugation for 15 min at 15.000 x g the supernatant was immunoprecipitated with GFP-Trap beads

(Chromotek) for 2 h, washed 5x with lysis buffer, 2x with lysis buffer supplemented with 500 mM NaCl, 2x with lysis buffer, and 1x with lysis buffer without Triton X-100 and finally eluted with SDS-sample buffer. Eluates and lysed cells (corresponding to 5% of the eluates) were analyzed. For colocalization experiments (Figure 2A), pEGFP3-Nup153hs or pEGFP3-Nup153hsV47E were co-transfected with mCherry-hLMNB2 (kind gift of Martin Hetzer) or mCherry-Nup62xl using jetPRIME (Polyplus transfection). 24 hours after transfection live cells were imaged at 37°C with a confocal microscope LSM780 (Zeiss) equipped with incubation chamber and using an Apochromat 63x/1.40 Oil DIC M27 objective.

GST Pulldown experiments

Fragments used for the GST pulldown experiments were cloned into a modified pET28a vector with GST tag followed by a recognition site for TEV protease and purified via the N-terminal His6 tag. 60 µl GSH–Sepharose (GE Healthcare) were incubated with 300 µg of the respective bait proteins, washed and blocked with 5% BSA in PBS. Beads were incubated with cytosol from *Xenopus* egg extracts (diluted 1:1 with PBS, and cleared by centrifugation for 30 min at 100,000 rpm in a TLA110 rotor (Beckman Coulter) for 2 h and washed six times with PBS. Bound proteins were eluted by cleavage with TEV protease (0.5 mg/ml) for 1 h at RT and analyzed by SDS-PAGE and Western blotting.

Supplemental References

Antonin, W., Franz, C., Haselmann, U., Antony, C., and Mattaj, I.W. (2005). The integral membrane nucleoporin pom121 functionally links nuclear pore complex assembly and nuclear envelope formation. Mol Cell *17*, 83-92.

Eisenhardt, N., Schooley, A., and Antonin, W. (2014). *Xenopus* in vitro assays to analyze the function of transmembrane nucleoporins and targeting of inner nuclear membrane proteins. Methods Cell Biol *122*, 193-218.

Makise, M., Mackay, D.R., Elgort, S., Shankaran, S.S., Adam, S.A., and Ullman, K.S. (2012). The Nup153-Nup50 protein interface and its role in nuclear import. J Biol Chem *287*, 38515-38522.

Mansfeld, J., Guttinger, S., Hawryluk-Gara, L.A., Pante, N., Mall, M., Galy, V., Haselmann, U., Muhlhausser, P., Wozniak, R.W., Mattaj, I.W.*, et al.* (2006). The conserved transmembrane nucleoporin NDC1 is required for nuclear pore complex assembly in vertebrate cells. Mol Cell *22*, 93-103.

Rabut, G., Doye, V., and Ellenberg, J. (2004). Mapping the dynamic organization of the nuclear pore complex inside single living cells. Nat Cell Biol, 1114-1121.

Sachdev, R., Sieverding, C., Flotenmeyer, M., and Antonin, W. (2012). The C-terminal domain of Nup93 is essential for assembly of the structural backbone of nuclear pore complexes. Mol Biol Cell *23*, 740-749.

Shah, S., and Forbes, D.J. (1998). Separate nuclear import pathways converge on the nucleoporin Nup153 and can be dissected with dominant-negative inhibitors. Curr Biol *8*, 1376-1386.

Theerthagiri, G., Eisenhardt, N., Schwarz, H., and Antonin, W. (2010). The nucleoporin Nup188 controls passage of membrane proteins across the nuclear pore complex. The Journal of cell biology *189*, 1129-1142.

Vollmer, B., Schooley, A., Sachdev, R., Eisenhardt, N., Schneider, A.M., Sieverding, C., Madlung, J., Gerken, U., Macek, B., and Antonin, W. (2012). Dimerization and direct membrane interaction of Nup53 contribute to nuclear pore complex assembly. EMBO J *31*, 4072-4084.

Walther, T.C., Alves, A., Pickersgill, H., Loiodice, I., Hetzer, M., Galy, V., Hulsmann, B.B., Kocher, T., Wilm, M., Allen, T.*, et al.* (2003). The conserved Nup107-160 complex is critical for nuclear pore complex assembly. Cell *113*, 195-206.